

Evolution of temperature and mobilization of
terrigenous organic matter in the subarctic Northwest
Pacific and adjacent Beringia since the Last Glacial
Maximum

Dissertation
zur Erlangung des Doktorgrades
der Naturwissenschaften
Dr. rer. nat.
am
Fachbereich Geowissenschaften
der Universität Bremen

Vorgelegt von:

Vera Meyer

Bremen

Februar 2016

Gutachter der Dissertation:

Prof. Dr. Gesine Mollenhauer

Prof. Dr. Bernhard Diekmann

Tag des Promotionskolloquiums:

25.05.2016

Mitglieder der Prüfungskommission:

Prof. Dr. Gesine Mollenhauer

Prof. Dr. Bernhard Diekmann

Prof. Dr. Gerhard Bohrmann

Prof. Dr. Heiko Pälke

Dr. Henning Kuhnert

Fr. Sara Trojahn

To my parents

Erklärung

Name: Vera Meyer

Datum: 17.02.2015

Anschrift: Brandtstraße 55/57

28215 Bremen

Hiermit versichere ich, dass ich

1. die vorliegende Arbeit ohne unerlaubte fremde Hilfe angefertigt habe,
2. keine anderen als die von mir angegebenen Quellen und Hilfsmittel benutzt habe und
3. die den benutzten Werken wörtlich oder inhaltlichen entnommenen Stellen als solche kenntlich gemacht habe.

Bremen, den 17.02.2015

Unterschrift

This PhD-project was conducted at the Marine Geochemistry group at the Alfred-Wegener-Institute Helmholtz Centre for Polar- and Marine Research, Bremerhaven, Germany. It was mainly funded by the Helmholtz association through the President's Initiative and Networking Fund. Additional funding for a research stay at the School of Palaeogeography, Palaeoarchaeology and Palaeoecology at Queen's University Belfast was provided by GLOMAR-Bremen Graduate School in Marine Sciences.



Abstract

In times of global warming a profound understanding of the climate system is necessary to develop mitigation strategies. Studying episodes of climate change during the Earth's history (e.g. Glacial-Interglacial cycles) allows insights into the climate system and its feedback processes. In the subarctic Northwest Pacific (NW Pacific) and adjacent Northeast Siberia (NE Siberia) mean climate changes between the Last Glacial Maximum and the Holocene are poorly understood since climate records (e.g. temperature records) spanning the full LGM-Holocene transition are sparse. This thesis shall contribute to a better understanding of climate and environmental change since the LGM and the controlling mechanisms in the region by investigating the development of temperature, glaciation and export of terrigenous organic matter into the North Pacific (N Pacific). Biomarkers in sediment cores from the Western Bering Sea and the NW Pacific/continental margin off Siberia are applied as palaeoclimate archives.

In the first part of the thesis LGM-to-Holocene sea surface temperature (SST) records for the marginal Northwest Pacific and the Western Bering Sea are established using the $\text{TEX}^{\text{L}_{86}}$ (Tetraether Index)-SST proxy. It focusses on the LGM and the early deglaciation since existing deglacial SST records from the region do not reach beyond 15 ka BP. $\text{TEX}^{\text{L}_{86}}$ -based SSTs in both settings closely follow millennial-scale climate fluctuations known from Greenland ice-cores until 15 ka BP, confirming other SST-records from the region which point to rapid atmospheric teleconnections with abrupt climate changes in the North Atlantic (N Atlantic). During Heinrich Stadial 1 (HS1), Western Bering Sea SSTs decline, similar to the N Atlantic realm, suggesting the Bering Sea was connected to the N Atlantic climate change. Progressively rising SSTs in the NW Pacific differ from the Western Bering Sea and the N Atlantic climate. Similarities between the climate in the Gulf of Alaska and the NW Pacific suggest that the Alaskan Stream accumulated in the NW Pacific during the LGM connecting the climates of the eastern and western N Pacific. Deviating trends in the climate from 12-10 ka onwards point to reduced influence of the Alaskan Stream in the NW Pacific and the end of the oceanic linkage.

The second part of the thesis investigates the LGM-to-Holocene evolution of mean air temperature (MAT) of the Kamchatka Peninsula. Climate archives, existing in Kamchatka, do not reach beyond 12 ka BP, so the climate evolution since the LGM is fairly unknown. Using the CBT/MBT'-palaeothermometry (Cyclisation of Branched Tetraethers and the Methylation of Branched Tetraethers indices) a continuous record in summer MAT is provided for the past

20 ka. It is found that glacial summers were as warm as at present. This is in line with summer conditions in continental Siberia but contrasts with the SST-development of the surrounding seas. Likely, strong southerly winds, associated with a pronounced North Pacific High pressure system (NPH) over the subarctic NW Pacific, accounted for the warm conditions on Kamchatka. A comparison with an Earth System Model reveals discrepancies between proxy-based inferences for temperature and atmospheric circulation. The deglacial temperature development was characterized by abrupt millennial-scale temperature oscillations. The Bølling/Allerød warm-phase (B/A) and the Younger Dryas cold-spell (YD) are pronounced events, providing evidence for a strong impact of N Atlantic climate variability on southeastern Siberia, at least during the past 15 ka BP. During HS1, similarities with the NW Pacific SST imply that the Alaskan Stream determined temperature change on the Peninsula rather than teleconnections with the N Atlantic.

Considering that NE-Siberian glaciation is supposed to have been more extensive than at present but restricted to mountain ranges during the LGM, the warm glacial-summers of Siberia suggest that summer temperature may have been an important limiting factor for ice sheet growth in the region. In the third part of the thesis, mass balance calculations for the LGM-glaciers on Kamchatka and the Kankaren Range (NE Siberia) are performed by degree-day-modelling in order to estimate the precipitation needed to sustain the glaciers under warm summer conditions. It is found that precipitation at least must have equaled or even exceeded the modern average. The precipitation estimates confirm the hypothesis that summer temperature limited ice-sheet expansion in NE Russia during the LGM, thereby countering the prevailing view that increased aridity (relative to present) hampered ice-sheet growth.

The fourth part of the thesis contributes to an ongoing debate about the sources of old, (^{14}C -depleted) carbon dioxide (CO_2) which increased atmospheric CO_2 -levels ($\text{CO}_{2\text{atm}}$) and concurrently decreased the atmospheric radiocarbon signature ($\Delta^{14}\text{C}_{\text{atm}}$) during the deglaciation. Permafrost-decomposition in the Northern Hemisphere (NH) triggered by deglacial warming and sea-level rise is considered as one possible source of ^{14}C -depleted CO_2 , particularly at the onset of the B/A-interstadial (14.6 ka BP). However, the timing of carbon mobilization in permafrost areas of the NH is underconstrained. In order to investigate the potential role of permafrost decomposition in the subarctic N Pacific realm in the atmospheric, changes mass accumulation rates and the radiocarbon signature ($\Delta^{14}\text{C}$) of leaf-wax lipids are analyzed in order to identify intervals of intensified export of ^{14}C -depleted terrigenous OM into the Western Bering Sea and the NW Pacific. Enhanced burial of nearly

^{14}C -free carbon commenced during the HS1 and was likely triggered by increased runoff in the Yukon River due to retreating American ice-sheets. Since the B/A mobilization of ^{14}C -depleted seems to have been dominantly controlled by sea-level rise and thus by erosion of permafrost-covered shelves. Enhanced OM-export associated with permafrost-thaw on Kamchatka likely initiated during the second half of the B/A-interstadial and peaked during the YD-stadial. Lagging the rapid $\text{CO}_{2\text{atm}}/\Delta^{14}\text{C}_{\text{atm}}$ changes at 14.6 ka BP, the permafrost degradation in the Kamchatka region was probably irrelevant for the atmosphere. Instead, enhanced OM-export in the region coincided with abrupt $\text{CO}_{2\text{atm}}/\Delta^{14}\text{C}_{\text{atm}}$ changes during the YD suggesting that permafrost may have contributed to the atmospheric carbon-pool at that time.

Kurzfassung

In Zeiten globaler Erwärmung ist ein profundes Verständnis des Klimasystems nötig, um Strategien zur Eindämmung der Konsequenzen des Klimawandels zu entwickeln. Das Untersuchen von vergangenen Klimaveränderungen in der Erdgeschichte (z. B. Glazial-Interglazial Zyklen) gewähren Einsichten in das Klimasystem und dessen Rückkopplungsprozesse. Sowohl im subarktischen Nordwestpazifik als auch im angrenzenden Nordost Sibirien sind Prozesse der Klimaveränderungen während des Übergangs aus dem Letzten Glazialen Maximums (LGM) ins Holozän kaum verstanden, da Klimaarchive dieser Region selten den gesamten Zeitraum erfassen. Diese Dissertation soll zu einem besseren Verständnis der deglazialen Klima- und Umweltveränderungen sowie deren Ursachen im Nordwestpazifikraum beitragen. Auf der Basis von Biomarkern in Sedimenten des westlichen Beringmeers und des Nordwestpazifiks (Kontinentalhang Sibirien), werden die Entwicklungen von Temperatur, Vergletscherung und des Eintrags terrigenem Materials in den Ozean untersucht.

Im ersten Teil der Dissertation werden Oberflächenwassertemperaturen (sea surface temperature, SST) mittels des $\text{TEX}^{L_{86}}$ (Tetraether Index) Temperaturproxys für das westliche Beringmeer und den marginalen Nordwestpazifik rekonstruiert. Der Fokus liegt dabei auf dem Heinrich Stadial 1 (HS1) und dem LGM, da existierende SST-Datensätze nicht weiter als 15 ka BP (BP: Before Present, vor heute) zurückreichen. Bis ca. 15 ka BP, zeichnen die auf $\text{TEX}^{L_{86}}$ basierenden Daten beider Lokationen Klimaoszillationen nach, die aus Grönland-Eiskernen bekannt sind. Dieses Muster bestätigt die Interpretationen vorangegangener Arbeiten, wonach atmosphärische Telekonnektionen mit dem Klima des Nordatlantiks die deglaziale SST-Entwicklungen im Nordpazifik bestimmten. Im HS1 verzeichnet die Temperaturkurve aus dem westlichen Beringmeer eine ähnliche Abkühlung, wie sie aus dem Nordatlantik bekannt ist, was eine Telekonnektion im HS1 suggeriert. Mit einer progressiven Erwärmung weicht der Nordpazifik sowohl vom Temperaturmuster des Beringmeeres als auch der Entwicklung des Nordatlantiks ab. Ähnlichkeiten mit dem Golf von Alaska deuten auf eine ozeanische Verbindung zwischen dem westlichen und östlichen Nordpazifik über den Alaska Strom an. Ab 10-12 ka BP suggerieren abweichende Trends zwischen Ost und West eine Abschwächung des Stroms und damit das Ende der ozeanographischen Verbindung.

Im zweiten Teil der Dissertation wird die Entwicklung der mittleren Lufttemperaturen (mean air temperature, MAT) auf Kamtschatka zwischen dem LGM und dem Holozän untersucht. Da existierende Klimaarchive der Halbinsel nur die letzten 12 ka umfassen, sind Kamtschatkas klimatische Bedingungen während des LGMs und des Deglazials nahezu

unbekannt. Mit dem CBT/MBT-Temperaturproxy (Cyclisation of Branched Tetraethers/Methylation of Branched Tetraethers) werden im Rahmen der Dissertation kontinuierliche Sommertemperaturdaten für die letzten 20 ka gewonnen. Die Daten zeigen, dass die Sommer des LGM genauso warm waren, wie heute. Dies passt zu den glazialen Temperaturbedingungen in Sibirien, nicht aber zur SST Entwicklung des Nordpazifiks. Es wird vermutet, dass verstärkte Südwinde, die mit einem intensivierten Nordpazifik-Hoch in Zusammenhang stehen können, für die warmen Bedingungen auf Kamtschatka verantwortlich waren. Im Vergleich mit einem Klimamodell (Earth System Model) fallen Diskrepanzen in Hinblick auf die klimatischen Bedingungen im LGM auf. Das Deglazial wird von abrupten Oszillationen charakterisiert. Die Bølling/Allerød-Warmphase (B/A) und die Jüngere Dryas-Kaltphase (Younger Dryas, YD) sind deutlich zu erkennen und zeugen von einer starken Verbindung zum Klimageschehen des Nordatlantiks. Ähnlichkeiten mit der Temperaturentwicklung des Nordwestpazifiks deutet darauf hin, dass der Alaska Strom während des HS1 einen größeren Einfluss auf Kamtschatkas Klima hatte, als eine atmosphärische Telekonnektion mit dem Nordatlantik.

Rekonstruktionen der glazialen Vergletscherung Sibiriens zeigen, dass die Eisausdehnung weiter als heute, jedoch auf Gebirgsketten eingeschränkt war. Vor diesem Hintergrund mögen warme Sommer als ein wichtiger hemmender Faktor für die Vereisung der Region gewesen sein. Um diese These zu überprüfen, werden im dritten Teil der Dissertation die jährlichen Niederschlagsmengen abgeschätzt, die für das Ausmaß der glazialen Gletscher unter warmen Sommerbedingungen erforderlich gewesen wären. Dazu werden Massenbilanzen für die Gletscher mit einem „Degree-Day-Model“ erstellt. Die Daten zeigen, dass die Niederschlagsmengen im LGM mindestens genauso groß oder sogar noch größer als heute gewesen sein müssen. Dies suggeriert, dass Sommertemperaturen die Eisausdehnung im LGM limitierten, und stellt die vorherrschende Hypothese in Frage, wonach trockene Bedingungen den limitierenden Faktor darstellten.

Der vierte Teil der Dissertation liefert einen Beitrag zur Suche nach Quellen für ^{14}C -angereichertes Kohlendioxid (CO_2), die den deglazialen Anstieg der atmosphärischen CO_2 -Konzentration verursachten und gleichzeitig das atmosphärische Kohlenstoffisotopenverhältnis ($^{14}\text{C}/^{12}\text{C}$) der Atmosphäre ($\Delta^{14}\text{C}_{\text{atm}}$) veränderten. Als eine mögliche Quelle werden tauende Permafrost-böden in der Nordhemisphäre angesehen und primär für den $\text{CO}_{2\text{atm}}$ -Anstieg zu Beginn der B/A-Warmphase diskutiert. Um die potenzielle Rolle deglazialer Permafrost-Destabilisierung im Nordpazifikraum für Veränderungen in $\text{CO}_{2\text{atm}}$ und $\Delta^{14}\text{C}_{\text{atm}}$ zu

untersuchen, werden Massenakkumulationsraten und die $\Delta^{14}\text{C}$ -Signatur terrigener Biomarker bestimmt. Ein erster verstärkter Eintrag von ^{14}C -abgereichertem organischen Material (OM) ist für das HS1 zu verzeichnen, und war vermutlich mit fluvialer Erosion im Einzugsgebiet des Yukon assoziiert. Ab dem B/A scheint die Mobilisierung des OM vornehmlich durch den steigenden Meeresspiegel und der damit zusammenhängenden Erosion der Schelfe kontrolliert worden zu sein. Verstärkter OM-Eintrag im Zuge tauender Permafrostböden auf Kamtschatka begann wahrscheinlich im späten B/A und spitzte sich in der YD zu. Da Phasen verstärkter OM-Mobilisierung in der Region um Kamtschatka nicht mit den atmosphärischen Veränderungen zu Beginn des B/A zusammenfallen, stattdessen aber mit denen der YD, könnten Permafrost-Destabilisierungen während der YD zum $\text{CO}_{2\text{atm}}$ -Anstieg beigetragen haben, erscheinen jedoch als unwahrscheinliche Quellen für den Beginn des B/A.

Table of contents

Abstract.....	I
Kurzfassung.....	IV
1. Introduction.....	1
1.2. <i>Scientific background</i>	1
1.3. <i>Past climate change</i>	5
1.4. <i>Biomarkers as proxies for past climate change</i>	6
1.5. <i>Motivation, aims and objectives of the thesis</i>	10
1.6. <i>Outline of the thesis</i>	17
2. Manuscript I: Glacial-to-Holocene evolution of sea surface temperature and surface circulation in the subarctic Northwest Pacific and the Western Bering Sea.....	18
3. Manuscript II: Summer-temperature evolution on the Kamchatka Peninsula during the past 20,000years.....	37
4. Manuscript III: Linking glacier extent and summer temperature in NE Russia: implications for precipitation during the last glacial maximum.....	62
5. Manuscript IV: Increased export of ¹⁴ C-depleted terrigenous organic matter into the NW Pacific and the Western Bering Sea during deglacial permafrost decomposition in Beringia.....	75
6. Summary and Perspectives.....	102
6.1. <i>Summary - temperature development</i>	102
6.2. <i>Summary - time-scales of carbon mobilization</i>	104
6.3. <i>Perspectives - temperature development</i>	105
6.4. <i>Perspectives – time-scales of carbon mobilization</i>	107
7. Acknowledgements.....	110
8. References.....	112
9. Description of Own Contributions.....	134

1. Introduction

1.1. Scientific background

It is unequivocal that anthropogenic greenhouse gas emissions (e.g. carbon dioxide and methane) as a result of fossil fuel burning cause global warming, since global mean temperature and atmospheric greenhouse-gas concentrations have progressively risen since the industrialization in the late 19th century (Figure 1.1.; IPCC, 2007, 2013 and references therein). There is consensus across various climate-models that the global warming trend will continue in the future and will induce severe climatic and environmental responses. Changing environmental conditions, such as e.g. sea-level rise or desertification represent long-term threats for society (IPCC, 2007; 2013).

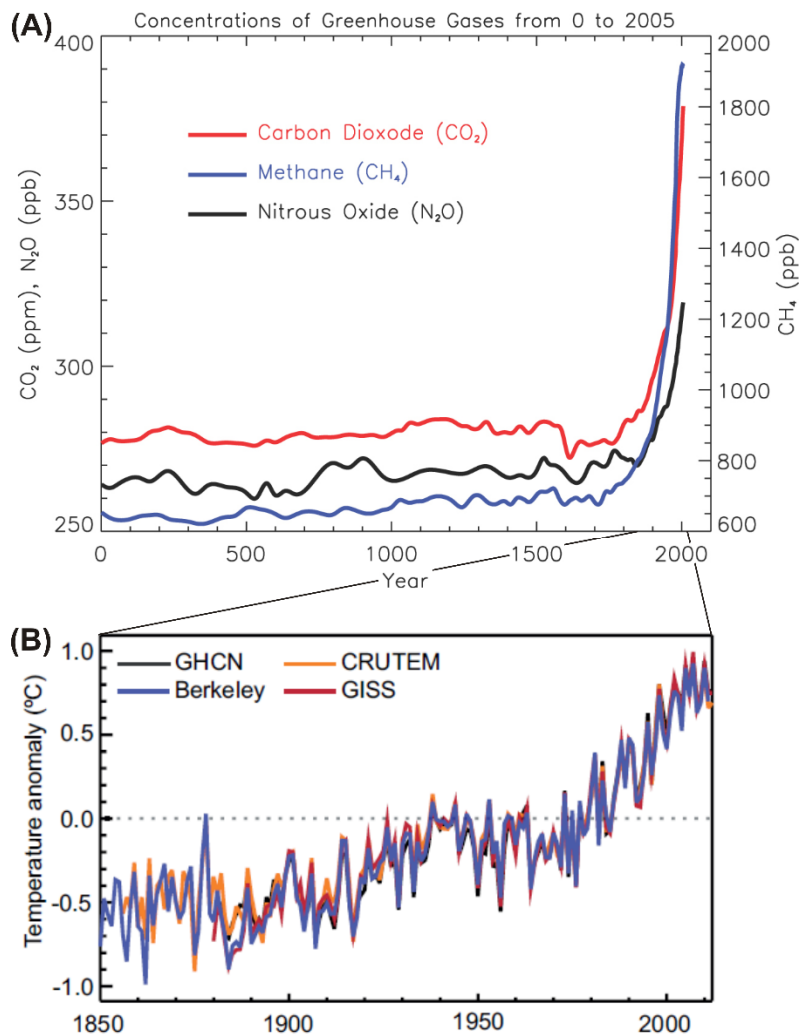


Figure 1.1. (A) Development of atmospheric greenhouse gases over the past 2000 years (adopted from: IPCC, 2007). (B) Global average land-surface temperature anomalies relative to 1961-1990, since the mid-19th century (adopted from: IPCC, 2013 and references therein).

In order to develop strategies to mitigate climate change and its consequences, precise predictions for the dimensions of future warming and environmental responses are necessary and require a profound understanding of the climate system. Future climate change is certainly dependent to the dimension of future anthropogenic greenhouse-gas emissions but also on the interaction of several internal feedback processes in the Earth's climate system (e.g. the carbon cycle; Huntingford et al., 2009; IPCC, 2013 and references therein) which may either intensify or hamper regional and global warming. So far, not all feedback processes are fully understood, which requires further research on the Earth's climate system.

A particular sensitivity and relevance to climate change is assigned to the high latitudes of the Northern Hemisphere (NH) as arctic mean temperature rose twice as much as the average of lower latitudes since the 1980s (AMAP, 2012). Such polar amplification is also consistently predicted for the future (Figure 1.2) across various climate models. Depending on different greenhouse-gas emission scenarios (Representative Concentration Pathway, RCP), temperature is expected to increase by 2.2-2.4 times the global average until the end of the 21st century (IPCC, 2013 and references therein). Hence, the arctic cryosphere and ecosystems will probably undergo drastic changes (AMAP, 2012) which will implicate various feedback processes and climate responses acting on regional and partly global scales. By way of example, the decay of the Greenland ice sheet may potentially cause a negative feedback of at least regional dimension as the input of melt-water from the retreating Greenland ice-sheet is predicted to weaken the Atlantic Meridional Overturning Circulation (AMOC) and thus the meridional heat transport (e.g. Driesschaert et al., 2007; Drifjhout et al., 2012) into the North Atlantic (N Atlantic) throughout the 21st century. This may result in cooling the North Atlantic realm (Figure 1.2) but may potentially also counteract warming in distant regions of the NH (IPCC, 2013).

In contrast, representing a net terrestrial carbon sink, the circumarctic permafrost soils may trigger a positive feedback process magnifying the Earth's greenhouse effect and hence global warming. Permafrost is perennial frozen ground (per definition: perennial frozen for at least two consecutive years) covering about 25% of the circumarctic land-area north of 50°N (Figure 1.3).

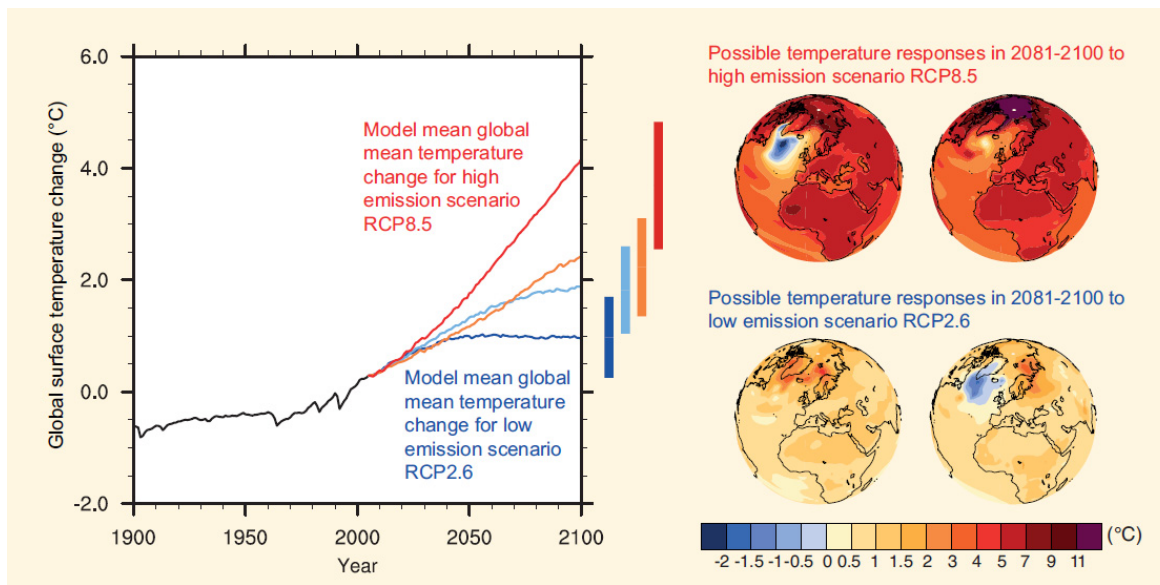


Figure 1.2. Left panel: Global mean temperature development for four scenarios of anthropogenic greenhouse gas emission (Representative Concentration Pathway, RCP), averaged across all climate models from the Coupled Model Intercomparison Phase 5 (CMIP5). Likely ranges for the scenarios are given by vertical bars. Right panel: Temperature anomalies for years 2081-2100 relative to 1986-2005 adopted from two CMIP5 models for the highest (RCP8.5) and lowest (RCP2.6) emission scenarios (from IPCC, 2013).

Owing to the frozen conditions microbial degradation of organic matter (OM) is strongly suppressed and restricted to the summer months when the uppermost soil layer (active layer) temporarily thaws. The frozen conditions allowed permafrost to accumulate and preserve large amounts of organic carbon during the Quaternary (Smith et al., 2004; Zimov et al., 2006). The size of the freeze-locked carbon pool is estimated to 1700 PgC (Tarnocai et al., 2009) which is approximately twice as much as the carbon stock of the atmosphere (Houghton, 2007; Dolman et al., 2010; Schuur et al., 2009, 2013) and amounts to half of the global soil-carbon pool. In the course of arctic warming permafrost is expected to thaw (Figure 1.3), so the carbon stocks would become accessible to biogeochemical cycling. As such it is very likely that permafrost will turn into a source of carbon dioxide (CO₂) and methane (CH₄) magnifying the Earth's greenhouse effect (e.g. Saito et al. 2007; Zimov et al., 2006, 2009; Schuur et al., 2008, 2009; 2013; 2015; Zhang et al. 2008a, b; Slater and Lawrence, 2013). Observations of permafrost conditions in the NH show that permafrost thaw/decomposition has already begun, as soil temperature has risen by up to 2°C since the 1980s (e.g.; Callaghan et al., 2011; IPCC, 2013) and the southern limit of permafrost extent has migrated northward since the 1970s (e.g. IPCC, 2013). Also, the active-layer thickness has grown since then (Akerman and Johansson, 2008; Smith et al., 2010; IPCC, 2013). Furthermore, permafrost decomposition will probably constitute itself by enhanced riverine and coastal erosion (e.g. Guo et al., 2007; AMAP, 2012) due to intensifying fluvial runoff,

sea-level rise and ocean warming (Lantuit et al., 2008; Rachold et al., 2000, IPCC, 2013; Lawrence and Slater, 2010; Koven et al., 2013). By now, the climatic relevance of permafrost degradation is poorly assessed since most climate models do not consider the permafrost carbon-pool for predictions of future atmospheric CO₂-levels (e.g. IPCC, 2013 and references therein). The few existing modelling approaches do predict the carbon sink would turn into a source of greenhouse gases and would cause a positive feedback-process acting on centennial to millennial time-scales (e.g. Koven et al., 2011; Schaefer et al., 2011; MacDougall et al., 2012; IPCC, 2013). However, these models largely vary among future development of regional extent of permafrost, active-layer thickness and magnitude of greenhouse-gas release. Consequently, a broad range of additional warming (ranging between 0.04-4.69°C by 2100) is currently suggested (MacDougall et al., 2012; Schneider von Deimling et al., 2012; IPCC, 2013). This variety is because uncertainty exists upon physical and chemical processes in degrading permafrost. This includes thawing rates, the time-scales of the thawing and carbon mobilization, as well as about the quantity of carbon which would be remineralized and would ultimately become climatically relevant by entering the atmosphere as CO₂ or CH₄ (Koven et al., 2011, 2013; Schaefer et al., 2011; McDougall et al., 2012; IPCC, 2013). Therefore, further research on the permafrost feedback is necessary.

As the impact of permafrost-thaw will certainly depend on the magnitude of future warming (e.g. Harden et al., 2012; Schneider von Deimling et al., 2012; IPCC, 2013 and references therein), further research investigating the controlling mechanisms of temperature-change in high latitudes of the NH is necessary, considering that climate models still have large discrepancies concerning the dimension of future warming in the Arctic and sub-arctic regions. Temperature predictions for these regions differ significantly in magnitude as the processes controlling temperature change are divers and differently represented in climate models. For instance, model simulations consistently predict a weakening of the AMOC throughout the 21st century but uncertainty exists upon the magnitude (Drifjhout et al., 2012; IPCC, 2013). As such arctic warming (by the end of the 21st century) is strongest in models with none or little AMOC-weakening (Figure 1.2) but weaker when AMOC-induced cooling spreads out into the NH (IPCC, 2013 and references therein). As a negative feedback process, AMOC-weakening may be important to hamper the permafrost-feedback.

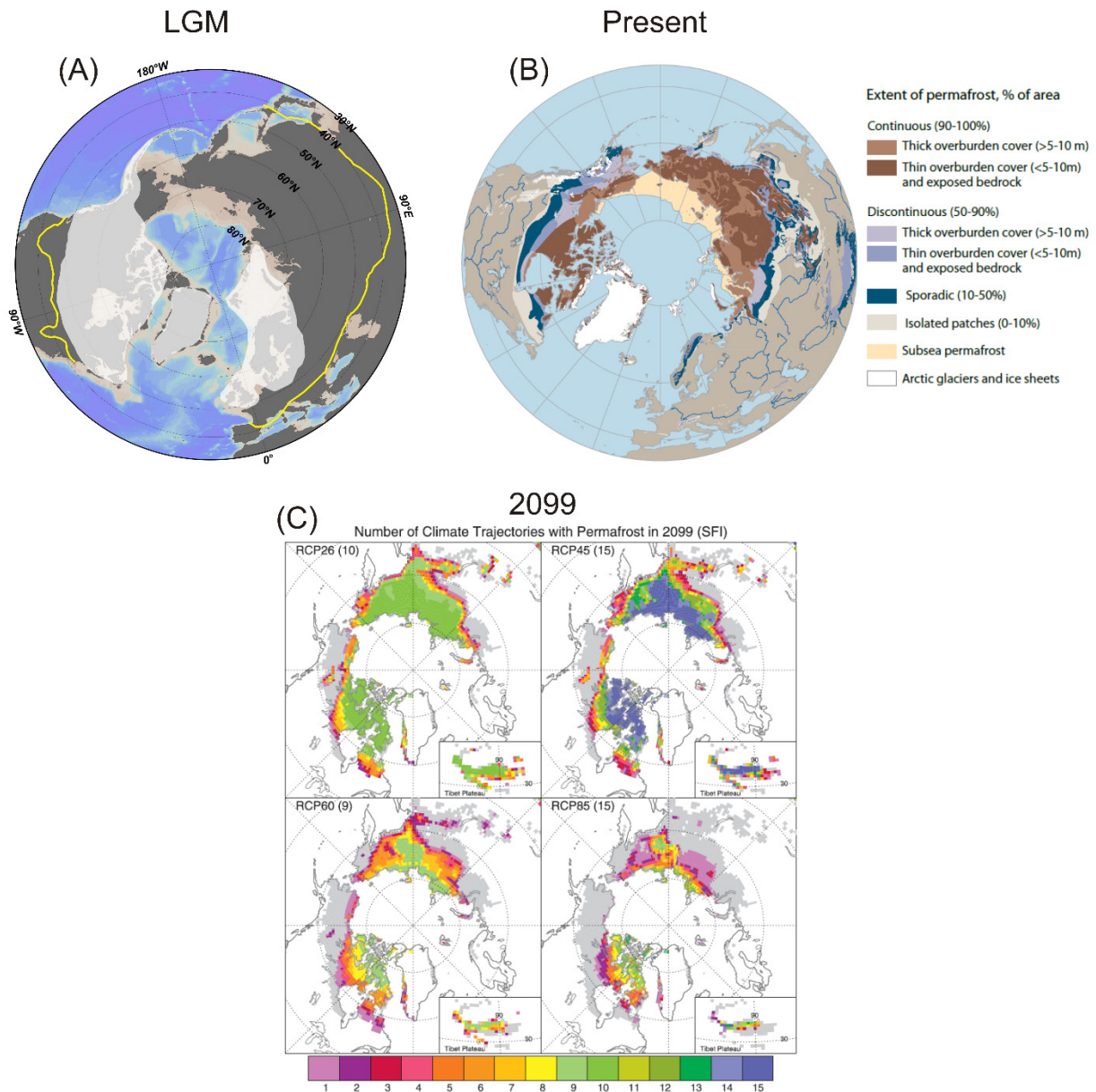


Figure 1.3. a) Southern boundary of permafrost during the Last Glacial Maximum (21-18 ka BP; yellow line; after Vandenberghe et al., 2014). White shaded areas indicate continental ice caps. b) Present-day permafrost extent (from AMAP, 2012). c) Climate model outputs for permafrost extent in 2099 based on different climate trajectories adopted from different RCP-scenarios. Grey areas sketch the modern permafrost extent. (From: Slater and Lawrence, 2013).

1.2. Past climate change

The study of past episodes of global warming and rising greenhouse-gas concentrations allows to improve the understanding of the climate system providing insights into the interaction of feedback processes and environmental responses to different forcings. The last deglaciation, the transition from the Last Glacial Maximum (LGM) into the current interglacial, the Holocene, is such analogue as it was characterized by several environmental changes which are also expected for the future. Between 18-8 ka before present (BP) average global temperature rose about 3-8 °C (e.g. Shakun et al., 2012), atmospheric CO₂-levels

(CO_{2atm}) increased by about 100 ppm and melting continental ice caps made sea-level rise by approximately 120 m (e.g. Stanford et al., 2011; Lambeck et al., 2014). Also, the extensive permafrost areas of the (NH) rapidly shrank during the deglacial climate amelioration (Figure 1.3) with the southern boundary migrating 10° farther north (Brown et al., 1998; Yershov, 1998; Vandenberghe et al., 2014). So the last deglaciation represents a suitable time interval to study the response of permafrost to warming, the contribution of formerly freeze-locked carbon to rising atmospheric CO₂ levels, but also the mechanisms controlling temperature change in subarctic and arctic regions.

Intending to contribute to a better understanding of temperature change in high-latitudes and the permafrost feedback, this thesis investigates deglacial temperature change and carbon turnover associated with permafrost dynamics in the Northwest Pacific (NW Pacific) realm, using biomarkers preserved in marine sediments as palaeoclimate archives.

1.3. Biomarkers and their application as proxies for past environmental changes

Biomarkers are molecular fossils indicative of a specific organism or a group of organisms. Being indicative of a specific biological sources they represent powerful tools to reconstruct past environmental conditions (e.g. Peters et al., 2005). Found in marine sediments marine and terrigenous biomarkers allow insights into both, continental as well as marine realm. They are common means to reconstruct past temperature and organic-matter turnover. In the following a brief overview of the biomarkers and appending proxies mentioned in this thesis are given. Examples of the molecular structure are shown in Figure 1.4.

Long-chain alkenones

Long-chain alkenones (C_{37:2}-C_{37:4}; Figure 1.4) are unsaturated long-chain ketones which are produced by haptophyte algae, predominantly by *Emiliana Huxleyi*, a coccolithophorid-species (e.g. Volkman et al., 1980). Since the degree of saturation, that is to say the number of double bonds (2-4), varies with temperature (number of double-bonds increases with decreasing temperature) the alkenone-unsaturation index (U^K₃₇) was developed as proxy for sea-surface temperature. (Brassel et al., 1986; Prahl and Wakeham, 1987; Prahl et al., 1988; Muller et al., 1998).

Isoprenoid Glycerol Dialkyl Glycerol Tetraethers

Isoprenoid Glycerol Dialkyl Glycerol Tetraethers (isoGDGTs) are membrane molecules of Marine Thaumarchaeota (e.g. Schouten et al., 2013 and references therein) which differ in the number of cyclopentyl moieties in the alkyl-chains (Figure 5). It has been observed in culture experiments that the growth temperature influences the distribution of isoprenoid GDGTs in the cell membrane in so far that the number of GDGTs with a higher amount of cyclopentyl-moieties increases with rising temperature (e.g. Schouten et al., 2002, 2007, 2013; Wuchter et al., 2004). Due to this observation the TetraEther-Index of Tetraethers consisting of 86 carbon atoms (TEX₈₆) was introduced as proxy for mean annual sea-surface temperature (Schouten et al., 2002) based on the relative abundances of isoGDGTs (GDGT 1-4 and the Crenarchaeol regio-isomer; Figure 1.4) in marine sediments. Due to uncertainties in the relation between TEX₈₆ and temperature modified versions of the calibration or advanced indices were proposed. Kim et al. (2010) introduced the TEX^L₈₆ and TEX^H₈₆ (L: low temperature; H: high temperature) which are supposed to work best in settings below and above 15°C, respectively. Since Thaumarchaeota also thrive in sub-surface waters the TEX_{86_0-200 m} was introduced to estimate mean annual temperature in the upper 200 m of the water column (Kim et al., 2012).

Branched Glycerol Dialkyl Glycerol Tetraethers

Similar to isoGDGTs, branched Glycerol Dialkyl Glycerol Tetraether (brGDGTs) are supposed to be membrane lipids but the exact species synthesizing these molecules are still unknown. Most likely brGDGT derive from anaerobic (Weijers et al., 2006a, b) and heterotrophic (Pancost and Sinningh  Damst , 2003) bacteria which are ubiquitous in peats and soils (Weijers et al., 2006a, 2007; Peterse et al., 2012). Some Acidobacteria have been suggested as producer of brGDGTs but so far culture experiments could only provide evidence for the presence of one GDGT in those bacteria (Weijers et al., 2009; Sinningh  Damst , 2011). Initially, brGDGT were supposed to be predominantly produced in terrestrial environments and to be fluvially transported into the marine realm. Based on this view Hopmans et al. (2004) introduced the Branched and Isoprenoid Tetraether index (BIT-index) as a means to quantify the relative abundance of terrigenous organic matter in marine sediments. The BIT is based on the sum of brGDGTs (GDGTs Ia, IIa, and IIIa; Figure 1.4) and the predominantly marine derived Crenarchaeol (isoGDGT). In soils and peats, hence where terrigenous GDGTs dominate, the index is close to 1 whereas open marine sediments with extremely low terrigenous inputs reach BIT-values close to 0 (Hopmans et al., 2004).

Later, it was found that the distribution of the nine different brGDGTs in terrestrial soils is dependent on temperature and soil-pH. Specifically, it was found that number of methyl groups in the alkyl chains of the brGDGT negatively correlated with temperature whereas the number of incorporated cyclopentyl-moieties show a negative correlation with soil pH (Weijers et al., 2007). Therefore, Weijers et al. (2007) introduced the Cyclisation of Branched Tetraether index (CBT) and Methylation of Branched Tetraether index (MBT) as proxies for mean annual air temperature and changes in soil-pH (based on all nine brGDGT, shown in Figure 1.4). MBT was modified (to MBT') by Peterse et al. (2012) who excluded GDGT IIIb and IIIc as they usually do not account for more than 1% in the GDGT distribution. During the last decade evidence was found that brGDGT are not exclusively produced in terrestrial soils but also in marine sediments, lake water and rivers (Peterse et al., 2009; Tierney et al., 2010; Zhu et al., 2011; Zell et al., 2013; deJonge et al., 2014). This complicates the application of the BIT-index and CBT/MBT proxies (e.g. Peterse et al., 2009, 2014; Zell et al., 2013).

Leaf-wax lipids

Long-chain *n*-alkanes ($> n\text{-C}_{23}$) and long-chain *n*-alkanoic acids ($> n\text{-C}_{24}$; Figure 1.4) are constituents of the protective epicuticular leaf-waxes of higher land plants (Eglinton and Hamilton, 1967). They are frequently used to reconstruct terrestrial climate change as the molecular structure and the stable carbon and hydrogen isotopic compositions contain information about continental vegetation (composition and distribution of different plant types) or humidity as well as variations in $p\text{CO}_2$ at the time of biosynthesis (e.g. Schefuß et al., 2005; Eglinton and Eglinton, 2008). Quantified in marine sediments they can also be applied as proxies to estimate variations in the export of terrigenous organic matter into the ocean. Compound-specific radiocarbon analysis of leaf-wax lipids has been applied to study terrestrial residence times of organic matter between the death of the plant and the final burial in marine sediments (e.g. Kusch et al., 2010), a means to obtain insights into the time-scales of processes controlling the fate of terrigenous organic matter prior to the final deposition in marine sediments. The time-scales are determined by the way of transport (e.g. aeolian or riverine), the temporary storage in terrestrial reservoirs (e.g. soils) and several biogeochemical and sedimentary processes affecting the organic matter after the death of the plant. Information about terrestrial residence times of biomarkers helps to understand past and present carbon cycle dynamics.

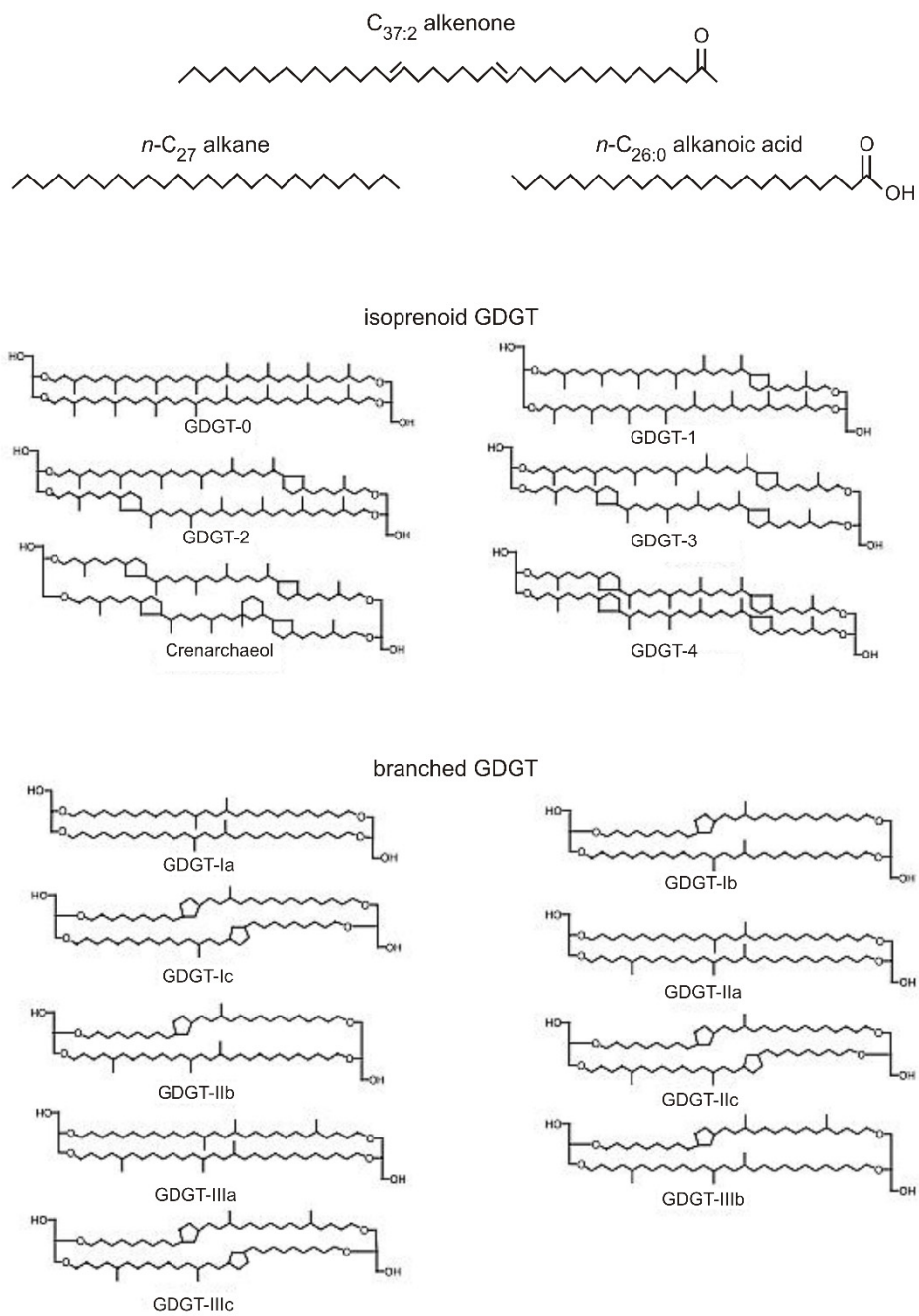


Figure 1.4. Molecular structure of biomarkers described in section 1.3.

1.4. Motivation, aims and objectives of the thesis

The deglacial increase in $\text{CO}_{2\text{atm}}$ was characterized by three distinct pulses between approximately 17.5 and 11.8 ka BP (Figure 1.5). Each of them was accompanied by a concurrent decrease in the radiocarbon-content of atmospheric CO_2 ($\Delta^{14}\text{C}_{\text{atm}}$, Figure 1.5). The first phase lasted from 17.5-14.6 ka BP, often referred to as the Mystery Interval (MI), and was followed by more rapid increase lasting for approximately 180 years at the onset of the Bølling/Allerød (B/A)-interstadial. Afterward, CO_2 -levels remained stable until the onset of the final phase which occurred between 12.8 and 11.8 ka BP (Figure 1.5). Deglacial variations of the carbon cycle that caused the changes in the atmospheric carbon pool are not completely understood. A reorganization of oceanographic conditions (e.g. circulation and stratification) particularly in the Southern Ocean leading to outgassing of ^{14}C -depleted CO_2 from a formerly isolated deep-water masses, is considered as primary cause (e.g. Broecker and Barker, 2007; Broecker and Clark, 2010; Fischer et al., 2010; Marchitto et al., 2010; Rose et al., 2010; Ronge et al., 2015). However, it is questionable whether oceanic outgassing alone can account for the entire changes in atmospheric CO_2 and $\Delta^{14}\text{C}$. It seems that this processes fuelled the $\text{CO}_{2\text{atm}}$ -rise during the first half of the MI (Skinner et al., 2010; Schmitt et al., 2012) but the sources for the abrupt changes from 14.6 ka BP onward are not fully identified (Köhler et al., 2014).

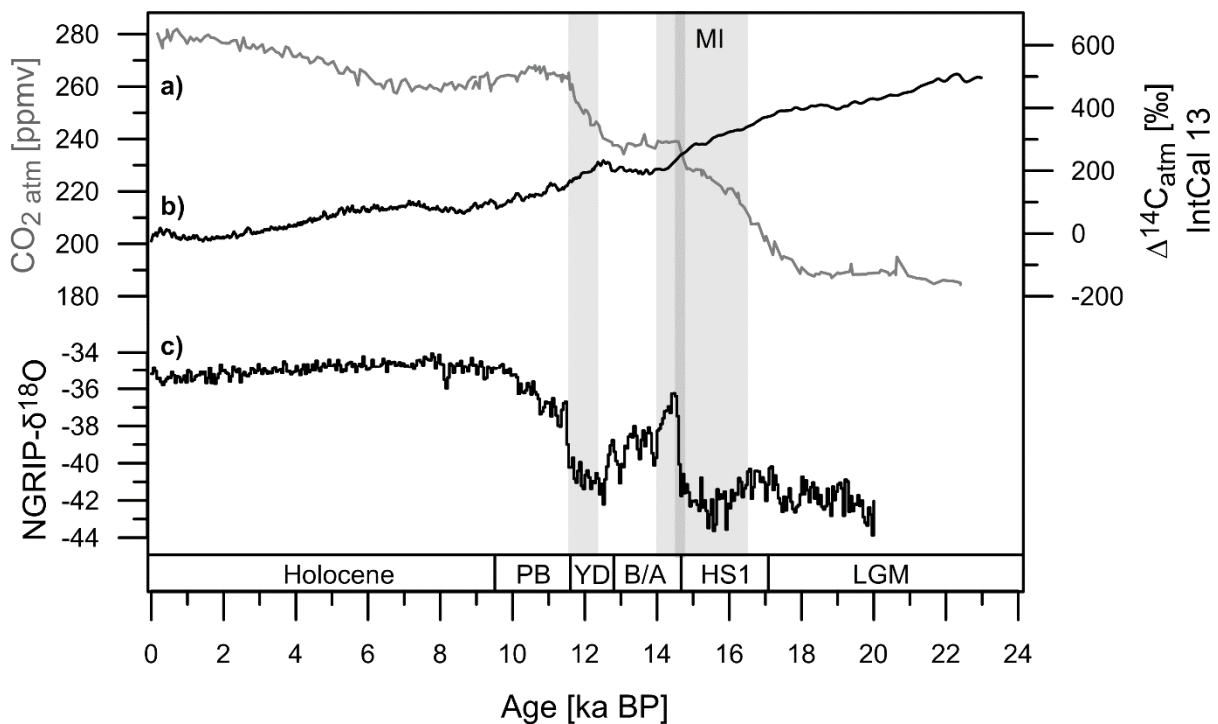


Figure 1.5. a) $\text{CO}_{2\text{atm}}$ from Epica Dome C (compiled from Monnin et al., 2001 and Parrenin et al., 2013). b) IntCal 13 from Reimer et al. (2013). c) Oxygen isotope record from Greenland ice cores (NGRIP, 2004). Grey bars mark the intervals of rising $\text{CO}_{2\text{atm}}$ and decreasing $\Delta^{14}\text{C}_{\text{atm}}$. MI: Mystery Interval.

Diverting OM from biogeochemical cycling over long periods of time permafrost represents a source of old organic matter OM. In this light, emissions of ^{14}C -depleted CO_2 during the deglacial permafrost retreat are suggested to have partly fuelled the deglacial changes in $\text{CO}_{2\text{atm}}$ and $\Delta^{14}\text{C}_{\text{atm}}$ (e.g. Ciais et al., 2013; Köhler et al., 2013, 2014). However, the potential impact of permafrost carbon on $\text{CO}_{2\text{atm}}$ and $\Delta^{14}\text{C}_{\text{atm}}$ is poorly understood since the age of carbon stored in permafrost during the LGM is unknown and the timing of carbon release as well as the portion that entered the atmosphere are current factors of uncertainty.

Various palaeoclimate records and models suggest that the deglacial climate and temperature development was strongly controlled by oscillations in the AMOC (e.g. Manabe and Stouffer, 1988; Contreras-Rosales, 2014; Hong et al., 2008; Wang et al., 2008; Sanchi et al., 2014). Alternating phases of weakening and strengthening of the AMOC lead to abrupt temperature oscillations in the North Atlantic realm (Figure 1.5.) with cold-spells during the Heinrich Stadial 1 (17.5-14.6 ka BP) and the Younger Dryas (12.9-11.7 ka BP) and abrupt warming during the Bølling/Allerød-interstadial (14.6-12.9 ka BP) and the early Holocene (11.7 ka BP; e.g. NGRIP, 2004). It is suggested that this climatic pattern spread widely throughout the NH due to atmospheric or oceanic teleconnections (e.g. Manabe and Stouffer, 1988; Wang et al., 2008). As such it is likely that permafrost dynamics and the associated mobilization of old OM were linked to this temperature pattern. Indeed, environmental indicators of permafrost thaw, such as stalagmite growth and thaw-lake expansion, point to permafrost thaw during the B/A and the early Holocene whereas stabilizing Eurasian permafrost conditions were reported for the YD (e.g. Sailer and Kernschner et al., 2000; Renssen and Vandenberghe, 2003; Gruber and Reitner, 2007; Fischer et al., 2008; Rostek and Bard, 2013). Therefore, permafrost appears likely to have fuelled the abrupt atmospheric changes at the onset of the B/A, a hypothesis which is corroborated by carbon cycle models (Köhler et al., 2014). However, it seems unlikely as source for $\text{CO}_{2\text{atm}}$ and $\Delta^{14}\text{C}_{\text{atm}}$ during the HS1 and YD cold-spells. As for the onset of the B/A it was further hypothesized that coastal permafrost erosion caused by rapid shelf-flooding during Meltwater Pulse 1a (MWP-1a) may have additionally triggered degradation of OM formerly stored in permafrost. However, constraints on the timing of mobilization of ^{14}C -depleted carbon during permafrost retreat are very sparse as most environmental indicators (e.g. stalagmite growth, or thaw-lake expansion) for deglacial permafrost dynamics (Walter et al., 2007; Lozhkin et al., 2011; Vaks et al., 2013) do neither provide insights into carbon mobilization nor the radiocarbon signature of the mobilized OM. Rostek and Bard (2013) analyzed the abundance of terrigenous biomarkers in Black-Sea sediments as a means to trace OM-mobilization during Eurasian permafrost-retreat. However,

radiocarbon data providing evidence that the mobilized OM was ^{14}C -depleted was not provided. Recently, mass accumulation rates together with the $\Delta^{14}\text{C}$ -signature of terrigenous biomarkers provided evidence for increased deglacial export of ^{14}C -depleted OM from the Amur River catchment into the Sea of Okhotsk and this was suggested to attest to deglacial permafrost dynamics in East Asia (Winterfeld, 2014; Dummann; 2015). This generally corroborates the idea of permafrost as potential source of ^{14}C -depleted CO_2 . Given the scarce information on the time-scales of carbon mobilization the application of the approach used for the Amur-River catchment is necessary elsewhere in the NH in order to identify regional differences and to ultimately better comprehend the role permafrost may have played in $\text{CO}_{2\text{atm}}$ and $\Delta^{14}\text{C}_{\text{atm}}$.

Beringia is one of those regions. It is defined as the area between NE Russia and the Yukon Territories in Canada (Figure. 1.6, Hopkins et al., 1982). Nowadays, NE Russia is separated from Alaska by the Bering Strait, a shallow seaway connecting the Bering Sea with the Arctic Ocean (Figure 1.6). In the course of Pleistocene sea-level variation (e.g. Manley, 2002) large parts of the Bering and Chukchi Shelves became exposed and connected northeast Russia and Alaska via the “Bering Land Bridge” (BLB)(Figure 1.6). In contrast to North America and Western Europe, where large continental ice caps persisted north of 50-60°N (Figure 1.4 & 1.6), Beringia remained widely unglaciated and glaciers were restricted to the mountain ranges (e.g. Gualtieri et al., 2000; Brigham-Grette et al., 2003; Gualter et al., 2003; Stauch and Gualtieri, 2008; Barr and Solomina, 2014). Those conditions made Beringia a glacial refuge for Arctic flora and fauna (e.g. Guthrie, 2001) and ultimately allowed permafrost to accumulate large amounts of organic carbon. Beringia is supposed to have been completely covered by continuous permafrost during the LGM (Vandenberghe et al., 2014). During the deglacial climate amelioration continuous permafrost in Alaska likely turned into discontinuous permafrost in Alaska. On Kamchatka, (a Peninsula attached to Siberia separating the Sea of Okhotsk from the NW Pacific, Figure 1.6) is assumed to have become almost permafrost-free (Vandenberghe et al., 2014). Under present-day conditions continuous permafrost still covers large areas in Siberia. Thermokarst processes have been described for the deglaciation (e.g. Walter et al., 2007) in Siberia and those probably attest to permafrost dynamics. Furthermore, the Beringian shelf areas were presumably covered by permafrost (Vandenberghe et al., 2014) and may have undergone erosion during sea-level rise. So it appears possible that permafrost-destabilization mobilized ^{14}C -depleted OM and potentially contributed to rising $\text{CO}_{2\text{atm}}$ and declining $\Delta^{14}\text{C}_{\text{atm}}$.

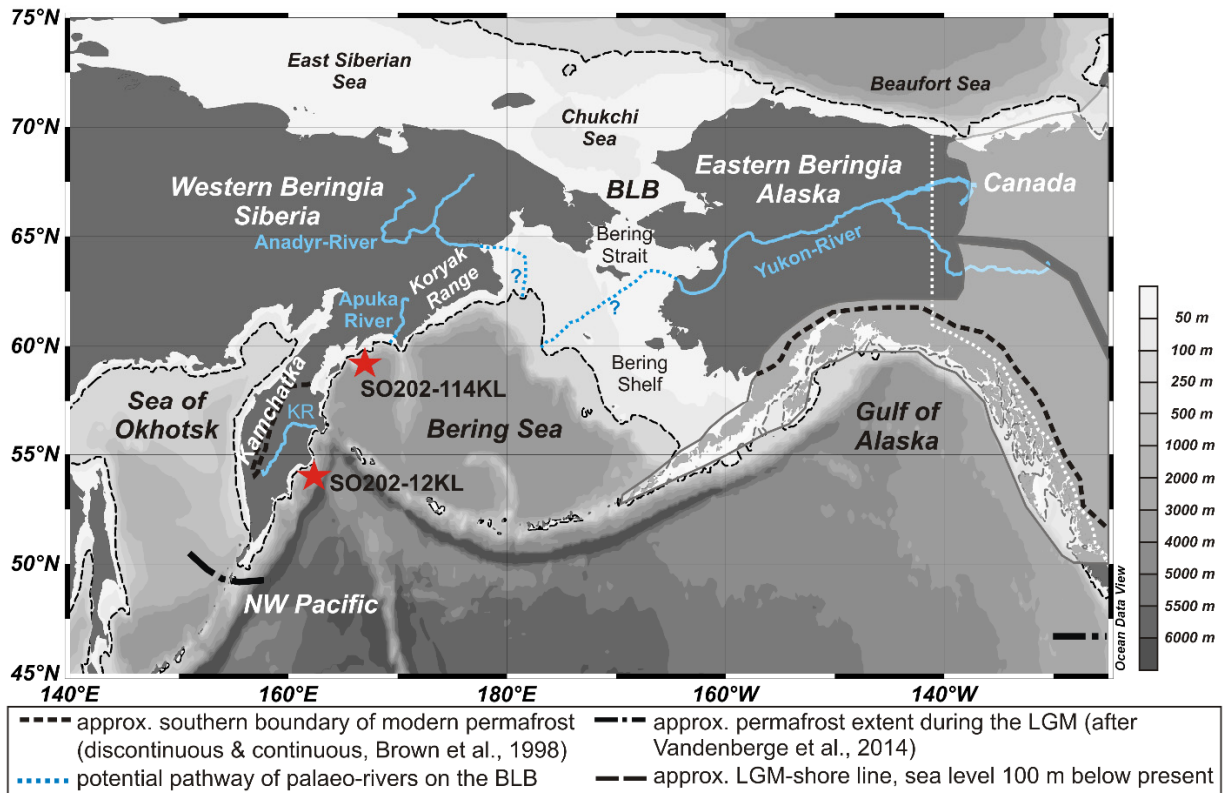


Figure 1.6. The subarctic North Pacific Ocean and Beringia. KR: Kamchatka River. White shaded areas mark the position of continental ice sheets. Red stars: study sites from this thesis.

In order to contribute to a better understanding of the region's potential to have fuelled $\text{CO}_{2\text{atm}}$ and $\Delta^{14}\text{C}_{\text{atm}}$ changes, this thesis aims at identifying the time-scales (onset and duration) of mobilization-events of ^{14}C -depleted OM during deglacial permafrost decomposition in Kamchatka and the Koryak area (NE Siberia, Figure 1.6).

However, gaps of knowledge exist upon the temperature development in the NW-Pacific realm between the LGM and the Holocene. In terms of deglacial temperature evolution, western Beringia (Siberia), the subarctic NW Pacific and its marginal seas (the Sea of Okhotsk and the Bering Sea, Figure 1.6) are one of the least studied areas across the NH since climate records spanning the entire LGM-Holocene transition are very sparse. Furthermore, many terrestrial records have poor chronologies (e.g. Kokorowski et al., 2008a,b). Kamchatka is one of the least studied areas of Beringia as terrestrial climate archives, such as peat sections or lake sediments, do not reach beyond 12 ka BP (e.g. Dirksen et al., 2013, 2015; Nazarova et al., 2013a; Hoff et al. 2015; Klimaschewski et al., 2015; Self et al., 2015; Solovieva et al., 2015). In the marine realm, HS1 and the LGM are underconstrained as far as the sea surface temperature (SST) evolution is concerned. This is because most existing records from the subarctic N Pacific and its marginal seas (the Bering Sea and the Sea of Okhotsk) are based on alkenone palaeothermometry ($U^{\text{K}^{37}}$) and alkenones are often

extremely low or even below detection limit in sediments corresponding to HS1 and the LGM (Ternois et al., 2000; Barron et al., 2003; Caissie et al., 2010; Seki et al., 2004a; Max et al., 2012). If alkenones are present (Sea of Okhotsk), adopted temperatures for the last glacial period and early deglaciation appear to be too warm (e.g. Seki et al., 2004b, 2007). It is assumed that these records are seasonally biased due to shifting blooming seasons of the coccolithophorids during the deglaciation. (Harada et al., 2003; Seki et al., 2004b, 2007). Temperature-inferences for the NW-Pacific realm adopted from foraminiferas do provide records for the full glacial/Holocene transition but those are often considered to reflect sub-surface (approx. 50-100 water depth) rather than sea surface (0-50 m) conditions (e.g. Gebhardt et al., 2008; Max et al., 2012; Riethdorf et al., 2013). Given the gaps in the temperature records, there is a lack in consensus regarding climate change since the LGM and the controlling mechanisms in the region. Uncertainties exist upon the LGM-to-Holocene development of regional climate drivers such as oceanic and atmospheric circulation, upon the nature of teleconnections with AMOC-variability, or upon the response to insolation or atmospheric CO₂-levels. Inconsistencies exist across climate model outputs for the LGM climatic conditions as well as for deglacial climate change. For the LGM some suggest that LGM SST were warmer than at present (Otto-Bliesner et al., 2006; Alder and Hostetler, 2015) while others predict a cooling relative to pre-industrial conditions (e.g. Yanase and Abe-Ouchi, 2007). As for the deglaciation it has been proposed that N-Pacific SST evolution was linked to North Atlantic climate oscillations. However, proxy-based SST reconstructions as well as general circulation models provide to an inconsistent picture regarding nature of the N Pacific response to AMOC-oscillations. Some climate models found an out-of-phase behavior with cooling in the N Atlantic and a concurrent warming in the N Pacific during stadials (Sarnthein et al., 2004, 2006; Gebhardt et al., 2008). General Circulation Models (GCMs) suggest that the weakening of the AMOC would result in the establishment of a Pacific Meridional Overturning Circulation (PMOC) and hence intensified poleward heat transport into the N Pacific (Schmittner et al., 2003; Saenko et al., 2004; Okazaki et al., 2010; Menviel et al., 2012). By contrast, GCMs also proposed that Atlantic and Pacific SST varied in-phase, a pattern which was attributed to rapid atmospheric teleconnections between both ocean basins (Mikolajewicz et al., 1997; Vellinga and Wood, 2002; Okumura et al., 2009; Chikamoto et al., 2012). Both scenarios are corroborated by SST, sub-surface temperature and salinity reconstructions (Barron et al., 2003; Gebhardt et al., 2008; Kiefer and Kienast, 2005; Max et al., 2012; Kuehn et al., 2014; Praetorius and Mix, 2014). Also, terrestrial archives generate an ambiguous picture as far as the sensitivity of Beringia to deglacial N Atlantic

climate change is concerned. Existing climate reconstructions from Siberia, the former BLB and Alaska reveal a rather inconsistent picture. Some studies found evidence for a late glacial warming during the B/A followed by a cold reversal corresponding to the YD while others do not show any climatic reversals during the deglacial climate amelioration (e.g. Lozhkin et al., 1993, 2007; Pisaric et al., 2001; Lozhkin and Anderson, 2006; Kokorowski et al., 2008a,b; Meyer et al., 2010; Fritz et al., 2012). The discrepancies among Beringian records may relate to regional differences in the sensitivity to N-Atlantic climate variability but also to poor chronologies or to sampling resolutions which are too coarse to monitor short-term oscillations (e.g. Kokorowski et al., 2008a, b).

The sparseness of continuous LGM-to-Holocene temperature records and the inconsistencies among climate inferences require additional records in SST and mean air temperature (MAT) which span the full LGM/Holocene transition in order to continue building up a better understanding of regional climate dynamics in the NW Pacific and NE Siberia. This is also the basis for comprehending the permafrost dynamics and carbon mobilization in the Kamchatka-region. So, the second aim of this thesis is to contribute to an improved picture of LGM climatic conditions and deglacial climate change in the NW Pacific realm and adjacent NE Siberia by establishing continuous LGM-to-Holocene SST records for the Western Bering Sea, the marginal NW Pacific and MAT-records for the Kamchatka Peninsula. The TEX^{L}_{86} and CBT/MBT-paleothermometries shall be applied in marine sediment cores from the continental margin off Kamchatka (sites SO201-2-12KL and SO201-2-114KL; Figure 1.6). The climatic history of the Kamchatka-area may provide important insights into the LGM and deglacial patterns of regional atmospheric and oceanic circulation and the impact of supra-regional climate drivers. Furthermore, a better understanding of the temperature during the LGM and the deglaciation, offers the possibility to investigate the role of temperature in restricted ice-sheet extent in Northeast Siberia. In contrast to North America and western Eurasia, Beringia remained widely unglaciated as glaciers were restricted to the mountain ranges (e.g. Brigham-Grette et al., 2003; Barr and Solomina, 2014). The prevailing hypothesis seeking to explain the limited ice-extent is that the region was too arid (e.g. Brigham-Grette et al., 2003; Barr and Clark, 2011). However, glacier growth is ultimately a function of snow accumulation and temperature. Considering that some Siberian records provide evidence for relatively warm summers during the LGM with conditions similar to modern (e.g. Berman et al., 2011). Temperature may have played an important role in restricted glaciation, next to arid conditions. On Kamchatka detailed reconstruction about palaeo-glaciation has been provided by Barr and Clark (2011) and includes the reconstruction of equilibrium line

altitudes (ELA). Those can be used to investigate a glacier's response to temperature or precipitation (e.g. Barr and Clark, 2011) as data on glacier extent combined with LGM air temperature would allow mass-balance calculations for the LGM-glaciers and would provide estimates about LGM precipitation (Braithwaite et al., 2006; Barr and Clark, 2011). Since, climate records from Kamchatka do not reach beyond 12 ka BP information about temperature and precipitation is not available so far. As such a quantitative air temperature record for Kamchatka represents a first puzzle piece to unravel how temperature and precipitation controlled ice-sheet growth in the Kamchatka-region. Estimates of glacial precipitation may also complement the temperature records with respect to inferences regarding atmospheric and oceanic circulation. All together this may provide important information to validate existing climate model outputs and a step towards comprehending the controls on the regional climate during the LGM.

Constraints on the deglacial SST development and on the deglacial MAT-development of Kamchatka may complement the existing knowledge about the connectivity of the NW Pacific, the Western Bering Sea and Siberia to N Atlantic climate change. Existing SST records from sites 12KL and 114KL provide evidence for the presence of the B/A warm phase and the YD cold-spell which attests to atmospheric teleconnections between the NW Pacific realm and the N Atlantic (Max et al., 2012). However, these records are established on alkenone paleothermometry and do not provide insights into HS1. The presence of the B/A-interstadial and the YD cold spell may suggest that HS1 would have been characterized by a cold-spell, similar to the N-Atlantic realm. However, in the open NW Pacific warm-spells have been identified which corroborate the idea of intensified oceanic heat transport (Gebhardt et al., 2008). Inferences for the AMOC-impact on Kamchatka are important for understanding temperature controls on permafrost dynamics in the region and to test the hypothesis that HS1 and the YD were intervals of stabilizing permafrost conditions. Warm-spells during HS1 may have already caused permafrost degradation and carbon mobilization prior to the B/A, so the region may have provided CO₂ to the atmosphere during the MI.

In summary, the thesis aims at improving the comprehension of LGM-climatic conditions (temperature and precipitation) and deglacial temperature change in the NW Pacific realm. It further aims at providing into the potential role of the region's permafrost carbon-pool in deglacial CO_{2atm} and $\Delta^{14}C_{atm}$ changes. In order to achieve these major aims marine and terrigenous biomarkers are analyzed in sediment cores SO201-2-12KL and SO201-2-114KL. Based upon the TEX₈₆ temperature proxy the SST development of the Western Bering Sea

and the NW Pacific between the LGM and the Holocene shall be reconstructed (**Objective 1**). The focus is the SST evolution during the LGM and HS1.

Objective 2 comprises the reconstruction of the evolution of mean air temperature on Kamchatka, using the CBT/MBT-temperature proxy. Objectives 1 and 2 shall provide insights into the impact of regional climate oceanic and atmospheric circulation and into the impact of AMOC-variability. Investigating the deglacial temperature variability on Kamchatka shall generate the basis to comprehend permafrost dynamics and carbon mobilization in the region. On the basis of the adopted temperature data for the LGM, the interplay of temperature and precipitation for restricted glacier extent on Kamchatka shall be investigated in a degree-day-model (mass balance calculations, **Objective 3**).

In order to trace permafrost decomposition in Kamchatka and the Koryak area, and to assess the time-scales of the associated carbon mobilization, the deglacial development of the export of terrigenous OM into the adjacent NW Pacific and the Western Bering Sea shall be reconstructed (**Objective 4**). Mass-accumulation rates and compound-specific radiocarbon analysis of leaf-wax lipids in cores SO201-2-12KL and SO202-2-114KL are supposed to identify periods of enhanced mobilization of ¹⁴C-depleted OM and to constrain the timing of carbon release during permafrost decomposition in the region.

1.5. Outline of the thesis

The three objectives are addressed in four manuscripts (chapters 2-5) which are either in the process or in preparation for publishing in peer-reviewed journals. The first part of the thesis (chapters 2 & 3) deal with the reconstruction of the SST and MAT development, tackling objectives 1 and 2. In the second part (chapters 4 & 5) the implications of temperature for the cryosphere (glaciation and permafrost) are addressed (objectives 3 & 4). Chapter 6 summarizes the main findings and the perspectives of this thesis.

2. Manuscript I:

Glacial-to-Holocene evolution of sea surface temperature and surface circulation in the subarctic Northwest Pacific and the Western Bering Sea

Vera D. Meyer^{1,2}, Lars Max¹, Jens Hefter¹, Ralf Tiedemann¹ and Gesine Mollenhauer¹

¹ Alfred Wegener Institute Helmholtz Centre for Polar and Marine Research, Am Alten Hafen 26, D-27568, Bremerhaven, Germany

² Department of Geosciences, University of Bremen, Klagenfurter Strasse, D-28359 Bremen, Germany

Revised version after first review. To be re-submitted to Palaeoceanography

Abstract

It has been proposed that North Pacific sea surface temperature (SST) evolution was intimately linked to North Atlantic climate oscillations during the last deglaciation. However, during the early deglaciation and the Last Glacial Maximum (LGM), the SST development in the subarctic Northwest Pacific and the Bering Sea is poorly constrained. Most existing deglacial SST records are based on alkenone palaeothermometry which is limited prior to 15 ka BP in the subarctic North Pacific realm. By applying the TEX^L₈₆ temperature proxy we obtain Glacial-Holocene-SST records for the marginal Northwest Pacific and the Western Bering Sea. We find that during the past 15 ka SSTs in the northwest Pacific and the Western Bering Sea closely follow millennial-scale climate fluctuations known from Greenland ice cores. This agrees with previous studies suggesting rapid atmospheric teleconnections with abrupt climate changes in the North Atlantic. Our SST reconstructions indicate that in the Western Bering Sea SSTs drops significantly during Heinrich Stadial 1 (HS1), similar to the known North Atlantic climate history. In contrast, progressively rising SST in the Northwest Pacific is significantly different to the North Atlantic climate development during HS1. Similarities between the Northwest Pacific SST and climate records from the Gulf of Alaska rather point to a stronger influence of Alaskan Stream waters connecting the eastern and western basin of the North Pacific during this time. During the Holocene, dissimilar trends in the climate point to reduced influence of the Alaskan Stream in the Northwest Pacific.

2.1. Introduction

During the last deglaciation, the North Pacific (N Pacific) and its marginal seas experienced millennial scale climate oscillations, which are proposed to be linked to variations in the strength of the Atlantic Meridional Overturning Circulation (AMOC) (e.g. Seki et al., 2002; Sagawa and Ikehara, 2004; Kiefer and Kienast, 2005; Gebhardt et al., 2008; Harada et al., 2012; Max et al., 2012). From the N Atlantic it has been proposed that AMOC weakened twice during the last deglaciation (Heinrich Stadial 1 and Younger Dryas stadials) due to vast freshwater supply from melting continental ice-sheets into the N Atlantic, which lead to colder conditions in the N Atlantic realm (e.g. McManus et al., 2004). Proxy-based SST reconstructions as well as general circulation models lead to an inconsistent picture regarding the N Pacific response and the underlying teleconnection mechanisms. Some studies (based on climate models and proxy data) found an out-of-phase behavior with cooling in the N Atlantic and a concurrent warming in the N Pacific during stadials (Sarnthein et al., 2004, 2006; Gebhardt et al., 2008). It has been proposed that the weakening of the AMOC would result in the establishment of a Pacific Meridional Overturning Circulation (PMOC) and hence intensified poleward heat transport in the N Pacific (Schmittner et al., 2003; Saenko et al., 2004; Okazaki et al., 2010; Menviel et al., 2012). By contrast General Circulation Models (GCMs) and the majority of proxy-based studies identified a similar pattern of N Pacific – N Atlantic climate evolution which was attributed to rapid atmospheric teleconnections connecting both ocean basins (Mikolajewicz et al., 1997; Kienast and McKay, 2001, Piasias et al., 2001; Vellinga and Wood, 2002; Barron et al., 2003; Okumura et al., 2009; Timmermann et al., 2010; Chikamoto et al., 2012; Harada et al., 2012; Max et al., 2012; Kuehn et al., 2014; Praetorius and Mix, 2014). Most proxy-based studies do not allow insights into the Heinrich Stadial 1 (HS1) and the LGM because for this time-interval alkenone palaeothermometry is afflicted by several limitations. So the SST development and its potential linkage to AMOC variations during during the early deglaciation remains underconstrained.

Specifically, alkenone concentrations are often extremely low or even below detection limit in sediments older than ca. 15 ka (Ternois et al., 2000; Barron et al., 2003; Caissie et al., 2010; Seki et al., 2004a; Max et al., 2012), which prevents the application of U^{k}_{37} during HS1 and LGM. The growth of coccolithophorids, the alkenone producers, may have been impeded by low temperatures during glacial times. Besides, in records where alkenones are present (Sea of Okhotsk), adopted temperatures for the last glacial period and early deglaciation appear to be too warm pointing to a seasonal bias (e.g. Seki et al., 2004b). It has been assumed that

longer lasting sea-ice seasons likely forced phytoplankton to bloom in late summer during glacial times, while under modern conditions phytoplankton blooms occur during early spring/autumn (Takahashi et al., 2002; Harada et al., 2003; Seki et al., 2004b, 2007).

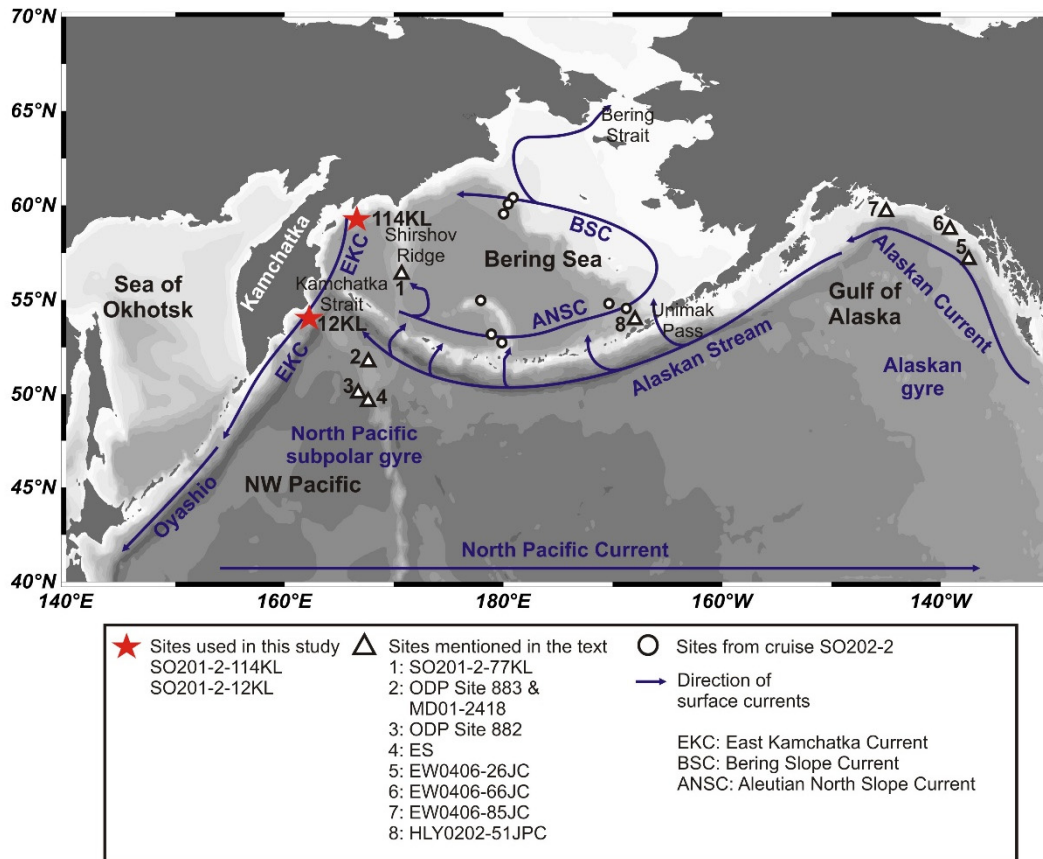


Figure 2.1. Map of the study area showing sites of the sediment cores used in this study together with core sites from other studies mentioned in the text. Additionally, the general surface circulation pattern of the N Pacific and the Bering Sea is sketched.

The TEX₈₆ (Tetra Ether indeX) has been introduced as SST proxy by Schouten et al. (2002) and quantifies the relative abundance of isoprenoid glycerol dialcyl glycerol tetraethers (isoGDGTs) consisting of 86 C-atoms with different numbers of cyclopentyl moieties. These lipids are synthesized by marine Thaumarchaeota (Archaea), planktonic ammonia oxidizing chemoautotrophes (Könneke et al., 2005; Martens-Habbena et al., 2009; Walker et al., 2010). In the subarctic gyre, the highest abundances of Thaumarchaeota have been observed in winter and summer (e.g. Karner et al., 2001; Yamamoto et al., 2012) but the strongest productivity of marine Thaumarchaeota in the N Pacific and the Sea of Okhotsk seems to be associated with the summer season (Seki et al., 2009; 2014). Having different ecological preferences than alkenone producers (phytoplankton) the Thaumarchaeota may not be affected by environmental stress factors which limit the alkenone producing algae, rendering the TEX₈₆ index potentially useful in settings where alkenone palaeothermometry is

problematic. Applying the TEX₈₆ temperature proxy to two sediment cores used in the study of Max et al. (2012) we were able to produce full glacial to Holocene records in SST for the Western Bering Sea and the marginal NW Pacific. Our SST data provides new insights into the nature of teleconnections between the N Pacific and N Atlantic during the early deglaciation. Our findings also reveal changes in the relative intensity of surface circulation patterns of the Bering Sea and the marginal NW Pacific and their impact on the N Pacific climate development.

2.2. Regional Setting

The surface circulation in the North Pacific and the Bering Sea is cyclonic (Figure 2.1). At 40°N the North Pacific Current, the extension of the subtropical Kuroshio Current, flows eastward carrying warm and saline surface waters into the Alaskan Gyre/Northeast Pacific (NE Pacific). The Alaskan Stream (AS) forms a northern boundary current flowing along the Aleutian Arc into the Western Sub-polar Gyre. Through several passages of the Aleutian Islands surface waters from the AS enter the Bering Sea where they form the Aleutian North Slope Current (ANSC), a surface current flowing eastwards along the Aleutian Arc. The ANSC acts as the southern boundary current of the counterclockwise circulation of the Bering Sea. In the north, the Bering Slope Current transports the water masses along the coastlines of Alaska and Siberia. The Bering Sea waters leave the Bering Sea via the Bering Strait into the Arctic Ocean. The main outflow, however, is through the Kamchatka Strait where surface waters enter the NW Pacific via the East Kamchatka Current (EKC). The EKC flows along the eastern coast of the Kamchatka Peninsula and forms the western boundary current of the Western Sub-polar Gyre (e.g. Stabeno and Reed, 1994).

The N Pacific and its marginal seas are characterized by strong seasonal contrasts in SST (winter: 0-3°C; summer 8-12°C; (Locarnini et al., 2010) and upper-water column stratification. The seasonal contrasts are linked to seasonal changes of the major atmospheric circulation over the N Pacific. During winter, the Aleutian Low develops over the N Pacific and brings cold air masses from the Arctic to the subarctic N Pacific. The cold air induces cooling of surface waters and sea ice formation in the Bering Sea (Ohtani et al., 1972; Niebauer et al., 1999). Brine rejection as well as wind stress cause vertical mixing of surface and subsurface waters. During summer the Aleutian Low weakens and the North Pacific High establishes over the N Pacific. This brings warm southerly winds to the subarctic N Pacific and the Bering Sea. Together with increasing insolation this causes sea-ice melt and warming

of surface waters. As a consequence a distinct upper-ocean stratification with pronounced seasonal pycnocline and thermocline develops (Ohtani et al., 1972).

2.3. Material and Methods

2.3.1. Core material and age control

For this study we used two piston cores from the Western Bering Sea (SO201-2-114KL) and the NW Pacific (SO201-2-12KL) recovered at the continental margin off Kamchatka Peninsula (Figure 2.1) during KALMAR Leg 2 cruise of R/V SONNE SO201 in 2009 (Dullo et al., 2009). Prior to sample preparation, cores were stored at 4°C. Integrated age models were developed by accelerator mass spectrometry (AMS) radiocarbon dating of planktonic foraminifera (*Neogloboquadrina pachyderma* sinistral) as well as by core-to-core correlations of high-resolution spectrophotometric (color b*) and X-ray fluorescence data. For a detailed description and AMS-¹⁴C results see Max et al. (2012). For this study, cores were sampled in 10 cm (12KL) and 5 cm (114KL) steps providing a temporal resolution of ca. 250-500 years. The cores have a total recovery of 11.78 m (12KL) and 7.89 m (114KL) representing the periods of 1-20 ka BP and 8.8-29 ka BP.

2.3.2. Lipid extraction

The sediment samples (5 g) were freeze-dried and homogenized. 10 µg of C₄₆-GDGT were added as internal standard. Samples were extracted with an accelerated solvent extractor (Dionex ASE 200) using 22 ml cells and dichloromethane (DCM):methanol (MeOH) 9:1 (v/v) as solvent at 100°C and 1000 psi with three cycles of 5 minutes each. The total lipid extracts were dried with a rotary evaporator. Afterwards they were hydrolyzed with 0.1 N potassium hydroxide (KOH) in MeOH:H₂O 9:1 (v/v). Neutral compounds (including GDGTs) were extracted with *n*-hexane. Compound classes were separated with column chromatography, using deactivated SiO₂. An apolar fraction was eluted using *n*-hexane. Polar compound-classes, including the GDGTs, were eluted with MeOH:DCM 1:1 (v/v). Dissolved in hexane:isopropanol 99:1 (v/v) the polar-fraction was filtered with a PTFE filter (0.45 µm pore size) according to Hopmans et al. (2004). Samples were brought to a concentration of 2 µg/µl prior to GDGT analysis.

2.3.3. GDGT analysis and SST determination

GDGTs were analyzed by high performance liquid chromatography (HPLC) coupled via an atmospheric pressure chemical ionization (APCI) interface to a single quadrupole mass selective detector (MSD), with a method slightly modified from Hopmans et al. (2000). Analyses were performed on an Agilent 1200 series HPLC system and an Agilent 6120 MSD. Separation of the individual GDGTs was achieved on a Prevail Cyano column (Grace, 3 μ m, 150 mm x 2.1 mm) maintained at 30°C. After sample injection (20 μ L) and 5 min isocratic elution with solvent A (hexane) and B (hexane with 5 % isopropanol) at a mixing ratio of 80:20, the proportion of B was increased linearly to 36 % within 40 min. The eluent flow was 0.2 ml/min. Prior to analysis of the next sample, the column was cleaned by back-flushing with 100% solvent B (8 min) and re-equilibrated with solvent A (12 min, flow 0.4 ml/min). GDGTs were detected using positive-ion APCI-MS and selective ion monitoring (SIM) of their (M+H)⁺ ions (Schouten et al., 2007) with APCI spray-chamber conditions as follows: nebulizer pressure 50 psi, vaporizer temperature 350°C, N₂ drying gas flow 5 l/min and 350°C, capillary voltage (ion transfer tube) -4 kV and corona current +5 μ A. The MS-detector was set for SIM of the following (M+H)⁺ ions: *m/z* 1302.3 (GDGT 0), 1300.3 (GDGT 1), 1298.3 (GDGT 2), 1296.3 (GDGT 3), 1292.3 (GDGT 4 + 4' / crenarcheol + regio-isomer), 1050 (GDGT III), 1036 (GDGT II), 1022 (GDGT I) and 744 (C₄₆ standard), with a dwell time of 67 ms per ion.

Peak areas from the individual GDGTs were obtained by integration. Compounds were quantified by using the respective peak areas and the response factor of the C₄₆ standard. The results were normalized to the amount of extracted sediment and total organic carbon (TOC) content. We applied the TEX^L₈₆ -index, which has been suggested for temperature ranges below 15°C by Kim et al. (2010). In order to convert TEX^L₈₆ into temperatures we applied the regional calibration for the Sea of Okhotsk and the NW Pacific by Seki et al. (2014).

The reported standard error for the regional calibration is $\pm 1.7^\circ\text{C}$. The standard deviation for TEX^L₈₆ was calculated from repeated measurements and was $< 0.0,1$ corresponding to a maximal uncertainty of $\pm 0.37^\circ\text{C}$ in the reconstructed temperatures.

This regional calibration has been suggested since in the Sea of Okhotsk and the N Pacific the global core-top calibrations by Kim et al. (2010, 2012) often overestimate mean annual SST and tend to produce excessively cold temperatures for the Glacial (Seki et al., 2014). This was explained by region-specific ecologic characteristics of the Thaumarchaeota such as seasonality and export production depth which may bias the TEX^L₈₆ (Seki et al., 2014).

According to the study of Seki et al. (2014) $\text{TEX}^{\text{L}}_{86}$ would reflect mean August temperatures in 20 m water depth (Figure 2.2).

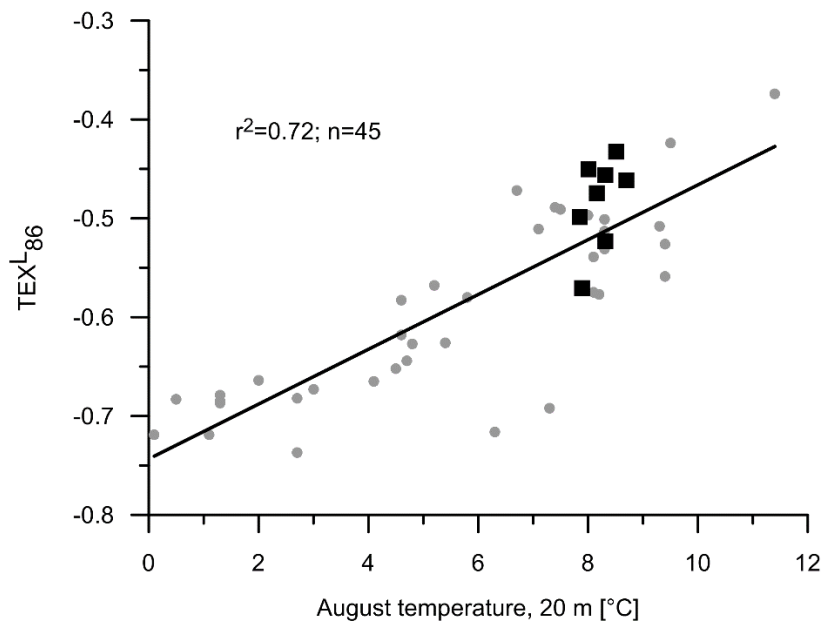


Figure 2.2. Core-top data from the Bering Sea (black squares, sites from cruise SO202-2, Ho et al., (2014) plotted together with the dataset used for the regional calibration for the Sea of Okhotsk and the N Pacific from Seki et al. (2014) (grey dots). Corresponding mean August temperatures at 20 m water depth for the sites in the Bering Sea were taken from WOA09 (Locarnini et al., 2010).

As the dataset from Seki et al. (2014) does not include data from the Bering Sea, we tested whether the proposed regional calibration would be applicable there by combining core-top data from the central Bering Sea (from Ho et al. (2014) and the dataset from (2014)). The data from the Bering Sea are based on sites from cruise SO202-2 with RV SONNE (Ho et al. (2014), Figure 2.1). Since data from the Bering Sea were within the range of values from the Sea of Okhotsk/N Pacific we concluded that the regional calibration is valid for the Bering Sea (Figure 2.2). Seki et al. (2014) argued that a highly stratified water column in summer restricted the summer warmth to 20 m and 40 m in the Sea of Okhotsk and the NW Pacific and that ammonium concentrations peaked in that depth interval at the same time. As Thaumarchaeota are ammonia oxidizing chemoautotrophs (Könneke et al., 2005; Martens-Habbena et al., 2009; Walker et al., 2010) they probably accumulate in that depth range during the summer months (Seki et al., 2014 and references therein). CTD-profiles from the Western Bering Sea show that the development of the water column is similar to the NW Pacific/Sea of Okhotsk with respect to the depth of summer stratification (Dullo et al., 2009; Riethdorf et al., 2013). Therefore, it is reasonable to assume that ammonium which is produced during the decay of organic matter after the first phytoplankton blooms in spring

would accumulate in the mixed layer of the Bering Sea during the summer months. This might be accompanied by enhanced productivity of the Thaumarchaeota.

As Weijers et al. (2006) pointed out that terrigenous GDGTs can bias the temperature signal of TEX₈₆ when terrigenous organic matter input is high, we determined the relative contribution of marine and terrigenous GDGTs in our samples using the BIT-index after Hopmans et al. (2004). The index is based on a ratio of terrigenous GDGTs (GDGT I-III) and the marine Crenarchaeol (GDGT 4). Repeated measurements resulted in a standard deviation of 0.01 which corresponds to an analytical error of ± 0.004 BIT units.

2.4. Results

2.4.1. BIT-values and applicability of TEX^L₈₆-based SST reconstructions

BIT values and TEX^L₈₆-derived SST (SST_{TEXL86}) are shown together with alkenone-based SST (SST_{UK37}) from Max et al. (2012) in Figure 2.3. Ranging between 0.04-0.22, BIT values are below the critical value of 0.3, defined by Weijers et al. (2006), where SST reconstructions are potentially biased by terrigenous isoGDGTs (Figure 2.3). Hence, at sites 12KL and 114KL marine derived GDGTs dominate over terrigenous GDGTs. Under these circumstances we are confident that TEX^L₈₆ is not biased by terrigenous input. At site 12KL TEX^L₈₆-based SST reconstructions for the core-top (1000 ka BP, 9.5°C) match modern summer SST in the Western Subarctic Gyre (ca. 9-11°C; satellite data from WOA09 (Locarnini et al. 2010) confirming that TEX^L₈₆ reflects summer SST. Since site 114KL does not cover the entire Holocene a comparison of late Holocene SST with modern satellite data is not possible. The TEX^L₈₆-derived SST from the early Holocene (10- 9.5°C) gives estimates slightly above modern summer SST (ca. 8°C; WOA09; Locarnini et al., 2010). This offset is likely because the reconstructed temperatures fall in the time-period of the Holocene thermal maximum that occurred between 11 and 8 ka BP in the NW Pacific and Siberia (e.g. Max et al., 2012; Biskaborn et al., 2012 and references therein) and was warmer than at present.

2.4.2. SST development over the past 22 ka

Whereas the previously published U^K₃₇-records span the last 15 ka only (Max et al., 2012), our TEX^L₈₆ records reach further back, (Figure 2.3). During the LGM Bering Sea SST_{TEXL86} range between 5°C and 6°C, while SST_{TEXL86} in the NW Pacific range between 8°C and 8.5°C. During the deglaciation SST_{TEXL86} increase about 4-5°C in the Western Bering Sea but, less in the NW Pacific. At site 12KL SST_{TEXL86} only rise by 3°C. SST_{TEXL86} in the NW Pacific reach their maximum at 8 ka BP and subsequently decrease progressively. While a

temperature offset between the Western Bering Sea and the NW Pacific of ca. 2°C is present during the late glacial /early deglaciation both locations reach similar temperatures during the early Holocene Thermal Maximum (10-11°C; 10 ka BP-8 ka BP; Figure 2.3).

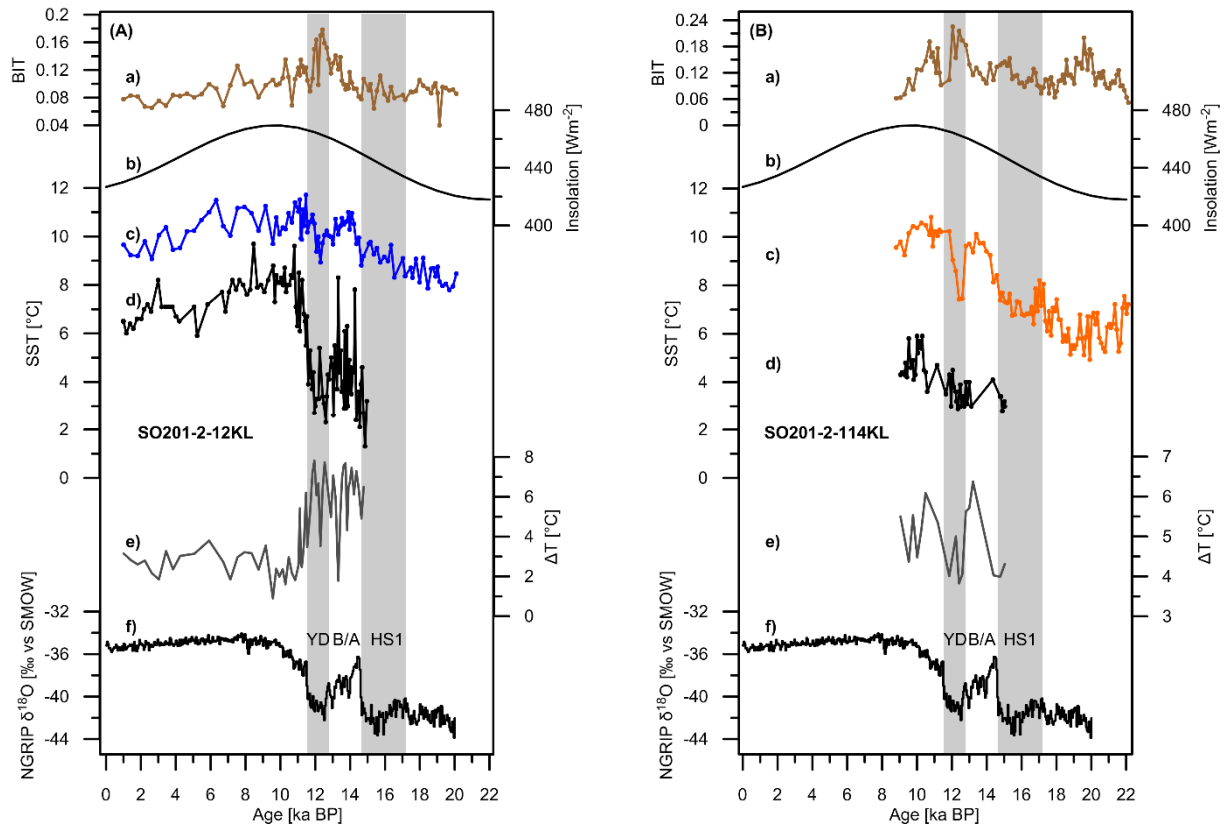


Figure 2.3. Sea surface temperature reconstruction and BIT-indices (a) over the past 22 ka for the NW Pacific (site 12KL, A) and the Western Bering Sea (site 114KL, B). TEX⁸⁶ based SSTs from this study (c) are plotted together with the SST_{UK'37} (d) by Max et al. (2012). The thermal difference between the two proxies is expressed as ΔT_{TEXL86-UK'37} (e). Additionally, mean July insolation at 65°N (b, Berger and Loutre, 1991) is shown. The NGRIP oxygen isotope record from Greenland (f) is shown in order to compare the N Pacific SST development with the climate variability in the N Atlantic. Grey shaded areas mark the YD and the HS1 stadials.

Since ca. 15 ka BP, the SST_{TEXL86} evolution at both sites has been in agreement with the previously published SST_{UK'37} from Max et al., 2012 (Figure 2.3). It is characterized by a sharp temperature increase at the onset of the B/A and a subsequent cooling into the YD cold-spell followed by an abrupt warming into the early Holocene (Figure 2.3). SST_{TEXL86} are generally higher than SST_{UK'37} at both sites (Figure 2.3). The difference (ΔT_{TEX-UK'}) is 6°C during the deglaciation (Figure 2.3). At site 12KL ΔT_{TEX-UK'} is abruptly reduced by about 3-4°C at the Holocene transition. This is mainly driven by a sharp increase in SST_{UK'37}.

Whereas the Bering Sea and the NW Pacific have experienced similar SST developments since the B/A, they are characterized by different patterns prior to 15 ka BP (Figure 2.3). In the Bering Sea the SST_{TEXL86} records an early warming phase during the late glacial (18-17 ka BP) which is followed by a drop in SST during at 17-16 ka BP. Warming rebounds at 15.5 ka

BP and an abrupt increase in temperature occurs at the transition to the B/A-interstadial (14.6 ka BP). In the NW Pacific the late glacial and the early deglaciation SST_{TEXL86} deviates from SST_{TEXL86} at site 114KL (Figure 2.3). At site 12KL SST_{TEXL86} continuously rises between 18 and 14.6 ka BP, without being interrupted by a cold-reversal (Figure 2.3). At 14.6 ka an abrupt temperature increase marks the onset of the B/A-interstadial.

2.5. Discussion

2.5.1. *Seasonal differences between summer and fall SST*

Based on the good correspondence of regional core-top data with summer SST (Seki et al., 2014; Ho et al., 2014, Figure 2), TEX^L₈₆ is regarded to reflect summer SST in the N Pacific and its marginal seas. In contrast, U^K₃₇ is supposed to reflect late summer/fall SST today (Harada et al., 2003; Seki et al., 2007). At site 12KL the Holocene $\Delta T_{\text{TEXL86-UK}^{\text{K}}37}$ (ca. 3°C) is in agreement with the thermal difference between summer and autumn recorded by the satellite data of WOA09 (Locarnini et al., 2010). Accordingly, the increased $\Delta T_{\text{TEXL86-UK}^{\text{K}}37}$ (prior to 12 ka BP) implies that the thermal contrast between summer and autumn was greater than during the Holocene (Figure 2.3). The temperature increase at the YD-Holocene boundary is stronger in the SST_{UK^K37} than in the SST_{TEXL86} which makes the alkenones the main driver of the decrease in $\Delta T_{\text{TEXL86-UK}^{\text{K}}37}$ (Figure 2.3). This suggests that autumn warming may have been more pronounced than summer warming. Prolonged summer seasons during the Holocene may have accounted for this. Several GCMs suggest that the Aleutian Low was stronger during the LGM than during the Holocene (Dong and Valdes, 1998; Shin et al., 2003; Yanase and Abe-Ouchi, 2007, 2010; Alder and Hostetler, 2015) and that a distinct low-pressure anomaly persisted throughout the deglaciation, until ca. 12 ka BP. In association with a stronger Aleutian Low northerly winds would intensify over the NW Pacific and would have enhanced the advection of cold arctic air during fall/winter. As a result, sea-surface cooling between summer and fall was likely more pronounced during the LGM/deglaciation than during the Holocene.

2.5.2. *SST evolution of the NW Pacific and Western Bering Sea over the past 22 ka*

2.5.2.1. *The late deglacial (10-15 ka)*

Our TEX^L₈₆-based SST-records resemble the previously published alkenone data from Max et al. (2012) and show a similar pattern as recorded in NGRIP- $\delta^{18}\text{O}$ (Figure 2.3). Similarity between N Pacific SST and the climate evolution in the N Atlantic realm was also described in the Sea of Okhotsk (e.g. Max et al., 2012), the NE Pacific (e.g. Kienast and McKay, 2001;

Pisias et al., 2001; Barron et al., 2003) and the Bering Sea (Caissie et al., 2010; Max et al., 2012) and interpreted as atmospheric coupling between both oceans. GCMs predicting simultaneous drops/increases in SST in the N Pacific indicate that enhanced westerly winds would have carried cold/warm air masses from the Atlantic to the N Pacific where the sea surface would have cooled/warmed due to heat exchange with the atmosphere (Manabe and Stouffer, 1988; Mikolajewicz et al., 1997; Schiller et al., 1997; Vellinga and Wood, 2002; Chikamoto et al., 2012). A key role has been attributed to the Aleutian Low pressure system since in model simulations the intensity and the position of the Aleutian Low was extremely sensitive to SST anomalies in the N Atlantic (e.g. Mikolajewicz et al., 1997, Okumura et al., 2009). In those models the Aleutian Low deepens and migrates southward during stadials resulting in anomalous advection of cold Arctic air via northerly winds and enhanced westerlies, which increase surface heat fluxes from the ocean to the atmosphere, as well as in a southward shift of the oceanic frontal zones. All these processes would cause SST cooling in the N Pacific.

However, being present from late fall until early spring, the Aleutian Low is a seasonal feature restricted to the boreal winter. Therefore, any anomaly in the Aleutian Low should not have a dominant control on the summer SST reflected by TEX^{L86} . Indeed, Okumura et al. (2009) found that the cyclonic anomaly over the N Pacific is strongest in winter but absent during the summer months. Interestingly, the magnitude of SST cooling did not show strong seasonal variations as the difference between summer and winter was less than 1°C in their model simulations. This robustness of the SST cooling in the N Pacific is confirmed by the clear presence of the YD stadal in the summer-SST records from TEX^{L86} . Furthermore, it becomes obvious when $SST_{TEX^{L86}}$ is compared to the $SST_{UK'37}$. Alkenones are supposed to reflect autumn SST and therefore would be under the influence of the Aleutian Low. Consequently, large seasonal variations in the magnitude of the YD cooling should cause large discrepancies in the $SST_{TEX^{L86}}$ and $SST_{UK'37}$. At site 12KL the magnitude of the cooling is 1°C in the $SST_{TEX^{L86}}$ smaller than in the $SST_{UK'37}$ (Figure 2.3) which supports the finding of the model simulations. Suggesting a response to N Atlantic climate change of SST throughout the annual cycle.

2.5.2.2. *Late glacial and HS1 – differences between the NW Pacific and the Western Bering Sea*

As cited above, previously published alkenone-based studies from the N Pacific and its marginal seas indicate that the subarctic N Pacific was widely connected to the N Atlantic via atmospheric teleconnections during the deglaciation (between ca. 10-15 ka). Therefore, it seems reasonable to assume that the atmospheric coupling would have also controlled the SST development during the early deglaciation and the late glacial. Indeed, SST_{TEXL86} from the Western Bering Sea resemble NGRIP- $\delta^{18}\text{O}$ and reveals a cooling during Heinrich Event 1 (17-16 ka BP; Figure 2.4 A) in the Western Bering Sea, indicating that the atmospheric linkage with the N Atlantic has already been present during the early deglaciation. However, a quite different pattern is visible in SST_{TEXL86} in the NW Pacific (site 12KL), where a gradual, uninterrupted increase in SST_{TEXL86} between 18 ka -15 ka does not agree with the North Atlantic climate evolution and shows no indication for a Heinrich-equivalent cold spell (Figure 2.4B). This contrasts model simulations which investigated the response of the N Pacific to freshwater perturbations in the N Atlantic under glacial boundary conditions (including lowered Sea-level and continental ice-caps) to explicitly investigate the SST-response during HS1 (Chikamoto et al. (2012), MIROC-simulation). The model predicted a clear decrease in SST in the Bering Sea as well as in the entire subarctic N Pacific. This suggest a rather widespread sensitivity of NW Pacific SST to atmospheric teleconnections with N Atlantic climate change already during the early deglaciation/HS1. However, our SST_{TEXL86}-record reveals that a clear similarity with the NGRIP- $\delta^{18}\text{O}$ and the SST-development in the NW Pacific can only be found since ca. 15 ka (Figure 2.3 & 2.4). This finding implies that during the late glacial and the early deglaciation the SST development in the NW Pacific was apparently less sensitive to an atmospheric teleconnection with the N Atlantic than the Western Bering Sea and was controlled by different processes.

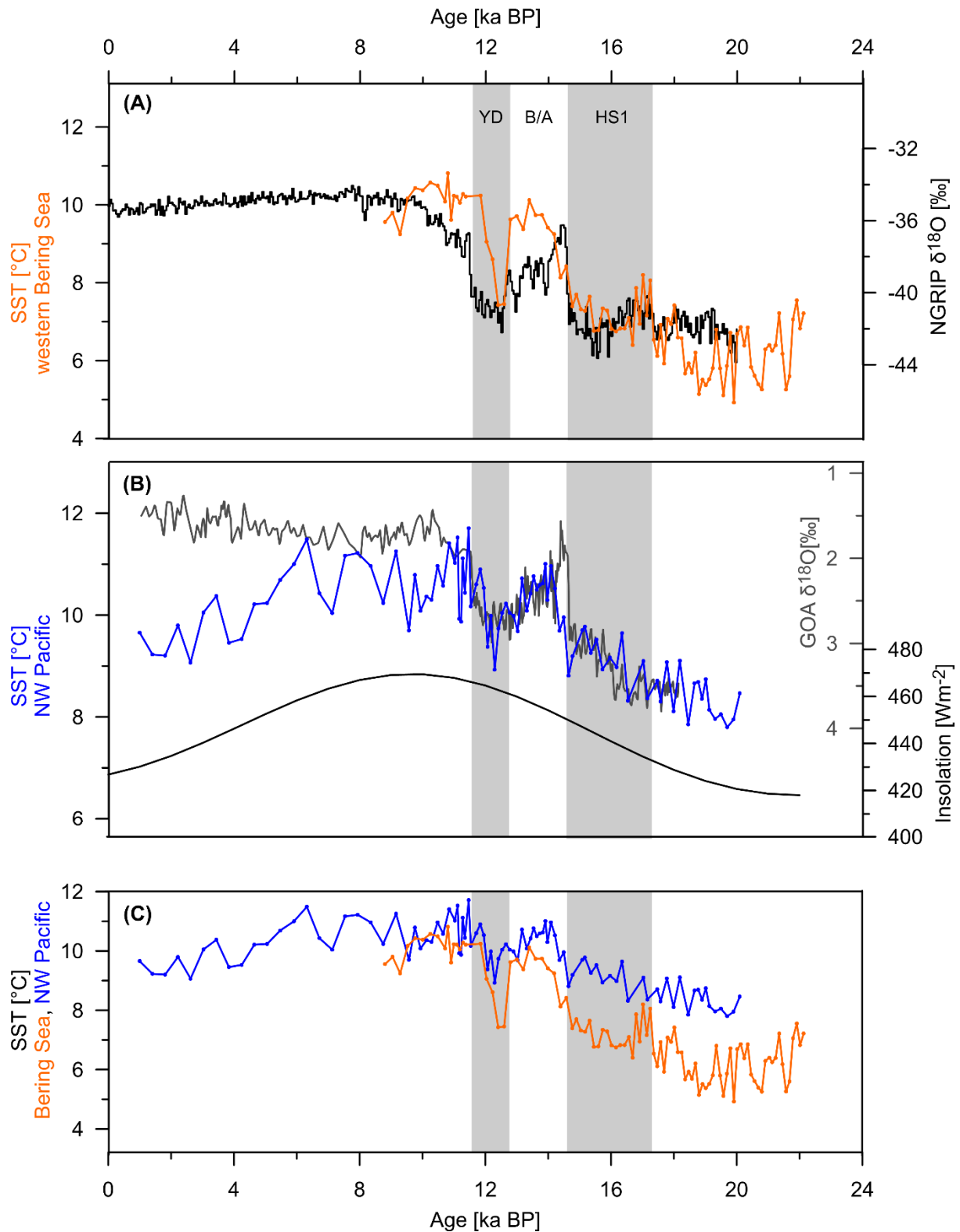


Figure 2.4. a) $\text{SST}_{\text{TEXL86}}$ from site 114KL, Western Bering Sea (orange) compared to Greenland ice core $\delta^{18}\text{O}$ (NGRIP, black). b) $\text{SST}_{\text{TEXL86}}$ from site 12KL, NW Pacific (blue) plotted together with the GOA- $\delta^{18}\text{O}$ measured on the planktonic foraminifera *Neogloboquadrina pachyderma* (sin.) (grey, Praetorius and Mix, 2014) and mean July-insolation at 65°N (Berger and Loutre, 1991). c) Comparison $\text{SST}_{\text{TEXL86}}$ from sites 12KL (blue) and 114KL (orange).

2.5.3. Controls on the early deglacial SST development in the NW Pacific

As the warming in SST_{TEXL86} at site 12KL during the late glacial/HS1 follows the trend of mean summer insolation (Figure 2.3 & Figure 2.4B) it seems likely that increasing insolation was an important factor driving the SST-evolution during this time. The temperature development from the NW Pacific also resembles the climate evolution in the Gulf of Alaska (GOA, Figure 4b). There, $\delta^{18}\text{O}$ -records, established on planktonic foraminifera, indicate that the climate of the NE-Pacific developed asynchronously with the N Atlantic realm during the late glacial/HS1 and became synchronized on centennial time-scales at ca. 15 ka (Praetorius and Mix (2014), Figure 2.4). It is noteworthy that $\delta^{18}\text{O}$ of planktonic foraminifera technically record a composite of temperature, salinity and global ice volume and cannot easily be interpreted as a temperature signal alone. However, Praetorius and Mix (2014) found that alkenone-based SST records from the NE Pacific and the southern Bering Sea track the GOA- $\delta^{18}\text{O}$ which made them conclude that a large component of the $\delta^{18}\text{O}$ would reflect upper-ocean temperature. Under this assumption, the similarity between the GOA- $\delta^{18}\text{O}$ and our data may even indicate a quite similar SST-evolution in the NW Pacific and the GOA (Figure 2.4 B). The asynchronicity between the climate development in the GOA and the N Atlantic realm was explained by a southward displacement of the westerly jet due to expanded ice caps on the American continent. This would have reduced the atmospheric connection between Greenland and GOA preventing the establishment of an atmospheric coupling (Praetorius and Mix, 2014 and references therein). At ca. 15.5 ka the coupling would have been initiated in response to falling ice height in the course of retreating continental ice caps (Praetorius and Mix, 2014). However, in case of site 12KL in the NW Pacific, it seems unlikely that a southward shift of the westerly jet accounts for the decoupling since an atmospheric connection is evident in SST_{TEXL86} from the Western Bering Sea, north of site 12KL (Figure 2.1 & 2.4). Instead, the similar trends in the GOA- $\delta^{18}\text{O}$ and SST_{TEXL86} suggest the existence of an oceanographic linkage between the eastern and western basin of the subarctic N Pacific which overprinted an atmospheric coupling with the N Atlantic. A prominent oceanic feature connecting the eastern and western part of the North Pacific is the Alaskan Stream (AS, Figure 2.1). Relatively strong accumulation of AS waters at site 12KL could have been more relevant to the SST development in the NW Pacific, than an atmospheric teleconnection there during HS1. This east-west linkage corroborates considerations by Riethdorf et al. (2013) who reconstructed sub-surface salinity at site 12KL and found a freshening between 17.5 and 15.5 ka BP in the NW Pacific. These authors supposed enhanced accumulation of low-salinity waters from the AS since the Alaskan Current/Alaskan Stream current system experienced

drops in salinity due to continental runoff and intensified ice-berg calving, associated with the beginning retreat of continental ice caps during HS1 (Gebhardt et al., 2008; Hendy and Cosma, 2008; Riethdorf et al., 2013; Taylor et al., 2014). The freshwater discharge from the American continent would have reduced surface salinity in the NE Pacific/GOA and the AS would have advected this low-salinity anomaly to the NW Pacific (Riethdorf et al., 2013). Hence, a pronounced influence of AS waters at site 12KL seems to have had an important impact on the surface conditions and the climate in the NW Pacific during the late glacial and the HS1.

2.5.4. Surface circulation changes – the AS-EKC interplay

Sites 12KL and 114KL are both under the influence of the EKC (Figure 2.1). Considering that the current transports surface water from the Western Bering Sea to site 12KL (Figure 2.1) one may expect that the SST development would be similar in both settings. Ice rafted detritus (IRD) was deposited in the open NW Pacific (sites ODP Site 882, MD01-2412) during glacial times until ca. 15 ka BP (St. John and Krissek, 1999; Gebhardt et al., 2008) and it has been found that the source of the IRD is the Kamchatka Peninsula and coastal Siberia (St. John and Krissek, 1999). Ice rafting along the coast of Kamchatka provides evidence for the presence of the EKC during the late glacial/HS1. So, the disagreement of the two SST_{TEXL86} records (Figure 2.4) implies that the AS was dominating over the influence of the EKC during the late glacial.

A glacial increase of AS waters accumulating in the marginal NW Pacific as inferred from our data is in agreement with studies that point to reduced inflow of AS waters into the Bering Sea (Katsuki and Takahashi, 2005; Tanaka and Takahashi, 2005) during the glacial sea-level low stand. Those authors speculated that some shallow passages between the Aleutian Islands were closed, including Unimak Pass, the main pathway of the AS into the Bering Sea today. The closure would have reduced the net inflow of AS waters into the Bering Sea and consequently, would have increased the accumulation of AS waters in the NW Pacific and ultimately established the climatic linkage between the eastern and western basins of the N Pacific. At the same time the reduced inflow of AS waters into the Eastern and Southern Bering Sea limited the influence of the N Pacific there and likely lead to a climatic isolation of the Bering Sea which allowed atmospheric teleconnections with the N Atlantic to affect the Bering Sea already prior to 15 ka BP. As our record is representative for the Western Bering Sea only, future SST studies should be carried out in the Eastern Bering Sea in order to test this hypothesis.

The relative influence of the two surface currents seems to have changed over the deglaciation as the GOA- $\delta^{18}\text{O}$ and our $\text{TEX}^{\text{L}}_{86}$ -based SST differ during the Holocene. While in the NW Pacific, SST progressively decreases over the Holocene and follows the trend of mean summer insolation (Figure 2.4B) Praetorius and Mix (2014) found relatively stable $\delta^{18}\text{O}$ -values in the NE Pacific throughout the entire Holocene (Figure 2.4B). This implies that the influence of the AS weakened over the deglaciation, which likely disconnected the NW Pacific SST from the NE Pacific. Also, the thermal difference between the Western Bering Sea and the NW Pacific becomes smaller over the deglaciation since the two SST-records show equal values during the Holocene (Figure 2.4C). Similar SST along the transect point to increased advection of Bering Sea waters into the NW Pacific and thus an increased influence of the EKC. The change in the relative intensities of the EKC and AS (AS strong during glacials, EKC more influential during the Holocene) may explain the relatively low thermal difference between the glacial and the Holocene SST at site 12KL. The deglacial temperature increase is ca. 2°C smaller than in the Western Bering Sea and glacial SST are only 1.5°C lower than modern. The MARGO-compilation (Waelbrock et al., 2009) suggested a temperature drop of $2\text{-}6^\circ\text{C}$ for the subarctic N Pacific. This attenuated glacial-Holocene warming may result from the deglacial changes in the EKC and AS-intensities in the NW Pacific. The increasing intensity of the relatively cold EKC and the concurrent reduction of the relatively warm AS may have dampened the deglacial SST increase at the site 12KL.

The change in the relative intensities of the EKC and the AS likely are a result of deglacial sea-level rise. When sea level rose the passages between the Aleutian Islands opened and probably allowed the AS waters to enter the Bering Sea. This in turn weakened the influence of the AS in the NW Pacific and at the same time the relative influence of the EKC could increase. Some evidence exists that the passages began to open during the B/A, since Riethdorf et al. (2013) reported sub-surface freshening at the southern tip of the Shirshov Ridge (site SO201-2-77KL, Figure 2.1) and considered enhanced inflow of relatively fresh AS waters into the Bering Sea. With the onset of the B/A, the thermal difference between the Bering Sea and the NW Pacific becomes reduced and $\text{SST}_{\text{TEX}^{\text{L}}_{86}}$ at sites 12KL and 114KL approach each other (Figure 2.4C) which may attest to contemporaneously reduced influence of the AS at site 12KL. However, diatom assemblages from site 12KL point to a pronounced influence of AS-waters in the NW Pacific during the B/A (Smirnova et al., 2015). Therefore, we assume that the relative intensities of the AS and the EKC may have not significantly differed from the glacial. In the southeastern Bering Sea the fractional abundances of the diatom species associated with AS-waters, have been increasing since ca. 11-12 ka BP (site

51-JPC, near Unimak Pass, Figure 2.1) which is indicative of pronounced inflow of AS waters into the Bering Sea and is associated with the opening of the Unimak Pass [Katsuki et al., 2004; Caissie et al., 2010]. Diatom assemblages from site 12KL indicate that the coastal Bering Sea waters have significant influence on the NW Pacific since ca. 11 ka BP (Smirnova et al. 2015) which coincides with the convergence of SST_{TEXL86} at sites 12KL and 114KL and the beginning deviation of SST_{TEXL86} and the GOA- $\delta^{18}\text{O}$. Therefore, we infer that the change in the relative intensities of the EKC and the AS likely occurred between the YD and the early Holocene and seems to be associated to the opening of Unimak Pass. We conclude that controlling the Glacial-Interglacial change in the relative intensities of the AS and EKC, sea level played an important role in regional differences of N Pacific climate change.

The glacial-interglacial interplay between the AS and EKC suggested here contrasts the conclusion regarding the evolution of the relative intensity of the two surface currents by Katsuki and Takahashi (2005). These authors proposed an opposite pattern with a strengthened EKC and weakened AS during glacial times and vice versa during Interglacials. Analyzing diatom assemblages in the southwestern Bowers Ridge and the open NW Pacific (site ES, Figure 2.1) they found high abundance of *N. seminae*, a species indicative of open water conditions and associated with the AS, in the NW Pacific during interglacials but decreasing abundances during glacials. The reduction of *Neodenticula seminae* combined with increasing abundances of species related to sea-ice and cold, low-salinity surface waters made them conclude that icebergs and sea-ice were transported along the coast of the Kamchatka Peninsula and lowered the surface salinity in the Western Bering Sea and the NW Pacific. Therefore, they considered reduced influence of AS and a strengthened EKC during glacial times. However, they also suggested that the low abundance of *N. seminae* would indicate a decrease of nutrients in the surface layer and this may explain the discrepancies with the data presented in our study.

2.6. Summary and conclusions

Using TEX₈₆^L we reconstructed SST development in the Western Bering Sea and the NW Pacific from the LGM to the Holocene. Our conclusions can be summarized as follows:

Providing a rather stable signal throughout the entire studied time period TEX₈₆^L appears to be a powerful tool for unravelling the SST-development during glacial periods where alkenone-palaeothermometry is often problematic. SST_{TEXL86} are slightly warmer than previously published alkenone data resulting from different production seasons of

Thaumarchaeota (summer) and coccolithophores (fall). We propose that the offset reflects the seasonal contrast. The seasonal contrasts were greater during the deglaciation than during the Holocene which is probably a result of a shortened period of summer stratification and/or a stronger Aleutian Low. While alkenone-based records do not reach beyond 15 ka TEX^L₈₆ allows SST reconstructions until the LGM and provides new insights into the SST development during the HS1.

The deglacial SST development (ca. 10-15 ka) recorded by TEX^L₈₆ corroborates previous studies which suggested that the SST evolution in the N Pacific was linked to the climate development in the N Atlantic via atmospheric teleconnections. However, our data reveal that the onset of the teleconnections in the NW Pacific is delayed compared to the Western Bering Sea. While the Bering Sea has already been influenced by N Atlantic climate change through an atmospheric coupling during the early deglaciation (HS1), the marginal NW Pacific remained insensitive to any atmospheric connection until ca. 15 ka BP. Before this time, SST evolution in the NW Pacific seems to have been driven by increasing summer insolation and was strongly linked to the climate development in the GOA. There, a southward migration of the westerly jet is suggested to have inhibited atmospheric teleconnection with the N Atlantic prior to ca. 15 ka BP. Relatively strong accumulation of AS waters in the NW Pacific overprinted the atmospheric teleconnections there.

Our study reveals a glacial-interglacial interplay between the relative strengths of the EKC and the AS surface currents. While the AS dominates the surface conditions during glacial times, its influence weakens during the deglaciation in the course of sea-level rise and the concurrently increasing inflow of AS waters into the Bering Sea. At the same time the EKC becomes more influential in the NW Pacific. During the Holocene, the weakened influence of the AS in the NW Pacific disconnects the eastern and the western basins of the N Pacific and allows regionally different SST developments.

Regulating the net inflow of AS waters into the Bering Sea variations in sea level seem to drive the relative intensities of the EKC and AS and consequently have an indirect impact on the Glacial-Holocene SST development in the subarctic N Pacific.

Acknowledgments

The study resulted from core material that was gained in the frame of the German-Russian research project “KALMAR” – Kurile-Kamchatka and Aleutian Marginal Sea Island Arc Systems: Geodynamic and Climate Interaction in Space and Time”. We thank the Master and

the crew of R/V SONNE for their professional support during cruise SO201-2. Dirk Nürnberg is thanked for providing sample material from site SO201-2-12KL. We acknowledge Alexander Weise for his assistance on the geochemical sample preparation. The study was part of a PhD project funded by the Helmholtz association through the President's Initiative and Networking Fund and is supported by GLOMAR – Bremen International Graduate School for Marine Sciences. The data of this study is available on the database "Pangaea" (www.pangaea.de).

3. Manuscript II:

Summer-temperature evolution on the Kamchatka Peninsula, Russian Far East, during the past 20,000 years

Vera D. Meyer^{1,2}, Jens Hefter¹, Gerrit Lohmann¹, Ralf Tiedemann¹ and Gesine Mollenhauer^{1,2,3}

1: Alfred Wegener Institute Helmholtz Centre for Polar and Marine Research, Bremerhaven, Germany

2: Department of Geosciences University of Bremen, Bremen, Germany

3: MARUM- Centre for Environmental Sciences, University of Bremen, Bremen, Germany

Submitted to *Climate of the Past*

Abstract

Little is known about the climate evolution on the Kamchatka Peninsula during the last deglaciation as existing climate records do not reach beyond 12 ka BP. In this study, a summer-temperature record for the past 20 ka is presented. Branched Glycerol Dialkyl Glycerol Tetraethers, terrigenous biomarkers suitable for continental air temperature reconstructions, were analyzed in a sediment core from the western continental margin off Kamchatka/marginal Northwest Pacific (NW Pacific). The record reveals that glacial summer temperatures on Kamchatka equaled modern. We suggest that strong southerly winds associated with a pronounced North Pacific High pressure system over the subarctic NW Pacific accounted for the warm conditions. A comparison with outputs from an Earth System Model reveals discrepancies between model and proxy-based reconstructions for the LGM-temperature and atmospheric circulation in the NW Pacific realm. The deglacial temperature development is characterized by abrupt millennial-scale temperature oscillations. The Bølling/Allerød warm-phase and the Younger Dryas cold-spell are pronounced events, providing evidence for a strong impact of North-Atlantic climate variability on temperature development in southeastern Siberia. Summer insolation and teleconnections with the North Atlantic determine the long-term temperature development during the Holocene.

3.1. Introduction

The Kamchatka Peninsula is attached to Siberia and protrudes into the North Pacific Ocean separating the Sea of Okhotsk from the Northwest Pacific (NW Pacific) and the Bering Sea (Figure 3.1A). The Peninsula is a remote part of western Beringia. “Beringia” extends from the Lena River in Northeast Russia to the lower Mackenzie River in Canada (Figure 3.1A, Hopkins et al., 1982). During Pleistocene sea-level low-stands the Bering Land Bridge (BLB) linked Eastern and Western Beringia as the Chukchi and Bering Shelves became exposed (Figure 3.1A). Kamchatka is one of the least studied areas of Beringia since the available terrestrial climate archives, such as peat sections or lake sediments, do not reach beyond 12 ka BP (e.g. Dirksen et al., 2013, 2015; Nazarova et al., 2013a; Hoff et al. 2015; Klimaschewski et al., 2015; Self et al., 2015; Solovieva et al., 2015) and the climatic conditions during the Last Glacial Maximum (LGM) and the deglaciation are poorly understood. However, the climatic history of Kamchatka may provide important insights into the deglacial development of regional atmospheric and oceanic circulation, since the Holocene climate evolution largely responds to those regional forcing mechanisms (Nazarova et al., 2013a; Brooks et al., 2015; Hammarlund et al., 2015; Self et al., 2015) next to global or supra-regional climate drivers, e.g. summer insolation (Savoskul, 1999; Dirksen et al., 2013; Brooks et al., 2015; Self et al., 2015). Particularly, information about atmospheric and oceanic circulation in the Northwest Pacific (NW Pacific) realm is important to confirm outputs from climate models.

The investigation of deglacial climate change on Kamchatka may also contribute to the understanding of the spatial dimension of atmospheric teleconnections with abrupt climate change in the North Atlantic (N Atlantic). The majority of sea surface temperature records from the subarctic NW Pacific and the marginal seas mirror the N Atlantic climate oscillations (e.g. Caissie et al., 2010; Max et al., 2012; Meyer et al., submitted b) suggesting that atmospheric teleconnections with the North Atlantic controlled deglacial temperature development in the N Pacific realm (Max et al., 2012; Meyer et al., submitted b). However, climate records from Siberia and Alaska provide an ambiguous picture concerning the sensitivity of Beringia to climate oscillations in the N Atlantic. Some studies in Siberia (west of 140°N) and interior Alaska found patterns similar to the N Atlantic climate variability, including a Bølling/Allerød (B/A)-equivalent warm-phase and a subsequent climatic reversal during the Younger Dryas (YD; Anderson et al., 1990; Andreev et al., 1997; Pisaric et al., 2001; Bigelow and Edwards, 2001; Brubaker et al., 2001; Anderson et al., 2002; Meyer et al., 2010; Anderson and Lozhkin, 2015), while other Alaskan and east Siberian (east of ca.

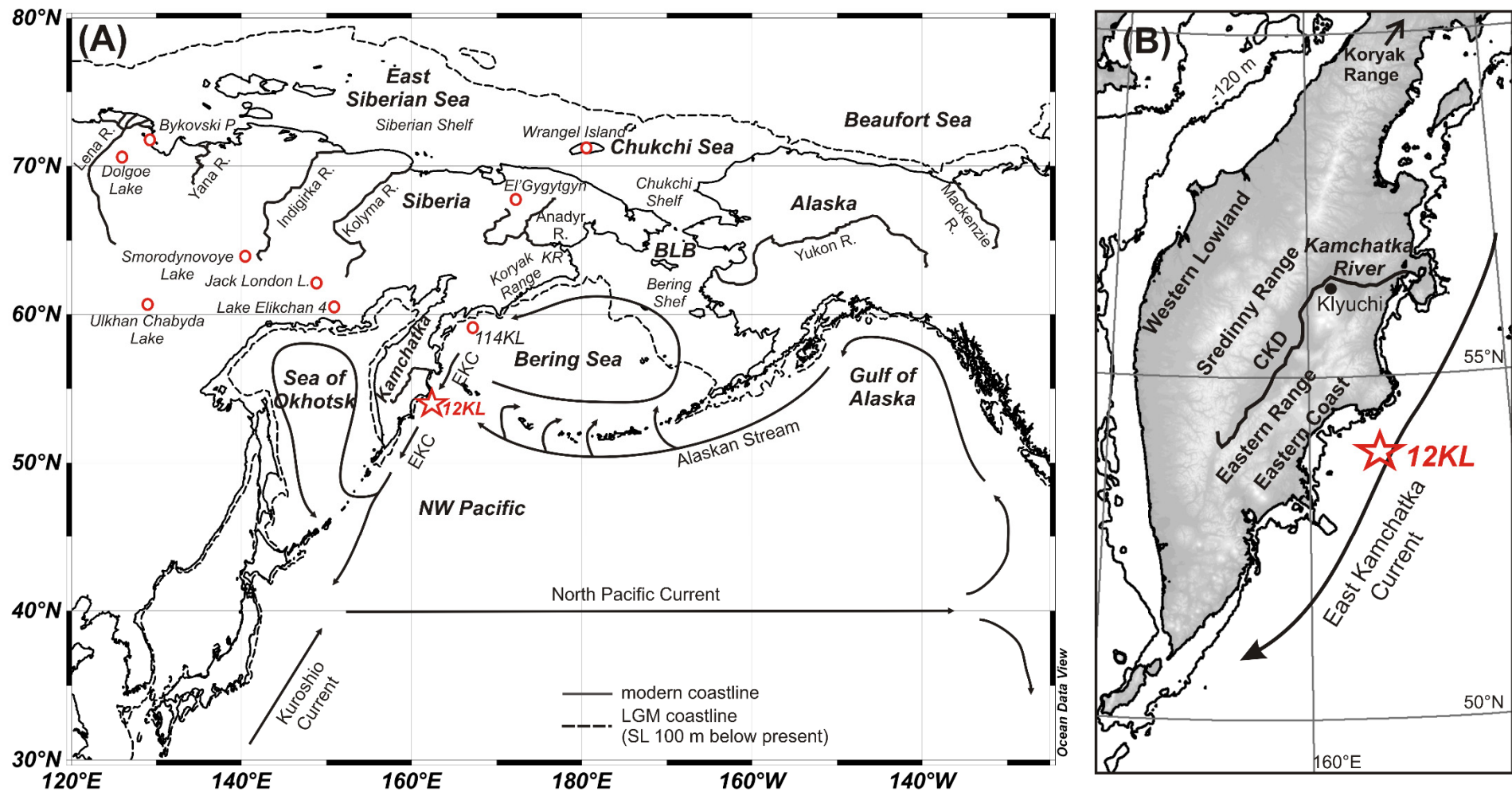


Figure 3.1. (A) Overview of Beringia and the N Pacific. Site SO201-2-12KL is marked by a red star. Circles represent sites mentioned in the text. Black arrows indicate the surface circulation patterns of the N Pacific (e.g. Stabeno and Reed, 1994). BLB = Bering Land Bridge, KR = Kankaren Range, R = River, EKC = East Kamchatka Current. P = Peninsula. L= Lake (B) Map of the Kamchatka Peninsula and its major orographic units. CKD = Central Kamchatka Depression.

150°N) records show progressive warming during the postglacial climate amelioration, without a YD-cold spell (Lozhkin et al., 1993, 2001; Anderson et al., 1996, 2002; Lozhkin and Anderson, 1996; Nowaczyk et al., 2002; Anderson et al., 2003; Nolan et al., 2003; Kokorowski et al., 2008a,b; Kurek et al., 2009). As pointed out by Kokorowski et al. (2008a,b) this may attest to regional differences or to uncertainties in chronologies. Therefore, further deglacial climate records with high resolution are necessary. This particularly applies for easternmost Siberia, since most deglacial records are obtained from sites west of 150°N and north of 65°N (Kokorowski et al., 2008a).

In this study, we analyzed branched glycerol dialkyl glycerol tetraethers (brGDGTs), terrigenous biomarkers as recorders of continental temperature (Weijers et al., 2006a, 2007), in a marine sediment core retrieved at the eastern continental margin off Kamchatka/NW Pacific (site SO201-2-12KL, NW Pacific, Figure 3.1). We present a continuous, quantitative record of summer-temperature on Kamchatka for the past 20 ka. The impact of global climate drivers, N Atlantic climate change, and regional atmospheric/oceanic circulation is investigated. The record reveals new aspects of LGM atmospheric circulation in the NW Pacific-realm, which are compared to an Earth System Model (ESM), and provides new insights into the interplay of global and regional climate drivers in the south-eastern edge of western Beringia since the LGM.

3.2. Regional Setting

The Kamchatka Peninsula is situated south of the Koryak Uplands in Siberia. It is characterized by strong variations in relief with lowlands in the coastal areas (Western Lowlands; Eastern Coast) and mountain ranges further inland (Figure 3.1B). The mountain ranges, the Sredinny and the Eastern Ranges, encircle the lowlands of the Central Kamchatka Depression (CKD; Figure 3.1B). The CKD is the largest watershed of the Peninsula and is drained by the Kamchatka River, the largest river of Kamchatka. The river discharges into the Bering Sea near 56°N (Figure 3.1B). The climate is determined by marine influences from the surrounding seas, by the East Asian continent, and by the interplay of the major atmospheric pressure systems over NE-Asia and the North Pacific (e.g. Mock et al., 1998; Glebova et al., 2009). In general the climate is classified as sub-arctic maritime (Dirksen et al., 2013). The winters are characterized by cold and relatively continental conditions since northerly winds prevail over Kamchatka which are mainly associated with the Aleutian Low over the N Pacific and the Siberian High over the continent (Mock et al., 1998). In summer, Kamchatka experiences warm maritime conditions owing to the East Asian Low over the continent and

the North Pacific High (NPH) over the N Pacific (Mock et al., 1998). Furthermore, there are the influences of the East Asian Trough (EAT) which has its average position over the northern shelves of central Beringia, as well as the influences of the westerly Jet and the associated polar front (Mock et al., 1998). Variations in the position and strength of the EAT affect precipitation and temperature over Beringia and can cause climatic contrasts between Siberia and Alaska (Mock et al., 1998 and references therein). With respect to Kamchatka westerly to northwesterly winds associated with the Jetstream and the EAT form a source of continental air masses from Siberia/East Asia (Mock et al., 1998).

The mountainous terrain with strongly variable relief results in pronounced climatic diversity on the Peninsula (Figure 3.1B). The coastal areas, the western Lowlands and the Eastern Coast, are dominated by marine influences. In the coastal areas, summers are cool and wet and winters are relatively mild. Precipitation is high along the coast and in the mountains throughout the year (Kondratyuk, 1974; Dirksen et al., 2013). Being protected from marine influences by the mountain ranges the CKD has more continental conditions with less precipitation and a larger annual temperature range than in the coastal areas (Ivanov, 2002; Dirksen et al., 2013, Kondratyuk, 1974; Jones and Solomina, 2015). Averaged for the entire Peninsula mean temperatures range from -8 to -26°C in January and from 10 to 15°C in July (Ivanov, 2002).

3.3. Material and Methods

3.3.1. Core material and chronology

Within a joint German/Russian research program (KALMAR Leg 2) core SO201-2-12KL (Figure 3.1) was recovered with a piston-corer device during cruise R/V SONNE SO201 in 2009 (Dullo et al., 2009). The core material was stored at 4°C prior to sample preparation. Age control is based on accelerator mass spectrometry (AMS) radiocarbon dating of planktic foraminifera (*Neogloboquadrina pachyderma* sin.) as well as on core-to-core correlations of high-resolution spectrophotometric (color b^*) and X-ray fluorescence (XRF) data. For detailed information and AMS- ^{14}C results, see Max et al. (2012).

3.3.2. Lipid extraction

For GDGT analyses, freeze-dried and homogenized sediment samples (ca. 5 g) were extracted with dichloromethane : methanol (DCM:MeOH, 9:1 v/v) using accelerated solvent extraction (ASE). Prior to extraction, 10 µg of a C₄₆-GDGT internal standard was added to each sample. The extraction was conducted on a “Dionex ASE 200”-device and was performed in three

cycles, each of them lasting for five minutes. During the extraction cycles the temperature was maintained at 100°C and the pressure at 1000 psi. After drying with a rotary-evaporator, extracts were hydrolyzed with 0.1N potassium hydroxide (KOH) in MeOH:H₂O 9:1 (v/v) to separate carbonic acids from neutral compound classes. After the hydrolyzation, neutral compounds such as hydrocarbons, ketones, alcohols and GDGTs were extracted with *n*-hexane, from the saponified solution. Dissolved in *n*-hexane the neutral compound-classes were separated using silica gel columns. Columns were built with Pasteur pipettes (6 mm diameter) which were filled with deactivated SiO₂ (mesh size 60, filling height 4 cm). After having eluted a less polar fraction with *n*-hexane, a polar fraction, containing the GDGTs, was eluted with DCM:MeOH (1:1 v/v). Dried polar fractions were dissolved in *n*-hexane:isopropanol (99:1, v/v) and were filtered through PTFE syringe filters (4 mm diameter, 0.45 µm pore size). Afterwards, samples were brought to a concentration of 2 µg/µl in order to prepare them for GDGT analysis.

3.3.3. GDGT analysis

GDGTs were analyzed by High Performance Liquid Chromatography (HPLC) and a single quadrupole mass spectrometer (MS). The systems were coupled via an atmospheric pressure chemical ionization (APCI) interface. The applied method was slightly modified from Hopmans et al. (2000). Analyses were performed on an Agilent 1200 series HPLC system and an Agilent 6120 MSD. Separation of the individual GDGTs was performed on a Prevail Cyano column (Grace, 3 µm, 150 mm x 2.1 mm) which was maintained at 30°C. After sample injection (20 µL) and 5 min isocratic elution with solvent A (hexane) and B (hexane with 5% isopropanol) at a mixing ratio of 80:20, the proportion of B was increased linearly to 36% within 40 min. The eluent flow was 0.2 ml/min. After each sample, the column was cleaned by back-flushing with 100% solvent B (8 min) and re-equilibrated with solvent A (12 min, flow 0.4 ml/min). GDGTs were detected using positive-ion APCI-MS and selective ion monitoring (SIM) of their (M+H)⁺ ions (Schouten et al., 2007). APCI spray-chamber conditions were set as follows: nebulizer pressure 50 psi, vaporizer temperature 350 °C, N₂ drying gas flow 5 l/min and 350 °C, capillary voltage (ion transfer tube) -4 kV and corona current +5 µA. The MS-detector was set in SIM-mode detecting the following (M+H)⁺ ions with a dwell time of 67 ms per ion: *m/z* 1292.3 (GDGT 4 + 4' / crenarcheol + regio-isomer), 1050 (GDGT IIIa), 1048 (GDGT IIIb), 1046 (GDGT IIIc), 1036 (GDGT IIa), 1034 (GDGT IIb), 1032 (GDGT IIc), 1022 (GDGT Ia), 1020 (GDGT Ib), 1018 (GDGT Ic) and 744 (C₄₆-internal standard).

GDGTs were quantified using the peak areas of the respective GDGTs and the obtained response factor from the C₄₆-standard. Concentrations were normalized to the dry weight (dw) of the extracted sediment and to total organic carbon contents (TOC). It has to be noted that the quantification should only be regarded as semi-quantitative because individual relative response factors between the C₄₆-standard and the different GDGTs could not be determined due to the lack of appropriate standards. Fractional abundances of single GDGTs were calculated relative to the total abundance of the all nine brGDGTs. The standard deviation was determined from repeated measurements of a standard sediment and resulted in an uncertainty of 9 % for the concentration of the sum of all nine brGDGT (Σ brGDGT).

3.3.4. *Temperature determination*

The Cyclisation of Branched Tetraether index (CBT) and Methylation of Branched Tetraether index (MBT) were introduced as proxies for soil-pH (CBT) and mean annual air temperature (MAT, CBT/MBT) by Weijers et al. (2007). The CBT-index was calculated after Weijers et al. (2007). For calculating the MBT-index we used a modified version of the original index, the MBT' which excludes GDGTs IIIb and IIIc. This modified index was introduced by Peterse et al. (2012), who argued that the brGDGTs IIIb and IIIc were often below detection limit, or accounted for not more than 1% of the total GDGT abundance on average. From repeated measurements the standard deviation for CBT and MBT' were determined as 0.01 and 0.04, respectively. CBT and MBT'-values were converted into temperature using the global-soil dataset calibration by Peterse et al. (2012). The residual standard mean error of this calibration is 5°C (Peterse et al., 2012). The standard deviation of CBT and MBT' translates into an uncertainty of max. 0.1°C.

Although terrestrial soils are supposed to be the main source of branched GDGTs (Weijers et al., 2007) brGDGT can also be produced in-situ in marine water systems (Peterse et al., 2009; Zhu et al., 2011; Zell et al., 2014) as well as in fresh water environments such as rivers or lakes (Tierney 2010; Zell et al., 2013; De Jonge et al., 2014; Dong et al., 2015). As in-situ production can bias temperature reconstructions, particularly in marine settings where the input of terrigenous GDGTs is low (Weijers et al., 2006b; Peterse et al., 2009, 2014; DeJonge et al., 2014), the contribution of brGDGTs to the marine sediments needs to be estimated prior to any palaeoclimatic interpretation of CBT/MBT'-derived temperatures. A common means to estimate the relative input of marine and terrestrial GDGTs is the BIT-index (Branched and isoprenoid tetraether index) which quantifies the relative contribution of the marine-derived

Crenarchaeol and terrigenous brGDGTs (Hopmans et al., 2004). BIT-values were adopted from Meyer et al. (submitted) who worked on the same sample used in this present study.

3.3.5. *Climate simulations with the Earth System Model COSMOS*

In order to compare inferences for atmospheric circulation during the summer months to computer model outputs, model simulations for the glacial climate were performed with the Earth System model COSMOS for pre-industrial (Wei et al., 2012) and glacial conditions (Zhang et al., 2013). The model configuration includes the atmosphere component ECHAM5 at T31 resolution ($\sim 3.75^\circ$) with 19 vertical layers (Roeckner et al., 2006), complemented by a land-surface scheme including dynamical vegetation (Brovkin et al., 2009). The ocean component MPI-OM, including the dynamics of sea ice formulated using viscous-plastic rheology, has an average horizontal resolution of $3^\circ \times 1.8^\circ$ with 40 uneven vertical layers (Marsland et al., 2003). The performance of this climate model was evaluated for the Holocene (Wei and Lohmann, 2012; Lohmann et al., 2013), the last millennium (Jungclauss et al., 2006), glacial millennial-scale variability (Gong et al., 2013; Weber et al., 2014; Zhang et al., 2014), and warm climates in the Miocene (Knorr and Lohmann, 2014) and Pliocene (Stepanek and Lohmann, 2012).

The climate model was integrated for 3000 model years and provides monthly output. Here, anomalies in sea-level pressure (SLP), wind directions (1000 hPa level) and surface air temperature (SAT) between the LGM and pre-industrial conditions were analyzed for the boreal summer season - June, July and August (JJA). All produced Figures show climatological mean characteristics averaged over a period of 100 years at the end of each simulation.

3.4. Results

3.4.1. *Concentrations and fractional abundance of brGDGT*

The summed concentration of all nine brGDGTs (Σ brGDGT) is shown in Figure 3.2a. The concentration of Σ brGDGTs vary between 40 and 160 ng/g dw throughout the record. Ranging between 60-80 ng/g dw, they are lowest during the LGM and the late Holocene. During the deglaciation and the early Holocene (17-8 ka BP) lowest values are ca. 80 ng/g dw, except for two peaks at 15-16 ka BP and 12-13 ka BP, respectively, where concentrations reach 160 ng/g dw (Figure 3.2a).

The fractional abundance of all nine brGDGTs, calculated relative to the Σ brGDGT, is shown in Figure 3.3. All samples are characterized by a similar pattern. The composition of the

brGDGT assemblage is dominated by brGDGTs without cyclopentyl moieties which together account for 60-80% of the total GDGT-assemblage (GDGT Ia, IIa, IIIa; Figure 3.3). GDGTs with a higher degree of methylation are more abundant than lesser methylated ones. In 83 out of 90 samples GDGT IIIa is the most prominent GDGT accounting for 22-37% of the total GDGT distribution. It is closely followed by GDGT IIa with 16-29% and GDGT Ia which accounts for 14-23% of the total GDGT distribution. As for GDGTs containing cyclopentyl moieties, GDGT IIb is most abundant accounting for 9-16% of the total GDGT assemblage. GDGT IIc, Ib, Ic, IIIb and IIIc are less abundant reaching 2-6%, 3-7%, 1-3%, 2-4%, and 1-2%. In one outlying sample GDGT IIc accounts for 24% (Figure 3.3).

3.4.2. Temperature development over the past 20 ka

The CBT/MBT'-derived temperatures are plotted in Figure. 2b. During the late Holocene (ca. 1 ka BP), the reconstructed temperature is 7.5°C. Interestingly, glacial temperatures (between 20-18 ka) are the same (Figure 3.2b). At 18 ka temperature drops by about 1.5°C. At 16 ka temperature jumps back to the glacial level. As this increase is based on one single data point, it cannot be excluded that this warming is an artifact resulting from an outlier. Deeming the data-point an outlier, temperature increases progressively until the onset of the Bølling/Allerød at ca. 14.6 ka BP, where it abruptly jumps back to the glacial and Holocene level of 7.5°C (Figure 3.2b). Between 14.6 and 13 ka, temperature progressively decreases about 1-0.5°C. During the Younger Dryas (YD) temperature abruptly decreases by about 2°C (at ca. 13 ka BP) and remains cold until 12 ka BP (Figure 3.2b). With ca. 4.5°C the YD is the coldest episode during the Glacial-Holocene transition. The cold spell is followed by a sharp temperature increase of ca. 3°C at the onset of the Preboreal (PB)/early Holocene (Figure 3.2b). After the abrupt temperature increase into the PB temperature progressively increases culminating in a Mid-Holocene Thermal Maximum (HTM) between 8.0-4.0 ka BP. With 8°C being reached between 6 and 4 ka BP, the mid-Holocene is the warmest episode since the Last Glacial Maximum (LGM). At 4 ka BP a cooling trend initiates and temperature decreases by about 0.5°C (Figure 3.2b). Compared to the deglacial temperature variations the Holocene variability is relatively small.

3.4.3. LGM-climate simulation with COSMOS

3.4.3.1. Sea-level pressure and wind patterns

Model-simulations for SLP (JJA) are shown Figure. 3.4A. The LGM-simulation is characterized by strong positive anomalies in sea-level pressure (SLP) over the American

Continent (Figure 3.4A). Positive SLP-anomalies also occur over the Arctic Ocean. Negative SLP anomalies occur south of 50°N and are centered over the NW Pacific and East Asia, but are also observed in a few grid-cells over the central and NE Pacific and over the Sea of Okhotsk. In the Bering Sea, the northern N Pacific (north of 50°N) and Beringia SLP does not change significantly relative to present.

The strong positive SLP-anomalies over North America are associated with pronounced anticyclonic anomalies in the wind directions, which expand to the Chukchi-Sea and to the formerly exposed BLB (Figure 3.4A). Over western Beringia as well as the adjacent Arctic Ocean small northerly anomalies are present. Between 100°E and 110°E pronounced anticyclonic anomalies are present over Russia. Over Kamchatka and the adjacent East Siberian Coast small northerly anomalies occur. The Western Bering Sea is characterized by easterly anomalies. Over the NW Pacific anomalies are small and show no general pattern. In the NE Pacific relatively strong westerly to southwesterly anomalies are present.

3.4.3.2. *Surface air temperature*

Model simulations for SAT (JJA) are shown in Figure 3.4B. The model predicts widespread negative surface air temperature (SAT)-anomalies over Beringia, East Asia, North America, the Arctic Ocean and the entire N Pacific (Figure 3.4B). However, in small parts of the formerly exposed BLB slightly warmer-than-present conditions are simulated. On the arctic shelf a small band where temperature may equal the PI-conditions as the SAT anomaly falls in the window of -1 to +1°C, occurs. The temperature anomalies are strongest over North America where they reach -17°C. Over western Beringia the SAT anomaly increases from east to west with SAT ranging between -1 and -5 over East Siberia and between -5 and -9 further west. Over the N Pacific SAT anomalies are smaller than over western Beringia and range between -1 and -5°C. SAT anomalies are smallest in the Bering Sea and along the eastern coast of Kamchatka. Over the Peninsula itself, the majority of grid-cells indicate a negative anomaly (-3 to -5°C). In the northern part and over the adjacent Bering Sea the SAT anomalies are very small within the window of -1 to +1°C (Figure 3.4B).

3.5. Discussion

3.5.1. *Sources of brGDGT and implications for CBT/MBT'-derived temperatures*

Considering that brGDGT are thought to be synthesized by terrestrial bacteria which thrive in peats and soils (e. g. Weijers et al., 2006b) it is most likely that the major origin of brGDGT in the marine sediments of the Bering Sea/NW Pacific would be the Kamchatka Peninsula.

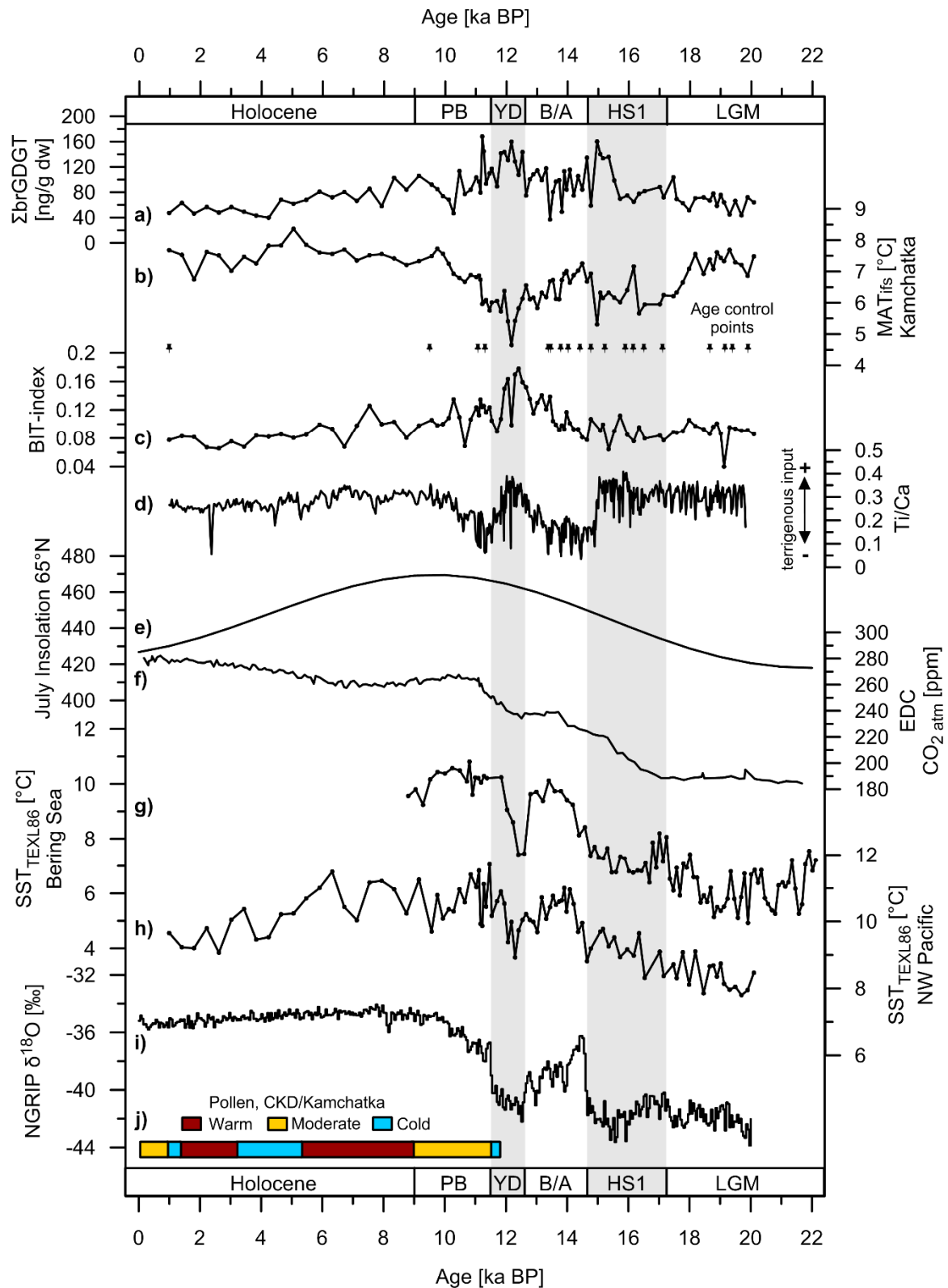


Figure 3.2. a) Concentrations of Σ brGDGT of core 12KL. b) CBT/MBT' derived MAT_{fis} from Kamchatka (this study). Black pins represent the age control points from core 12KL (based on radiocarbon dating of planktonic foraminifera, Max et al., 2012). c) BIT-index values of core 12KL (Meyer et al., submitted b). d) Titanium/Calcium ratios (Ti/Ca, XRF-scan core 12KL, Max et al., 2012). e) Mean July insolation at 65°N (Berger and Loutre, 1991). f) Atmospheric CO₂ concentration (EPICA dome C, Monnin et al., 2001). g) SST development in the marginal NW Pacific (site 12KL, Meyer et al., submitted b). h) SST evolution in the Western Bering Sea (site 114KL, Meyer et al., submitted b). i) NGRIP- $\delta^{18}\text{O}$ (NGRIP, 2004) represents climate change in the N Atlantic. j) Pollen-based temperature reconstructions from the CKD (after Dierksen et al., 2013). Grey-shaded bars mark the HS1 and YD stadials.

However, BIT-values from core 12KL range between 0.08 and 0.2 (Meyer et al., submitted b) throughout the entire record, indicating that marine derived GDGT dominate the total GDGT composition and that terrigenous input is low (Figure 3.2c). Since a bias from in-situ production is particularly eminent in marine settings where terrigenous input is low (e.g. Weijers et al., 2006b; Peterse et al., 2009; Zhu et al., 2011), non-soil derived brGDGTs potentially have a considerable effect on the temperature reconstruction at site 12KL. However, the concentrations of Σ brGDGT show strong similarities with the trend of Titanium/Calcium ratios (Ti/Ca-ratios, Figure 3.2d) from core 12KL (XRF-data from Max et al. (2012)). Reflecting the proportion of terrigenous and marine derived inorganic components of the sediment, Ti/Ca-ratios can be used as an estimator of terrigenous input. With relatively high values at 15.5 and 12 ka BP, and minima at 14 and 11 ka BP. As intervals of relatively high/low terrigenous input (as suggested by Ti/Ca) coincide with relatively high/low Σ brGDGT-concentrations brGDGTs seem to be terrigenous (Figure 3.2b, d). Moreover, the distribution of the brGDGTs the samples from site 12KL resemble the GDGT composition described for soils world-wide (Weijers et al., 2007; Blaga et al., 2010) as GDGT Ia, IIa and IIIa dominate over GDGTs with cyclopentyl moieties (e.g. Ib, IIb) accounting for 60-80% of the total brGDGT assemblage (Figure 3.3).

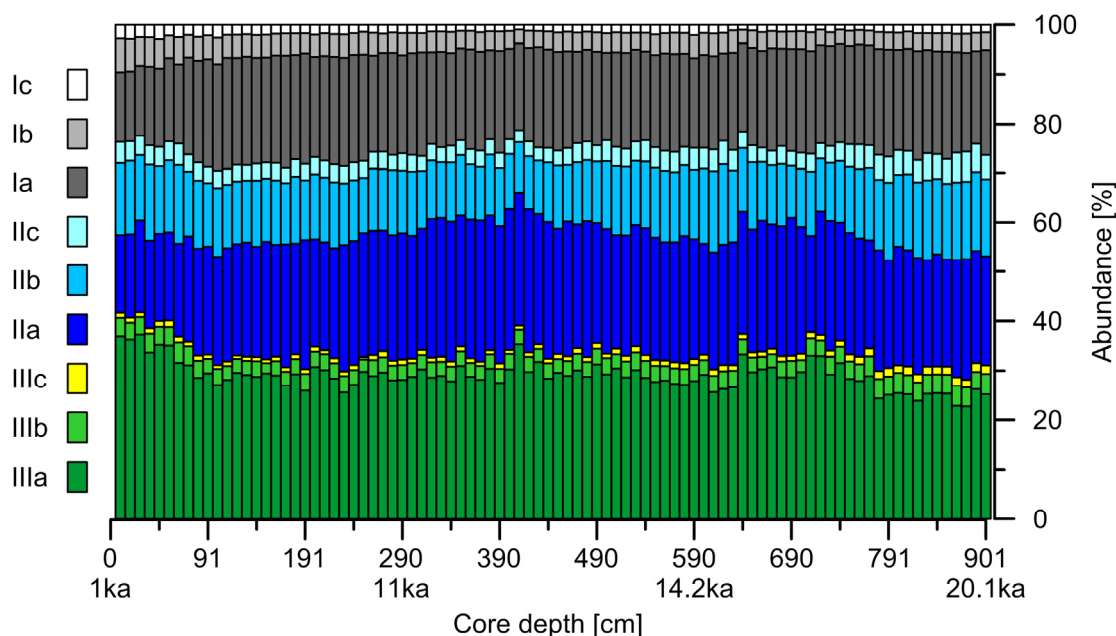


Figure 3.3. Fractional abundances of all nine brGDGT in core 12KL, given in percentage relative to the amount of Σ brGDGTs. For four samples the corresponding age is given, based on the core chronology from Max et al., [2012].

By contrast, in areas where GDGTs are thought to be produced in-situ, the GDGT compositions were dominated by GDGTs containing cyclopentyl moieties (Peterse et al., 2009; Zell et al., 2014). Thus, brGDGT seem to be soil-derived and a bias from in-situ

production is unlikely. We also exclude changes in the source of brGDGTs through time because the relative abundance of the brGDGTs is similar in all samples indicating that the source of brGDGTs remained constant throughout the past 20 ka (Figure 3.3). We consider the catchment of the Kamchatka River (CKD and inner flanks of the mountains) and the Eastern Coast as the likely sources of brGDGTs deposited in the marine sediments at the core site since the Kamchatka River and several small rivers draining the Eastern Coast discharge into the Western Bering Sea. Flowing southward along Kamchatka, the East Kamchatka Current would carry the load of the Kamchatka River to site 12KL (Figure 3.1A)

Although the CBT/MBT-palaeothermometre has been suggested to generally record mean annual air temperatures (Weijers et al., 2007) it is assumed to be biased to the summer months/ice-free season in high latitudes (Rueda et al., 2009, Shannahan et al., 2013; Peterse et al., 2014). According to Klyuchi climate station (for location see Figure 1b), mean annual air temperatures in the northern CKD are ca. -0.5°C (<http://en.climate-data.org/location/284590/>). The CBT/MBT'-derived temperatures for the core-top/late Holocene (7.5°C ; Figure 3.2b) exceed the annual mean by ca. 8°C and are similar to mean air temperatures from the ice-free season (Mai-October) at Klyuchi (ca. 9°C). Therefore, they are interpreted as summer temperature and will be referred to as "Mean Air Temperature of the ice-free season" (MAT_{ifs}) henceforth.

3.5.2. *Temperature evolution over the past 20 ka*

3.5.2.1. *The last glacial maximum – warm summers and the regional context*

The finding that LGM and Holocene MAT_{ifs} are equal contrasts with the general understanding of the glacial climate according to which the extratropics were significantly colder than today, as documented by several proxy-based temperature reconstructions (e.g. MARGO compilation, Kageyama et al., 2006; Waelbroeck et al., 2009) and computer model simulations (e.g. Kutzbach et al., 1998; Kageyama et al., 2006; Kim et al., 2008; Alder and Hostetler, 2015). The general cooling tendency is thought to result from low summer insolation, reduced carbon-dioxide concentrations in the atmosphere and extensive continental ice caps (Berger and Loutre 1991; Monnin et al., 2001; Kageyama et al., 2006, Shakun et al., 2012). Therefore, one may expect that the Kamchatka Peninsula would experience a glacial-interglacial warming trend. As MAT_{ifs} deviates from the trends in $\text{CO}_{2\text{atm}}$ and insolation (Figure 3.2.b, e, f) regional climate drivers may have overprinted the effects of $\text{CO}_{2\text{atm}}$ and summer insolation. Interestingly, several studies investigating climate in Beringia based on pollen and beetle-assemblages indicate that in NE Siberia and the formerly exposed BLB

(catchments of the Lena, Kolyma and Indigirka Rivers, Ayon Island, Anadyr Lowlands, Lake El'Gygytgen, Seward Peninsula, Figure 3.4C) summers during the LGM were as warm as at present or were even warmer (Figure 3.4C; Elias et al., 1996, 1997; Elias, 2001; Alfimov and Berman, 2001; Kienast, 2002; Kienast et al., 2005; Sher et al., 2005; Berman et al., 2011). Only a few pollen and insect-data from Markovo, Lakes Jack London and El'Gygytgin (Figure 1a), point to colder-than-present conditions (Figure 3.4C; Lozhkin et al., 1993; Alfimov and Bermann, 2001; Lozhkin et al., 2007; Pitul'ko et al., 2007). The fairly large number of sites indicating warm summers in Siberia suggests that a thermal anomaly was widespread over western/central Beringia (Figure 3.4.c) and extended to Kamchatka. The thermal anomaly did probably not extend to eastern Beringia as insect-data as well as pollen consistently point to summer cooling of up to 4°C (Figure 3.4.c; e.g. Mathews and Telka, 1997; Elias, 2001; Kurek et al., 2009).

3.5.2.2. *Controls on MAT_{ifs}*

The warm Siberian summers were attributed to increased continentality, which would arise from the exposure of the extensive Siberian and Chukchi shelves at times of lowered sea-level (Figure 3.1A; e.g. Guthrie, 2001; Kienast et al., 2005; Berman et al., 2011). The greater northward extent of the Beringian landmass (ca. +800 km relative to today) would have minimized maritime influences from the cold Siberian and Chukchi Seas (Guthrie, 2001; Alfimov and Berman, 2001; Kienast et al., 2005; Sher et al., 2005; Berman et al., 2011). Increased seasonal contrasts resulting in warmer summers and colder winters would have been the result (e.g. Guthrie, 2001; Kienast et al., 2005). Winter cooling in Siberia (relative to modern) is indicated by ice-wedge data (Meyer et al., 2002) from Bykovski Peninsula (Figure 3.1.A). Also, the presence of stronger-than-present sea-ice cover in the Bering Sea (Caissie et al., 2010; Smirnova et al., 2015) points to cold winter during the LGM.

However, for Kamchatka it is unlikely that the thermal anomaly and an increased seasonal contrast were a direct result from lowered sea-level as the bathymetry around the Peninsula is relatively steep and the exposed shelf area was very small. (Figure 3.1.A, B). Thus, other climate drivers were likely responsible for the relatively warm summer conditions. Potential mechanisms are changes in oceanic or atmospheric circulation.

A prominent oceanic conveyor of heat into the subarctic N Pacific is the Kuroshio-Current which flows northward along the coast of Japan and transports warm tropical water masses into the North-Pacific current system (Figure 3.1A). Today, it turns eastward at 40°N. Warm summers on Kamchatka could be a consequence of a northward expansion of Kuroshio water

into the proximity of the Kamchatka Peninsula. A northward expansion of the Kuroshio Current would have made the surface and sub-surface warmer and saltier than today and would have weakened the stratification. However, this scenarios seems unlikely as palaeoceanographic studies provide evidence for relatively fresh and colder-than-present surface (Meyer et al. submitted) and sub-surface waters (Gebhardt et al., 2008; Riethdorf et al., 2013) in the subarctic NW Pacific which points to pronounced stratification during the LGM (Gebhardt et al., 2008; Riethdorf et al., 2013). The work carried out by Riethdorf et al. (2013) suggests that at site 12KL these conditions persisted until the Bølling/Allerød. Intriguingly, alkenone-based SST reconstructions from the Sea of Okhotsk indicate that glacial SST were slightly warmer than today or equal to modern conditions (Seki et al., 2004b, 2009; Harada et al., 2004, 2012; Figure 3.4C). However, these records are considered to be biased by seasonal variations in the alkenone production rather than to reflect real temperature anomalies (Seki et al., 2004b, 2009; Harada et al., 2004, 2012). This seems to be supported by a few TEX^{L}_{86} -based SST reconstruction from the Sea of Okhotsk suggesting that LGM SST were ca. 5°C colder than at present (Seki et al. 2009; 2014). In this light, a climatic relation between alkenone-based SST and MAT_{ifs} seems very unlikely. Interestingly, LGM-SST in the subarctic NW Pacific (site 12KL) were only 1°C lower than at present (Figure 3.2.h), a relatively small temperature difference compared to other SST records from the NW Pacific and its marginal seas which suggest a cooling of 4-5°C on average (e.g. Seki et al., 2009; 2014; Harada et al., 2012, Meyer et al., submitted b). The relatively warm SST at site 12KL were explained by a stronger-than-present influence of the Alaskan Stream (Figure 3.1.A) in the marginal NW Pacific during the LGM (Meyer et al., submitted b). Such warm SST may have supported the establishment of warm conditions on Kamchatka. However, it is unlikely, that the temperature development on Kamchatka was fully controlled by oceanic influences since this would probably cause a similar temperature reduction as in the SST record of site 12KL.

If oceanic circulation alone is unlikely to have caused the warm temperatures on Kamchatka, atmospheric circulation may have exerted a strong control on glacial summer temperatures in the region. In terms of atmospheric circulation the summer climate of the Kamchatka is largely determined by the strength and position of the North Pacific High (NPH) over the N Pacific (Mock et al., 1998). As the southerly flow at the southwestern edge of the NPH brings

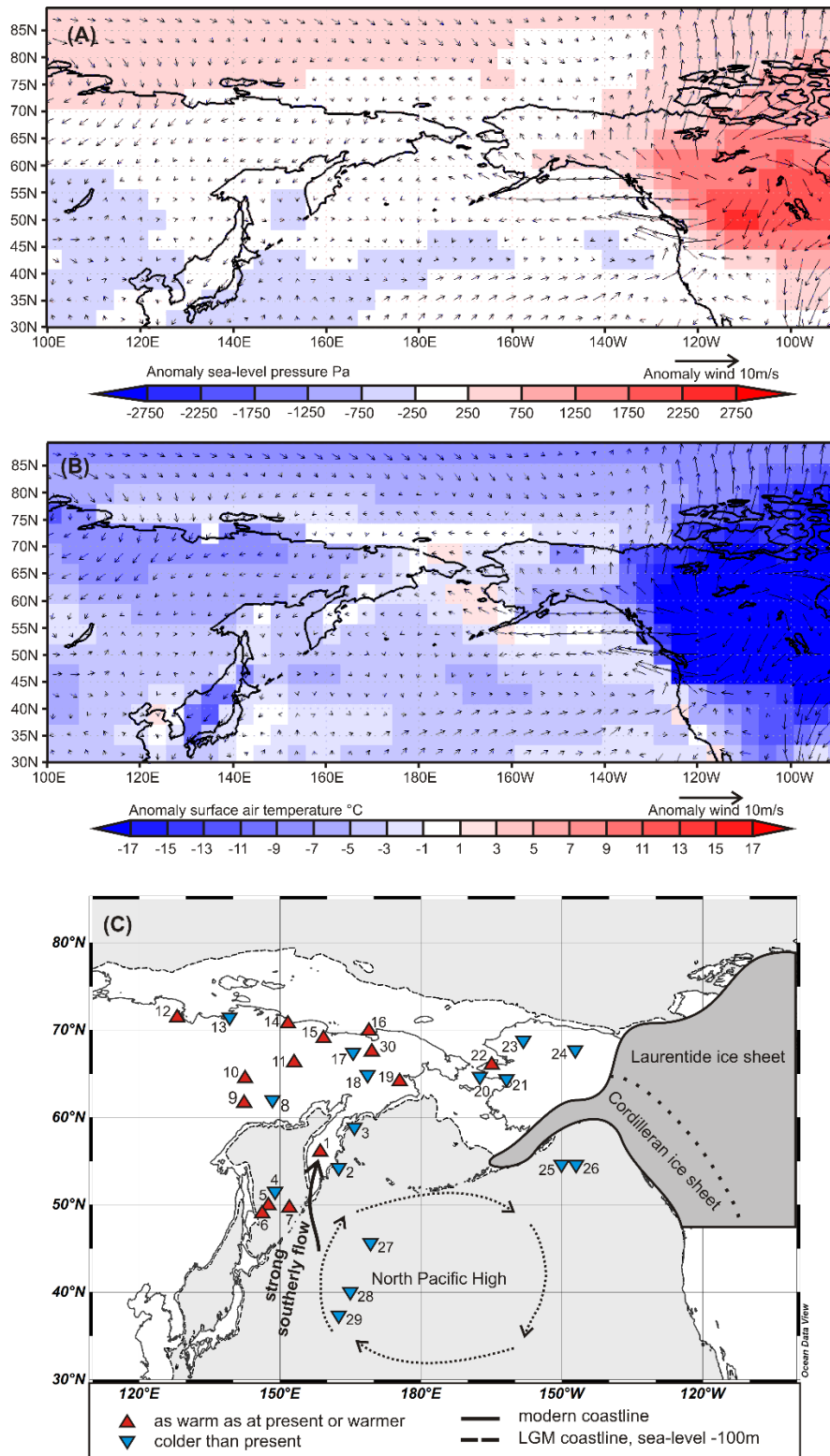


Figure 3.4. Comparison of proxy- and model-based inferences regarding glacial anomalies in temperature and atmospheric circulation over the N Pacific and Beringia relative to present. (A) COSMOS-simulation for the SLP-anomaly over Beringia and the N Pacific during the LGM (21 ka) relative to PI. Arrows represent the wind anomaly. Note that the model predicts a northerly anomaly over Kamchatka. (B) COSMOS-simulation for the SAT-anomaly together with the wind-anomaly. (C) Compilation of proxy based anomalies of summer air temperature in Beringia and of summer/autumn SST reconstructions in the N Pacific for the LGM. Sites and corresponding references are given in the appendix, Table A3.1. Dotted arrows sketch the general summer anticyclone over the N Pacific, the NPH. Based MAT_{ifs}, the NPH and associated southerly winds over the subarctic NW Pacific were stronger than at present (represented by solid arrow).

warm and moist air masses to Kamchatka summers on the Peninsula become warmer when the NPH and the associated warm southerly flow increase in strength (Mock et al., 1998). This modern analogue suggests that the LGM-NPH over the subarctic NW was stronger than today and the resulting warming effect may have balanced the cooling effects of CO_{2atm} and insolation. This atmospheric pattern could be explained by an increased thermal gradient between western/central Beringia and the N Pacific Ocean. While warm summers were widespread in western Beringia, the majority of sea surface temperature (SST) records from the open N Pacific and the Bering Sea indicate colder conditions during the LGM (Figure 3.4.A; deVernal and Pedersen, 1997; Seki et al., 2009, 2014; Kiefer and Kienast, 2005; Harada et al., 2004; 2012; Maier et al., 2015; Meyer et al., submitted b). Under the assumption that alkenone-based reconstructions of LGM SST in the Sea of Okhotsk are biased, also the Sea of Okhotsk may have been 4-5°C colder than at present as suggested by TEX^L₈₆-based SST reconstruction (Seki et al. 2009; 2014). An increased thermal gradient between the subarctic N Pacific and western Beringia would translate into an increased pressure gradient between the low-pressure over western Beringia and the high pressure over the subarctic NW Pacific, and in response the southerly flow over the Kamchatka would have intensified relative to today. (Figure 3.4C).

3.5.2.2.1. Comparison to the COSMOS-simulations

These inferences contrast with results from the climate simulations with COSMOS. For JJA the model predicts a decrease in SLP over the NW Pacific suggesting that the southerly flow at the western edge of the NPH was reduced rather than strengthened (Figure 3.4A). The weakening of the southerly flow is also discernable in the anomaly of the major wind-patterns over the NW Pacific (Figure 3.4.A) as a small northerly anomaly occurs north of Kamchatka (Figure 3.4A). The weakening of the NPH is agreement with several other General Circulation Model (GCM) outputs, which consistently predict a reduction in SLP over the N Pacific (Kutzbach and Wright, 1985; Bartlein et al., 1998; Dong and Valdes, 1998; Vetteoretti et al., 2000; Yanase and Abe-Ouchi, 2007; Alder and Hostetler, 2015). According to the climate synopsis by Mock et al (1998) a northerly anomaly would have caused summer cooling on Kamchatka. It has been suggested that a pronounced positive SLP-anomaly and a persistent anticyclone over the American continent resulted in reduced SLP over the Western North Pacific (Yanase and Abe Ouchi, 2010). The positive SLP-anomaly and the strong anticyclonic tendencies are clearly present in the COSMOS simulation of SLP and wind-patterns (Figure 3.4A) and were also simulated by several other GCMs (e.g. Yanase and Abe-

Ouchi, 2007; 2010; Alder and Hostetler, 2015). Its development was attributed to the presence of extensive ice sheets on the American continent (Yanase and Abe-Ouchi, 2010), which would have caused severe cooling of the overlying atmosphere. Considering the consistency of different GCMs, the anticyclonic anomalies over North America as well as resulting cyclonic anomalies over the N Pacific seem to be a robust feature of the glacial atmospheric circulation. As this contrast with the inferences made from the MAT_{ifs}-record, one may speculate that the effect of the ice-caps on the NPH mainly influenced the NE Pacific and that a strengthened anticyclone (as suggested in sec. 5.2.2) was restricted to the subarctic NW Pacific. In other words, the NPH may have shifted westward in response to the presence of a strong anticyclonic anomaly over the LIS.

The COSMOS-simulation also contrasts with the temperature patterns in western Beringia suggested by proxy-based climate reconstructions (see. Sec. 5.1) as summers were simulated to be colder than at present on Kamchatka and in Siberia (Figure 3.4B). However, in small parts of the formerly exposed BLB and the arctic shelves temperatures level or exceed PI-conditions (Figure 3.4B). These positive anomalies in the model are probably associated with the dominant anticyclonic flow over North America and the associated easterly to southeasterly winds over south-Alaska and the BLB (Figure 3.4B). The exposure of the Siberian Shelf may also have an effect. However, these anomalies are restricted to a relatively small area and are not comparable with the widespread warming tendencies over Siberia, which are visible in the proxy-compilation (Figure 3.4B, C). Given the discrepancies between proxy-based temperature reconstructions for Siberia and computer-model simulations, the thermal gradient between western Beringia and the subarctic NW Pacific may also differ. In the model simulation the thermal contrast between land and ocean tends to become smaller since the negative temperature anomaly over western Beringia for the most part is more pronounced than over the subarctic N Pacific (Figure 3.4B). This contrasts with the proxy compilation according to which the thermal gradient was increased relative to present (Figure 3.4C). As the model predicts a reduction of the thermal gradient the preconditions for the increased landward air-flow are not given. In contrast a reduced thermal gradient would support a northerly anomaly, which is in accordance with the simulated wind-patterns over Kamchatka (Figure 3.4A). Hence, the discrepancies between proxies and model-outputs concerning glacial summer temperature over western Beringia potentially entail the mismatch regarding the atmospheric circulation patterns over the NW Pacific.

3.5.2.3. *The deglaciation (18 ka-10 ka BP)*

The deglacial short-term variability strongly resembles the climate development in the N Atlantic as MAT_{ifs} follows the deglacial oscillations recorded in the NGRIP- $\delta^{18}\text{O}$ (Figure 3.2b, i), particularly after 15 ka BP. MAT_{ifs} clearly mirrors the Bølling/Allerød (B/A)-interstadial, the Younger Dryas (YD)-cold reversal and the subsequent temperature increase into the Preboreal (PB; Figure 3.2b, i). This similarity suggests a strong coupling with climate change in the N Atlantic realm and hence variations in the AMOC-strength. The pronounced response to N Atlantic climate change is in line with the temperature development in the surrounding seas where the majority of climate-records shows a Greenland-like pattern (Ternois et al., 2000; Seki et al., 2004b; Max et al., 2012; Caissie et al., 2010; Praetorius and Mix, 2014; Meyer et al., submitted b). This in-phase variability is assumed to result from atmospheric teleconnections between the N Atlantic and the N Pacific Oceans (e.g. Manabe and Stouffer, 1988; Mikolajewicz et al., 1997; Vellinga and Wood, 2002; Okumura et al., 2009; Chikamoto et al., 2012; Max et al., 2012; Kuehn et al., 2014). While the effects of an atmospheric coupling with the N Atlantic are undoubtedly present between 15 and 10 ka BP their relevance is questionable during Heinrich Stadial 1 (HS1). The cold-spell between 18 ka BP and 14.6 ka BP as evident in the MAT_{ifs} record may coincide with the HS1 in the N Atlantic but initiates 2 ka earlier than in NGRIP- $\delta^{18}\text{O}$. Considering that also SST records from the Western Bering Sea indicate that the Heinrich-equivalent cold-spell commenced at ca. 16.5 ka BP (site 114KL, Meyer et al., submitted b), the event in MAT_{ifs} is probably not associated with climate change in the N Atlantic (Figure 3.2b, g). This temporal offset cannot be explained by age-model uncertainties in core 12KL since the error (1σ) of the calibrated radiocarbon ages is smaller than 100 yrs (Max et al., 2012). If the cooling was not associated with climate change in the N Atlantic, it could perhaps represents a local event on Kamchatka, and potentially western Beringia, marking the abrupt end of the warm LGM-conditions. Since, to the knowledge of the authors, such an event is not reported in the terrestrial realm of western Beringia, it is difficult to identify the driving processes.

A clear similarity between MAT_{ifs} and NGRIP- $\delta^{18}\text{O}$ establishes at ca. 15 ka BP. This has recently been described for the SST in the marginal NW Pacific (Meyer et al., submitted b) reconstructed for the same core site as investigated in the present study (site 12KL, Figure 3.2h). This record implies that the climate of the Kamchatka Peninsula until 15 ka BP was tied to the climate change in the NW Pacific rather than to climate change in the Western Bering Sea (Figure 3.2). For SST this pattern was explained by accumulation of AS waters in

the NW Pacific, which likely overprinted the effect of the atmospheric teleconnection by linking the western and the eastern basins of the N Pacific (Meyer et al., submitted b). Hence, the effect of the AS may have also determined temperature evolution on Kamchatka during the early deglaciation, restricting the teleconnection to the period after 15 ka BP.

The clear and constant impact of N Atlantic climate change between 15 and ca. 10 ka BP on Kamchatka is in agreement with palynological data from the Kankaren Range/Northeast Siberia (Figure 3.1a) where abrupt climatic changes corresponding to the B/A and the YD are reported (Anderson and Lozhkin, 2015). Abrupt warming at the onset of the B/A is also evident in a high resolution record from Lake Elikchan 4 (Lozhkin and Anderson, 1996; Kokorowski et al., 2008b) and may indicate a linkage to N Atlantic climate change. However, a climatic reversal equivalent to the YD is often absent in records from northeast Siberia (east of 140°N and north of 65°N; Figure 3.1A; e.g. Lake Jack London, Lake El'Gygytgyn and Wrangel Island; Lozhkin et al., 1993, 2001, 2007; Lozhkin and Anderson, 1996; Nowaczyk et al., 2002; Nolan et al., 2003, Kokorowski et al., 2008a,b), as compiled by Kokorowski et al. (2008a). By contrast, palynological data from Siberia (e.g. Lakes Dolgoe, Smorodynovoye and Ulkhan Chabyda, Figure 3.1A) indicates that a YD climatic reversal was present west of 140°N (Pisaric et al., 2001; Anderson et al., 2002, Kokorowski et al., 2008a). This east-west gradient was explained by a westward shift of the East Asian Trough (normally situated over the central Beringian coast; Mock et al., 1998) which caused cooling in west of 140°N by enhancing cold northerly winds, and together with an anticyclone over the Beaufort Sea brought warming through stronger easterlies into the region (Kokorowski et al., 2008a). The presence of a YD-cold reversal on Kamchatka and in the Kankaren Range implies that the southeastern edge of Siberia was probably not affected by the shifting EAT. Several general circulation models investigating the nature of teleconnections between the N Atlantic and N Pacific realms suggest that the westerly Jet played an important role by acting as heat-conveyor between the N Atlantic and the N Pacific-Oceans (e.g. Manabe and Stouffer, 1988; Okumura et al., 2009). Considering the modern average position of the westerly Jet (between 30 and 60°N) Kamchatka likely received the YD-cold reversal through the westerlies. Also, relatively strong marine influences from the N Pacific may have induced cooling on Kamchatka and may have also affected the Kankaren Range. Together with the atmospheric patterns suggested by Kokorowski et al. (2008a), northward decreasing influences of the westerly Jet and the Pacific Ocean north may explain north-south differences in northeast Siberia.

3.5.2.4. *The Holocene*

Although not quite pronounced in magnitude, the long-term MAT_{ifs} evolution during the Holocene is characterized by a mid-Holocene Thermal Maximum (HTM) between 8 and 4 ka BP which is followed by neoglacial cooling (Figure 3.2b). This long-term development is in good agreement with existing climate records from central and southern Kamchatka (Figure 3.2j) where pollen-based records indicate warm and wet conditions between 8 and 5 ka BP, which are associated with the HTM (Dirksen et al., 2013). According to MAT_{ifs} the climate deterioration after the HTM started at ca. 4 ka BP. This timing is consistent with diatom-based climate reconstructions as well as chironomid-based temperatures from central and south Kamchatka (Dirksen et al., 2013; Hoff et al., 2014) and with re-advancing mountain glaciers (Savoskul et al., 1999, Barr and Solomina, 2014). As already discussed in previous studies this long-term temperature development is thought to respond to changes in mean summer insolation (Figure 3.2b, e, j). As summarized by Brooks et al. (2015), the timing of the HTM (ca. 9-4 ka BP) on Kamchatka as well as in southern parts of eastern Siberia is delayed compared to northern parts of Chukotka and Siberia where the HTM initiated at 9-8 ka BP (Biskaborn et al., 2012 and references therein; Nazarova et al., 2013b; Anderson and Lozhkin, 2015). Since a similar delay of the HTM has been found in northern Europe (Seppä et al., 2009), Brooks et al. (2015) concluded that the climate on Kamchatka was connected with the N Atlantic realm by an atmospheric coupling. Furthermore, the fact that Andrén et al. (2015) detected an 8.2 cooling-event in pollen-based climate records from Kamchatka also points to a linkage with N Atlantic climate.

Hence, it seems that the atmospheric linkage that determined climate variability during the deglaciation likely persisted into the Holocene where it acted as an important driver for long-term climate changes as well as for abrupt, short-lived climatic events.

3.6. Summary and Conclusion

Based on the CBT/MBT^{*}-palaeothermometre a continuous LGM-to-late Holocene record of summer-temperature in Kamchatka is presented. The temperature evolution and the driving mechanisms were investigated. The record allows inferences for the glacial atmospheric circulation patterns (i) and to describe how regional climate drivers (such as oceanic and atmospheric circulation) as well as global and supra-regional drivers (including CO_{2atm}, summer insolation and N Atlantic climate variability) influenced the climate change on Kamchatka (ii). The findings can be summarized as follows:

- (i) LGM-summer temperatures were as high as at present. The warm summers likely result from a change in the regional atmospheric circulation including a stronger-than-present southerly winds over Kamchatka as a result of a stronger-than-present anticyclone over the subarctic NW Pacific. This was potentially driven by increased thermal gradients between western Beringia and the N Pacific Ocean. The temperature reconstruction as well as the inferences for atmospheric circulation contrasts with model simulations, which predict widespread cooling over Siberia and Kamchatka, and a weakening of the NPH over the NW Pacific together with a reduction of southerly winds over Kamchatka. These discrepancies underline the need of further investigations of the LGM-climate in the NW Pacific realm using environmental indicators and model simulations. During the LGM the warming effect of the altered regional atmospheric circulation likely balanced the cooling-effects of lowered CO_{2atm} and summer insolation.
- (ii) Abrupt millennial-scale fluctuations characterize the deglacial temperature development and represent the most prominent temperature changes during the past 20 ka. A first abrupt cooling-event at 18 ka BP marks the end of the warm LGM conditions and is likely caused by regional climate change, the origin of which cannot be identified, yet. From 15 ka onwards the temperature variations are obviously linked to climate change in the N Atlantic, presumably via rapid atmospheric teleconnections, as the B/A-interstadial and the YD cold reversal are clearly present. Regional differences regarding the presence of a YD-cold reversal in Siberia are possibly related to the position of the westerly Jet. During the Holocene the atmospheric linkage with the N Atlantic remained active and together with summer insolation is a primary driver for the long-term temperature development.

Acknowledgments

The study was part of a PhD project funded by the Helmholtz association through the President's Initiative and Networking Fund and is supported by GLOMAR – Bremen International Graduate School for Marine Sciences. Core SO201-2-12KL was recovered during cruise SO201-2 which took place in 2009 within the frame of the German-Russian research project “KALMAR” – Kurile-Kamchatka and Aleutian Marginal Sea Island Arc Systems: Geodynamic and Climate Interaction in Space and Time”. We thank the Master and the crew of R/V SONNE for their professional support during the cruise. Dirk Nürnberg is thanked for providing sample material. Alexander Weise is acknowledged for his assistance on the geochemical sample preparation in the laboratories at the University of Bremen. The

data obtained during this study are available online on the “Pangaea”-database (www.pangaea.de).

Appendix A - 3

Table A 3.1. Sites and references for the data compiled in Figure 3.4 C.

No.	Site	Region	Proxy	Reference
1	SO201-2-12KL	NW Pacific/Kamchatka	CBT/MBT'	This study
2	SO201-2-12KL	NW Pacific	TEXL86	Meyer et al., submitted b
3	SO201-2-114KL	Western Bering Sea	TEXL86	Meyer et al., submitted b
4	MR0604-PC7	Sea of Okhotsk	UK'37	Seki et al., 2009, 2014
5	XP98-PC2	Sea of Okhotsk	UK'37	Seki et al., 2004
6	XP98-PC4	Sea of Okhotsk	UK'37	Seki et al., 2004
7	MR00K03-PC04	Sea of Okhotsk	UK'37	Harada et al., 2004, 2012
8	unknown	Sosednee Lake/Siberia	pollen	Lozhkin et al., 1993
9	unknown	Oymyakon Depression/Siberia	beetle	Berman et al. (2011)
10	unknown	Middle stream of Indigirka River/Siberia	beetle	Berman et al. (2011)
11	unknown	Lower and middle reaches Kolyma River/Siberia	beetle	Berman et al. (2011)
12	Mkh	Bykovski Peninsula/Siberia	pollen/beetle	Kienast et al. (2005); Sher et al. (2005)
13	YA02-Tums1	Yana lowlands/Siberia	pollen	Pitul'ko et al. (2007)
14	unknown	Indigirka Lowland/Siberia	beetle	Alfimov and Berman, (2001); Kieselev (1981)
15	unknown	Kolyma Lowland/Siberia	beetle	Alfimov and Berman, (2001); Kieselev (1981)
16	unknown	Ayon Island/Siberia	beetle	Alfimov and Berman, (2001); Kieselev (1981)
17	PG1351	Lake El'Gygytgyn	pollen	Lozhkin et al. (2007)
18	unknown	Markovo/Siberia	beetle	Alfimov and Berman, (2001); Kieselev (1981)

Continued on the next page

No.	Site	Region	Proxy	Reference
19	unknown	Anadyr River middle stream /Siberia	beetle	Berman et al. (2011);
20	Bering Shelf 78-15	Shelf off Seward Peninsula/BLB	beetle	Elias et al. (1996, 1997); Elias (2001)
21	Zagoskin Lake	western Alaska	chironomids	Kurek et al. (2009)
22	Bering Land Bridge Park	Seward Peninsula/Alaska	beetle	Elias et al. (2001)
23	Burial Lake	St. Michael Island /BLB, Alaska	chironomids	Kurek et al. (2009)
24	Bluefish	Bluefish Basin/Alaska	beetle	Mathews and Telka, (1997); Elias et al. (2001)
25	SO202-27-6	Gulf of Alaska	U ^K ₃₇	Maier et al. (2015)
26	PAR87A-10	Gulf of Alaska	dinocysts	deVernal and Pedersen (1997)
27	MR97-02 St. 8s	NW Pacific	U ^K ₃₇	Harada et al. (2004, 2012)
28	MR98-05 St. 5	NW Pacific	U ^K ₃₇	Harada et al. (2004, 2012)
29	MR98-05 St. 6	NW Pacific	U ^K ₃₇	Harada et al. (2004, 2012)
30	unknown	Chaun Depression/Siberia	beetle	Berman et al. (2011)

4. Manuscript III:

Linking glacier extent and summer temperature in NE Russia: Implications for precipitation during the Last Glacial Maximum

Vera D. Meyer^{1,2} and Iestyn D. Barr³

1: Alfred-Wegener-Institute, Helmholtz Centre for Polar and Marine Research, Bremerhaven, Germany

2: Department of Geosciences University of Bremen, Germany

3: Department of Geography, Archaeology and Palaeoecology, Queen's University Belfast, Northern Ireland

In preparation for Palaeogeography, Palaeoclimatology and Palaeoecology

Abstract

It is generally assumed that during the Last Glacial Maximum (LGM) dry climatic conditions in Northeast Russia inhibited the growth of large ice caps and restricted glaciers to mountain ranges. The Kamchatka Peninsula and the Kankaren Range are examples of two such locations. However, recent evidence has been found to suggest that glacial summers on Kamchatka and the Kankaren Range were as warm as at present while glaciers were more extensive than today. As a result, we hypothesize that precipitation must have been relatively high in order to compensate for the high summer temperatures and the resulting glacial ablation. We estimate precipitation abundance by mass balance calculations for the palaeoglaciers on Kamchatka and in the Kankaren Range using a degree-day-modelling approach. We find that, precipitation must have either equalled or exceeded the modern average, according to our mass-balance calculations by approximately 13-28%. We suggest that stronger than present southerly winds over the Northwest Pacific may have accounted for the abundant precipitation. The DDM-results imply that summer temperature rather than aridity limited glacier extent in the southern Pacific Sector of NE Russia during the LGM.

4.1. Introduction

An understanding of the extent of glaciers in East Asia during the Last Glacial Maximum (LGM), and an appreciation of the underlying controlling mechanisms are important for the palaeoclimate modelling community, as the presence of large ice-caps during this period would strongly impact climatic conditions in the North Pacific (N Pacific) region (Felzer et al., 2001, Bigg et al., 2008). Glacier extent in Northeast Russia (NE Russia) during the LGM has been controversially discussed in the literature. For a long time the idea that a large pan-arctic ice sheet stretched over Beringia dominated the scientific debate (Grosswald, 1988, 1998; Grosswald and Hughes, 2002; Grosswald and Hughes, 2005). However, this hypothesis was challenged by many studies in which Pleistocene moraines in NE Russia were dated. These studies provided evidence that Beringia (the region stretching from Siberia to Alaska) remained largely ice-free during the LGM, and that glaciers were restricted to mountain ranges and did not extend further than 20 km in length (Velichko et al., 1984; Arkhipov et al., 1986; Glushkova, 2001; Gualtieri et al., 2000; Gualtieri et al., 2003; Brigham-Grette et al., 2003; Zamoruyev, 2004; Stauch and Gualtieri, 2008; Barr and Clark, 2012). By now, the idea of limited mountain glaciation has become widely accepted, and it is generally supposed that the Beringian climate was too dry to allow ice sheet growth (e.g. Brigham-Grette et al., 2003). Interestingly, several proxy-based palaeoclimate studies indicate that in Siberia, and in parts of the formerly exposed Bering Land Bridge (BLB), summers were as warm as, or even warmer than under present-day conditions (Elias et al., 1992, 1996, 1997, 2001; Alfimov and Berman, 2001; Kienast et al., 2005; Berman et al., 2011; Anderson and Lozhkin, 2015; Meyer et al., submitted a). This applies also for Kamchatka, a mountainous Peninsula (attached to the south-eastern edge of Siberia Figure 4.1A, B), and the Kankaren Range, situated north of the Koryak Range (Figure 4.1A, C; Berman et al., 2011; Anderson and Lozhkin, 2015; Meyer et al., submitted a). Glacier reconstructions from these regions suggest that during the LGM glaciation was restricted to mountain-glaciers but was more extensive than during the Holocene (St. John and Krissek, 1999, Bigg et al., 2008; Barr and Clark, 2011; Barr and Solomina, 2014). If warm summers accompanied this comparatively extensive mountain-glaciation, annual precipitation was probably abundant so that snow accumulation could compensate for the temperature-induced ablation during the warm summers. If this was the case, glacial summer temperatures would have been an important limiting factor for ice-expansion in these areas during the LGM. This would challenge the prevailing view that ice extent was limited by the region's aridity.

In this paper we test this hypothesis by estimating precipitation on Kamchatka and in the Kankaren area during the LGM - performing mass-balance calculations for palaeo-glaciers in the Sredinny (Kamchatka) and Kankaren mountain ranges (Figure 4.1). This is conducted using a degree-day-modelling approach (DDM, e.g., Hughes and Braithwaite, 2008). The results provide a new view of palaeo-climatic conditions in the Pacific sector of Siberia (Figure 4.1A) during the LGM and the mechanisms controlling glaciation in the region.

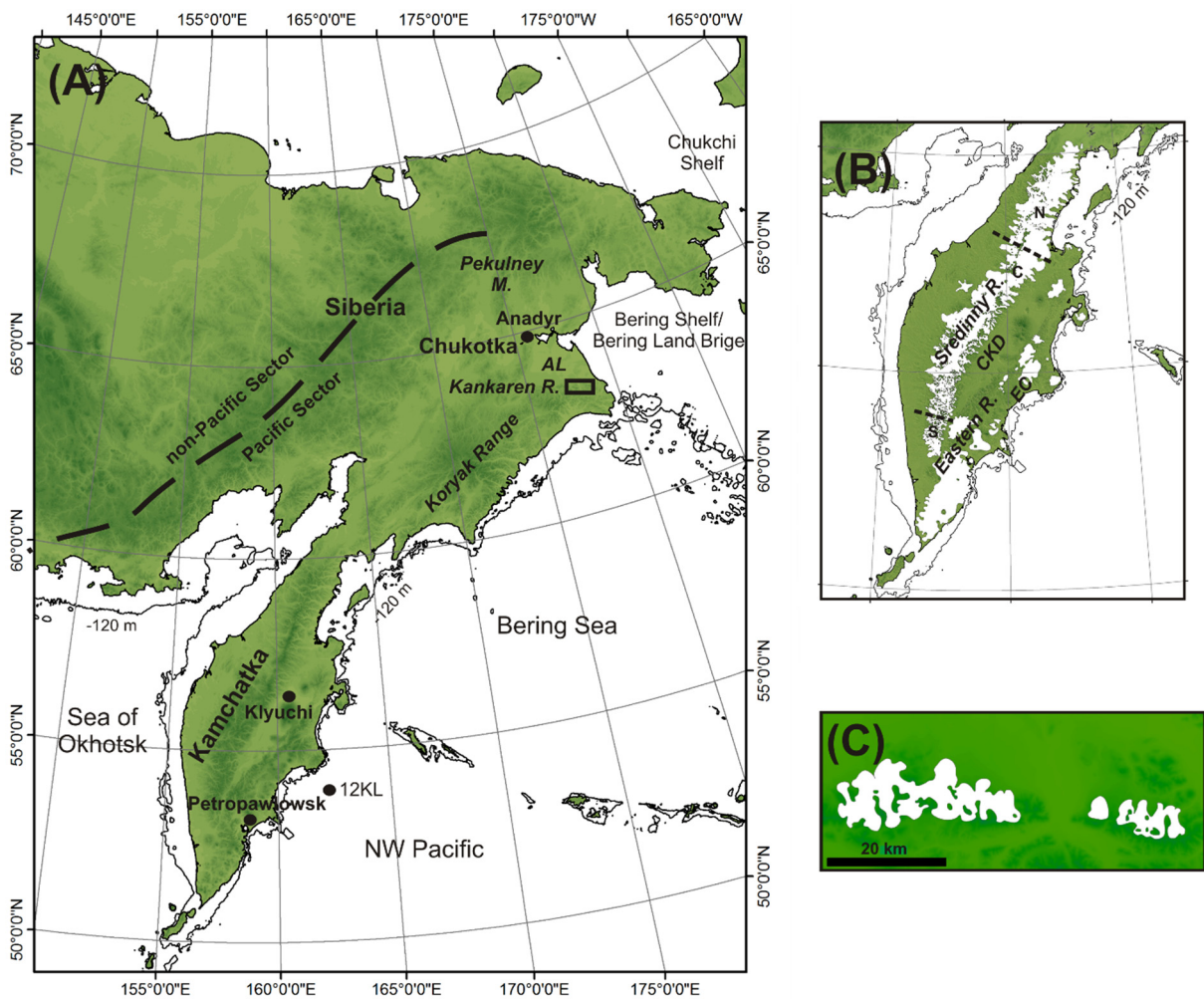


Figure 4.1. (A) Overview of Northeast Russia showing the regions mentioned in the text. The division into Pacific and non-Pacific sector is based upon Grosswald and Kotlyakov (1969). The LGM-shore line is indicated (solid line, sea-level ca. 120 m below present). M: Mountains; R: Range; AL: Anadyr Lowland. The rectangle marks the position of the Kankaren Range. (B) Glacier reconstruction in the Sredinny Range and the Eastern Range for the LGM after Barr and Clark (2011) and Barr and Solomina (2014) & references therein. EC: Eastern Coast; CKD: Central Kamchatka Depression. Dashed lines indicate the different sectors of the Sredinny ice field. N: northern sector, C: central sector, S: southern sector. (C) Reconstructed glaciation in the Kankaren Range during the LGM after Barr and Clark (2011).

4.2. Regional Setting

The climate in NE Russia is generally classified as strongly continental and characterized by warm summers, cold winters and strong aridity (Ivanov, 2002). A general gradient towards less extreme conditions exists from the interior towards the Pacific coast as the marine influence increases. Kamchatka and the Kankaren Range are part of the milder Pacific Sector (Figure 4.1A). Therefore, the climate is milder and wetter than in central Siberia. The general climatic conditions in NE Siberia are controlled by the interplay of the major atmospheric pressure systems over the North Pacific and the East Asian Continent. The winter climate is mainly determined by the presence of the Aleutian Low over the N Pacific and the Siberian High over Siberia. The atmospheric constellation lets northerly winds predominate over East Siberia which bring cold, arctic air masses. In summer, the North Pacific High develops over the North Pacific together with the East Asian Low over the continent. Southerly winds drive warm and moist maritime air masses to East Siberia (Mock et al., 1998; Shahgedanova et al., 2002; Yanase and Abe-Ouchi, 2007).

4.2.1. Kamchatka Peninsula/Sredinny Mountains

Kamchatka is bordered by the Sea of Okhotsk to the West, the Northwest Pacific to the Southeast and the Bering Sea to the East (Figure 4.1A). Its topography is characterized by strong variations in relief with lowlands along the coast and in the interior (Central Kamchatka Depression, CKD), and two major mountain Ranges, the Sredinny Range and the Eastern Range (Figure 4.1B). The Sredinny Range reaches a maximal altitude of 3621 m above sea-level (a.s.l.). The general climate of Kamchatka is cold maritime with cool and wet summers and mild, snowy winters (Dierksen et al., 2013). Mean July and January temperature of the entire Peninsula range from 10 to 15°C and from -8 to -26°C, respectively (Ivanov, 2002). In the coastal areas, precipitation is abundant throughout the year (ca. 900 mm yr⁻¹). Precipitation is highest in the mountain ranges where values typically range between 1200 mm yr⁻¹ and 1500 mm yr⁻¹, but can reach maximal values of 2000 mm yr⁻¹ in the southeast (Ivanov, 2002; Dierksen et al., 2013). In the interior valley, precipitation is lower (ca. 300 mm yr⁻¹) as the Mountain Ranges shield the marine influences. Today, small glaciers are only present at the highest peaks of the mountain ranges (Solomina and Calkin, 2003; Ananicheva et al., 2008; Barr and Solomina, 2014). A glacier reconstruction by Barr and Clark (2011) suggests that during the LGM a continuous, mountain-centred ice field existed in the Sredinny Mountains (Figure 4.1B). Its outlet glaciers extended up to 80 km into the valleys and the ice-field covered 57,363 km² (Barr and Clark, 2011). End-moraines of potential LGM age also exist in the

Eastern Range. As accurate dates to clearly ascribe these Eastern Range moraines to MIS 2 are missing (Barr and Solomina, 2014) this paper focusses on the Sredinny Range alone.

4.2.2. *The Kankaren Range and adjacent Anadyr-Lowlands*

The Kankaren Range is attached to the northern flanks of the Koryak Range and faces the Anadyr-Lowlands (AL) in the North (Figure 4.1A). The Kankaren Mountains reach maximal altitudes of 1200 m a.s.l. Direct observations of modern climate conditions in the mountains themselves are lacking, as the closest climate station is situated in Anadyr which lies ca. 150 km further north (Barr and Clark, 2011), where average July, January and annual temperatures are 12.6°C, -26.7°C and -10.1°C (Anderson and Lozhkin, 2015). Precipitation values for the Kankaren Mountains are also lacking, though in the Anadyr region modern precipitation is ca. 475 mm yr⁻¹ (Glushkova, 2001). According to the glacier reconstruction by Barr and Clark (2011), the western part of the Kankaren range was covered by a mountain-centred ice-field during the LGM, while the eastern sector was occupied by a group of five valley glaciers (Figure 4.1C). The reconstruction revealed glaciers up to 7 km in length and a total ice covered area of 215 km².

4.3. Degree Day Modelling

4.3.1. *General Model setup*

In order to estimate the amount of precipitation necessary to sustain the reconstructed LGM glaciers in the Sredinny and Kankaren Ranges, we used the degree day modelling approach used by Barr and Clark (2011). This approach allows estimating the annual accumulation needed to balance annual ablation at the equilibrium line altitudes (ELA) of former glaciers (Braithwaite et al., 2006). A glacier's ELA is defined as the altitude where net annual accumulation and ablation are in equilibrium. In the DDM approach, the annual melt at the glaciers ELA is calculated from the sum of daily melt values. The latter are dependent on daily air temperatures at the palaeo ELA. Assuming that the annual distribution of temperatures is described by a sine curve, (eq. 1; Hughes and Braithwaite, 2008; Hughes, 2009) daily temperatures at the palaeo-ELA can be calculated as follows (eq.1):

$$T_d = A_y \sin\left(\frac{2\pi d}{\lambda} - \phi\right) + T_a \quad (\text{eq. 1}),$$

where T_d is the daily mean temperature, A_y is the amplitude of annual temperature variations (1/2 of the total annual temperature range), d the ordinal day, λ is the period (365 days), ϕ is

the phase angle of the sine curve (here 1.93 radians based on the assumption that temperature is maximal in July and minimal in January), and T_a is the mean annual air temperature.

After modelling temperatures for every day of the year, the daily melt (M_d) at the palaeo-ELAs was calculated as a function of daily mean temperature using a degree-day melt factor (f) of $4 \text{ mm d}^{-1} \text{ }^\circ\text{C}^{-1}$ (eq. 2).

$$M_d = T_d * f \quad (\text{eq. 2})$$

The sum of these daily melt values was then assumed to be equalled by accumulation (expressed in mm) at the ELA (since, at the ELA, annual accumulation = annual ablation).

4.3.2. *Setup of simulated scenarios for Kamchatka and in the Kankaren Range*

In order to estimate the LGM precipitation for Kamchatka and the Kankaren area, the model was applied to the palaeo-ELA data for the Sredinny Range and the Kankaren Range from Barr and Clark (2011). In the Sredinny Range, the model was run with the mean annual ELAs of the entire ice-field and with average ELAs for the southern sector, the central sector and the northern part (Figure 4.1B). In the Kankaren Range, an ELA gradient was not reconstructed, and the mean values (shown in Table 4.1) were adopted from Barr and Clark (2011). LGM conditions were simulated assuming that glacial summer temperatures (T_{July}) equal modern conditions (Beerman et al., 2011; Anderson and Lozhkin, 2015; Meyer et al., submitted a), but that winters were colder than at present (Meyer et al., 2002). Modern T_{July} (12°C , Table 4.1) were compiled from two different Kamchatkan climate stations, Klyuchi (56.32°N , 160.83°E) and Petropavlovsk (52.99°N , 158.66°E ; Figure 4.1A) which represent the continental climate of the CKD and the maritime conditions at the eastern coast (<http://en.climate-data.org>). These stations were chosen, as the temperature record is considered to reflect climate change in the CKD and the Eastern Coast (Meyer et al., submitted a). T_{July} for the Kankaren Range (13°C) were adopted from Anderson and Lozhkin, 2015). Since no proxy-based absolute estimates for annual or winter LGM-temperature exists for the Kankaren and Sredinny Ranges, climate-model data (Kim et al., 2008) were adopted. For eastern Siberia as a whole, this climate model predicts a decrease in mean annual air temperature (T_a) of ca. $6\text{-}14^\circ\text{C}$ at the LGM, relative to present. A_y was calculated according to equation 3 using both values for T_a to obtain maximal and minimal estimates. As the summer-temperature is assumed to equal modern, winters are warmer in the scenario based on the minimal amplitude than in the scenario with maximal amplitude.

$$T_a = T_{\text{July}} - A_y \quad (\text{eq. 3})$$

Adopted T_a , T_{July} , and A_y values for Kamchatka and the Kankaren area are shown in Table 4.1. As all temperature-data reflect the conditions approximately at sea-level, T_a was lowered using a lapse-rate of $0.63^\circ\text{C}/100\text{ m}$ altitude (Osipov, 2004) in order to obtain the mean annual air temperature at the palaeo-ELAs of the LGM glaciers reconstructed by Barr and Clark (2011).

4.4. Results

Results for precipitation and the duration of the ablation season for the minimal and maximal amplitudes (i.e., A_y) are given in Table 4.1. Precipitation based on the greatest temperature amplitude ($A_y = 25.5^\circ\text{C}$) are always lower than in its counterpart ($A_y = 17.5^\circ\text{C}$). If scenarios based on both temperature altitudes are considered, the model suggests that $1399\text{-}1698\text{ mm yr}^{-1}$ precipitation would be necessary to sustain the mean ELA (897 m.a.s.l.) of the entire ice field in the Sredinny Range (Table 4.1). The results for the average ELAs in the different sectors suggests an increasing palaeo-precipitation gradient from south to north. Average ELA of the southern sector requires the lowest accumulation ($1119\text{-}1350\text{ mm yr}^{-1}$) while accumulation is maximal in the northern part of the ice-field ($1590\text{-}1920\text{ mm yr}^{-1}$). In the central part the estimated accumulation is $1443\text{-}1742\text{ mm yr}^{-1}$ (Table 4.1).

Table 4.1. DDM temperature-setup for the LGM simulations and results for precipitation and the length of the ablation season. The model was run with minimal and maximal T_a , based on climate-model estimates from Kim et al. (2008). Summer-temperature data for the LGM was adopted from Beerman et al. (2011); Anderson and Lozhkin (2015), and Meyer et al. (submitted a), and Klyuchi and Petropawlowsk climate stations. Calculated precipitation for the Sredinny Range is compared to modern values for the mountain ranges on Kamchatka (modern precipitation data is taken from, Ivanov et al. (2002) and Dierksen et al. (2013)). Such a comparison is not possible for the Kankaren Range as data for modern precipitation in the mountains is not available.

Average ELA [m.a.s.l.]	LGM Sredinny R.								LGM Kankaren	
	1035 south	876 centre	808 north	897 mean	1035 south	876 centre	808 north	897 mean	575 mean	
$T_{July}[^\circ\text{C}]$	12	12	12	12	12	12	12	12	13	13
$T_a[^\circ\text{C}]$	-0.5	-0.5	-0.5	-0.5	-2.7	-2.7	-2.7	-2.7	-16.1	-24.1
$A_y[^\circ\text{C}]$	17.5	17.5	17.5	17.5	25.5	25.5	25.5	25.5	29.1	37.1
Ablation [days]	93	102	105	101	76	83	86	82	96	82
annual prec. [mm yr ⁻¹]	1350	1742	1920	1698	1119	1443	1590	1399	2359	2081
Prec. [% modern] (relative to 1200/1500 mm yr ⁻¹)	112/ 90	145/ 116	160/ 128	141/ 113	93/ 74	120/ 96	132/ 106	116/ 93	-	-

In the Kankaren range the average ELA at the LGM was 575 m a.s.l. according to Barr and Clark (2011). Given this value, the accumulation required to keep the glaciers in equilibrium is higher than in the Sredinny Range (2505-2210 mm yr⁻¹, Table 4.1).

Barr and Clark (2011) pointed out that annual precipitation cannot be directly compared to the calculated annual accumulation at the ELA, since annual precipitation comprises snow and rainfall, whereas annual accumulation at a glacier mainly reflects snowfall (since rain contributes little to the glacier growth). Precipitation during the ablation season (presumed to be dominated by rainfall) is therefore not included in the output of the DDM. The ablation season in all our scenarios ranged between 76-105 days (Table 4.1) meaning that the values for accumulation are a rough estimate for annual precipitation but likely slightly underestimate true values.

It should also be kept in mind that there are additional uncertainties in these palaeo precipitation estimates as several parameters are approximated in the modelling approach (e.g. the amplitude of temperature change) and slight variations in these values would change accumulation/precipitation estimates. Hence, the obtained results should only be regarded as order of magnitude approximations of LGM precipitation and of how it differed relative to today.

4.5. Discussion

4.5.1. Inferences for LGM precipitation relative to present

Precipitation-values corresponding to the ELAs of the Sredinny ice-field assuming the maximal LGM temperature-amplitude, fall in the range of modern precipitation values on Kamchatka (1200-1500 mm yr⁻¹; Ivanov, 2002; Dierksen et al., 2013). However, the result for the minimal amplitude (warmer winters) at the mean ELA of the entire ice-field, the northern sector and the center indicate that LGM precipitation exceeds the modern annual mean by 13, 28 and 16 %, respectively (calculated relative to modern value of 1500 mm yr⁻¹). The results from the Kankaren Range cannot be compared to modern values because modern precipitation-data are lacking in the area (see section 2). A comparison with Anadyr climate station is probably not sensible as the Anadyr Lowlands are situated in the rain shadow of the Kankaren and Koryak Ranges (Mock et al., 1998). However, since the calculated precipitation amounts for the Kankaren are higher than the results for the Sredinny Mountains (see Table 4.1) the values might be assumed to exceed the modern average in the Kankaren Range.

These results indicate that annual precipitation must have been at least as high as today or must have even exceeded the modern average if summers were as warm as present while mountain glaciers were more extensive than today. An assessment of whether precipitation on Kamchatka during the LGM was greater than today cannot be made on the basis of proxy-data, since data is not available for the LGM or the period of deglaciation (i.e., leading into the early Holocene). In the Kankaren Range it is unclear whether or not published proxy-based precipitation reconstructions are in agreement with the DDM results from the present study. Pollen-based vegetation reconstructions provide evidence for the presence of snow-bed plant-communities indicating abundant snow-accumulation during the LGM. Although this is generally in concert with the presence of glaciers and abundant precipitation (as suggested by the DDM), the pollen assemblages also contrast with our findings as the paucity of shrubs in the region points to reduced available moisture (relative to today) implying that the LGM-climate of southern Chukotka was more arid than at present (Anderson and Lozhkin, 2015). However, NE-Russia's moisture may have been trapped in glaciers and ground ice during this period (Sergin and Scheglova, 1976; Alfimov and Beerman, 2001), meaning that precipitation, even if abundant, may not have been available to the plants. The sparseness of records and the uncertainty in the Kankaren Range indicates that further records of glacial precipitation in the region are required in order to confirm or discount our hypothesis.

However, the DDM-results from this investigation certainly suggest that warm summer temperature have the potential to limit glacier growth in the Pacific Sector of Siberia, in contrast with prevailing view that ice-sheet expansion was hampered by increased aridity (Seigert et al., 2001; Brigham-Grette et al., 2003; Stauch and Gualtieri, 2008; Barr and Clark, 2011; Barr and Spagnolo, 2013).

Summer temperature may have also limited glacier growth in the Pekulney Mountains (north of the Anadyr-Lowlands, Figure 4.1A) since DDM-results from Barr and Clark (2011) suggest that precipitation must have been 126% increased relative to modern conditions, if summer temperature was 3.1-4.1°C lower than at present (Alfimov and Beerman, 2001; Barr and Clark, 2011). However, LGM temperature reconstructions for the Pekulney-area vary considerably (Alfimov and Beerman, 2001; Lozhkin et al., 2007; Barr and Clark, 2011), and calculations based on a temperature reduction of 6.4°C (Lozhkin et al., 2007), would suggest that annual LGM accumulation was ca. 40% less than the modern mean, supporting the hypothesis that aridity hampered glacier growth (Barr and Clark, 2011). The ambiguity in the Pekulney Mountains requires further records in air temperature in the region (Barr and Clark,

2011). Nevertheless, based on the results adopted for the Sredinny and Kankaren Ranges it seems likely that temperature was the limiting factor for ice-sheet growth in the southern Pacific Sector of NE Russia.

4.5.2. *Possible mechanisms for increased annual precipitation at the LGM*

Glacier growth is mainly dependent to the snow accumulation/precipitation in winter. However (as outlined in section 5.1.), in the Beringian/N Pacific realm several palaeo-environmental indicators argue for a decrease in winter and annual precipitation during the LGM (relative to present) rather than an increase (as suggested in section 5.1.). During the LGM, the Bering and Chukchi-Shelves were exposed, reducing marine influences in western and central Beringia (Laukhin et al., 2006; Barr and Clark et al., 2011; Yanase and Abe-Ouchi, 2007), and proxy-based studies point to extensive sea-ice coverage (Sakamoto et al., 2005; Caissie et al., 2010; Smirnova et al., 2014) which also suggests that winter sea surface temperatures were lower than at present. These factors would reduce evaporation over the marginal N Pacific (Sancetta, 1983). Also, a study based on climate-models found no indication for increased winter precipitation in the N Pacific realm during the LGM (Yanase and Abe-Ouchi, 2007). Additionally, the growth of ice-sheets elsewhere in the Northern Hemisphere is presumed to have deprived NE Russia of moisture (e.g. Seigert et al., 2001; Stauch and Gualtieri, 2008). These factors are essentially the basis of the aridity-hypothesis (e.g. Brigham-Grette et al., 2003). Hence, the existing palaeo-environmental indicators generate a palaeoclimatic scenario for the NW Pacific realm in which extensive mountain glaciation, warm summers and arid conditions coexisted. However, this picture appears to contradict inferences made from the DDM approach adopted here. As such, the assertion that extensive glaciers and warm summer temperatures coincided at the LGM is brought into question. However, uncertainties in the chronologies of either temperature or glaciation may potentially explain the discrepancies; yet the chronology for the marine sediment-core on which the temperature record for Kamchatka was established, accurately defines the LGM in the record (Max et al., 2012; Meyer et al. submitted a,b). In terms of glaciation, a small number of radiocarbon ages in the Sredinny Mountains and cosmogenic dating (^{36}Cl) in the Kankaren Range assigns the terminal glaciation to the LGM and the late glacial (Braitseva et al., 1968; Melekestsev et al., 1970; Gualtieri et al., 2000). Moreover, ice rafted detritus (IRD), which evidently originated from the Kamchatka Peninsula (St John and Krissek, 1999), was constantly deposited in the NW Pacific during MIS 2 and is no longer found after ca. 15 and 14 ka BP (St. John and Krissek, 1999; Kiefer et al., 2001; Bigg et al., 2008; Gebhardt et al.,

2008). This suggests that outlet glaciers from the eastern coast of Kamchatka reached the shore-line during the LGM - indicating extensive glaciation (Figure 1B). Therefore, uncertainties in the glaciation-chronology can probably also be ruled out (i.e., they fail to account for the discrepancies noted in this paper). Since Meyer et al. (submitted a) consider a bias in the temperature record unlikely, the coexistence of warm summers and extensive mountain glaciation during the LGM seems likely and the view of abundant precipitation is supported.

Interestingly, Meyer et al. (submitted a) suggested that the warm summers on Kamchatka resulted from stronger-than-present southerly winds over the Northwest Pacific due to a strengthening or a westward displacement of the North Pacific High (NPH). Besides summer warming, increased advection of maritime air masses from the south simultaneously leads to more precipitation during the summer months in southeast Siberia, as summarized in the climate synopsis for Beringia by Mock et al. (1998). Given this interpretation, the temperature record may be an indirect indication for wet or maybe wetter-than-present conditions on the Peninsula/Coastal Siberia during the summer season. Unfortunately, no direct proxy-based reconstruction for precipitation is available for Kamchatka, so this assumption needs to be tested in the future. However, increased precipitation in the summer months contrasts with several studies utilising General Circulation Models, which predict that summer precipitation in East Asia was significantly reduced during the LGM (ca. 30-60%; Budiko et al., 1992; Velichko, 1993; Yanase and Abe-Ouchi, 2007). Yanase and Abe-Ouchi (2007) suggested two underlying mechanisms: (I) weakened advection of maritime air masses to the East Asian coast in response to a weakened NPH. (II) A reduction of precipitable moisture as a consequence of reduced evaporation over the NW Pacific due to lowered SST. (I) can be challenged by the proxy-based inference for increased southerly flow over Kamchatka (Meyer et al. submitted a). However, (II) seems to be a robust scenario since various SST records from the open North Pacific (south of 45°N) show lowered temperature during the LGM (e.g. Harada et al., 2012). However, in the marginal NW Pacific, in the vicinity of Kamchatka (site 12KL, Figure 4.1A) summer SST was probably only 1°C lower than at present (Meyer et al., submitted b). This is in accordance with model simulations which indicate that the thermal anomaly was relatively weak north of 50°N (Yanase and Abe-Ouchi, 2007). Hence, evaporation over the subarctic NW Pacific potentially did not differ significantly from present. According to alkenone-based SST records the same may have applied for the Sea of Okhotsk, since these records suggest that glacial temperatures in the area were the same as at present (Seki et al., 2004; Harada et al., 2012). However, these records are suspected to be

biased by shifting production-seasons of Coccolithophores (e.g. Seki et al., 2004b, 2009), a hypothesis which is supported by SST reconstructions based on TEX^L₈₆ (another SST-proxy) which indicate a cooling of ca. 5°C relative to modern (Harada et al., 2012; Seki et al., 2014). Nevertheless, in the subarctic NW Pacific little changes in evaporation (between LGM and present) combined with increased southerly winds in the subarctic NW Pacific may have resulted in increased precipitation in the southern Pacific sector of Siberia. So, summer precipitation may have mainly accounted for the precipitation necessary to sustain the glaciers during the LGM. Considering that the DDM does not include precipitation of the ablation season as it would fall as rain at the ELA, this scenario is difficult to envisage. However, if LGM-winter precipitation is unlikely to have been increased relative to present, increased summer precipitation must have significantly contributed to the glacier growth. Potentially, abundant snow accumulation occurred above the ELA even during the summer season. Additionally, a short summer season/ablation season may have supported glacier stability by limiting the total ablation. However, since palaeo data for LGM temperatures through the annual cycle do not exist for Kamchatka, this hypothesis is difficult to test, yet.

4.6. Summary and Conclusion

As evidence exists that LGM-summers in Kamchatka and the Kankaren Range were as warm as at present while mountain glaciation was more extensive than today, we hypothesized that, during this period, precipitation must have been abundant and that summer-temperature limited ice-sheet growth in the Pacific Sector of NE Russia. Our DDM-results support this hypothesis indicating that annual precipitation at the LGM was either equal to, or higher than, the modern mean on the Kamchatka. This finding is in contrast to the prevailing view that strong aridity restricted glaciation to the mountain ranges in NE Russia during the LGM. It seems possible that summer-precipitation was increased relative to today due to stronger southerly winds and relatively warm SST in the marginal NW Pacific, and this may have resulted in heavy snowfall above the ELA, allowing glaciers to develop and persist despite warm summer temperatures. Additionally the summer season may have been notably short (limiting total ablation). However, the majority of palaeo-environmental indicators from Siberia and the subarctic N Pacific point to dryer-than-present conditions in the NW Pacific realm at the LGM, particularly during winter. As winter precipitation is more important for glacier growth, than summer precipitation, it is questionable whether summer precipitation at the LGM accounted for the relatively high annual precipitation suggested by the DDM. In light of this, the coincidence of warm summers, decreased annual and/or winter precipitation

and extensive mountain glaciation provides a conflicting picture of LGM-palaeoenvironmental conditions in NE Russia—highlighting the necessity to further investigations of the regions glacial and climatic history.

Acknowledgements

This study was conducted within the frame of a PhD-project which was funded by the by the Helmholtz association through the President's Initiative and Networking Fund. GLOMAR – Bremen Graduate School for Marine Sciences is thanked for funding V. Meyer's research stay at Queen's University Belfast which allowed the realization of the project. The staff of the department of Geography, Archaeology and Palaeoecology at Queen's University Belfast are thanked for their kind support during the research stay.

5. Manuscript IV:

Increased export of ^{14}C -depleted terrigenous organic matter into the NW Pacific and the Western Bering Sea during deglacial permafrost decomposition in Beringia

Vera D. Meyer^{1,2}, Jens Hefter¹, Enno Schefuss³, Ralf Tiedemann¹, Rainer Gersonde¹ and Gesine Mollenhauer^{1,2,3}

1 Alfred-Wegener-Institute Helmholtz Center for polar and marine research, Bremerhaven, Germany

2 Department of Geosciences, University of Bremen, Bremen, Germany

3 MARUM – Center for Marine Environmental Sciences, Bremen, Germany

In preparation for Quaternary Science Reviews

Abstract

During the last deglaciation warming and sea-level rise likely triggered large-scale decomposition of permafrost soils in the Northern Hemisphere. Resulting release of ^{14}C -depleted carbon is assumed to have contributed to rising atmospheric carbon dioxide ($\text{CO}_{2\text{atm}}$) and declining atmospheric radiocarbon activity ($\Delta^{14}\text{C}_{\text{atm}}$), particularly at 14.6 ka BP. However, the impact of permafrost-degradation is not well understood as the timing of the carbon release is poorly constrained. In order to trace mobilization-events of ^{14}C -depleted terrigenous organic matter (OM) and permafrost decomposition on the Kamchatka Peninsula, we analyzed mass accumulation rates and the radiocarbon activity of leaf-wax lipids in two sediment cores from the Western Bering Sea and the Northwest Pacific. We find that enhanced mobilization of nearly ^{14}C -free carbon commenced during the Heinrich Stadial 1 and was likely triggered by retreating American ice-sheets and the associated meltwater-runoff through the Yukon River. Afterwards, deglacial mobilization of ^{14}C -depleted carbon was dominantly controlled by sea-level rise and permafrost erosion during shelf-flooding. Enhanced OM-export from Kamchatka associated with thawing of permafrost likely initiated during the second half of the Bølling/Allerød-interstadial and peaked during the Younger Dryas (YD). Increased OM-export from the Kamchatka region ends at 9 ka BP. The mobilization events lag the rapid $\text{CO}_{2\text{atm}}/\Delta^{14}\text{C}_{\text{atm}}$ changes at 14.6 ka BP suggesting that the region can be ruled out as drivers. Instead, carbon mobilized from degrading permafrost may have been a source of ^{14}C -depleted CO_2 during the YD.

5.1. Introduction

During the last glacial termination atmospheric carbon dioxide rose by about 100 ppm (e.g. Monnin et al., 2001; Parrenin et al., 2013), and this rise was accompanied by a decrease in atmospheric radiocarbon activity ($\Delta^{14}\text{C}$; Hughen et al., 2004; Fairbanks et al., 2005; Reimer et al., 2013). The underlying mechanisms for the changes in the atmospheric carbon pool are still not fully understood. Venting of formerly isolated deep-water masses is considered as a prominent driver for the atmospheric changes (Broecker, 1982; Broecker and Barker, 2007; Broecker and Clark, 2010; Fischer et al., 2010; Skinner et al., 2010; Schmitt et al., 2012). However, mobilization of terrigenous carbon may have additionally contributed since the glacial size of inert terrestrial carbon pool has been estimated to be larger than under Holocene conditions (Ciais et al., 2013). Among the terrestrial carbon reservoirs, it is the carbon pool of the permafrost-soils (perennially frozen ground) in the Northern Hemisphere (NH) which is regarded as a potentially important source of ^{14}C -depleted (old) CO_2 . Permafrost acts as a carbon sink, as its frozen state suppresses microbial degradation of organic matter. Therefore, the carbon stocks of permafrost are characterized by low radiocarbon activity.

Since permafrost extent rapidly shrank during the deglaciation (Yershov, 1998; Vandenberghe et al., 2014), vast amounts of old carbon may have been mobilized from thawing permafrost and released as greenhouse gases (CO_2 and CH_4) into the atmosphere (Zimov et al., 2006, 2009; Schuur et al., 2008, 2009; Köhler et al., 2013; 2014). The permafrost-feedback has been suggested to have particularly fueled the atmosphere at the onset of the Bølling/Allerød-interstadial (B/A, approx. 14.6 ka BP; Köhler et al., 2013; 2014), where the $\text{CO}_{2\text{atm}}/\Delta^{14}\text{C}_{\text{atm}}$ increase/decrease abruptly accelerated (Parrenin et al., 2013; Durand et al., 2013) with $\text{CO}_{2\text{atm}}$ rising about six times faster than during the early deglaciation (approx. 10 ppmv within 180 years; Parrenin et al., 2013, Veres et al., 2013). Based on a carbon-cycle model, Köhler et al. (2013; 2014) showed that release of old permafrost-soil derived carbon would have been able account for the atmospheric changes and may have “provided the final push out of the ice age” (Köhler et al. 2014). These authors hypothesized that abrupt warming of the NH at the onset of the B/A, together with rapid flooding of the Siberian shelves during Meltwater Pulse 1a (MWP-1a) triggered widespread permafrost decomposition. Supporting evidence for widespread permafrost-thaw and concurrent mobilization of terrigenous OM at that time may come from increasing concentrations of terrigenous biomarkers in Black Sea sediments (Rostek and Bard, 2013) and the beginning expansion of thermokarst lakes in Eurasia and Alaska (Walter et al., 2007). $\text{CO}_{2\text{atm}}$ and $\Delta^{14}\text{C}_{\text{atm}}$ also increased/decreased during HS1 and the

YD, but those events represent cold-reversals in the Northern Hemisphere (NH). So permafrost decomposition is unlikely to be important for the atmosphere at that time. This is corroborated by environmental indicators which point to permafrost-stabilization during the YD (Renssen and Vandenberghe, 2003; Gruber and Reitner, 2007; Fischer et al., 2008; Rostek and Bard, 2013). However, the timing of deglacial mobilization of ^{14}C -depleted carbon during permafrost thaw in the NH is only poorly constrained as proxy-data recording mobilization-events of ^{14}C -depleted terrigenous carbon are sparse.

On the Kamchatka Peninsula (attached to Siberia, Figure 5.1) permafrost is supposed to have almost completely disappeared during the deglaciation (Vandenberghe et al., 2014). In this light, carbon export from the Peninsula into the Northwest Pacific (NW Pacific) and the Western Bering Sea may contain information about the timing of permafrost decomposition in East Asia and may contribute to a better understanding of the role permafrost may have played in deglacial $\text{CO}_{2\text{atm}}/\Delta^{14}\text{C}_{\text{atm}}$ changes.

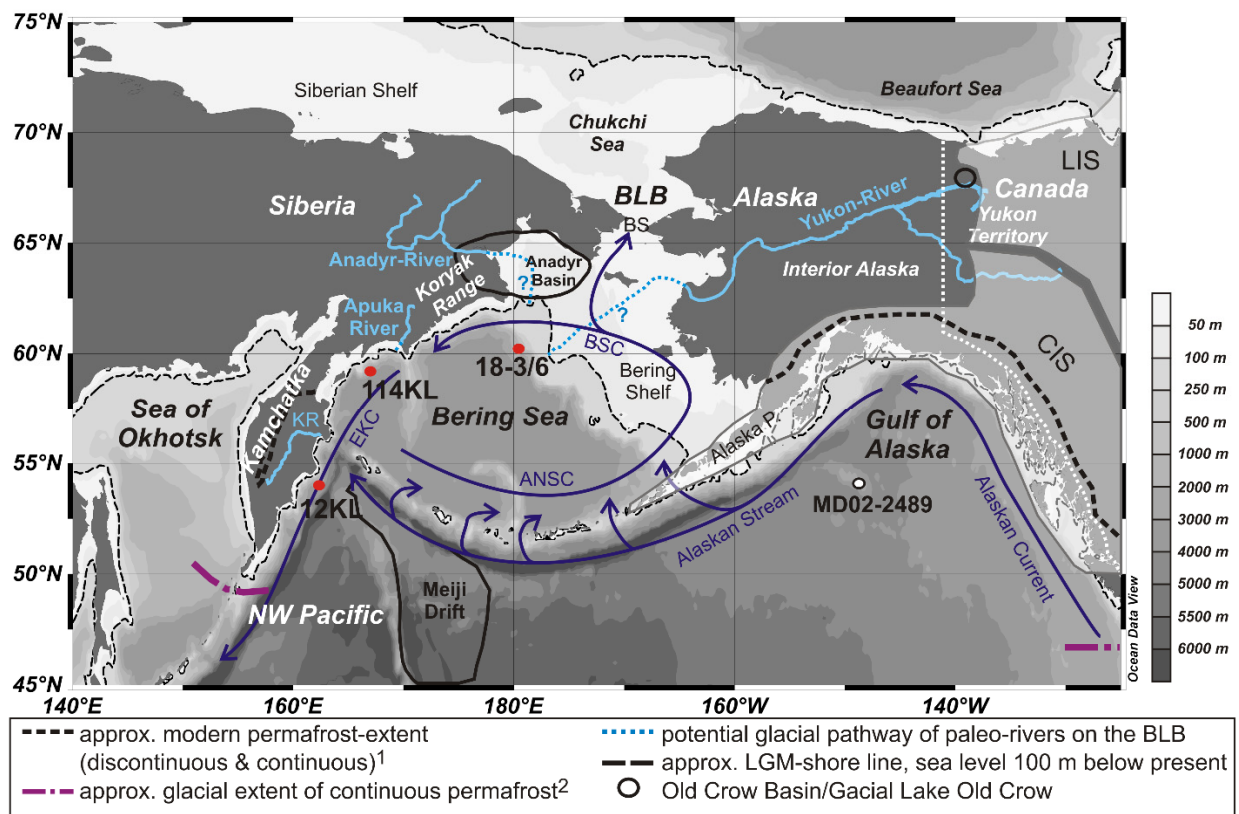


Figure 5.1. Map of the North Pacific Ocean and adjacent Beringia. Red dots represent sites investigated in this study. The white circle denotes a site mentioned in the text. Blue arrows indicate the modern surface circulation patterns of the N Pacific and the Bering Sea (e.g. Stabeno and Reed, 1994). EKC: East Kamchatka Current, ANSC: Aleutian North Slope Current, BSC: Bering Slope Current. White shaded areas sketch the extent of continental ice sheets during the LGM. LIS: Laurentide Ice Sheet, CIS: Cordilleran Ice Sheet. KR: Kamchatka River, BS: Bering Strait, BLB: Bering Land Bridge, P: Peninsula. 1: modified after Brown et al, (1998); 2: modified after Vandenberghe et al. (2014).

Quantifying terrigenous biomarkers and analyzing their compound-specific $\Delta^{14}\text{C}$ -signature in two sediment cores from the Western Bering Sea and the subarctic NW Pacific (sites 114KL and 12KL, Figure 5.1), we identify time intervals of enhanced export of terrigenous organic matter and reconstruct deglacial permafrost dynamics on Kamchatka and the adjacent shelves. Our results provide new insights into the timing and underlying mechanisms of deglacial organic matter mobilization in the NW Pacific realm, and into the potential role of permafrost decomposition in deglacial $\text{CO}_{2\text{atm}}/\Delta^{14}\text{C}_{\text{atm}}$ changes.

5.2. Regional Setting

The source areas of terrestrial material deposited in sediments along the core-transect (114KL and 12KL, Figure 5.1) spreads from eastern Siberia (114KL), to Kamchatka (12KL), a mountainous peninsula separating the Bering Sea from the Sea of Okhotsk (Figure 5.1). The Apuka-River drains the southern flanks of the Koryak Ranges and the adjacent coastal lowlands until it discharges into the Western Bering Sea (Figure 5.1), in front of site 114KL. The landscape of Kamchatka is characterized by strong variations in relief as two parallel mountain chains separate the coastal lowlands from the interior depression. Draining the interior valley and the inner flanks of the mountain ranges, the Kamchatka River is the largest watershed of the Peninsula and, by discharging into the Bering Sea, it is probably the most prominent supplier or terrigenous sedimentary load for site 12KL (Figure 5.1). Additionally, terrigenous material may also derive from the Eastern Coast.

Under present-day conditions eastern Siberia is dominantly covered by continuous permafrost (Brown et al., 1998). However, in the Apuka catchment, discontinuous permafrost prevails spreading to the northern tip of Kamchatka (down to approx. 57°N , Brown et al., 1998). South of 57°N the Peninsula is widely permafrost-free and only small patches of sporadic permafrost occur. Continuous permafrost is restricted to the high mountains (Brown et al., 1998).

The east Siberian climate is in general continental with strong aridity, cold winters and warm summers. Continental conditions are strongest in the Siberian interior and become less extreme towards the Pacific coast where marine influences become more prevalent (Ivanov, 2002). In NE Siberia mountain ranges along the coast cause climatic gradients between north and south by preventing maritime influences from migrating further inland (Mock et al., 1998). The same applies for Kamchatka where the parallel mountain chains cause climatic gradients between the interior valley and the coastal areas (Dirksen et al., 2013 and references therein). Therefore, the climate of Kamchatka and along the Bering-Sea coasts is relatively

mild compared to central Siberia, with smaller annual temperature ranges and abundant precipitation (Mock et al., 1998; Dirksen et al., 2013). Averaged for the entire Kamchatka Peninsula, mean July and January temperature range from 10 to 15°C and from -8 to -26°C, respectively (Ivanov, 2002).

5.3. Material and Methods

5.3.1. Core material and chronology

During cruise RV SONNE SO201 piston-cores SO201-2-114KL (Western Bering Sea) and SO201-2-12KL (NW Pacific) have been recovered in 2009 (Dullo et al., 2009) within the frame of KALMAR Leg 2. Prior to sample preparation, cores were stored at 4°C. Integrated age models were developed by accelerator mass spectrometry (AMS) radiocarbon dating of planktonic foraminifera (*Neogloboquadrina pachyderma* sinistral) as well as core-to-core correlations of high-resolution spectrophotometric (color b*), X-ray fluorescence data and ash-layers. For details, the reader is referred to Max et al. (2012). For the quantification of leaf-wax lipids (long-chain *n*-alkanes and long-chain *n*-alkanoic acids) and the calculation of mass accumulation rates, cores were sampled every 10 cm (12KL) or 5 cm (114KL). Samples for CSRA were taken from 5-6 selected horizons of 2-3.5 cm thickness.

5.3.2. Lipid extraction

Samples were freeze-dried and homogenized using an agate mortar and pestle. Prior to extraction Squalane and Erucic Acid (10 µg) were added as internal standards. Samples for compound-specific radiocarbon analyses (CSRA) were processed without internal standards, as the standards were regarded as potential contaminants. The sample set at regular 10 and 5 cm intervals was extracted by accelerated solvent extraction (Dionex ASE 200) using 22 ml cells and dichlormethane (DCM):methanol (MeOH) 9:1 (v/v) as solvent. Every sample was treated with three cycles, each of them run at 100°C and 1000 psi for five min. Samples for CSRA were extracted with a Soxhlet-apparatus (60°C, 48 hours, DCM:MeOH 9:1 (v/v)). Total lipid extracts were dried with a rotary evaporator. In order to break up wax-esters and to separate carbonic acids from neutral compounds, samples were hydrolyzed with 0.1 N potassium hydroxide (KOH) in MeOH:H₂O 9:1 (v/v) at 80°C for two hours. Neutral compounds were extracted with *n*-hexane. Seralpur-e water was added before the saponified solution was acidified to pH~1 with hydrochloric acid (HCl; 37%). Subsequently, carbonic acids were extracted with DCM. The neutral fraction was further separated into hydrocarbons and polar compounds using column chromatography, performed in Pasteur pipettes (0.5 mm

diameter) which were filled with deactivated SiO₂ (mesh size 60, filling height 4 cm). Hydrocarbons were first eluted with 4 mL *n*-hexane. MeOH:DCM 1:1 (v/v) was used to elute the remaining polar compound-classes. In a second chromatographic step, unsaturated compounds were separated from saturated hydrocarbons using SiO₂ coated with silver nitrate (filling height 4 cm). Saturated hydrocarbons were eluted with 4 mL *n*-hexane.

Carboxylic acids were derivatized to fatty acid methyl esters (FAME) in order to facilitate chromatographic separation. The derivatization was achieved by adding MeOH of known $\Delta^{14}\text{C}$, together with 20 μl HCl. Air in the headspace of the sample-tube was replaced by Nitrogen gas (N₂) and the solutions were heated overnight, at 50°C. After adding Seralpur-e water to the methylated solutions, FAMES were extracted with *n*-hexane. FAMES were separated from polar compounds with column-chromatography using deactivated SiO₂ (mesh size 60, filling height 4 cm) and NaSO₄ (0.5 cm on top of SiO₂). FAMES were eluted with DCM:Hexane 2:1 (v/v).

5.3.3. *Analysis of n-alkanes and n-alkanoic acids and determination of mass accumulation rates*

N-alkanes and FAMES were analyzed using an Agilent7890A gas chromatograph coupled to a flame ionization detector (GC-FID). The system was equipped with an on-column injector and an Agilent J&W DB5-ms column (length 60 m, diameter 250 μm , film thickness 0.25 μm). Helium (He) was used as carrier-gas, maintained at a constant flow of 1.5 ml/min. The temperature program of the GC-oven was set as follows: for both compound-classes: 60°C (1min); 20°C/min up to 150°C; 6°C/min to 320°C; 320°C (35 min). The FID was maintained at 330°C throughout the measurement. Long-chain *n*-alkanes and the respective FAMES of long-chain *n*-alkanoic acids were identified with an external standard mixture. Single compounds were quantified using the peak areas of the respective compounds and the response factor of the internal standard (Squalane and Erucic Acid). The measurement uncertainty was obtained from repeated injections of the external standard. The standard deviation was 0.01%. Concentrations of the compounds were normalized to the dry weight (dw) and total organic carbon content (TOC) of the extracted sediment.

In order to estimate terrigenous input, mass accumulation rates were calculated for the sum of the odd-numbered *n*-alkanes (C₂₃-C₃₃; MAR $_{\Sigma\text{C}_{23}\text{-C}_{33}}$) using the concentrations of the compounds, the dry bulk density (dbd) of the sediment and the sedimentation rates. Dbd and sedimentation rates were obtained from Max et al., (2012). As for core 114KL dbd values are not available, MAR $_{\Sigma\text{C}_{23}\text{-C}_{33}}$ were calculated using a constant value of 0.9 g/cm³.

In order to identify potential contributions of petrogenic OM, the Carbon Preference Index (CPI) was calculated. It quantifies the relative abundance of odd versus even-numbered *n*-alkanes in an *n*-alkane-assemblages, and can be used to estimate thermal maturity of organic matter (Bray and Evans, 1961).

5.3.4. Purification of single compounds for CSRA

For CSRA the *n*-C_{26:0} and *n*-C_{28:0} alkanolic acids were purified using preparative capillary gas chromatography (e.g. Eglinton et al., 1996). The purification was performed on an Agilent HP6890N gas chromatograph, with a Gerstel CIS injection-system, connected to a Gerstel preparative fraction collector (PFC-GC), using a method similar to Kusch et al. (2010). The system was equipped with a Restek Rtx-XLB fused silica capillary column (30 m, 0.53 mm diameter, 0.5 µm film thickness). Samples were injected in solvent vent mode, with a split vent flow of 100 ml/min until 0.12 min and a purge flow of 50 mL/min until 2 min. The temperature program of the CIS injector was set as follows: 40°C (0.06 min), 12 °C/s to 320 °C (5 min), 12 °C/s to 340 °C (5 min). The program of the GC-oven was: 50°C (1 min), 6°C/min up to 320°C (20 min). The interface between the GC and the PFC was maintained at 320°C. Helium was used as carrier-gas with a constant flow-rate of 4 ml/min. All samples were stepwise injected into the PFC-GC system with 5 µl per injection. Depending on the sample size, 20-110 injections were necessary to process the entire sample. Purified compounds were transferred into pre-combusted quartz-tubes, together with 150 µg pre-combusted copper (II)-oxide (CuO; wire shaped) which served as oxidizing agent. Quartz tubes were evacuated (10⁻⁵ mbar) and flames-sealed with a hydrogen/oxygen torch. The sealed tubes were combusted at a temperature of 950°C for four hours to convert the solid FAMES into CO₂.

5.3.5. Compound-specific radiocarbon analysis

The isotopic ratio (¹⁴C/¹²C) of the *n*-alkanoic acids was determined by Accelerator Mass Spectrometry (AMS). The measurements were carried out on the MICADAS-system equipped with a gas-ion source (Ruff et al., 2007; Synal et al., 2007; Wacker et al., 2013) at the Institute of Ion Beam Physics, ETH Zurich.

AMS-results are reported as “fraction modern carbon” (fMC), conventional radiocarbon ages (¹⁴C-ages, given in ¹⁴C yrs BP) and Δ¹⁴C (Stuiver and Pollach, 1977). In order to account for contamination from modern and fossil carbon from unknown sources during the sample-treatment, process-blanks were assessed by processing standards of know radiocarbon

activity. *n*-hexadecanoic acids (*n*-C_{16:0}) from apple peel served as representative of the modern end-member, and Triacosanoic acid (*n*-C_{30:0}) Sigma, Prod. No. T3527-100MG, Lot 018K3760, Rethemeyer et al., 2013) was used as fossil standard. A list of processed samples and respective sample sizes is given in the Appendix (Table A5.1). Blank assessment was performed graphically similar to Shah and Pearson, (2007). A description of the blank assessment, the fMC-value and the mass of the blank as well as the respective uncertainties are given in the appendix (Figure A5.1). Blank-correction was performed after Wacker and Christl (2011). fMC-values were further corrected for the methyl-group, which had been added during the derivatization process, using isotopic mass balance. Errors have been propagated after Wacker and Christl (2011).

5.3.6. Reporting ¹⁴C-content

¹⁴C-contents of *n*-alkanoic acids are henceforth reported as the difference between initial $\Delta^{14}\text{C}$ values ($\Delta^{14}\text{C}_{\text{initial}}$, $\Delta^{14}\text{C}$ -value corrected for the decay between measurement and deposition; calculated after Ohkouchi et al., 2002) and atmospheric $\Delta^{14}\text{C}$ -values at the time of deposition ($\Delta\Delta^{14}\text{C}$). Atmospheric $\Delta^{14}\text{C}$ -values were extracted from IntCal 13 (Reimer et al., 2013), and the time of deposition was obtained from the age models of cores 12KL and 114KL (Max et al., 2012).

5.4. Results

5.4.1. Mass accumulation rates and CPI-values

MAR_{ΣC23-C33} are given in Figure 5.2. All MAR_{ΣC23-C33} display similar general patterns. Deglacial MAR_{ΣC23-C33} (between approx. 17 and 10 ka BP) tend to be higher than MAR_{ΣC23-C33} of the Holocene and the LGM (Figure 2). During the deglaciation, MAR_{ΣC23-C33} are characterized by two striking maxima which coincide with the Heinrich Stadial 1 (HS1) and the Preboreal (PB, Figure 5.2). The first event in MAR_{ΣC23-C33} abruptly initiates between 16.8 and 16.3 ka BP and abruptly ends at approx. 15-14.6 ka BP, shortly before the onset of the B/A. The second maximum initiates at approx. 11.5 ka BP and lasts until 10.5 ka BP at site 114KL, but is shorter at site 12KL where it ends at approx. 11 ka; Figure 5.2). MAR_{ΣC23-C33} of both cores reach their highest values during this event, (Figure 5.2). Different patterns characterize the period between the B/A and the onset of the PB (approx. 13.2-11.5 ka BP). At site 12KL a third peak occurs between 14 and 13.3 ka BP while MAR_{ΣC23-C33} of core 114KL remain constant during this interval (Figure 5.2). MAR_{ΣC23-C33} of core 12KL increase again at 13.2 culminating into a fourth peak during the YD (at approx. 12.3 ka BP). A similar

event is also present in core 114KL (between 13.2-12.8 ka; Figure 2) but in contrast to site 12KL, it does not persist into the YD (Figure 5.2). Instead, $MAR_{\Sigma C_{23-C_{33}}}$ at site 114KL exhibit a deglacial minimum at that time. After the PB-maximum $MAR_{\Sigma C_{23-C_{33}}}$ decrease until approx. 9 ka BP and become lower than during most parts of the deglaciation. At core 12KL, $MAR_{\Sigma C_{23-C_{33}}}$ even out and remain constant throughout the Holocene (Figure 5.2).

CPI-values of both cores are rather stable during the LGM and the early deglaciation, scattering between 5.5 and 6.5 (Figure 5.3). Strikingly decreased CPI-values of 3.5 are exhibited between 17 and approx. 14.6 ka BP. During the deglaciation and the Holocene, values range between 5 and 7 (Figure 5.3).

5.4.2. CSRA and $\Delta\Delta^{14}C$

$\Delta\Delta^{14}C$ -values for the long-chain *n*-alkanoic acids of cores 12KL and 114KL are shown in Table 51 together with the corresponding blank- and methyl-group-corrected fMC-values, conventional radiocarbon ages (^{14}C -ages), $\Delta^{14}C$ and $\Delta^{14}C_{\text{initial}}$. $\Delta\Delta^{14}C$ -values are also plotted in Figure 2, together with $MAR_{\Sigma C_{23-C_{33}}}$. The raw data from the AMS-measurement are given in Appendix 2 (Table A5.2). In both cores, $\Delta\Delta^{14}C$ -values are highest during the LGM (1413‰ & 1405‰) and lowest during the Holocene (372‰ & 52‰; Figure 2). The *n*-C_{28:0} *n*-alkanoic acid is generally more depleted in ^{14}C than the *n*-C_{26:0} homologue. A $\Delta\Delta^{14}C$ -signature exceeding 1000 ‰, implies that the *n*-alkanoic acids are virtually ^{14}C -free which is also expressed by infinite ^{14}C -ages (Table 5.1).

Between the LGM and HS1 the $\Delta\Delta^{14}C$ signatures decrease and range between 966.3‰ (*n*-C_{26:0} 114KL) and 1323.7‰ (*n*-C_{28:0}, 12KL). The $\Delta\Delta^{14}C$ -values further decline into the B/A reaching values between 831.4‰ (*n*-C_{26:0}, 114KL) and 1231.2‰ (*n*-C_{28:0}, 12KL). Although two $\Delta\Delta^{14}C$ -values fall below the threshold of 1000‰ (HS1, 114KL *n*-C_{26:0} & B/A, 12KL, *n*-C_{26:0}), they still have to be considered as ^{14}C -free and hence beyond the limit of radiocarbon dating, when the error bars are taken into account (Figure 5.2; Table 5.1). Therefore, the decrease of the $\Delta\Delta^{14}C$ -values between the LGM and the B/A is only determined by the differing $\Delta^{14}C$ -signature of the atmosphere (Figure 5.4a) and does not allow for any palaeo-environmental inferences. The lipids significantly fall below the threshold of 1000 ‰ during the B/A (site 114KL) and the YD (site 12KL). Considering the error bars of the $\Delta\Delta^{14}C$ -values, the $\Delta\Delta^{14}C$ -signature of *n*-C_{26:0} and *n*-C_{28:0} remains constant in core 114KL throughout the B/A, the YD and the PB. (Figure 5.2, Table 5.1).

Table 5.1. CSRA-data of long-chain *n*-alkanoic acids for cores SO201-2-12KL and SO201-2-114KL. Raw-data, respectively AMS-results, are given in the appendix, Table A2.

1: corrected for process-blanks (for blank data, see appendix, Table A5.1 and Figure A5.1) and methylation 2: adopted from the age model of cores 12KL and 114KL (Max et al., 2012). 3: Difference between $\Delta^{14}\text{C}_{\text{initial}}$ and $\Delta^{14}\text{C}_{\text{atm}}$ at the respective time of deposition. $\Delta^{14}\text{C}_{\text{atm}}$ -data was taken from IntCal 13 (Reimer et al., 2013).

Sample (core, depth [cm], compound)	Corrected fMC ¹	Deposition age, mid-point [cal. ka BP] ² , time interval	¹⁴ C-age [ka BP]	$\Delta^{14}\text{C}$ [‰]	$\Delta^{14}\text{C}_{\text{initial}}$ [‰]	$\Delta\Delta^{14}\text{C}$ [‰] ³
12KL, 1-4.5, <i>n</i> -C _{26:0}	0.5366 ± 0.0429	1.07	5.180 ± 0.500	-467.5 ± 3.3	-389.2 ± 38.0	372.0 ± 36.3
12KL, 203-205, <i>n</i> -C _{26:0}	0.1408 ± 0.0085	9.35	15.800 ± 0.500	-859.5 ± 0.8	-561.3 ± 27.2	660.6 ± 34.7
12KL, 203-205, <i>n</i> -C _{28:0}	0.1242 ± 0.0106	9.35	16900 ± 0.720	-876.7 ± 1.1	-615.1 ± 34.9	714.4 ± 32.4
12KL, 295-297, <i>n</i> -C _{26:0}	0.1049 ± 0.0894	11.10	18.300 ± 5.200	-895.8 ± 10.0	-597.9 ± 383.8	751.9 ± 381.6
12KL, 295-297, <i>n</i> -C _{28:0}	-0.1514 ± 0.2219	11.10	infinite	-999.9 ± 11.6	-999.6 ± 448.5	1153.6 ± 292.3
12KL, 419-422, <i>n</i> -C _{26:0}	0.0813 ± 0.0122	12.31	20.100 ± 1.200	-918.7 ± 1.2	-636.9 ± 55.7	852.2 ± 52.8
12KL, 419-422, <i>n</i> -C _{28:0}	0.0707 ± 0.0141	12.31	21.400 ± 1.700	-929.1 ± 1.5	-683.4 ± 65.8	898.7 ± 62.8
12KL, 609-612, <i>n</i> -C _{26:0}	0.0516 ± 0.0199	14.51	23.800 ± 2.700	-948.7 ± 3.6	-701.1 ± 208.7	932.9 ± 202.9
12KL, 609-612, <i>n</i> -C _{28:0}	-0.0393 ± 0.0504	14.51	infinite	-999.9 ± 2.7	-999.4 ± 154.7	1231.2 ± 148.9
12KL, 693-696, <i>n</i> -C _{26:0}	0.0425 ± 0.0117	16.03	25.400 ± 2.300	-957.5 ± 2.8	-702.1 ± 197.8	1026.5 ± 148.9
12KL, 693-696, <i>n</i> -C _{28:0}	-0.0017 ± 0.0239	16.03	infinite	-999.9 ± 1.3	-999.3 ± 87.8	1323.7 ± 188.7
12KL, 896-898, <i>n</i> -C _{26:0}	-0.0147 ± 0.0270	19.61	infinite	-999.9 ± 1.4	-998.9 ± 153.4	1413.6 ± 141.6
114KL, 3-5.5, <i>n</i> -C _{26:0}	0.0924 ± 0.0313	9.01	8.480 ± 0.520	-654.7 ± 3.2	34.9 ± 96.4	52.0 ± 18.7
114KL, 39-41.5, <i>n</i> -C _{26:0}	0.3479 ± 0.0060	10.72	19.150 ± 0.750	-908.5 ± 0.6	-662.8 ± 22.1	786.2 ± 96.4
114KL, 39-41.5, <i>n</i> -C _{28:0}	0.0869 ± 0.0063	10.72	19.700 ± 0.600	-914.6 ± 0.6	-685.1 ± 23.8	808.5 ± 20.4
114KL, 101-103.5, <i>n</i> -C _{26:0}	0.0794 ± 0.0105	12.69	20.500 ± 1.100	-922.7 ± 1.1	-638.3 ± 50.3	860.4 ± 43.1
114KL, 101-103.5, <i>n</i> -C _{28:0}	0.0534 ± 0.0162	12.69	23.600 ± 2.300	-947.4 ± 3.5	-754.1 ± 165.4	976.2 ± 158.2

Continued on the next page

Sample (core, depth [cm], compound)	Corrected fMC ¹	Deposition age, mid-point [cal. ka BP] ² , time interval	¹⁴ C-age [ka BP]	$\Delta^{14}\text{C}$ [‰]	$\Delta^{14}\text{C}_{\text{initial}}$ [‰]	$\Delta\Delta^{14}\text{C}$ [‰] ³
114KL, 144-146.5, <i>n</i> -C _{26:0}	0.0677 ± 0.0091	14.40	21.600 ± 1.200	-932.6 ± 1.0	-612.1 ± 57.4	831.4 ± 51.5
114KL, 174-176.5, <i>n</i> -C _{26:0}	0.0493 ± 0.0121	15.33	24.100 ± 2.100	-950.6 ± 1.3	-682.2 ± 81.0	966.3 ± 72.8
114KL, 174-176.5, <i>n</i> -C _{28:0}	0.0021 ± 0.0314	15.33	49.800 ± 21.900	-998.0 ± 1.8	-987.0 ± 43.1	1271.1 ± 104.9
114KL, 301-303.5, <i>n</i> -C _{26:0}	-0.0327 ± 0.0188	18.41	infinite	-999.9 ± 1.0	-999.1 ± 90.0	1405.5 ± 81.9

$\Delta\Delta^{14}\text{C}$ -values range between 976.2‰ and 786.2‰. $\Delta\Delta^{14}\text{C}$ -values of core 12KL progressively decline between the B/A and the PB (Figure 5.2). This trend is exhibited by both the *n*-C_{28:0} and the *n*-C_{26:0} but can only be regarded as significant in the *n*-C_{28:0} which yields smaller error bars than the *n*-C_{26:0} (Figure 5.2).

From the B/A to the PB, $\Delta\Delta^{14}\text{C}$ varies between 1231.2 (B/A, *n*-C_{28:0}) and 751.9 (PB, *n*-C_{26:0}) and is in a similar range as in core 114KL (Table 5.1, Figure 5.2).

After the PB, the $\Delta\Delta^{14}\text{C}$ -signatures of the cores strongly deviate from each other since the abrupt decrease about approx. 700 ‰ which characterizes site 114KL, is not present at site 12KL (Figure 5.2, Table 5.1). Instead, at 9 ka BP $\Delta\Delta^{14}\text{C}$ -values of core 12KL (*n*-C_{26:0}: 714.4‰ & *n*-C_{28:0}: 660.6‰) are lowered by approx. 100 ‰-points relative to the PB and the YD (Figure 5.2, Table 5.1). The $\Delta\Delta^{14}\text{C}$ -signature of the *n*-C_{26:0} further declines over the Holocene and reaches a value of 372‰ during the late Holocene, at approx. 1 ka BP (Figure 5.2, Table 5.1).

5.5. Discussion

5.5.1. Sources of terrigenous organic matter and mobilization of ¹⁴C-depleted carbon

5.5.1.1. Steady state conditions – Late Holocene and LGM

Considering that the late Holocene and the LGM were periods with rather stable climatic conditions (compared to the deglaciation), the $\Delta\Delta^{14}\text{C}$ signature of the long-chain *n*-fatty acids from these time-intervals reflect the background (permafrost-) conditions during the two steady states. As core 114KL contains only late glacial to early Holocene sediment (core top at approx. 9 ka), the modern steady state is only recorded at site 12KL. During the late

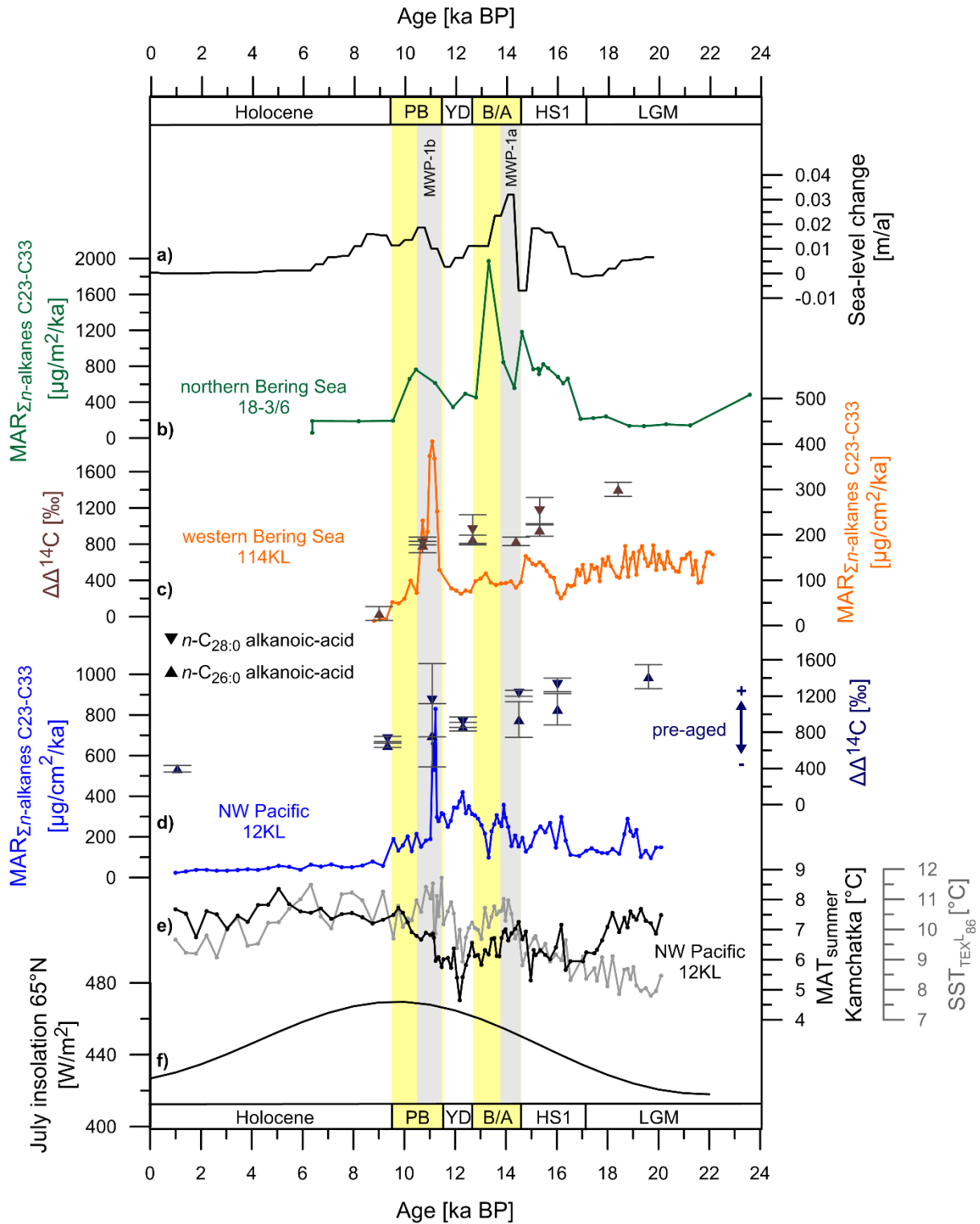


Figure 5.2. a) Global rate of sea-level change (Lambeck et al., 2014). b) Mass accumulation rate of long-chain *n*-alkanes ($\Sigma_{C_{23}-C_{33}}$) of core 18-3/6 (unpublished data V. Meyer), c) Mass accumulation rate of long-chain *n*-alkanes ($\Sigma_{C_{23}-C_{33}}$) and radiocarbon data of long-chain *n*-alkanoic acids of core 114KL (this study), d) Mass accumulation rate of long-chain *n*-alkanes ($\Sigma_{C_{23}-C_{33}}$) and radiocarbon data of long-chain *n*-alkanoic acids of core 12KL (this study). e) Mean Air Temperature if the ice-free season/summer season on Kamchatka (MAT_{ifs} Meyer et al., submitted a) and SST from the marginal subarctic NW Pacific (site 12KL, Meyer et al., submitted b). f) Mean July insolation at 65°N (Berger and Loutre, 1991). Yellow shaded areas mark the warm-phases of the Bølling/Allerød and the Preboreal. Grey bars represent MWP-1a and MWP-1b (after Hanebuth et al., 2000; Deschamps et al., 2012).

Holocene, the *n*-C_{26:0} alkanolic acid has a $\Delta\Delta^{14}\text{C}$ -signature of 372.0 ‰ which is considered here as the background signal of the *n*-alkanoic acids exported from Kamchatka. With a $\Delta\Delta^{14}\text{C}$ -signature of approx. 1400‰, the LGM *n*-fatty acids from sites 12KL and 114KL indicate that the turnover of leaf-wax lipids was much slower during the LGM than during the late Holocene. As compound-specific $\Delta^{14}\text{C}$ -values of lipids in modern sediments off the Siberian permafrost draining rivers (-530 to -660‰, Gustafsson et al., 2011) are higher than off rivers with permafrost free catchments (e.g. 200‰, Kusch et al., 2010) the difference points to extensive permafrost coverage on Kamchatka during the LGM. Interestingly, Meyer et al. (submitted b) found that LGM summers were as warm as at present which may counter the view of extended permafrost during the LGM (relative to modern). Assuming that Kamchatka experienced colder-than-present winter conditions during the LGM, mean annual air temperatures would have been lowered as well. Such harsh conditions may have allowed permafrost to persist despite relatively warm summers.

Astonishingly, the $\Delta\Delta^{14}\text{C}$ -signature of sites 12KL and 114KL (approx. 1400 ‰, Table 1, Figure 5.2) exceeds the modern values of the Siberian Rivers by 900 to 700 ‰-points. This suggests that glacial terrestrial residence times of leaf-wax lipids in permafrost areas was increased relative to modern. Values above 1000 ‰ even indicate that the OM deposited in the sediments at the LGM was ¹⁴C-free implying that the contribution of fresh, weakly pre-aged OM, e.g. from the vegetation or top-soils, was strongly suppressed during the LGM. A scarce vegetation coverage on Kamchatka and in the Apuka-catchment could have accounted for this. However, glacial and deglacial vegetation history of Kamchatka and the Apuka-catchment is poorly known (e.g. Dirksen et al., 2013). Assuming scarce vegetation, erosion of relatively old organic-rich layers preserved in the permafrost-soils along the riverbanks and coastlines may have formed the dominant source of exported OM during the LGM. Also, pronounced contributions petrogenic OM, a prominent source of ¹⁴C-free carbon, could explain the $\Delta\Delta^{14}\text{C}$ -signature (e.g. Kusch et al., 2010). However, CPI-values in cores 12KL and 114KL are around 6 suggesting that the OM composition is dominated by fresh, immature OM (Figure 5.3). Furthermore, due to their reactivity *n*-fatty acids are prone to degradation (Sun and Wakeham, 1994; Canuel and Martens, 1996) and would lose their functional groups during diagenesis. Hence, a significant contribution of petrogenic carbon to the *n*-alkanoic acids is rather unlikely.

Considering that a few studies suggested that during the LGM, NE Russia's moisture was trapped in glaciers and ground ice during the LGM (Sergin and Scheglova, 1976; Alfimov and

Berman, 2001), overland drainage was probably weak and may have reduced the transport of vegetation-derived OM into rivers systems. Slow riverine runoff/reduced fluvial energy would have certainly increased terrestrial residence times of OM.

5.5.1.2. *Early deglaciation (17-14.6 ka BP)*

5.5.1.2.1. *Contribution of thermally mature OM and provenance of leaf-wax lipids*

During the HS1 (between approx. 17 and 14.6 ka BP) all sites exhibit a first pronounced event of intensified supply of ^{14}C -depleted terrigenous OM as can be inferred from the increased $\text{MAR}_{\Sigma\text{C}_{23-\text{C}_{33}}}$ and a high $\Delta\Delta^{14}\text{C}$ -signature of the $n\text{-C}_{26:0}$ from sites 12KL and 114KL. Coevally to the increased terrigenous OM-input all cores are characterized by strongly decreasing CPI-values (Figure 5.3). A change towards lower values indicates that the portion of thermally mature OM, and probably petrogenic carbon, abruptly increased in the course of the mobilization event and may imply that the carbon source changed. Numerous oil-shale and coal deposits exist in Alaska and the Yukon Territories/Canada (USGS; Barnes, 1967), but also the Anadyr basin, the catchment of the Anadyr River, (stretching from the Anadyr Lowlands to the western Bering Shelf, Figure 5.1) holds several source rocks of oil and gas (Clarke, 1988; Burlin and Agapitov, 2002; Poludedkina, 2007). Considering the anti-clockwise circulation of the Bering Sea (consisting of the BSC and the EKC) OM matter from the Anadyr and Yukon catchments may have been carried to the marginal NW Pacific (Figure 5.1). This idea is confirmed by MAR of long-chain n -alkanes and CPI-values (unpublished data from V. Meyer) from a sediment core retrieved at the continental margin off the Bering Shelf (site 18-3/6, Figure 5.1). The site is near Navarin Canyon (Gersonde, 2012), which was presumably formed by the palaeo-Anadyr and Yukon Rivers when the Bering and Chukchi-Shelves were exposed during Pleistocene sea-level regressions (Carlson and Karl, 1984, 1988). The $\text{MAR}_{\Sigma\text{C}_{23-\text{C}_{33}}}$ and CPI-values of core 18-3/6 show the same pattern with more pronounced amplitudes as cores 12KL and 114KL (Figures 5.2 and 5.3). As increased $\text{MAR}_{\Sigma\text{C}_{23-\text{C}_{33}}}$ coincides with a first peak in the global rate of sea-level change (Figure 5.2), shelf flooding may have resulted in erosion of thermally mature deposits from the Anadyr Basin. This would be in agreement with the flooding-scenario for the Bering Shelf (Manley, 2002), according to which submergence mainly initiated in the western part of the Bering Shelf at that time (Figure 5.3). However, unpublished data of the clay-mineral composition at site 18-3/6 which indicate that fluvial discharge intensified at 16.8 ka BP (pers.

Communication R. Wang, May, 2015) suggesting that also the intensified export of OM and the mobilization of thermally mature OM was associated with strong fluvial activity of either

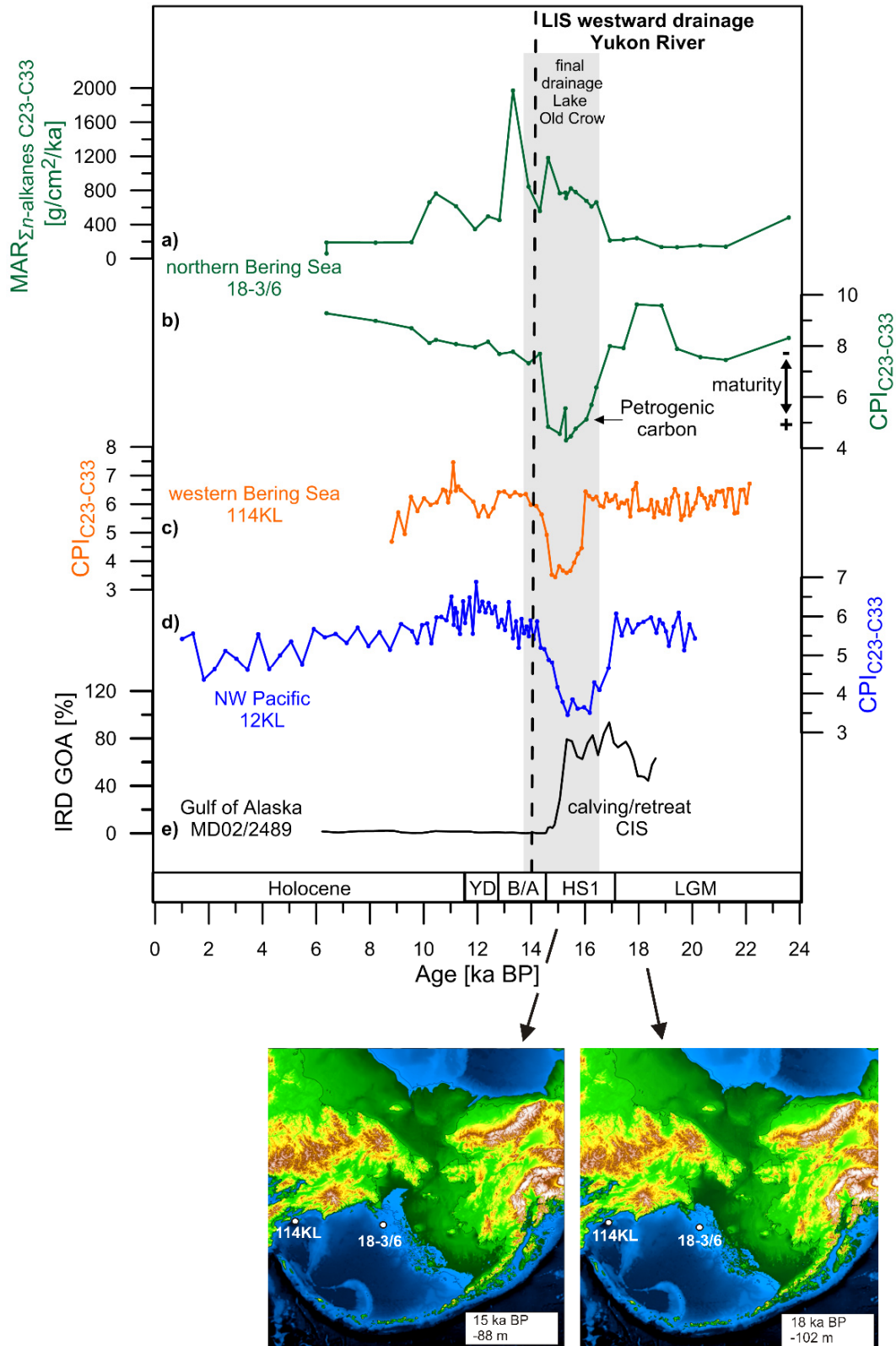


Figure 5.3. a) Mass accumulation rate of long-chain n-alkanes ($\Sigma C_{23-C_{33}}$) of core 18-3/6 and CPI-values of cores 18-3/6, 114KL and 12KL (b, c, d, this study). e) Abundance of ice rafted detritus in core MD02/2489 (Gebhardt et al., 2008). The grey bar represents the maximum time interval for the final drainage of proglacial Lake Old Crow (after Harrington, 2003; Zazula et al., 2004; Kennedy et al., 2010). The dashed line indicates when the LIS retreated from its northwestern limits (after Dyke and Prest, 1987; Dyke et al., 2002, 2003). Beforehand, the LIS blocked eastward drainage into the Beaufort Sea, causing drainage through the Yukon River (Dyke and Prest, 1987; Dyke et al., 2002, 2003). BLB-shore lines are adopted from the shelf-flooding scenario for the Bering Shelf by Manley (2002).

the Yukon or Anadyr Rivers. Hence, shelf erosion may have played a secondary role. Increased fluvial activity in the Yukon River is likely considering that the Cordilleran and Laurentide ice sheets (CIS, LIS, Figure 5.1) began to retreat between approx. 19 ka-15ka BP (e.g.: Mann and Peteet, 1994; Mann and Hamilton, 1995; Dyke et al., 2002; Gebhardt et al., 2008; Hendy and Cosma, 2008; Kennedy et al., 2010; Davies et al., 2011; Taylor et al., 2014). The timing is probably best documented by ice-rafted detritus (IRD) in the NE Pacific where intensified IRD supply attests to calving-events of retreating outlet glaciers from the Alaska Peninsula and the CIS between 17.5 and 15 ka BP (Mann and Peteet, 1994; Mann and Hamilton, 1995; Porter and Swanson, 1998; Mosher and Hewitt, 2004; Cosma and Hendy, 2008; Gebhardt et al., 2008; Hendy and Cosma, 2008, Figure 5.3). Also, the final drainage of proglacial Lake Old Crow (Figure 5.1) initiated around approx. 13.7 ¹⁴C ka BP (16.3 ka BP; Kennedy et al., 2010) and was accomplished by approx. 12.6-11.9 ¹⁴C ka BP (15,0-13.7 ka BP; Harrington, 2003; Zazula et al., 2004; Kennedy et al., 2010). As the LIS remained close to its northwestern limits until approx. 15-14 ka BP, thereby blocking northward drainage of its proglacial lakes into the Beaufort Sea (Dyke and Prest, 1987; Dyke et al., 2002, 2003; Fritz et al., 2012), the Lake Old Crow drained westward into the Yukon-River and confluences (Dud-Rodkin and Hughes, 1994; Dud-Rodkin et al., 2004; Kennedy et al., 2010). This timing of peaking IRD-supply and lake drainage fits well with the increased MAR_{ΣC23-C33} and decreased CPI-values in our sediment cores (Figure 5.3), implying that enhanced fluvial discharge from the Yukon River accounted for the intensified export of OM and the deposition of thermally mature OM, potentially derived from Alaskan or Canadian oil-shale or coal deposits. A strong influence of Alaskan sources on the sedimentary composition of the NW Pacific (as suggested here) is also supported by the glacial provenance pattern of inorganic sediment components according to which approx. 50% of siliciclastic sediment components from the Meji Drift body (marginal NW Pacific, near site 12KL, Figure 5.1) originated from Alaska and the Yukon-River catchment during glacial intervals (VanLaningham et al., 2009).

5.5.1.2.2. Sources of ¹⁴C-depleted n-alkanoic acids

Given the conclusion that melt-water runoff during the early phase of the LIS/CIS-retreat and deglacial drainage of Lake Old Crow caused the increased organic supply to sites 18-3/6, 114KL and 12KL it should consequentially also account for the intensified mobilization of strongly ¹⁴C-depleted OM. Note that radiocarbon data are not available for site 18-3/6 which is why the assumed linkage between the $\Delta\Delta^{14}\text{C}$ has to be confirmed by future CSRA of core

18-3/6. Although thermally mature organic matter is a potential source of fossil/¹⁴C-free carbon, it is questionable whether ¹⁴C-depleted *n*-alkanoic acids are directly associated with thermally mature OM. Since *n*-alkanoic acids are prone to degradation during diagenesis and catagenesis they are barely present in strongly mature deposits. Instead, intensified runoff in the Yukon River probably enhanced permafrost erosion along the riverbanks and mobilization of ¹⁴C-depleted OM increased. Widespread thawing of Alaskan permafrost seems unlikely since sea surface temperature reconstructions for the Gulf of Alaska and the Bering Sea imply that the climate was similarly cold as during the LGM (Maier et al., 2015; Meyer et al. submitted). Furthermore, thermokarst processes seem to have begun after 15 ka BP (Walter et al., 2007; Lozhkin et al., 2011; Reyes and Cooke, 2011).

5.5.1.3. *The deglaciation (14.6-9 ka BP)*

5.5.1.3.1. *Sea-level induced mobilization of ¹⁴C-depleted carbon*

Between approx. 15 and 14.6 ka BP increasing CPI-values and decreasing $MAR_{\Sigma C_{23-C_{33}}}$ in all cores, including site 18-3/6, likely attest to the end of the mobilization event associated with the LIS-drainage (Figure 5.2 & 5.3). Afterwards, the deglacial pattern in the $MAR_{\Sigma C_{23-C_{33}}}$ at sites 12KL and 114KL shows strong similarities with the global rate of sea-level change as peaks in $MAR_{\Sigma C_{23-C_{33}}}$ during the B/A and the PB coincide with the rapid sea-level change during melt-water pulses 1a and 1b (MWP-1a, MWP-1b, Figure 5.2; Lambeck et al., 2014). The pronounced similarity suggests that shelf erosion on the shelves along the eastern coast of Siberia/Kamchatka was the dominant mechanism for OM mobilization between 14.6 and approx. 10 ka BP. However, site 114KL is missing a peak in $MAR_{\Sigma C_{23-C_{33}}}$ during MWP-1a (Figure 5.2) indicating that sea-level rise had hardly any impact on the shelf adjacent to site 114KL, while it seems to have been effective along the shelves off Kamchatka. Interestingly, site 18-3/6 also exhibits a pronounced peak in $MAR_{\Sigma C_{23-C_{33}}}$ during MWP-1a (Figure 5.2). The discrepancies between site 114KL and 18-3/6 indicate that the supply from the Yukon-River catchment ceased during the B/A and that sites 114KL and 12KL are dominated by Siberian sources. While the impact of MWP-1a was inconsistently present in the NW Pacific/western Bering-Sea, MWP-1b was consistently effective, causing the strongest mobilization-event of OM during the deglaciation, since $MAR_{\Sigma C_{23-C_{33}}}$ of cores 114KL and 12KL become maximal (Figure 5.2). $\Delta\Delta^{14}C$ -values varying between 1231-751‰ at sites 114KL and 12KL imply that the mobilized OM was nearly ¹⁴C-free (Figure 5.2). Hence, it likely that shelf-erosion during MWP-1a and 1b triggered permafrost decomposition on the flooded shelves areas. Given this

interpretation, coastal erosion and associated permafrost decomposition along Kamchatka/Siberia was strongest during the PB/MWP-1b.

Sea-level rise seems to have mobilized terrigenous OM on the BLB, as $MAR_{\Sigma C23-C33}$ of core 18-3/6 are similar to the rate of sea-level change (Figure 5.2). So pronounced coastal permafrost decomposition may have potentially occurred on the BLB during MWP-1a and MWP-1b. However, radiocarbon-data confirming that the OM was ^{14}C -depleted are not available.

5.5.1.3.2. *The deglaciation (14.6-9 ka BP) – mobilization of ^{14}C -depleted OM in the Kamchatka hinterland*

Although sea-level seems to have played a major role in OM-mobilization, additional processes mobilizing ^{14}C -depleted carbon seem to have acted on Kamchatka as $MAR_{\Sigma C23-C33}$ at site 12KL deviate from the global rate of sea-level change between 13.3 and approx. 11.3 ka BP. $MAR_{\Sigma C23-C33}$ exhibit a peak while the rate of sea-level change is relatively low (Figure 5.2). A parallel development establishes again at 11.3 ka BP when MWP-1b causes shelf-erosion (Figure 5.2). A similar event which is likely not related to sea-level, is also displayed at site 114KL but the event is less pronounced and shorter (restricted to 13.3-12.9 ka). Since erosional activity along the coastlines presumably weakened in response to slowly rising sea-level, the strongly pre-aged OM could have been mobilized in the catchments of the Kamchatka and Apuka Rivers. The onset of the export event coincides with peat-land expansion on Kamchatka, which has been dated to the period between 13.9 and 8.5 ka BP (Khotinsky, 1977; Dirksen et al., 2013 and references therein; Klimaschewski et al., 2015).

The initiation of peat-formation likely occurred in response to climate amelioration including warming and increased moisture availability (Dirksen et al., 2013 and references therein; Klimaschewski et al., 2015). Warming during the B/A would be in concert with rising summer insolation at 65°N (e.g. Berger and Loutre, 1991) and temperature records from Siberia, and eastern Beringia (Kokorowski et al., 2008; Kurek et al., 2009; Anderson and Lozhkin, 2015) as well as in the adjacent seas (Seki et al., 2004b; Max et al., 2012; Meyer et al., submitted a). As the $\Delta\Delta^{14}C$ -signature of the *n*-alkanoic acids provides evidence for mobilization of strongly ^{14}C -depleted OM, it seems likely that warming also triggered permafrost-thaw and increased soil erosion on Kamchatka at that time. Permafrost thaw may have also supported peat formation on the Peninsula by raising the ground water table and increasing moisture in the soils. Initiating permafrost-thaw during the B/A is in line with the beginning expansion of thermokarst lakes in Siberia and Alaska (Walter et al., 2007; Jones

and Yu, 2010; Reyes and Cooke, 2011). Conflictingly, the biomarker data from site 12KL suggest that the mobilization event culminated during the mid-YD where several temperature records from Siberia, Kamchatka and the adjacent Sea of Okhotsk, the Western Bering Sea and the NW Pacific consistently indicate a cold-spell (Seki et al., 2004b; Caissie et al., 2010; Max et al., 2012; Dirksen et al., 2013; Smirnova et al., 2015; Meyer et al., submitted a, b). As suggested by Meyer et al. (submitted b) summer temperatures on Kamchatka declined by approx. 2°C, relative to the late B/A (Figure 2). Owing to the cold-reversal, one may assume that permafrost would have stabilized on Kamchatka and that soil erosion and the associated OM export weakened. However, as $MAR_{\Sigma C_{23-C_{33}}}$ do not track the abrupt climate-deterioration suggesting the export of OM-mobilization may not have responded to the abrupt temperature-forcing. Interestingly, SST and mean air temperature (MAT) records indicate that the severe cold-spell in the Kamchatka region was relatively short (lasting only for the first half of the YD-stadial; Figure 5.2). So, one may speculate that the response of permafrost-thaw on Kamchatka and the associated carbon release, was too slow react to this short event. Furthermore, SST records from the NW Pacific indicate that YD-SST were as warm as at present and warmer than during the LGM, despite the presence of a cold reversal (Figure 5.2). The MAT record from Kamchatka may indicate that YD summers were colder than at present, but if the annual mean or winter temperatures on Kamchatka developed similar to the NW Pacific SST (including a relatively warm YD), permafrost decomposition may have proceeded through the YD despite the abrupt and pronounced summer cooling on Kamchatka. At this point, the establishment of records of winter temperature would be helpful to fully understand the carbon export dynamics on the Peninsula at that time.

5.5.1.4. *The early Holocene (approx. 10 - 9 ka BP) – end of strong OM mobilization*

$MAR_{\Sigma C_{23-C_{33}}}$ of cores 114KL and 12KL progressively decrease after the pronounced mobilization-event at approx. 11.0-10.5 ka BP/MWP-1b until they fall below the average deglacial level at approx. 9 ka BP and remain constant throughout the Holocene (sites 12KL and 18-3/6; Figure 2). During this time-interval, the $\Delta\Delta^{14}C$ -signature of the *n*-alkanoic acids of core 12KL exceeds the background value of the late Holocene and is still similar to the period of intense sea-level rise and permafrost-thaw on Kamchatka (Figure 5.2). This suggests that the export of strongly pre-aged OM into the NW Pacific associated with permafrost decomposition was still in progress but gradually declined, as suggested by the decreasing $MAR_{\Sigma C_{23-C_{33}}}$, until it probably ended at 9 ka BP (Figure 5.2). Palynological data from peat-profiles on Kamchatka show that aquatic and marsh plants spread on the Peninsula between

approx. 10.4 and 8.5 ka BP (Klimaschewski et al., 2015) which would be in line with permafrost thaw. As sea-level globally rose until 6-7 ka BP (Stanford et al., 2011; Lambeck et al., 2014) shelf erosion may also have contributed to the ^{14}C -depleted carbon pool at site 12KL, until 9 ka BP. In contrast to site 12KL, the $\Delta\Delta^{14}\text{C}$ -signature at site 114KL decreases abruptly together with the $\text{MAR}_{\Sigma\text{C}23\text{-C}33}$ (Figure 5.2). As the core-top of 114KL represents 9 ka BP, the $\Delta\Delta^{14}\text{C}$ -signature may potentially be biased by carbon exported later than 9 ka BP, so the data-point has to be interpreted with caution. The decrease in the $\Delta\Delta^{14}\text{C}$ -signature may indicate that the export of strongly pre-aged OM associated with permafrost decomposition ended at approx. 10.5 ka BP. According to the flooding scenario for the Bering Shelf by Manley (2002), major parts of the Bering Shelf were inundated after the Bering Strait had opened between 13-10 ka BP (Elias et al., 1992, 1996; Manley, 2002; Bradley and England, 2008), and the coastline changed only slightly after approx. 10 ka BP. Hence, reduced sea-level change in the Bering-Sea realm may have stopped permafrost erosion on the shelves adjacent to site 114KL.

5.5.2. *Implications for atmospheric CO_2 and $\Delta^{14}\text{C}$*

The first mobilization-event of ^{14}C -depleted carbon, which is associated with the LIS-retreat, initiates during the Mystery Interval (MI, lasting from 19-14 ka BP; Broecker et al., 2007). Although the atmospheric changes during the MI are assumed to have largely been fueled by outgassing from ^{14}C -depleted deep ocean carbon (Broecker, 2007; Schmitt et al., 2012; Skinner et al., 2012) and by the production rate of radiocarbon in the atmosphere (Köhler et al., 2006) our CSRA-results suggest that reworked pre-aged terrigenous OM was a possible additional contribution to the $\text{CO}_{2\text{atm}}$ and $\Delta^{14}\text{C}_{\text{atm}}$. The same potentially applied for the retreating Fennoscandian Ice Sheet (FIS), as intensified OM-mobilization associated with increasing drainage from the FIS during the early HS1/MI is also recorded in sediments from the Black Sea (Rostek and Bard, 2013; Soulet et al., 2013). However, to the knowledge of the authors, radiocarbon data to confirm or counter this idea are not available for the biomarkers in the Black-Sea sediments.

During the B/A, the mobilization-event on the shelf along Kamchatka associated with MWP-1a lags the accelerated increase in $\text{CO}_{2\text{atm}}$ and decrease in $\Delta^{14}\text{C}_{\text{atm}}$ by approx. 600 years (Figure 5.4). Together with the absence of a pronounced export event during MWP-1a at site 114KL this suggests that the sea-level induced destabilization of permafrost soils in the NW Pacific/western Bering-Sea realm was probably irrelevant for the abrupt changes of $\text{CO}_{2\text{atm}}/\Delta^{14}\text{C}_{\text{atm}}$. Since the sea-level induced mobilization of ^{14}C -depleted carbon around

Kamchatka seem to have been strongest during the B/A and PB when $\text{CO}_{2\text{atm}}$ was stagnating and $\Delta^{14}\text{C}_{\text{atm}}$ changed relatively slowly (Figure 5.4), sea-level induced destabilization of permafrost in the NW Pacific/Western Bering Sea region seems to have been insignificant for the major changes of $\text{CO}_{2\text{atm}}$ and $\Delta^{14}\text{C}_{\text{atm}}$. Initiating during the second half of the B/A on Kamchatka, thaw-induced mobilization of ^{14}C -depleted carbon occurs also too late to be

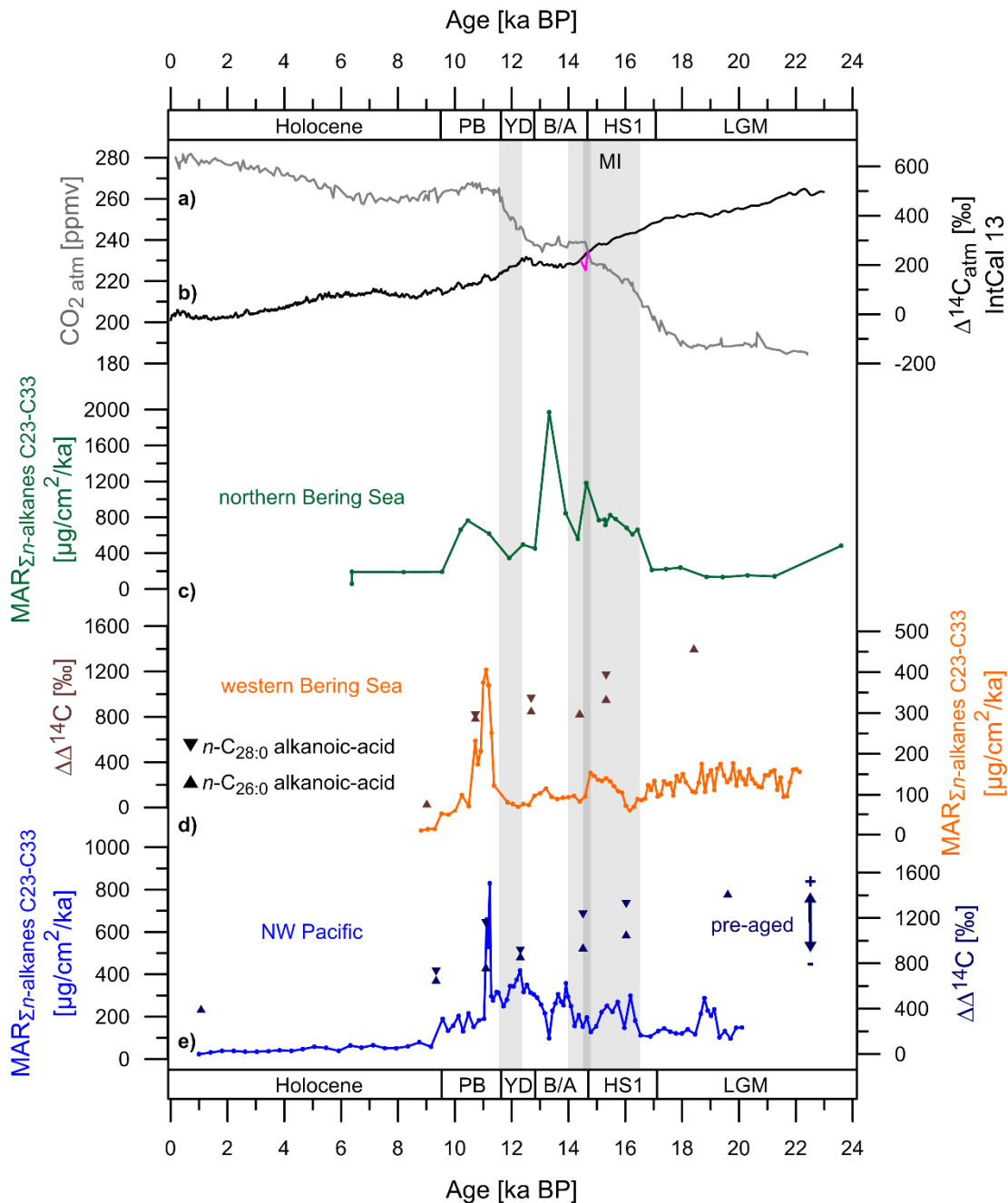


Figure 5.4. a) $\text{CO}_{2\text{atm}}$ from Epica Dome C (based on the age models of Monnin et al., 2001 and Parrenin et al., 2013). b) $\Delta^{14}\text{C}_{\text{atm}}$ from IntCal 13 (Reimer et al., 2013). The $\Delta^{14}\text{C}_{\text{atm}}$ -record from IODP-cores # 310, corals off Tahiti, is superimposed (pink line, modified after Durand et al., 2013). c) Mass accumulation rate of long-chain n -alkanes ($\Sigma\text{C}_{23}\text{-C}_{33}$) of core 18-3/6 (unpublished data V. Meyer). d) Mass accumulation rate of long-chain n -alkanes ($\Sigma\text{C}_{23}\text{-C}_{33}$) and radiocarbon data of long-chain n -alkanoic acids of core 114KL (this study), e) Mass accumulation rate of long-chain n -alkanes ($\Sigma\text{C}_{23}\text{-C}_{33}$) and radiocarbon data of long-chain n -alkanoic acids of core 12 KL (this study). Grey bars represent the pronounced phases of deglacial $\text{CO}_{2\text{atm}}/\Delta^{14}\text{C}_{\text{atm}}$ changes. MI: Mystery Interval.

relevant for the atmospheric changes. Hence, permafrost dynamics in the NW Pacific realm can probably be ruled out as important drivers for the increase/decrease in $\text{CO}_{2\text{atm}}/\Delta^{14}\text{C}_{\text{atm}}$ at that time. This counters the hypothesis of Köhler et al., (2014) according to which permafrost in Eurasia may have rapidly released carbon into the atmosphere in the course of abrupt warming and sea-level rise at 14.6 ka BP. Considering that $\text{MAR}_{\Sigma\text{C}_{23-\text{C}_{33}}}$ at site 18-3/6 indicate that shelf-flooding mobilized OM from the BLB (Figure 5.2) and display a maximum at 14.6 ka BP (Figures 5.2 & 5.3) it seems still possible that the shelves from the northern Bering Sea represented a source ^{14}C -depleted CO_2 . Since, the BLB, together with the Siberian shelves (Figure 5.1), was among the largest permafrost-covered shelf-areas during the LGM (Vandenberghe et al., 2014; Köhler et al., 2014) it may have been an important for the rapid atmospheric changes (Köhler et al., 2014). However, the sampling resolution of core 18-3/6 is too coarse to precisely constrain the mobilization-timing and CSRA-data for the OM is not available. Therefore, the authors plan to analyze the radiocarbon activity of leaf-wax lipids in core 18-3/6 in order to investigate the timing of sea-level induced permafrost decomposition on the BLB.

Persisting into the YD, enhanced thaw-induced carbon release (on Kamchatka) may have presented an additional source to fuel the $\text{CO}_{2\text{atm}}/\Delta^{14}\text{C}_{\text{atm}}$ changes between approx. 12.6 and 11.2 (Figure 5.4), next to oceanic outgassing which is suggested as driver of the atmospheric changes (e.g. Skinner et al., 2010). The timing of Kamchatka contrasts the idea that permafrost is unlikely to have provided CO_2 at that time given the widespread cold-spell at that time. Considering the small size of Kamchatka (relative to permafrost covered regions in Eurasia, Vandenberghe et al., 2014) the inferences for atmospheric changes (during both, the onset of the B/A and the YD) adopted here would only apply if carbon export during permafrost thaw in large parts of Eurasia had a similar timing as Kamchatka. However, at the onset of the B/A (14.6 ka BP) biomarker concentrations in Black-Sea sediments abruptly increase which was assumed to reflect abruptly initiating permafrost decomposition in southeastern Europe (Rostek and Bard, 2013). In contrast to the Kamchatka data, this would support the hypothesis of Köhler et al., (2014). As for the YD, existing studies indicate that European permafrost stabilized during the cold-reversal (Renssen and Vandenberghe, 2003; Gruber and Reitner, 2007; Fischer et al., 2008; Rostek and Bard, 2013). Rostek and Bard (2013) suggested that diminishing input of terrigenous biomarkers into the Black Sea were in connection with reduced soil erosion due to stabilizing permafrost conditions. Considering the discrepancies between the Kamchatka data and other studies regional differences regarding the timing of permafrost decomposition seem likely and permafrost thaw on the Peninsula

could have been decoupled from continental Eurasia. So, a large-scale relevance of permafrost decomposition as suggested by the Kamchatka-data from this study, seems questionable but not impossible considering the sparseness of data constraining the timing of carbon mobilization during Eurasian permafrost-thaw. This highlights the need of further investigations of the deglacial mobilization of ^{14}C -depleted OM in Eurasia.

5.6. Summary and Conclusions

This study provides insights into the LGM-to-Holocene-development of terrestrial residence times (i) and provenance of terrigenous OM in the NW Pacific/Bering Sea realm (ii). The data allow inferences for the timing of deglacial permafrost destabilization in adjacent Beringia and the potential relevance for $\text{CO}_{2\text{atm}}$ and $\Delta^{14}\text{C}_{\text{atm}}$ (iii). The main findings can be summarized as follows.

- (i) During the LGM the terrestrial long-chain *n*-alkanoic acids are significantly more pre-aged when deposited in marine sediments than during the late Holocene. Transport of OM from the vegetation or the top-soils is probably strongly suppressed (relative to present) and OM may have mainly derived from riverbank erosion of permafrost soils. We hypothesize that this may have resulted from weak overland drainage during the LGM. However, the underlying mechanisms remain poorly understood and require further investigations of OM-transport in high latitudes during the LGM.
- (ii) During HS1 increased contributions of thermally mature OM (relative to the LGM and the later deglaciation), associated with the retreat of the LIS and the drainage of proglacial Lake Old Crow, point to a provenance-change of terrigenous OM in the Yukon-catchment. Having spilled out into the Western Bering Sea and the NW Pacific the Yukon-River load seems to have played an important role in the sedimentation processes in the NW Pacific/Western Bering Sea realm, until the early B/A. A significant influence of the Yukon load in the NW Pacific complicates biomarker-based reconstruction of palaeo-environmental conditions in the western Beringian realm.
- (iii) Mobilization of ^{14}C -depleted carbon intensifies during HS1 (16.8 and 14.6 ka BP) and is associated with enhanced melt-water runoff in the Yukon River. Thermally mature OM, riverbank erosion of permafrost and outwash from the retreating LIS may have provided ^{14}C -depleted OM. After approx. 14.6 ka BP, the sediment cores predominantly record mobilization of nearly ^{14}C -free OM associated with permafrost erosion during shelf-flooding. OM export is most pronounced during MWP-1b/PB. Thaw-induced OM-export in the Kamchatka-hinterland likely initiated during the late B/A and culminated during

the early YD. While shelf-erosion causes abrupt variations in OM-export, carbon release during permafrost-thaw seems to be a slow process and does not vary in-phase with abrupt temperature-fluctuations. Pronounced carbon mobilization and permafrost decomposition (from both processes) ended at approx. 9 ka BP. With a duration of more than 1000 years the carbon-mobilization event associated with permafrost thaw in the Kamchatka hinterland lasted significantly longer than the abrupt sea-level induced erosion events (200-700 years).

Terrigenous organic carbon, mobilized during ice-sheet retreat, presents a potential carbon source during the MI and further research should address the mechanisms that may have made the OM available for conversion to CO₂ and release to the atmosphere. The hypothesis of Köhler et al. (2014) according to which permafrost decomposition induced by shelf-flooding and abruptly rising temperatures was an important carbon source at the onset of the B/A, is challenged since mobilization-events of ¹⁴C-depleted OM (associated with both, MWP-1a and warming) lag the atmospheric event. Instead, the timing of permafrost thaw on Kamchatka implies that Eurasian permafrost soils may have fueled the atmosphere during the YD. Discrepancies with other studies require further research on the timing of deglacial permafrost decomposition and the associated carbon release in Eurasia.

Acknowledgements

The study was conducted within a PhD-project funded by the Helmholtz association through the President's Initiative and Networking Fund. Additional funding was obtained from GLOMAR – Bremen International Graduate School for Marine Sciences. Cores SO201-2-12KL and SO201-2-114KL were recovered within the frame of KALMAR-Leg 2 whereas cores SO202-18-3 and SO202-18-6 were obtained in the course of the INOPEX-research program. We acknowledge the support of Master and crew of R/V SONNE during cruises SO201 and SO202 in 2009. Dirk Nürnberg is thanked for providing sample material for site 12KL. We thank Alexander Weise and Arnaud Nicolas for their assistance on the geochemical sample-preparation in the laboratories. Negar Haghipour is thanked for her kind guidance and assistance on the sample preparation for AMS-measurements at the ETH Zurich. We very much appreciate the effort and help of Cameron McIntyre during the AMS-measurement at the Institute for Ion Beam Physics at ETH. The data of this study can be found on the online-database "Pangaea" (www.pangaea.de).

Appendix - 5

Table A 5.1. Samples sizes (expressed in μg carbon, μgC) together with the fMC-values and the respective measurement uncertainties (σ_{fMC}) from the AMS-measurement of fossil and modern standards used for the process-blank assessment (fossil: $n\text{-C}_{30:0}$ alkanolic acid; modern: $n\text{-C}_{16:0}$ alkanolic acid). 1: adopted from Rethemeyer et al. (2013).

Standard material	Mass [μgC]	fMC	σ_{fMC}
Apple peel bulk unprocessed	38.3	1.0103	0.0089
Apple peel $n\text{-C}_{16:0}$ processed	150.6	0.9650	0.0078
Apple peel $n\text{-C}_{16:0}$ processed	22.4	0.9013	0.0083
Sigma Aldrich $n\text{-C}_{30:0}$ unprocessed	n.a.	0.0025 ¹	0.0007 ¹
Sigma Aldrich $n\text{-C}_{30:0}$ processed	24.0	0.1453	0.0038

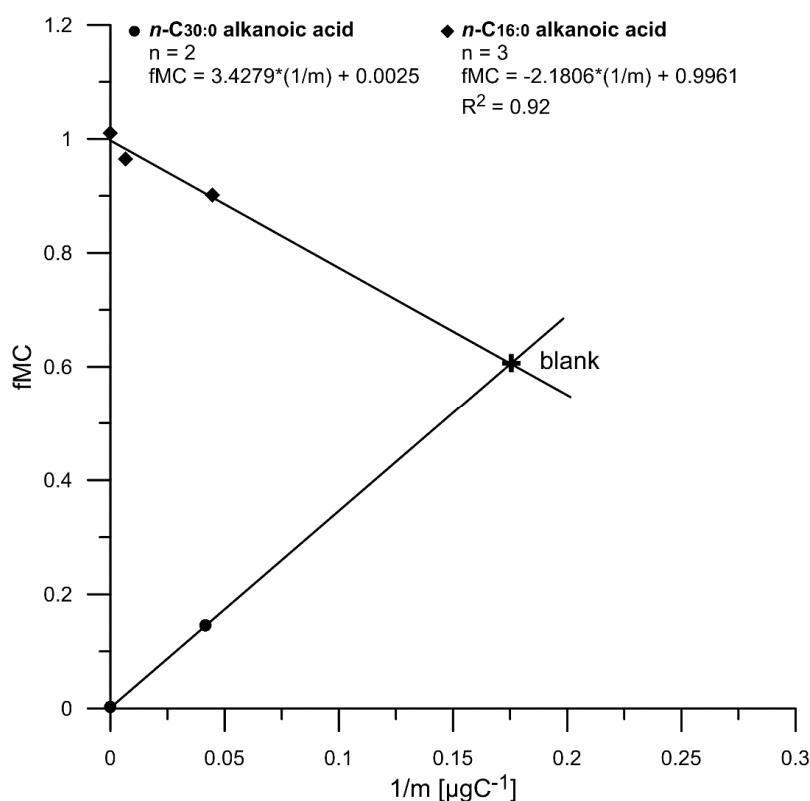


Figure A 5.1. Graphical assessment of the fMC-value and the mass of the process blank ($\text{fMC}_{\text{blank}}$ & m_{blank}) based on the AMS-results of modern and fossil standards shown in Table A1. The intercept of the two regression lines yields an $\text{fMC}_{\text{blank}}$ of **0.6097** and an m_{blank} of **5.6 μg Carbon (μgC)**. The uncertainty for $\text{fMC}_{\text{blank}}$ (σ_{fMC}) and m_{blank} (σ_m) were determined by the regression coefficient R^2 of the $n\text{-C}_{16:0}$ dataset. The dataset of the $n\text{-C}_{30:0}$ was ignored since $n = 2$. Based on the R^2 of 0.92 σ_{fMC} would be **0.08**. According to Shah and Pearson (2007), the R^2 -value of 0.92 implies that the both, the $\text{fMC}_{\text{blank}}$ and the m_{blank} , are predicted with 92% certainty by the respective regression line. Therefore, these authors inferred that σ_m can be determined by: $\sigma_m = m_{\text{blank}} \cdot (1 - R^2)$. Based on $R^2 = 0.92$ the equation yields $\sigma_m = \mathbf{0.5 \mu\text{gC}}$. It has to be acknowledged that σ_m and σ_{fMC} are likely underestimated since the uncertainties of the $n\text{-C}_{30:0}$ -dataset could not be taken into account.

Table A 5.2. List of CSRA-samples from cores SO201-2-12KL and SO201-2-114KL, the respective sample sizes (expressed in μgC) and the AMS-results for long-chain *n*-alkanoic acids (expressed as fMC-values). σ_{fMC} represents the respective measurement uncertainties from the AMS. Radiocarbon data for site 18-3/6 are not available yet.

Sample (core, depth [cm], compound)	Sample size [μgC]	fMC	σ_{fMC}
12KL, 1-4.5, <i>n</i> -C _{26:0}	17.6	0.5730	0.0074
12KL, 203-205, <i>n</i> -C _{26:0}	100.2	0.1636	0.0029
12KL, 203-205, <i>n</i> -C _{28:0}	81.8	0.1542	0.0032
12KL, 295-297, <i>n</i> -C _{26:0}	13.09	0.3232	0.0064
12KL, 295-297, <i>n</i> -C _{28:0}	9.4	0.3046	0.0074
12KL, 419-422, <i>n</i> -C _{26:0}	72.3	0.1228	0.0028
12KL, 419-422, <i>n</i> -C _{28:0}	63.2	0.1183	0.0029
12KL, 609-612, <i>n</i> -C _{26:0}	46.4	0.1214	0.0030
12KL, 609-612, <i>n</i> -C _{28:0}	22.4	0.1302	0.0037
12KL, 693-696, <i>n</i> -C _{26:0}	71.2	0.0858	0.0026
12KL, 693-696, <i>n</i> -C _{28:0}	40.08	0.0862	0.0029
12KL, 896-898, <i>n</i> -C _{26:0}	36.9	0.0847	0.0029
114KL, 3-5.5, <i>n</i> -C _{26:0}	25.5	0.4132	0.0055
114KL, 39-41.5, <i>n</i> -C _{26:0}	151.2	0.1092	0.0026
114KL, 39-41.5, <i>n</i> -C _{28:0}	144.4	0.1048	0.0026
114KL, 101-103.5, <i>n</i> -C _{26:0}	83.5	0.1136	0.0028
114KL, 101-103.5, <i>n</i> -C _{28:0}	56.1	0.1102	0.0029

Continued on the next page

Sample (core, depth [cm], compound)	Sample size [μgC]	fMC	σ_{fMC}
114KL, 144-146.5, <i>n</i> -C _{26:0}	98.3	0.0983	0.0029
114KL, 174-176.5, <i>n</i> -C _{26:0}	74.3	0.0926	0.0027
114KL, 174-176.5, <i>n</i> -C _{28:0}	31.2	0.1131	0.0033
114KL, 301-303.5, <i>n</i> -C _{26:0}	51.7	0.0404	0.0025

6. Summary and Perspectives

The studies carried out within this thesis ultimately aimed at (i) contributing to a better understanding of climatic conditions of the subarctic NW Pacific realm during the LGM and the last deglaciation, emphasizing on temperature development and the controls, and (ii) reconstructing the time-scales of mobilization of ^{14}C -depleted OM during deglacial permafrost thaw in Northeast Siberia (Kamchatka and the adjacent Koryak region) in order to identify time-intervals when the region potentially represented a source of ^{14}C -depleted CO_2 . The LGM-to-Holocene temperature development of the NW Pacific realm was investigated by establishing continuous LGM-to-Holocene summer-SST records for the Western Bering Sea and the NW Pacific using the $\text{TEX}^{L_{86}}$ -palaeothermometry, and by establishing a record in summer MAT (MAT_{ifs}) for Kamchatka applying the CBT/MBT²-temperature proxy. It was intended to obtain insights into the impact of regional and supra-regional climate drivers, such as insolation, atmospheric CO_2 , N Atlantic climate change or regional oceanic and atmospheric circulation. Mass balance calculations for the palaeo glaciers on Kamchatka and the Kankaren Range (NE Siberia) were used to estimate LGM precipitation abundance and to investigate the controls for restricted glaciation in the region during the LGM. Temperature development and inferences for precipitation were used to validate climate-model outputs.

The established temperature records were used to investigate infer temperature controls on deglacial permafrost dynamics Beringia (particularly on Kamchatka and the Koryak area) and the associated mobilization of ^{14}C -depleted OM. Mass accumulation rates and the $\Delta^{14}\text{C}$ -signature of terrigenous biomarkers was used to identify periods enhanced OM-export into the NW Pacific and the Western Bering Sea. It was aimed to test the hypothesis that AMOC-induced temperature variation controlled permafrost decomposition in the region and making permafrost a potential source ^{14}C -depleted CO_2 at the onset of the B/A-interstadial, but not during HS1 and the YD-cold reversals. Furthermore, it was tested whether or not rapid shelf-flooding during MWP-1a mobilized ^{14}C -depleted OM on the shelves in the Bering Sea/NW Pacific shelves.

The main findings can be summarized as follows:

6.1. LGM climatic conditions and deglacial temperature change

LGM SST in the Western Bering Sea and the NW Pacific were both colder than at present but the magnitude of glacial cooling was more pronounced in the Western Bering Sea than in the NW Pacific ($3^\circ\text{C}/1.5^\circ\text{C}$; see chapter 2). MAT_{ifs} were as warm as at present (see chapter 3).

Ocean cooling is in general agreement with lowered CO_{2atm} and summer insolation during the LGM but altered configurations of oceanic surface and atmospheric circulation seem to have counteracted the cooling effects of the CO_{2atm} and insolation in the NW Pacific and on Kamchatka. The SST data imply that the Alaskan Stream accumulated in the NW Pacific during the LGM when sea-level was 120 m below present so Unimak Pass and other Aleutian passes became exposed (chapter 2). This weakened the inflow of relatively warm Pacific waters into the Bering Sea and at the same time made the relatively warm water masses of the Alaskan Stream (warm relative to the East Kamchatka Current) more influential in the marginal NW Pacific. This led to relatively weak cooling in the NW Pacific compared to the Bering Sea (chapter 2). At the same time stronger than present southerly winds over the marginal NW Pacific, presumably resulting from a strengthened North Pacific High Pressure System over the marginal NW Pacific, likely accounted for warm summers on Kamchatka. As summer temperature in large parts of NE Siberia were similar to today or even warmer while the N Pacific was colder than at present (see chapter 3 and references therein) it is suggested that an increased thermal pressure gradient may have amplified the southerly flow during the LGM. Moreover, a westward displacement of the NPH due to a persistent anticyclone over the American ice sheets may have accounted for the strong southerly flow over the subarctic NW Pacific (chapter 3). The relatively small reduction of summer SST in the NW Pacific (1.5°C) probably supported the establishment of warm summers on Kamchatka as the cooling marine influences may have been small compared to today. In turn, the increased southerly winds over the subarctic NW Pacific (as suggested in chapter 2) may have additionally weakened the influence of the East Kamchatka Current in the subarctic NW Pacific during the last glacial, and may have contributed to the relatively warm SST during the LGM, at least during the summer season.

Based on the summer temperature data for Kamchatka and existing data for the Kankaren Range it was hypothesized that glacial precipitation must have been abundant if mountain glaciation was more extensive than today while summers were as warm as at present. This view was supported by mass-balance calculations for the palaeo glaciers, suggesting that precipitation must have been similar or even more abundant than at present (chapter 4). It was inferred that summer temperature restricted glacier growth which contrasts the prevailing hypothesis according to which aridity hampered ice sheet growth in the region. The strengthened southerly winds potentially supplied the Pacific Sector of Siberia with enough moisture.

The HS1 was characterized by heterogenous temperature development which is largely caused by the accumulation of Alaskan Stream waters in the NW Pacific. In the Bering Sea a cold-spell equivalent to the Heinrich Event 1 in the N Atlantic provided evidence for atmospheric teleconnections. In contrast, SST in the NW Pacific warmed progressively without being interrupted by a similar cold spell as in the Western Bering Sea/N Atlantic. The Alaskan Stream waters seem to have linked the NW Pacific with the Gulf of Alaska, where a southward displacement of the westerly Jet, caused by the presence of the Laurentide ice sheet, inhibited the establishment of an atmospheric coupling with the N Atlantic (chapter 2 and references therein) prior to 15 ka BP. On Kamchatka a pronounced cold spell between 18 and 15 ka BP was probably not associated with AMOC-variability. Its origin could not be identified. Similarities between MAT_{ifs} and the NW Pacific SST during HS1 suggested that the temperature evolution on Kamchatka responded to the influence of the Alaskan Stream. The oceanographic linkage between the eastern and western Pacific ended with the opening of the Aleutian Passes between approximately 12 and 10 ka BP, as adopted from the SST-data.

From 15 ka BP onwards the temperature development in the NW Pacific realm and Kamchatka seems to be strongly determined by atmospheric teleconnections with the N Atlantic since the B/A-warm phase, the YD cold-spell and the subsequent abrupt warming into the Preboreal are clearly exhibited by the SST and MAT-records. This is in line with several SST records from the NE Pacific and the Sea of Okhotsk, suggesting that atmospheric teleconnections widely determined temperature variation in the subarctic N Pacific realm (chapters 2 & 3 and references therein).

As for summer temperature on Kamchatka, LGM atmospheric circulation and LGM precipitation in the NW Pacific several climate-models contrast with the result of this thesis. Models suggest cold summers, a weakened HPH and decreased precipitation (see Chapters 3 and 4). Also, the temperature development during HS1 is only partly in line with climate model outputs as models which suggest atmospheric teleconnections, predict widespread cooling over the entire N Pacific (see chapter 2 and references therein).

6.2. *Time-scales of OM-mobilization*

The SST and MAT_{ifs} records provided evidence for cold conditions during HS1 and the YD and for abrupt warming into the B/A-interstadial. On Kamchatka the stadials have even been the coldest episodes since the LGM as far as summer temperature is concerned. So the deglacial temperature evolution corroborates the idea that permafrost decomposition and the associated mobilization of ¹⁴C-depleted OM may have followed N Atlantic temperature

variations and that permafrost in the Kamchatka region may have represented a source of ^{14}C depleted CO_2 at 14.6 ka BP. It is found that enhanced export (relative to the LGM and the late Holocene) of ^{14}C -depleted OM into the N Pacific happened between approximately 17 and 9 ka BP and occurred in four pulses. Although HS1 was a cold episode with colder than or similar temperatures as during the LGM (see chapters 2 & 3) permafrost erosion seems to have strengthened at that time. Instead of temperature it was likely associated with strengthened fluvial erosion in the Yukon-River catchment triggered by the beginning retreat of the Laurentide ice sheet and drainage of proglacial lakes (chapter 5). Coinciding with increasing $\text{CO}_{2\text{atm}}$ and decreasing $\Delta^{14}\text{C}_{\text{atm}}$ permafrost erosion appears as potential source of ^{14}C -depleted OM during the Mystery Interval. During MWP-1a and MWP-1b rapid flooding of permafrost covered shelves along the Koryak Range and Kamchatka caused abrupt and pronounced mobilization of ^{14}C -depleted OM. Permafrost thaw in the Kamchatka interior likely initiated in the second half of the B/A-warm phase, peaked during the YD-cold spell and ended around 9 ka BP (chapter 5). Mobilization of ^{14}C -depleted OM was strongest during the Preboreal and likely associated with MWP-1b. As for duration of carbon mobilization and permafrost degradation sea-level rise caused abrupt short events in the range of approximately 200-700 years. By contrast the retreat of permafrost in the Kamchatka hinterland appears as a process of millennia (see chapter 5).

The identified timing of carbon mobilization counters the hypotheses that permafrost decomposition and the associated carbon release followed abrupt temperature variations caused by N Atlantic climate change. Carbon mobilization in the Kamchatka-region the rapid atmospheric CO_2 and $\Delta^{14}\text{C}$ changes at 14.6 ka BP and was probably not important for the atmospheric event. Also, the shelf erosion during MWP-1a initiated too late in the area to be considered as CO_2 source during the early B/A. Not responding to the YD cold-spell the carbon mobilization on Kamchatka represents itself as possible source of ^{14}C -depleted CO_2 for rising $\text{CO}_{2\text{atm}}$ -levels and declining $\Delta^{14}\text{C}_{\text{atm}}$.

6.3. Perspectives – LGM climatic conditions and deglacial temperature development.

This thesis provides the first continuous and quantitative temperature records for the Western Bering Sea, the marginal subarctic NW Pacific and the Kamchatka Peninsula. This allowed for new insights into regional oceanic and atmospheric circulation patterns during the LGM. The combination of MAT_{ifs} with data on LGM-glacier extent on Kamchatka provided a first but indirect insight into glacial precipitation on Kamchatka and the Pacific Sector of Siberia. The SST and MAT records also identified new aspects regarding the nature of teleconnections

(particularly during HS1) and contributes to better comprehension of the connectivity of the NW Pacific and adjacent Siberia to N Atlantic climate variability. As AMOC-weakening is predicted for the future, this might be useful for assessing the supra-regional impact of a potential future negative feedback triggered by AMOC-weakening.

The information on summer temperature, precipitation, atmospheric circulation and SST-development during HS1 is important for the modelling community since several discrepancies with climate models regarding these points were identified. Those discrepancies highlight the need to further investigate precipitation and temperature development in the region, using both, proxies and climate models, in order to identify where climate models may insufficiently represent the interaction of several climatic forcings in the region (e.g. the effect of continentality in Siberia), or where proxy-interpretations go wrong due to (e.g. biases). More proxy-based data on precipitation are necessary to confirm the newly established hypotheses of increased precipitation in the region and of summer temperature as limiting factor for ice sheet growth. This particularly applies to Kamchatka where no proxy-data on precipitation is available. Pollen-data from terrestrial archives would be a desirable complement to the degree-day-model data. The need of further proxy-based reconstructions of precipitation and (summer) temperature in western Beringia also manifests itself by inconsistencies within proxy-based inferences for LGM-climatic conditions. Proxies generate the picture of warm summers, extensive mountain glaciation and dryer-than-present conditions in NE Siberia. The finding from the DDM indicates that these conditions are very unlikely to have co-existed. The application of different proxies (e.g. beetles, pollen brGDGTs for summer temperature) at the same location may represent a way to identify potential biases or misinterpretations.

The temperature reconstruction from this thesis are indicators for the summer season. However, information on winter or annual mean temperatures would be important to better understand the interaction of temperature and cryosphere in the region. It is not clear why carbon mobilization - likely associated with permafrost-decomposition - proceeded through and even culminated during the YD, despite a pronounced cold-spell at that time. Also, it remains an open question how far the annual temperature cycle, (the length of the summer and winter season) may have influenced glacier extent in the Sredinny and Kankaren Ranges. Together with the existing summer temperature data palaeo-winter temperature would provide insights into the annual temperature range and may also allow insights into the length of the season, e.g. by modelling the annual temperature cycle. Oxygen isotopes from ice-wedges

have been applied as winter temperature archives in Siberia (e.g. Meyer et al., 2002) and if present in the vicinity of Kamchatka, those might help to better constrain climate change in the region.

In terms of SST reconstruction in the subarctic N Pacific and its marginal seas, chapter 2 identifies the $\text{TEX}^{\text{L}}_{86}$ as alternative to the unsaturation of alkenones. Since the $\text{U}^{\text{K}'}_{37}$ is often afflicted with several problems in sediments deposited prior to 15 ka BP, the $\text{TEX}^{\text{L}}_{86}$ is promising for unravelling oceanographic changes during the early deglaciation. For instance constraints on water column stratification may help to understand intermediate water formation during HS1 in the Bering Sea (e.g. Riethdorf et al., 2013; Knudson and Ravelo, 2015). From the SST records (provided in this thesis) for the Western Bering Sea and the NW Pacific one may hypothesize that the marginal seas (the Bering Sea and the Sea of Okhotsk) were affected by atmospheric teleconnections with the N Atlantic during HS1 (since a cold-spell is shown for the Bering Sea but not for the N Pacific). Future applications of the $\text{TEX}^{\text{L}}_{86}$ in the Sea of Okhotsk may help to test this hypothesis. Although there is consensus that the existing $\text{U}^{\text{K}'}_{37}$ -based LGM-SST in the Sea of Okhotsk are biased by shifting blooming seasons of coccolithophorids, the conclusion that precipitation must have been at least as abundant as at present challenges this idea since warm summer conditions in the Sea of Okhotsk would have represented a source of moisture (see chapter 4). $\text{TEX}^{\text{L}}_{86}$ -based SST-reconstruction may help to improve the understanding of LGM surface conditions.

6.4. *Perspectives – export of terrigenous OM*

In Chapter 5 it was identified that the provenance of the OM changed during HS1 as a significant portion of the lipid-biomarkers in the sediments from the NW Pacific and the Western Bering Sea likely derived from the Yukon catchment. This complicates the application of biomarkers as palaeo-environmental indicators for western Beringia. So one may question the CBT/MBT-derived temperatures during HS1. However, brGDGTs seem to be too prone to degradation to be transported over long distances, in contrast to the refractory *n*-alkanes (e.g. Schouten et al., 2013). So it seems very likely that brGDGT do monitor Kamchatka temperatures during HS1. Nevertheless, given the provenance change, data on terrigenous biomarkers (e.g. distribution of compounds or adopted climate signals) should be compared to biomarker assemblages from the eastern Bering Sea, in order to identify groups of biomarkers that are concerned by this provenance pattern.

By analyzing mass accumulation rates and $\Delta^{14}\text{C}$ of terrigenous biomarkers in marine sediments from the subarctic NW Pacific and the Bering Sea, new insights into the timing of

mobilization of ^{14}C -depleted OM during deglacial permafrost decomposition could be adopted. When discussing the relevance of permafrost decomposition for the atmosphere one has to keep in mind that the approach does not allow inferences regarding the fraction of the mobilized carbon that entered the atmosphere as CO_2 . It is possible to make assessments of the timing and relative intensity of pronounced mobilization phases and this can be used for estimating the likelihood during which intervals permafrost may have contributed to the atmospheric greenhouse gases. By generating the counterintuitive idea that permafrost-thaw may have represented a source of CO_2 during the YD-cold spell instead of the early B/A it also revealed new aspects about the general role permafrost may have played in atmospheric $\text{CO}_2/\Delta^{14}\text{C}$ changes since such timing as found here has not been described beforehand. This makes further studies investigating OM-mobilization during permafrost thaw elsewhere in the NH, in order to assess the spatial dimension of this timing. This would be an important step to unravelling the potential role of permafrost in influencing the atmospheric carbon pool. As such, the combination of mass accumulation rates of biomarkers combined with CSRA should be applied off Eurasian river systems with larger catchments than the Kamchatka Peninsula, for instance in the Black Sea. Chapter 5 of this thesis suggests that shelf-erosion during rapid sea-level rise was a powerful mechanism to mobilize permafrost derived OM during the deglaciation. In this light, carbon mobilization and the $\Delta^{14}\text{C}$ -signature of the mobilized OM should be investigated on the Siberian Shelf and the Bering Shelf as those areas were the largest permafrost covered shelves during the LGM and represent a potentially important carbon sources for the atmosphere. This is highlighted by the biomarker data from 18-3/6 which indicates that OM was mobilized from the Bering Shelf at 14.6 ka BP (Chapter 5). As it remains unclear whether or not the mobilized OM was depleted in ^{14}C , CSRA-data for this core is highly necessary to confirm this hypothesis core.

Providing evidence that the mobilization ^{14}C -depleted terrigenous OM in formerly permafrost covered areas increased during the deglaciation supports the hypothesis that formerly freeze-locked, ^{14}C -depleted carbon potentially became available for biogeochemical cycling and potentially entered the atmosphere as greenhouse gases. This corroborates the expectation of future mobilization of the carbon stock preserved in permafrost today, highlighting the need to include permafrost modules into carbon cycle models. The data adopted in this thesis (regarding the timing of carbon mobilization and $\Delta^{14}\text{C}$ -signature of the mobilized OM) could be implemented into permafrost modules of (transient) carbon cycle models which estimate the impact of deglacial as well as future permafrost decomposition on atmospheric greenhouse gas concentrations.

7. Acknowledgements

The three years I spent working on my PhD-project were an awesome and intensive experience in which I learned incredibly much and made many new friends.

My very special thanks go to my supervisor Gesine Mollenhauer. Thank you, Gesine, very much for entrusting me with this super interesting, exciting, fiddling, sometimes challenging and complex project. It fit my scientific interests perfectly and I enjoyed working on it very much. I really appreciate your good guidance, the time you were always willing to spend for helping me and your readiness to support me in realizing my own ideas, or to join summer schools and conferences and to organize research stays. Furthermore, I am grateful you sent me on a research cruise with RV Maria S. Merian so I could make the exciting experience of working on board a research vessel.

I enjoyed being part of Gesine's working group where scientific discussion, joint trouble shooting in the lab, our conversations at lunch time and joint coffee-breaks, our Christmas parties or our canoeing adventures, created a friendly and motivating atmosphere which made working in the group big fun. So thanks to all group members Maria Winterfeld, Célia Santos, Eunmi Park, Sarah Trojahn, Thorsten Riedel, Katja Hockun, Wenwen Chen, Andreas Basse, Shuwen Sun and Jens Hefter as well as to the former members Sze Ling Ho, Wolf Dummann and Pai Han.

I am also really grateful to Jens Hefter for providing important support in the lab, and his tireless willingness to help with any problems that may have occurred. I enjoy thinking back to the fun we had in the lab and moreover very much appreciate his abilities as "AWI-postman" who would carry countless important documents or samples from Bremen to Bremerhaven and vice versa.

I enjoyed sharing an office with the PhD students Shuwen Sun, Hanna Lührs, Kristin Hoffmann, and Li Wang. Together we went through all ups and downs of a PhD-life and helped each other through various problems.

I thank Bernhard Diekmann for reviewing my thesis.

As members of my thesis committee Ralf Tiedemann and Peter Köhler are thanked for providing constructive ideas and advice during the meetings.

I am very grateful to have received additional funding from GLOMAR - Bremen Graduate School in Marine Sciences, which allowed the participation in conferences, the Urbino Summer School in Palaeoclimatology and ,most important, the research stay at Queen's

University Belfast/Northern Ireland. Owing to these social events I met many colleagues from all over the world, found many new friends and could very much enjoy the international aspect of science.

At this point, I would like to warmly thank Iestyn Barr for providing the opportunity to spend four weeks in his working group and for introducing me into the world of palaeo-glacier reconstruction. Without the research stay at Queen's I would not have been able to develop the third manuscript. His friendly and helpful cooperation during the research stay at Queen's made the time in Northern Ireland an efficient episode of my PhD which I thoroughly enjoyed.

I would like to thank my co-authors Lars Max and Gerrit Lohmann for the fruitful and inspiring discussion about my data. Lars is thanked for helping me getting started by sharing his knowledge about palaeoceanography of the N Pacific realm. Those discussions gave me a good impulse to bring the interpretations of my data on their ways.

Furthermore, I thank Hella Buschoff and Stephanie Buchmeister for support during TOC-measurements at the University of Bremen. Arnaud Nicolas and Alexander Weise are acknowledged for their assistance during the laboratory sample preparations at the University of Bremen. Cameron McIntyre and Negar Haghypour are thanked for their professional and kind assistance and guidance during the sample preparation and the AMS measurements at ETH Zürich.

Apart from scientific staff, I very much thank friends and family who were a good balance for the sometimes stressful life as PhD-student. The time I spent at the horse-stables or riding along the Wümme-River or talking with friends over drinks has always been a refreshing and most welcome break from PhD-related work.

Last but not least I express my gratitude to my parents who forwarded all my ambitions always believing in my talents and skills. Without their motivation, support and confidence in me, I would not be where and who I am.

8. References

- Akerman, H. J., and Johansson, M.: Thawing permafrost and thicker active layers in sub-Arctic Sweden, *Permafr. Process.*, 19, 279–292, 2008.
- Alder, J. R., Hostetler, S. W. and Sciences, A.: Global climate simulations at 3000-year intervals for the last 21 000 years with the GENMOM coupled atmosphere – ocean model, *Clim. Past*, 11, 449–471, doi:10.5194/cp-11-449-2015, 2015.
- Alfimov, A. V. and Berman, D. I.: Beringian climate during the Late Pleistocene and Holocene, *Quat. Sci. Rev.*, 20(1-3), 127–134, doi:10.1016/S0277-3791(00)00128-1, 2001.
- AMAP: Snow, water, ice and permafrost in the Arctic (SWIPA). Oslo: Arctic Monitoring and Assessment Programme (AMAP), 2012.
- Ananicheva, M. D., Krenke, A. N., Hanna, E., 2008. Mountain glaciers of NE Asia in the near future: a projection based on climate-glacier systems interaction. *Cryosphere Discussion*, 2, 1-21.
- Anderson, P. M., Edwards, M. E., Brubaker, L. B.: Results and Palaeoclimate implications of 35 years of palaeoecological research in Alaska, *Development in Quaternary Science* 1, 427–440, 2003.
- Anderson, P. A., and Lozhkin, A. V.: Late Quaternary vegetation of Chukotka (Northeast Russia), implications for Glacial and Holocene environments of Beringia, *Quat. Sci. Rev.*, 107, 112-128, 2015.
- Anderson, P. M., Lozhkin, A. V., Brubaker, L. B.: A lacustrine pollen record from North Priokhot'ya: new information about late Quaternary vegetational variations in western Beringia, *Arctic Alpine Res.*, 28, 93–98, 1996.
- Anderson, P. M., Lozhkin, A. V., Brubaker, L. B.: Implications of a 24000-yr palynological record for a Younger Dryas cooling and for boreal forest development in northeastern Siberia, *Quat. Res.* 57, 325–333, 2002.
- Anderson, P. M., Reanier, R. E., Brubaker, L. B.: A 14000-year pollen record from Sithylenkat Lake, north-central Alaska. *Quat. Res.*, 33, 400–404, 1990.
- Andrén, E., Klimaschewski, A., Self, A. E., Amour, N. St., Andreev, A. A., Bennett, K. D., Conley, D. J., Edwards, T. W. D., Solovieva, N. and Hammarlund, D.: Holocene climate and environmental change in north-eastern Kamchatka (Russian Far East), inferred from a multi-proxy study of lake sediments, *Glob. Planet. Change*, 134, 41–54, doi:10.1016/j.gloplacha.2015.02.013, 2015.
- Andreev, A. A., Klimanov, V. A. and Sulerzhitsky, L. D.: Younger Dryas pollen records from central and southern Yakutia, *Quat. Int.*, 41/42, 111–117, 1997.
- Arkipov, S. A., Isaeva, L. L., Bepaly, V. G., Glushkova, O. Y.: Glaciation of Siberia and North-East USSR, *Quat. Sci. Rev.* 5, 463–474, 1986.
- Barnes, F. F.: Coal Resources of Alaska, Geological Survey Bulletin 1242-B, United States Printing Office, 1962.
- Barr, I. D. and Clark, C. D.: Glaciers and climate in Pacific Far NE Russia during the Last Glacial Maximum, *J. Quat. Sci.* 26, 227–237, 2011.
- Barr, I. D. and Clark, C. D.: Late Quaternary glaciations in Far NE Russia: combining moraines, topography, and chronology to assess regional and global glaciation synchrony, *Quat. Sci. Rev.* 53, 72–87, 2012.
- Barr, I. D. and Solomina, O.: Pleistocene and Holocene glacier fluctuations upon the Kamchatka Peninsula, *Glob. Planet. Change*, 1–11, 2014.

- Barr, I. D. and Spagnolo, M.: Palaeoglacial and Palaeoclimatic conditions in the NW Pacific, as revealed by a morphometric analysis of cirques on the Kamchatka Peninsula, *Geomorphology*, 192, 15–29, 2013.
- Barron, J. A., Heusser, L., Herbert, T. and Lyle, M.: High-resolution climatic evolution of coastal northern California during the past 16,000 years, *Palaeoceanography*, 18(1), 1020, doi:10.1029/2002PA000768, 2003.
- Bartlein, P. J., Anderson, K. H., Anderson, P. M., Edwards, M. E., Mock, C. J., Thompson, R. S., Webb, R. S., Webb, T. and Whitlock, C.: Palaeoclimate simulations for North America over the past 21,000 years: Features of the simulated climate and comparisons with palaeoenvironmental data, *Quat. Sci. Rev.*, 17(6-7), 549–585, doi:10.1016/S0277-3791(98)00012-2, 1998.
- Berger A. and Loutre M. F.: Insolation values for the climate of the last 10 million years. *Quat. Sci. Rev.*, 10, pp. 297-317, 1991.
- Berman, D., Alfimov, A. and Kuzmina, S.: Invertebrates of the relict steppe ecosystems of Beringia, and the reconstruction of Pleistocene landscapes, *Quat. Sci. Rev.*, 30(17-18), 2200–2219, doi:10.1016/j.quascirev.2010.09.016, 2011.
- Bigelow, N. H. and Edwards, M. E.: A 14000 yr palaeoenvironmental record from Windmill Lake, central Alaska: evidence for high-frequency climatic and vegetation fluctuations, *Quat. Sci. Rev.*, 20, 203–215, 2001.
- Bigg, G. R., Clark, C. D., Hughes, A. C. L.: A last glacial ice sheet on the Pacific Russian Coast and catastrophic change arising from coupled ice-volcanic interactions, *Earth Planet Sci. Lett.*, 265, 559-570, 2008.
- Biskaborn, B. K., Herzschuh, U., Bolshiyakov, D., Savelieva, L. and Diekmann, B.: Environmental variability in northeastern Siberia during the last ~13,300yr inferred from lake diatoms and sediment-geochemical parameters, *Palaeogeogr. Palaeoclimatol. Palaeoecol.*, 329-330, 22–36, doi:10.1016/j.palaeo.2012.02.003, 2012.
- Bradley, R. S. and England, J. H.: The Younger Dryas and the Sea of Ancient Ice, *Quat. Res.*, 70(1), 1–10, doi:10.1016/j.yqres.2008.03.002, 2008.
- Braithwaite R. J., Raper, S. C. B., Chutko, K.: Accumulation at the equilibrium line altitude of glaciers inferred from a degree–day model and tested against field observations, *Annals of Glaciology*, 43, 329–334, 2006
- Brassell, S. C., Eglinton, G., Marlowe, I. T., Pflaumann, U., Sarnthein, M.: Molecular stratigraphy: a new tool for climatic assessment. *Nature*. 320, 129-133, 1986.
- Bray, E. E. and Evans, E. D.: Distribution of *n*-paraffins as a clue to Recognition of source beds, *Geochim. Cosmochim. Acta* 22, 2-15, 1961.
- Brigham-Grette, J., Gualtieri, L. M., Glushkova, O. Yu., Hamilton, T.D., Mostoller, D., Kotov, A.: Chlorine-36 and ¹⁴C chronology support a limited last glacial maximum across central Chutotka, north-eastern Siberia, and no Beringian ice sheet, *Quat. Res.* 59, 386–398, 2003.
- Broecker, W. S.: Glacial to interglacial changes in ocean chemistry, *Prog. Oceanogr.*, 11(2), 151–197, doi:10.1016/0079-6611(82)90007-6, 1982.
- Broecker, W. and Barker, S.: A 190‰ drop in atmosphere’s $\Delta^{14}\text{C}$ during the “Mystery Interval” (17.5 to 14.5 kyr), *Earth Planet. Sci. Lett.*, 256(1-2), 90–99, doi:10.1016/j.epsl.2007.01.015, 2007.
- Broecker, W. and Clark, E.: Search for a glacial-age ¹⁴C-depleted ocean reservoir, *Geophys. Res. Lett.*, 37(13), L13606, doi:10.1029/2010GL043969, 2010.

- Brooks, S. J., Diekmann, B., Jones, V. J. and Hammarlund, D.: Holocene environmental change in Kamchatka: A synopsis, *Glob. Planet. Change*, 134, 166–174, doi:10.1016/j.gloplacha.2015.09.004, 2015.
- Brovkin, V., Raddatz, T. Reick, C., Claussen, M. and Gayler, V.: Global biogeophysical interactions between forest and climate, *Geophys. Res. Lett.* 36, L07405, doi:10.1029/2009GL037543, 2009.
- Brown J., Ferrians, O. J., Heginbottom, J. A. and Melnikov, E. S.: Circum-Arctic Map of Permafrost and Ground-Ice Conditions. Boulder (CO): National Snow and Ice Data Center/World Data Center for Glaciology, 1998.
- Brubaker, L. B., Anderson, P. M. and Hu, F. S.: Vegetation ecotone dynamics in southwest Alaska during the late Quaternary, *Quat. Sci. Rev.* 20, 175–188, 2001.
- Budiko, M. I., Borzenkova, I. I., Menzhulin, G. B., Selyakov, K. I., 1992. Expecting changes of regional climate. *Izvestiya AN SSSR, Series Geographica*, 4, 36-52 (in Russian).
- Burlin, Y. K. and Agapitov, D. D.: Priority Directions of Oil-Gas Exploration in Anadyr Oil-Gas Basin, *Petroleum Geology: A digest of Russian literature on Petroleum Geology*, 36, 4, 307-314, 2002.
- Caissie, B. E., Brigham-Grette, J., Lawrence, K. T., Herbert, T. D. and Cook, M. S.: Last Glacial Maximum to Holocene sea surface conditions at Umnak Plateau, Bering Sea, as inferred from diatom, alkenone, and stable isotope records, *Palaeoceanography*, 25(1), PA1206, doi:10.1029/2008PA001671, 2010.
- Callaghan, T. V., Johansson, M., Anisimov, O., Christiansen, H. H., Instanes, A., Romanovsky, and V., Smith, S.: Changing permafrost and its impacts. In: *Snow, Water, Ice and Permafrost in the Arctic (SWIPA). Arctic Monitoring and Assessment Program (AMAP)*, 2011.
- Canuel, E.A. and Martens, C.S.: Reactivity of recently deposited organic matter: Degradation of lipid compounds near the sediment-water interface, *Geochim. Cosmochim. Acta*, 60, 1793-1806, 1996.
- Carlson, P. R. and Karl, H. A.: Development of large submarine canyons in the Bering Sea, indicated by morphologic, seismic, and sedimentologic characteristics, *Geol. Soc. Am. Bull.*, 100(10), 1594–1615, 1988.
- Chikamoto, M. O., Menviel, L., Abe-Ouchi, A., Ohgaito, R., Timmermann, A., Okazaki, Y., Harada, N., Oka, A. and Mouchet, A.: Variability in North Pacific intermediate and deep water ventilation during Heinrich events in two coupled climate models, *Deep Sea Res. Part II Top. Stud. Oceanogr.*, 61-64, 114–126, doi:10.1016/j.dsr2.2011.12.002, 2012.
- Ciais, P., Tagliabue, a., Cuntz, M., Bopp, L., Scholze, M., Hoffmann, G., Lourantou, a., Harrison, S. P., Prentice, I. C., Kelley, D. I., Koven, C. and Piao, S. L.: Large inert carbon pool in the terrestrial biosphere during the Last Glacial Maximum, *Nat. Geosci.*, 5(1), 74–79, doi:10.1038/ngeo1324, 2011.
- Clarke, J. W.: Sedimentary basins of Northeastern USSR. United States Department of the Interior Geological Survey, Open file report, 88-246, 1988.
- Climate data from Klyuchi climate station. <http://de.climate-data.org/location/284590/>, 2015
- Climate data from Petropawlowsk Kamtschatski climate station. <http://de.climate-data.org/location/1810/>, 2015
- Contreras-Rosales, A., Jennerjahn, T., Tharammal, T., Lückge, A., Meyer, V., Paul, A. and Schefuß, E.: Evolution of the Indian Summer Monsoon eastern branch and terrestrial vegetation since the Last Glacial, *Quat. Sci. Rev.*, 16, 2728, doi:10.1016/j.quascirev.2014.08.010, 2014.
- Cosma T. and Henty I. L. 2008, Pleistocene glacio-marine sedimentation on the continental slope off Vancouver Island, British Columbia: *Marine Geology*, v. 255, p. 45, doi: 10.1016/j.margeo.2008.07.001.

- Davies, M. H., Mix, a. C., Stoner, J. S., Addison, J. a., Jaeger, J., Finney, B. and Wiest, J.: The deglacial transition on the southeastern Alaska Margin: Meltwater input, sea level rise, marine productivity, and sedimentary anoxia, *Palaeoceanography*, 26, 1–18, doi:10.1029/2010PA002051, 2011.
- De Jonge, C., Stadnitskaia, A., Hopmans, E. C., Cherkashov, G., Fedotov, A. and Sinninghe Damsté, J. S.: In situ produced branched glycerol dialkyl glycerol tetraethers in suspended particulate matter from the Yenisei River, Eastern Siberia, *Geochim. Cosmochim. Acta*, 125, 476–491, doi:10.1016/j.gca.2013.10.031, 2014.
- Deschamps, P., Durand, N., Bard, E., Hamelin, B., Camoin, B., Thomas, A. L., Henderson, G., M., Okuno, J. and Yokohama, Y.: Ice-sheet collapse and sea-level rise at the Bolling warming 14,600 years ago, *Nature* 483, 559–564, 2012.
- de Vernal, A. and Pedersen, T. F.: Micropalaeontology and palynology of core PAR87A-10: A 23,000 year record of palaeoenvironmental changes in the Gulf of Alaska, northeast North Pacific, *Palaeoceanography*, 12(6), 821, doi:10.1029/97PA02167, 1997.
- Dirksen, V., Dirksen, O. and Diekmann, B.: Holocene vegetation dynamics and climate change in Kamchatka Peninsula, Russian Far East, *Rev. Palaeobot. Palynol.*, 190, 48–65, doi:10.1016/j.revpalbo.2012.11.010, 2013.
- Dirksen, V., Dirksen, O., van den Bogaard, C. and Diekmann, B.: Holocene pollen record from Lake Sokoch, interior Kamchatka (Russia), and its palaeobotanical and palaeoclimatic interpretation, *Glob. Planet. Change*, 134, 129–141, doi:10.1016/j.gloplacha.2015.07.010, 2015.
- Dolman, A., van der Werf, G., van der Molen, M., Ganssen, G., Erisman, J., and Strengers, B.: A carbon cycle science update since IPCC AR-4, *Ambio*, 39, 402–412, 2010.
- Dong, L., Li, Q., Li, L. and Zhang, C. L.: Glacial – interglacial contrast in MBT/CBT proxies in the South China Sea: Implications for marine production of branched GDGTs and continental teleconnection, *Org. Geochem.*, 79, 74–82, doi:10.1016/j.orggeochem.2014.12.008, 2015.
- Dong, B. and Valdes, P. J.: Simulations of the Last Glacial Maximum climates using a general circulation model: prescribed versus computed sea surface temperatures, *Clim. Dyn.*, 14, 571– 591, 1998.
- Drijfhout, S., van Oldenborgh, G. J., and Cimadoribus, A.: Is a decline of AMOC causing the warming hole above the North Atlantic in observed and modeled warming patterns? *J. Clim.*, 25, 8373–8379, 2012.
- Driesschaert, E., et al.: Modeling the influence of Greenland ice sheet melting on the Atlantic meridional overturning circulation during the next millennia, *Geophys. Res. Lett.*, 34, L10707, 2007.
- Dullo, W. C., Baranov, B. and van den Bogaard, C.: FS Sonne Fahrtbericht/Cruise Report SO201–2. IFM-GEOMAR, Report 35, Kiel, IFM262 GEOMAR, 2009.
- Durand, N., Deschamps, P., Bard, E., Hamelin, B., Camoin, G., Thomas, A. L., Henderson, G. M., Yokoyama, Y. and Matsuzaki, H.: Comparison of 14C and U-Th Ages in Corals from IODP #310 Cores Offshore Tahiti, *Radiocarbon*, 55(4), 1947–1974, doi:10.2458/azu_js_rc.v55i2.16134, 2013.
- Duk-Rodkin, A., Barendregt, R. W., Froese, D.G., Weber, F., Enkin, R., Smith, I., Zazula, G.D., Waters, P., Klassen, R.: Timing and extent of Plio-Pleistocene glaciations in northwestern Canada and east-central Alaska. In: Ehlers, J., Gibbard, P.L. (Eds.), *Quaternary Glaciations—Extent and Chronology, Part II: North America*. Elsevier, Amsterdam, pp. 313–345, 2004.
- Duk-Rodkin, A. and Hughes, O. L.: Tertiary-quaternary drainage of the Pre-glacial Mackenzie basin, *Quat. Int.*, 22-23, 221–241, doi:10.1016/1040-6182(94)90015-9, 1994.

- Dumann, W.: Thaw-induced release of carbon from permafrost in Eastern Siberia during the last deglaciation. Master Thesis, University of Bremen, 2015.
- Dyke, A. S., Andrews, J. T., Clark, P. U., England, J. H., Miller, G. H., Shaw, J. and Veillette, J. J.: The Laurentide and Innuitian ice sheets during the Last Glacial Maximum, *Quat. Sci. Rev.*, 21(1-3), 9–31, doi:10.1016/S0277-3791(01)00095-6, 2002.
- Dyke, A. S. and Prest, V. K.: Late Wisconsinan and Holocene history of the Laurentide Ice Sheet, *Géographie Physique et Quaternaire* 41, 237–263, 1987.
- Dyke, A.S., Moore, A. and Robertson, L.: Deglaciation of North America. Geological Survey of Canada Open File 1574, 2003
- Eglinton, T.I., Aluwihare, L.I., Bauer, J.E., Druffel, E.R.M. and McNichol, A.P.: Gas Chromatographic Isolation of Individual Compounds from Complex Matrices for Radiocarbon Dating, *Anal. Chem.* 68, 904-912, 1996.
- Eglinton, T. I. and Eglinton, G.: Molecular proxies for palaeoclimatology, *Earth Planet. Sci. Let.* 275, 1-16, 2008.
- Elias, S. A.: Mutual climatic range reconstructions of seasonal temperatures based on Late Pleistocene fossil beetle assemblages in Eastern Beringia, *Quat. Sci. Rev.*, 20, 77–91, doi:10.1016/S0277-3791(00)00130-X, 2001.
- Elias, S. A., Short, S. K. and Birks, H. H.: Late Wisconsin environments of the Bering Land Bridge, *Palaeogeogr. Palaeoclimatol. Palaeoecol.*, 136(1-4), 293–308, doi:10.1016/S0031-0182(97)00038-2, 1997.
- Elias, S.A., Short, S.K. and Phillips, R.L.: Palaeoecology of late-glacial peats from the Bering Land Bridge, Chukchi Sea shelf region, northwestern Alaska. *Quat. Res.* 38, 371–378, 1992.
- Elias, S. A., Short, S. K., Nelson, C. H. and Birks, H. H.: Life and times of the Bering land bridge, *Nature*, 382(6586), 60–63, doi:10.1038/382060a0, 1996.
- Fairbanks, R. G., Mortlock, R. a., Chiu, T.-C., Cao, L., Kaplan, A., Guilderson, T. P., Fairbanks, T. W., Bloom, A. L., Grootes, P. M. and Nadeau, M.-J.: Radiocarbon calibration curve spanning 0 to 50,000 years BP based on paired $^{230}\text{Th}/^{234}\text{U}/^{238}\text{U}$ and ^{14}C dates on pristine corals, *Quat. Sci. Rev.*, 24(16-17), 1781–1796, doi:10.1016/j.quascirev.2005.04.007, 2005.
- Felzer, B., 2001. Climate impacts of an ice sheet in East Siberia during the Last Glacial Maximum. *Quat. Sci. Rev.* 20, 437–447.
- Fischer, H., Schmitt, J., Lüthi, D., Stocker, T. F., Tschumi, T., Parekh, P., Joos, F., Köhler, P., Völker, C., Gersonde, R., Barbante, C., Le Floch, M., Raynaud, D. and Wolff, E.: The role of Southern Ocean processes in orbital and millennial CO_2 variations – A synthesis, *Quat. Sci. Rev.*, 29(1-2), 193–205, doi:10.1016/j.quascirev.2009.06.007, 2010.
- Fischer, H., Behrens, M., Bock, M., Richter, U., Schmitt, J., Loulergue, L., Chappellaz, J., Spahni, R., Blunier, T., Leuenberger, M. and Stocker, T. F.: Changing boreal methane sources and constant biomass burning during the last termination, *Nature*, 452(7189), 864–7, doi:10.1038/nature06825, 2008.
- Fritz, M., Herzschuh, U., Wetterich, S., Lantuit, H., De Pascale, G. P., Pollard, W. H. and Schirrmeister, L.: Late glacial and Holocene sedimentation, vegetation, and climate history from easternmost Beringia (northern Yukon Territory, Canada), *Quat. Res.*, 78(3), 549–560, doi:10.1016/j.yqres.2012.07.007, 2012.
- Gebhardt, H., Sarnthein, M., Grootes, P. M., Kiefer, T., Kuehn, H., Schmieder, F. and Röhl, U.: Palaeonutrient and productivity records from the subarctic North Pacific for Pleistocene glacial terminations I to V, *Palaeoceanography*, 23(4), PA4212, doi:10.1029/2007PA001513, 2008.

- Gersonde, R.: The Expedition of the Research Vessel “Sonne” to the Subpolar North Pacific and the Bering Sea in 2009 (SO202-INOPEX), in: Reports on Polar and Marine Research, Alfred Wegener Institute, Bremerhaven, 323 pp., 2012.
- Glebova, S., Ustinova, E. and Sorokin, Y.: Long-term changes of atmospheric centers and climate regime of the Okhotsk Sea in the last three decades. *PICES Sci. Rep.* 36, 3–9, 2009.
- Gong, X., Knorr, G., Lohmann, G. and Zhang, X.: Dependence of abrupt Atlantic meridional ocean circulation changes on climate background states. *Geophys. Res. Lett.* 40 (14), 3698–3704, doi:10.1002/grl.50701, 2013.
- Glushkova, O. Y.: Geomorphological correlation of Late Pleistocene glacial complexes of Western and Eastern Beringia, *Quat. Sci. Rev.* 20, 405–417, 2001
- Grosswald, M. G.: An Antarctic-style ice sheet in the Northern Hemisphere: towards a new global glacial theory, *Polar Geography and Geology*, 12, 239–267, 1988.
- Grosswald, M. G.: Late Weichselian ice sheets in Arctic and Pacific Siberia, *Quat. Int.* 45/46, 3–18, 1998.
- Grosswald, M. G. and Hughes, T. J.: The Russian component of an Arctic Ice Sheet during the Last Glacial Maximum, *Quat. Sci. Rev.* 21, 121–146, 2002.
- Grosswald, M. G. and Hughes, T. J.: “Back-arc” marine ice sheet in the Sea of Okhotsk, *Rus. J. Earth. Sci.* 7. doi:10.2205/2005ES000180, 2005.
- Grosswald, M. G. and Kotlyakov, V. M.: Present-day glaciers in USSR and some data on their mass balance, *J. Glaciol.* 8, 9–21, 1969.
- Gruber, A. and Reitner, J. M.: Dating of mass movements by rock glaciers: examples from the eastern Alps *Geophysical Research Abstracts*, 9. European Geoscience Union, p. 03945 (SRef-ID: 1607-7962/gra/EGU2007-A-03945), 2007.
- Gualtieri, L., Glushkova, O. and Brigham-Grette, O. J.: Evidence for restricted ice extent during the last glacial maximum in the Koryak mountains of Chukotka, far eastern Russia, *Geol. Soc. Amer. Bull.* 112, 1106–1118, 2000.
- Gualtieri, L., Vartanyan, S., Brigham-Grette, J., Patricia, M., Anderson, P. M.: Pleistocene raised marine deposits on Wrangel Island, NE Siberia: implications for Arctic ice sheet history. *Quat. Res.* 59, 399–410, 2003.
- Guo, L., Ping, C.-L. and Macdonald, R. W.: Mobilization pathways of organic carbon from permafrost to arctic rivers in a changing climate, *Geophys. Res. Lett.*, 34 (13), doi:10.1029/2007GL030689, 2007.
- Gustafsson, Ö., van Dongen, B., Vonk, J., Dudarev, O. and Semiletov, I.: Widespread release of old carbon across the Siberian Arctic echoed by its large rivers, *Biogeosciences*, 8 (6), 1737–1743, doi:10.5194/bg-8-1737-2011, 2011.
- Guthrie, R. D.: Origin and causes of the mammoth steppe: a story of cloud cover, woolly mammal tooth pits, buckles, and inside-out Beringia, *Quat. Sci. Rev.*, 20, 549–574, 2001.
- Hammarlund, D., Klimaschewski, A., St. Amour, N. A., Andrén, E., Self, A. E., Solovieva, N., Andreev, A. A., Barnekow, L. and Edwards, T. W. D.: Late Holocene expansion of Siberian dwarf pine (*Pinus pumila*) in Kamchatka in response to increased snow cover as inferred from lacustrine oxygen-isotope records, *Glob. Planet. Change*, 134, 91–100, doi:10.1016/j.gloplacha.2015.04.004, 2015.
- Hanebuth, T., Stattegger, K., and Grootes, P. M.: Rapid flooding of the Sunda shelf: a late-glacial sea-level record, *Science*, 288 (5468), 1033–1035, 2000.

- Harada, N., Ahagon, N., Uchida, M. and Murayama, M.: Northward and southward migrations of frontal zones during the past 40 kyr in the Kuroshio – Oyashio transition area. *Geochem. Geophys. Geosyst.* 5, Q09004, 2004.
- Harada, N., Sato, M., Seki, O., Timmermann, A., Moossen, H., Bendle, J., Nakamura, Y., Kimoto, K., Okazaki, Y., Nagashima, K., Gorbarenko, S. A., Ijiri, A., Nakatsuka, T., Menviel, L., Chikamoto, M. O., Abe-Ouchi, A. and Schouten, S.: Sea surface temperature changes in the Okhotsk Sea and adjacent North Pacific during the last glacial maximum and deglaciation, *Deep Sea Res. Part II Top. Stud. Oceanogr.*, 61-64, 93–105, doi:10.1016/j.dsr2.2011.12.007, 2012.
- Harada, N., Shin, K. H., Murata, A., Uchida, M. and Nakatani, T.: Characteristics of alkenones synthesized by a bloom of *Emiliana huxleyi* in the Bering Sea, *Geochim. Cosmochim. Acta*, 67(8), 1507–1519, doi:10.1016/S0016-7037(02)01318-2, 2003.
- Harden, J. W., et al.: Field information links permafrost carbon to physical vulnerabilities of thawing. *Geophys. Res. Lett.*, 39, L15704, 2012.
- Harington, C. R.: *Annotated Bibliography of Quaternary Vertebrates of Northern North America with Radiocarbon Dates*. University of Toronto Press, Toronto, Ontario, 539, 2003.
- Hendy, I. L., T. Cosma, T.: Vulnerability of the Cordilleran Ice Sheet to iceberg calving during late quaternary rapid climate change events, *Palaeoceanography*, 23, PA2101, doi:10.1029/2008PA001606, 2008
- Ho, S. L., Mollenhauer, G., Fietz, S., Martínez-García, A., Lamy, F., Rueda, G., Schipper, K., Méheust, M., Rosell-Melé, A., Stein, R. and Tiedemann, R.: Appraisal of TEX₈₆ and thermometries in subpolar and polar regions, *Geochim Cosmochim Acta*, 131, 213–226, doi:10.1016/j.gca.2014.01.001, 2014.
- Hoff, U., Biskaborn, B. K., Dirksen, V. G., Dirksen, O., Kuhn, G., Meyer, H., Nazarova, L., Roth, A. and Diekmann, B.: Holocene environment of Central Kamchatka, Russia: Implications from a multi-proxy record of Two-Yurts Lake, *Glob. Planet. Change*, 134, 101–117, doi:10.1016/j.gloplacha.2015.07.011, 2015.
- Hoff, U., Dirksen, O., Dirksen, V., Kuhn, G., Meyer, H. and Diekmann, B.: Holocene freshwater diatoms: palaeoenvironmental implications from south Kamchatka, Russia, *Boreas*, 43(1), 22–41, doi:10.1111/bor.12019, 2014.
- Hong, Y. T., Hong, B., Lin, Q. H., Shibata, Y., Zhu, Y. X., Leng, X. T. and Wang, Y.: Synchronous climate anomalies in the western North Pacific and North Atlantic regions during the last 14,000 years, *Quat. Sci. Rev.*, 28(9-10), 840–849, doi:10.1016/j.quascirev.2008.11.011, 2009.
- Hopkins, D. M., Matthews Jr., J. V., Schweger, C. E. and Young, S. B. (Eds.): *Palaeoecology of Beringia*. Academic Press, New York, 1982.
- Hopmans, E. C., Schouten, S., Pancost, R. D., Van Der Meer, M. T. J., & Sinninghe Damsté, J. S.: Analysis of intact tetraether lipids in archaeal cell material and sediments by high performance liquid chromatography/atmospheric pressure chemical ionization mass spectrometry, *Rapid Commun. Mass Spectrom.* RCM, 14(7), 585–9, 2000.
- Hopmans, E. C., Weijers, J. W. ., Schefuß, E., Herfort, L., Sinninghe Damsté, J. S. and Schouten, S.: A novel proxy for terrestrial organic matter in sediments based on branched and isoprenoid tetraether lipids, *Earth Planet. Sci. Lett.*, 224(1-2), 107–116, doi:10.1016/j.epsl.2004.05.012, 2004.
- Houghton, R. A.: Balancing the Global Carbon Budget, *Annu. Rev. Earth Planet. Sci.*, 35 (1), 313–347, doi:10.1146/annurev.earth.35.031306.140057, 2007.

- Hughen, K. A.; Southon, J. R.; Lehman, S. J.; Overpeck, J. T.: Synchronous Radiocarbon and Climate Shifts During the Last Deglaciation, *Science* 290(5498), 1951–1954, doi:10.1126/science.290.5498.1951, 2000.
- Hughes, P. D.: Loch Lomond Stadial (Younger Dryas) glaciers and climate in Wales, *Geol. J.*, 44, 375–391, 2009.
- Hughes, P. D., and Braithwaite, R. J.: Application of a degree-day model to reconstruct Pleistocene glacial climates, *Quat. Res.* 69, 110–116, 2008.
- Huntingford, C., Lowe, J., Booth, B., Jones, C., Harris, G., Gohar, L., and Meir, P.: Contributions of carbon cycle uncertainty to future climate projection spread, *Tellus B*, 61, 355–360, 2009.
- IPCC: Climate change 2007. The physical science basis: Working group I contribution to the fourth assessment report of the IPCC, edited by S. Solomon, D. Qin, M. Manning, Z. Chen, M. Marquis, K. B. Averyt, M. Tignor, and H. L. Miller, IPCC, 4, pp. 996., Cambridge University Press, Cambridge, UK and New York, USA, 2007.
- IPCC: Climate change 2013. The physical science basis: Working group I contribution to the fifth assessment report of the IPCC, edited by Stocker, T.F., Qin, D., Plattner, G.-K., Tignor, M.M.B., Allen, S.K., Boschung, J., Nauels, A., Xia, Y., Bex, V. and Midgley, P.M., IPCC, 5, pp.1525, Cambridge University Press, Cambridge, UK and New York, USA, 2013.
- Ivanov, A.: The Far East. In: *The Physical Geography of Northern Eurasia*, Shahgedanova M. (ed.). Oxford University Press: Oxford, 422-447, 2002.
- Jones, V. and Solomina, O.: The Geography of Kamchatka, *Glob. Planet. Change*, 134, 3–9, doi:10.1016/j.gloplacha.2015.06.003, 2015.
- Jungclauss, J. H., Keenlyside, N., Botzet, M., Haak, H., Luo, J.-J., Latif, M., Marotzke, J., Mikolajewicz, M. and Roeckner, E.: Ocean circulation and tropical variability in the coupled model ECHAM5/MPI-OM, *J. Climate*, 19, 3952–3972, 2006.
- Kageyama, M., Laine, a., Abe-Ouchi, a., Braconnot, P., Cortijo, E., Crucifix, M., de Vernal, a., Guiot, J., Hewitt, C. D., Kitoh, a., Kucera, M., Marti, O., Ohgaito, R., Otto-Bliesner, B., Peltier, W. R., Rosell-Melé, A., Vettoretti, G., Weber, S. L. and Yu, Y.: Last Glacial Maximum temperatures over the North Atlantic, Europe and western Siberia: a comparison between PMIP models, MARGO sea-surface temperatures and pollen-based reconstructions, *Quat. Sci. Rev.*, 25(17-18), 2082–2102, doi:10.1016/j.quascirev.2006.02.010, 2006.
- Karner, M. B., Delong, E. F. and Karl, D. M.: Archaeal dominance in the mesopelagic zone of the Pacific Ocean, *Nature*, 409(6819), 507-510, doi:10.1038/35054051, 2001.
- Katsuki, K. and Takahashi, K.: Diatoms as palaeoenvironmental proxies for seasonal productivity, sea-ice and surface circulation in the Bering Sea during the late Quaternary, *Deep Sea Res., Part II*, 52, 2110–2130, doi:10.1016/j.dsr2.2005.07.001, 2005.
- Katsuki, K., Takahashi, K. and Matsushita, K.: Diatom palaeoceanography during the past 340 kyr in the Bering Sea and the western subarctic Pacific, in *Seventeenth International Diatom Symposium*, edited by M. Poulin, pp. 147–159, Biopress, Bristol, U. K., 2004.
- Kennedy, K. E., Froese, D. G., Zazula, G. D. and Lauriol, B.: Last Glacial Maximum age for the northwest Laurentide maximum from the Eagle River spillway and delta complex, northern Yukon, *Quat. Sci. Rev.*, 29(9-10), 1288–1300, doi:10.1016/j.quascirev.2010.02.015, 2010.
- Khotinsky, N. A.: *Holocene of the Northern Eurasia*. Nauka, Moscow, 1977. (In Russian)

- Kiefer, T. and Kienast, M.: Patterns of deglacial warming in the Pacific Ocean: a review with emphasis on the time interval of Heinrich event 1, *Quat. Sci. Rev.*, 24(7-9), 1063–1081, doi:10.1016/j.quascirev.2004.02.021, 2005.
- Kienast, F.: Die Rekonstruktion der spätquartären Vegetations- und Klimageschichte der Laptevsee-Region auf der Basis botanischer Großrestuntersuchungen. Ph.D. Dissertation, Potsdam University, 116pp, 2002.
- Kienast, S. S., and McKay, J. L.: Sea surface temperatures in the subarctic northeast Pacific reflect millennial-scale climate oscillations during the last 16 kyrs. *Geophys. Res. Lett.*, 28(8), 1563–1566, doi:10.1029/2000GL012543, 2001.
- Kienast, F., Schirmer, L., Siegert, C. and Tarasov, P.: Palaeobotanical evidence for warm summers in the East Siberian Arctic during the last cold stage, *Quat. Res.*, 63(3), 283–300, doi:10.1016/j.yqres.2005.01.003, 2005.
- Kiselev, S. V.: Beetles in North-East Siberia during the Late Cenozoic. Nauka Press, Moscow, 1981 (in Russian).
- Kim, J.-H., Crosta, X., Willmott, V., Renssen, H., Bonnin, J., Helmke, P., Schouten, S. and Sinninghe Damsté, J. S.: Holocene subsurface temperature variability in the eastern Antarctic continental margin, *Geophys. Res. Lett.*, 39, L06705, doi:10.1029/2012GL051157, 2012.
- Kim, S. J., Crowley, T. J., Erickson, D. J., Govindasamy, B., Duffy, P. B. and Lee, B. Y.: High-resolution climate simulation of the last glacial maximum, *Clim. Dyn.*, 31(1), 1–16, doi:10.1007/s00382-007-0332-z, 2008.
- Kim, J.-H., van der Meer, J., Schouten, S., Helmke, P., Willmott, V., Sangiorgi, F., Koç, N., Hopmans, E. C., and Sinninghe Damsté, J. S.: New indices and calibrations derived from the distribution of crenarchaeal isoprenoid tetraether lipids: Implications for past sea surface temperature reconstructions, *Geochim. Cosmochim. Acta*, 74(16), 4639–4654, doi:10.1016/j.gca.2010.05.027, 2010.
- Klimaschewski, A., Barnekow, L., Bennett, K. D., Andreev, A. A., Andrén, E., Bobrov, A. A. and Hammarlund, D.: Holocene environmental changes in southern Kamchatka, Far Eastern Russia, inferred from a pollen and testate amoebae peat succession record, *Glob. Planet. Change*, 134, 142–154, doi:10.1016/j.gloplacha.2015.09.010, 2015.
- Knorr, G. and Lohmann, G.: Climate warming during Antarctic ice sheet expansion at the Middle Miocene transition, *Nature Geosci.* 7, 376–381, 2014.
- Knudson, K. P. and Ravelo, A. C.: North Pacific Intermediate Water circulation enhanced by the closure of the Bering Strait, *Palaeoceanography*, 30, 1287–1304, 2015.
- Köhler, P. and Bard, E.: Abrupt carbon release at the onset of the Bolling : Permafrost thawing with inter-hemispheric impact, *Proc. Natl. Acad. Sci. U. S. A.*, 110(1), doi:10.1073/pnas, 2013.
- Köhler, P., Knorr, G. and Bard, E.: Permafrost thawing as a possible source of abrupt carbon release at the onset of the Bolling/Allerød, *Nat. Commun.*, 5, 5520, doi:10.1038/ncomms6520, 2014.
- Kokorowski, H. D., Anderson, P. M., Mock, C. J. and Lozhkin, A. V.: A re-evaluation and spatial analysis of evidence for a Younger Dryas climatic reversal in Beringia, *Quat. Sci. Rev.*, 27, 1710–1722, doi:10.1016/j.quascirev.2008.06.010, 2008a.
- Kokorowski, H. D., Anderson, P. M., Sletten, R. S., Lozhkin, A. V. and Brown, T. A.: Late Glacial and Early Holocene Climatic Changes Based on a Multiproxy Lacustrine Sediment Record from Northeast Siberia, Arctic, *Antarct. Alp. Res.*, 40(3), 497–505, doi:10.1657/1523-0430(07-036), 2008b.

- Kondratyuk, V. I.: Climate of Kamchatka. Hydrometeoizdat, Moscow, 1974. (In Russian)
- Könneke, M., de la Torre, A. E., Walker, J. R., Waterbury, J. B. and Stahl, D. A.: Isolation of an autotrophic ammonia-oxidizing marine archaeon. *Nature*, 437(7058), 543–546, doi:10.1038/nature03911, 2005.
- Koven, C. D., Riley, W. J., and Stern, A.: Analysis of permafrost thermal dynamics and response to climate change in the CMIP5 Earth system models, *J. Clim.*, 26, 1877–1900, 2013.
- Koven, C. D., Ringeval, B., Friedlingstein, P., Ciais, P., Cadule, P., Khvorostyanov, D., Krinner, G. and Tarnocai, C.: Permafrost carbon-climate feedbacks accelerate global warming, *P Natl. A. Sci.*, 108 (36), 14769–14774, doi:10.1073/pnas.1103910108/-/DCSupplemental/pnas.1103910108_SI.pdf, 2011.
- Kuehn, H., Lembke-Jene, L., Gersonde, R., Esper, O., Lamy, F., Arz, H., Kuhn, G. and Tiedemann, R.: Laminated sediments in the Bering Sea reveal atmospheric teleconnections to Greenland climate on millennial to decadal timescales during the last deglaciation, *Clim. Past*, 10(6), 2215–2236, doi:10.5194/cp-10-2215-2014, 2014.
- Kurek, J., Cwynar, L. C., Ager, T. A., Abbott, M. B. and Edwards, M. E.: Late Quaternary palaeoclimate of western Alaska inferred from fossil chironomids and its relation to vegetation histories, *Quat. Sci. Rev.*, 28(9-10), 799–811, doi:10.1016/j.quascirev.2008.12.001, 2009.
- Kusch, S., Rethemeyer, J., Schefuß, E. and Mollenhauer, G.: Controls on the age of vascular plant biomarkers in Black Sea sediments, *Geochim. Cosmochim. Acta*, 74(24), 7031–7047, doi:10.1016/j.gca.2010.09.005, 2010.
- Kutzbach, J., Gallimore, R., Harrison, S., Behling, P., Selin, R. and Laarif, F.: Climate and Biome simulations for the past 21,000 years, *Quat. Sci. Rev.*, 17(6-7), 473–506, 1998.
- Kutzbach, J. E. and Wright, E.: Simulation of the climate of 18 000 years BP: results for the North American / North Atlantic/ European sector and comparison with the geological record of North America, *Quart. Sci. Rev.*, 4, 147–185, 1985.
- Lambeck, K., Rouby, H., Purcell, A., Sun, Y. and Sambridge, M.: Sea level and global ice volumes from the last glacial maximum to the Holocene, *PNAS*, 111 (43), 15,296_15,303, 2014.
- Lantuit, H., Overduin, P. P., Couture, N., Wetterich, S., Aré, F., Atkinson, D., Brown, J., Cherkashov, G., Drozdov, D., Forbes, D. L., Graves-Gaylord, A., Grigoriev, M., Hubberten, H.-W., Jordan, J., Jorgenson, T., Ødegård, R. S., Ogorodov, S., Pollard, W. H., Rachold, V., Sedenko, S., Solomon, S., Steenhuisen, F., Streletskaia, I. and Vasiliev, A.: The Arctic Coastal Dynamics Database: A New Classification Scheme and Statistics on Arctic Permafrost Coastlines, *Estuaries and Coasts*, 35(2), 383–400, doi:10.1007/s12237-010-9362-6, 2012.
- Laukhin, S. A., Zhimin, J., Pushkar, V. S., and Cherepanova, M. V.: Last Glaciation in the northern part of the Eastern Chukchi Peninsula and palaeoceanography of the North Pacific, *Dokl. Earth Sci.*, 441A, 1422-1426, 2006.
- Lawrence, D., and Slater, A.: The contribution of snow condition trends to future ground climate, *Clim. Dyn.*, 34, 969–981, 2010.
- Locarnini R. A., Mishonov, A. V., Antonov, J. I., Boyer, T. P., Garcia, H. E., Baranova, O. K., Zweng, M. M. and Johnson, D. R.: World Ocean Atlas 2009: Volume 1: Temperature. In NOAA Atlas NESDIS 68, edited by S. Levitus, p. 184, U.S. Government Printing Office, Washington, D.C, 2010.
- Lohmann, G., Pfeiffer, M., Laepple, T., Leduc, G. and Kim, J.-H.: A model-data comparison of the Holocene global sea surface temperature evolution, *Clim. Past*, 9, 1807-1839, 2013

- Lozhkin, A. V. and Anderson, P. M.: A late Quaternary pollen record from Elikchan 4 Lake, northeast Siberia, *Geol. Pac. Ocean*, 12, 609–616, 1996.
- Lozhkin, A. V., Anderson, P., Eisner, W. R. and Solomatkina, T. B.: Late glacial and Holocene landscapes of central Beringia, *Quat. Res.*, 76(3), 383–392, doi:10.1016/j.yqres.2011.08.003, 2011.
- Lozhkin, A. V., Anderson, P. M., Matrosova, T. V. and Minyuk, P. S.: The pollen record from El'gygytgyn Lake: Implications for vegetation and climate histories of northern Chukotka since the late middle Pleistocene, *J. Palaeolimnol.*, 37(1), 135–153, doi:10.1007/s10933-006-9018-5, 2007.
- Lozhkin, A. V. Anderson, P. M. Ravako, L. G. Hopkins, D. M. Brubaker, L. B., Colinvaux, P. A. Miller, M. C.: Late Quaternary Lacustrine Pollen Records from Southwestern Beringia, *Quat. Res.*, 39, 314–324, 1993.
- Lozhkin, a. V., Anderson, P. M., Vartanyan, S. L., Brown, T. A., Belaya, B. V. and Kotov, A. N.: Late Quaternary palaeoenvironments and modern pollen data from Wrangel Island (Northern Chukotka), *Quat. Sci. Rev.*, 20(1-3), 217–233, doi:10.1016/S0277-3791(00)00121-9, 2001.
- MacDougall, A. H., Avis, C. A. and Weaver, A. J.: Significant contribution to climate warming from the permafrost carbon feedback. *Nature Geosci.*, 5, 719–721, 2012.
- Maier, E., Méheust, M., Abelman, A., Gersonde, R., Chaplignin, B., Ren, J., Stein, R., Meyer, H. and Tiedemann, R.: Deglacial subarctic Pacific surface water hydrography and nutrient dynamics and links to North Atlantic climate variability and atmospheric CO₂, *Palaeoceanography*, 30(7), 949–968, doi:10.1002/2014PA002763, 2015.
- Manabe, S. and Stouffer, R. J.: Two stable equilibria of a coupled ocean-atmosphere model. *J. Climate*, 1, 841–861, 1988.
- Manley, W.F.: Postglacial Flooding of the Bering Land Bridge: A Geospatial Animation: INSTAAR, University of Colorado, v1, http://instaar.colorado.edu/QGISL/bering_land_bridge, 2002.
- Mann, D. H., and Hamilton, T. D.: Late Pleistocene and Holocene Palaeoenvironments of the North Pacific Coast, *Quat. Sci. Rev.*, 14, 449–471, 1995.
- Mann, D. H., and Peteet, D. M.: Extent and Timing of the Last Glacial Maximum in Southwestern Alaska, *Quat. Res.*, 42, 136–148, 1994.
- Marchitto, T. M., Lehman, S. J., Ortiz, J. D., Flückinger, J., and van Geen, A.: Marine radiocarbon evidence for the mechanism of deglacial atmospheric CO₂ rise, *Science* 316, 1456–1459, 2007.
- Marsland, S. J., Haak, H., Jungclaus, J. H., Latif, M. and Röske, F.: The Max-Planck-Institute global ocean/sea ice model with orthogonal curvilinear coordinates. *Ocean Modell.* 5, 91–127, doi:10.1016/S1463-5003(02)00015-X, 2003.
- Martens-Habbena, W., Berube, P. M., Urakawa, H., de la Torre, J. R. and Stahl, D. A.: Ammonia oxidation kinetics determine niche separation of nitrifying Archaea and Bacteria, *Nature*, 461(7266), 976–979, doi:10.1038/nature08465, 2009.
- Mason, O. K., Bowers, P. M., and Hopkins, D.M.: The early Holocene Milankovitch thermal maximum and humans: Adverse conditions for the Denali complex of eastern Beringia, *Quat. Sci. Rev.* 20, 525–548, 2001.
- Matthews Jr., J.V. and Telka, A.: Insect fossils from the Yukon. In: Danks, H.V., Downes, J.A. (Eds.), *Insects of the Yukon*. Ottawa, Biological Survey of Canada (Terrestrial Arthropods), pp. 911–962, 1997.
- Max, L., Riethdorf, J.-R., Tiedemann, R., Smirnova, M., Lembke-Jene, L., Fahl, K., Nürnberg, D., Matul, A. and Mollenhauer, G.: Sea surface temperature variability and sea-ice extent in the subarctic northwest Pacific during the past 15,000 years, *Palaeoceanography*, 27(3), PA3213, doi:10.1029/2012PA002292, 2012.

- McManus, J. F., Francois, R., Gherardi, J. M., Keigwin, L., D. and Brown-Leger, S.: Collapse and rapid resumption of Atlantic meridional circulation linked to deglacial climate change. *Nature*, 428(6985), 834–837, doi:10.1038/nature02494, 2004.
- Meyer, H., Dereviagin, A., Siegert, C., Schirrmeister, L. and Hubberten, H.-W.: Palaeoclimate reconstruction on Big Lyakhovsky Island, north Siberia - Hydrogen and oxygen isotopes in ice wedges, *Permafr. Periglac. Process.*, 13(2), 91–105, doi:10.1002/ppp.416, 2002.
- Meyer, V. D., Hefter, J., Lohmann, G., Tiedemann, R., Mollenhauer, G., submitted a. Development of summer temperature on the Kamchatka Peninsula, Russian Far East, over the past 20,000 years, *Clim. Past*, submitted a.
- Meyer, V. D., Max, L., Hefter, J., Tiedemann, R. and Mollenhauer, G.: Glacial-to-Holocene evolution of sea surface temperature and surface circulation in the subarctic Northwest Pacific and the Western Bering Sea, *Palaeoceanography*, submitted b.
- Meyer, H., Schirrmeister, L., Yoshikawa, K., Opel, T., Wetterich, S., Hubberten, H. W. and Brown, J.: Permafrost evidence for severe winter cooling during the Younger Dryas in northern Alaska, *Geophys. Res. Lett.*, 37(3), 1–5, doi:10.1029/2009GL041013, 2010.
- Menviel, L., Timmermann, A., Elison Timm, O., Mouchet, A., Abe-Ouchi, A., Chikamoto, M. O., Harada, N., Ohgaito, R., and Okazaki, Y.: Removing the North Pacific halocline: Effects on global climate, ocean circulation and the carbon cycle, *Deep Sea Res., Part II*, 61–64, 106–113, doi:10.1016/j.dsr2.2011.03.005, 2012.
- Mikolajewicz, U., Crowley, T. J., Schiller, A. and Voss, R.: Modelling teleconnections between the North Atlantic and North Pacific during the Younger Dryas, *Nature*, 387, 384–387, 1997.
- Mock, C. J., Mock, C. J., Bartlein, P. J., Bartlein, P. J., Anderson, P. a and Anderson, P. A.: Atmospheric circulation patterns and spatial climatic variations, Beringia, *Int. J. Climatol.*, 10, 1085–1104, 1998.
- Monnin, E., Indermühle, A., Dällenbach, A., Flückiger, J., Stauffer, B., Stocker, T. F., Raynaud, D. and Barnola, J. M.: Atmospheric CO₂ concentrations over the last glacial termination, *Science*, 291(5501), 112–114, doi:10.1126/science.291.5501.112, 2001.
- Muller, P.J., Kirst, G., Ruhland, G., von Storch, I., Rosell-Mele, A.: Calibration of the alkenone palaeotemperature index U_{37K'} based on core-tops from the eastern South Atlantic and the global ocean (60°N–60°S). *Geochim. Cosmochim. Acta*, 62, 1757–1772, 1998.
- Nazarova, L., de Hoog, V., Hoff, U., Dirksen, O. and Diekmann, B.: Late Holocene climate and environmental changes in Kamchatka inferred from the subfossil chironomid record, *Quat. Sci. Rev.*, 67, 81–92, doi:10.1016/j.quascirev.2013.01.018, 2013a.
- Nazarova, L., Lüpfer, H., Subetto, D., Pestryakova, L. and Diekmann, B.: Holocene climate conditions in central Yakutia (Eastern Siberia) inferred from sediment composition and fossil chironomids of Lake Temje, *Quat. Int.* 290–291, 264–274, 2013b.
- Niebauer, H. J., Bond, N. A., Yakunin, L. P. and Plotnikov, V. V.: An update on the climatology and sea ice of the Bering Sea, in *Dynamics of the Bering Sea*, edited by T. R. Loughlin, and K. Ohtani, pp. 29–59, University of Alaska Sea Grant, doi:10.1029/2003GC000559, 1999.
- Nolan, M., Liston, G., Prokein, P., Brigham-Grette, J., Sharpton, V. L. and Huntzinger, R.: Analysis of lake ice dynamics and morphology on Lake El'gygytgyn, NE Siberia, Siberia, using synthetic aperture radar (SAR) and Landsat, *J. Geophys. Res.*, 108, 1–12, 2003.

- North Greenland Ice Core Project members: High-resolution record of northern hemisphere climate extending into the last interglacial period, *Nature*, 431, 147–151, doi:10.1038/nature02805, 2004.
- Nowaczyk, N. R., Minyuk, P., Melles, M., Brigham-Grette, J., Glushkova, O., Nolan, M., Lozhkin, A. V., Stetsenko, T. V., Anderson, P. M. and Forman, S. L.: Magneto-stratigraphic results from impact crater Lake El'gygytgyn, northeast Siberia: a 300 kyr long high-resolution terrestrial palaeoclimatic record from the Arctic, *Geophys. J. Int.*, 150, 109–126, 2002.
- Ohkouchi, N., Eglinton, T., Keigwin, L. and Hayes, J.: Spatial and temporal offsets between proxy-records in a sediment drift, *Science*, 298 (5596), 1224–1227, doi:10.1126/science.1075287, 2002
- Ohtani, K., Akiba, Y. and Takenouti, A., Y.: Formation of western subarctic water in the Bering Sea, in *Biological oceanography of the northern North Pacific Ocean*, edited by A. Y. Takenouti, pp. 32–44, Idemitsu Shoten Publ. Co, doi:10.1029/2003GC000559, 1972.
- Okazaki, Y., Timmermann, A., Menviel, L., Harada, N., Abe-Ouchi, A., Chikamoto, M. O., Mouchet, A. and Asahi, H.: Deepwater formation in the North Pacific during the Last Glacial Termination, *Science*, 329(5988), 200–204, doi:10.1016/j.dsr2.2005.07.003, 2010.
- Okumura, Y. M., Deser, C., Hu, A., Timmermann, A., and Xie, S.-P.: North Pacific Climate Response to Freshwater Forcing in the Subarctic North Atlantic: Oceanic and Atmospheric Pathways, *J. Clim.*, 22(6), 1424–1445 doi:10.1175/2008JCLI2511.1, 2009.
- Otto-Bliesner et al.. Last Glacial Maximum and Holocene Climate in CCSM3, *J. of Clim.* 19: 2526, 2006.
- Pancost, R. D. and Sinninghe Damsté, J. S.: Carbon isotopic compositions of prokaryotic lipids as tracers of carbon cycling in diverse settings, *Chem. Geol.* 195, 29–58. doi:10.1016/S0009-2541(02) 00387-X, 2003.
- Parrenin, F., Masson-Delmotte, V., Köhler, P., Raynaud, D., Paillard, D., Schwander, J., Barbante, C., Landais, a, Wegner, a and Jouzel, J.: Synchronous change of atmospheric CO₂ and Antarctic temperature during the last deglacial warming., *Science*, 339(6123), 1060–3, doi:10.1126/science.1226368, 2013.
- Peters, K.E., Walters, C.C. and Moldowan, J.M.: *The Biomarker Guide*, Cambridge University Press, Cambridge, 2005.
- Peterse, F., Kim, J.-H., Schouten, S., Kristensen, D. K., Koç, N. and Sinninghe Damsté, J. S.: Constraints on the application of the MBT/CBT palaeothermometer at high latitude environments (Svalbard, Norway), *Org. Geochem.*, 40(6), 692–699, doi:10.1016/j.orggeochem.2009.03.004, 2009.
- Peterse, F., van der Meer, J., Schouten, S., Weijers, J. W. H., Fierer, N., Jackson, R. B., Kim, J.-H. and Sinninghe Damsté, J. S.: Revised calibration of the MBT–CBT palaeotemperature proxy based on branched tetraether membrane lipids in surface soils, *Geochim. Cosmochim. Acta*, 96, 215–229, doi:10.1016/j.gca.2012.08.011, 2012.
- Peterse, F., Vonk, J., Holmes, M., Giosan, L., Zimov, N. and Eglinton, T. I.: Branched glycerol dialkyl glycerol tetraethers in Arctic lake sediments: Sources and implications for palaeothermometry at high latitudes, *J. Geophys. Res. Biogeosciences*, 119, 1738–1754, doi:10.1002/2014JG002639., 2014.
- Pisaric, M. F. J., MacDonald, G. M., Velichko, A. A. and Cwynar, L. C.: The late-glacial and post-glacial vegetation history of the northwestern limits of Beringia based on pollen, stomates, and tree stump evidence, *Quat. Sci. Rev.*, 20, 235–245, 2001.
- Pisias, N., Mix, A., and Heusser, L.: Millennial scale climate variability of the northeast Pacific Ocean and northwest North America based on radiolaria and pollen, *Quat. Sci. Rev.*, 20(14), 1561–1576, doi:10.1016/S0277-3791(01)0018-X, 2001.

- Pitul'ko, V. V., Pavlova, E. Y., Kuz'mina, S. A., Nikol'skii, P. A., Basilyan, A. E., Tumskoi, V. E. and Anisimov, M. A.: Natural-climatic changes in the Yana-Indigirka lowland during the terminal Kargino time and habitat of late Palaeolithic man in northern part of East Siberia, *Dokl. Earth Sci.*, 417(1), 1256–1260, doi:10.1134/S1028334X07080284, 2007.
- Poludetkina, E.: Oil- and Gas-Bearing Prerequisites in the Anadyr Basin Based on Geochemical Indicators, *Vestnik Moskovskogo Universiteta, Geologiya*, 3, 65–71, 2007.
- Porter, S. C. and Swanson, T. W.: Radiocarbon Age Constraints on Rates of Advance and Retreat of the Puget Lobe of the Cordilleran Ice Sheet during the Last Glaciation, *Quat. Res.*, 50, 205–213, 1998.
- Praetorius, S. K. and Mix, A. C.: Synchronization of North Pacific and Greenland climates preceded abrupt deglacial warming, *Science*, 345(6195), 444–8, doi:10.1126/science.1252000, 2014.
- Prahl, F. G., Muehlhausen, L. A. and Zahnle, D. A.: Further evaluation of long-chain alkenones as indicators of palaeoceanographic conditions, *Geochim. et Cosmochim. Acta* 52, 2303–2310, 1988.
- Prahl, F. G. and Wakeham, S. G.: Calibration of unsaturation patterns in long-chain ketone compositions for palaeotemperature assessment, *Nature*, 330, 367–369, 1987.
- Rachold, V., Grigoriev, M. N., Are, F. E., Solomon, S., Reimnitz, E., Kassens, H. and Antonow, M.: Coastal erosion vs riverine sediment discharge in the Arctic Shelf seas, *Int. J. Earth Sci.*, 89(3), 450–460, doi:10.1007/s005310000113, 2000.
- Reimer, P.: IntCal13 and Marine13 Radiocarbon Age Calibration Curves 0–50,000 Years cal BP, *Radiocarbon*, 55(4), 1869–1887, doi:10.2458/azu_js_rc.55.16947, 2013.
- Renssen, H. and Vandenberghe, J.: Investigation of the relationship between permafrost distribution in NW Europe and extensive winter sea-ice cover in the North Atlantic Ocean during the cold phases of the Last Glaciation, *Quat. Sci. Rev.* 22, 209–223, 2014.
- Rethemeyer, J., Fülöp, R.-H., Höfle, S., Wacker, L., Heinze, S., Hajdas, I., Patt, U., König, S., Stapper, B. and Dewald, a.: Status report on sample preparation facilities for ¹⁴C analysis at the new CologneAMS center, *Nucl. Instruments Methods Phys. Res. Sect. B Beam Interact. with Mater. Atoms*, 294, 168–172, doi:10.1016/j.nimb.2012.02.012, 2013.
- Reyes, A. V and Cooke, C. a: Northern peatland initiation lagged abrupt increases in deglacial atmospheric CH₄, *Proc. Natl. Acad. Sci. U. S. A.*, 108(12), 4748–53, doi:10.1073/pnas.1013270108, 2011.
- Riethdorf, J.-R., Max, L., Nürnberg, D., Lembke-Jene, L. and Tiedemann, R.: Deglacial development of (sub) sea surface temperature and salinity in the subarctic northwest Pacific: implications for upper-ocean stratification, *Palaeoceanography*, 28, 1–14, doi:10.1002/palo.20014, 2013.
- Roeckner, E., Brokopf, R., Esch, M., Giorgetta, M., Hagemann, S. and Kornbueh, L.: Sensitivity of simulated climate to horizontal and vertical resolution in the ECHAM5 Atmosphere Model, *J. Climate*, 19, 3771–3791, doi:10.1175/JCLI3824.1, 2006.
- Rose, K. A., Sikes, E. L., Guilderson, T. P., Shane, P., Hill, T. M., Zahn, R., and Spero, H. J.: Upper-ocean-to-atmosphere radiocarbon offsets imply fast deglacial carbon dioxide release, *Nature*, 466, 1093–1097, 2010.
- Rostek, F. and Bard, E.: Hydrological changes in Eastern Europe during the last 40,000yr inferred from biomarkers in Black Sea sediments, *Quat. Res.*, 80(3), 502–509, doi:10.1016/j.yqres.2013.07.003, 2013.
- Rueda, G., Rosell-Melé, A., Escala, M., Gyllencreutz, R. and Backman, J.: Comparison of instrumental and GDGT-based estimates of sea surface and air temperatures from the Skagerrak, *Org. Geochem.*, 40(2), 287–291, doi:10.1016/j.orggeochem.2008.10.012, 2009.

- Ruff, M., Wacker, L., Gaggeler, H. W., Suter, M., Synal, H.-A., Szidat, S.: A Gas Ion Source for Radiocarbon Measurements at 200 kV, *Radiocarbon*, 49, 307-314, 2007.
- Saenko, O. A., Schmittner, A., and Weaver, A. J.: The Atlantic – Pacific Seesaw, *J. Clim.*, 17(11), 2033–2038, doi:10.1175/1520-0442(2004)017<2033:TAS>2.0.CO;2, 2004.
- Sagawa, T. and Ikehara, K.: Intermediate water ventilation change in the subarctic northwest Pacific during the last deglaciation, *Geophys. Res. Lett.*, 35, L24702, doi:10.1029/2008GL035133, 2008.
- Sailer, R. and Kerschner, H.: Equilibrium line altitudes and rock glaciers in the Ferwall Group (Western Tyrol, Austria) during the Younger Dryas cooling event, *Annals of Glaciology* 28, 141–145, 2000.
- Saito, K., Kimoto, M., Zhang, T., Takata, K. and Emori, S.: Evaluating a high-resolution climate model: simulated hydrothermal regimes in frozen ground regions and their change under the global warming scenario. *J. Geophys. Res.*, 112, doi:10.1029/2006JF000577, 2007.
- Sakamoto, T., Ikehara, M., Aoki, K., Iijima, K., Kimura, N., Nakatsuka, T., Wakatsuchi, M.: Ice-rafted debris (IRD)-based sea-ice expansion events during the past 100 kyrs in the Okhotsk Sea, *Deep Sea Res. Part II* 52 (16-18), 2275-2301, 2005.
- Sancetta, C.: Effect of Pleistocene glaciation upon oceanographic characteristics of the North Pacific Ocean and the Bering Sea, *Deep Sea Res.*, 30, 851-869, 1983.
- Sanchi, L., Ménot, G. and Bard, E.: Insights into continental temperatures in the northwestern Black Sea area during the Last Glacial period using branched tetraether lipids, *Quat. Sci. Rev.*, 84, 98–108, doi:10.1016/j.quascirev.2013.11.013, 2014.
- Sarnthein, M., H. Gebhardt, T. Kiefer, M. Kucera, M. Cook, and H. Erlenkeuser (2004), Mid Holocene origin of the sea-surface salinity low in the subarctic North Pacific, *Quat. Sci. Rev.*, 23(20-22), 2089–2099, doi:10.1016/j.quascirev.2004.08.008, 2004.
- Sarnthein, M., Kiefer, M. T., Grootes, P. M., Elderfield, H. and Erlenkeuser, H.: Warmings in the far northwestern Pacific promoted pre-Clovis immigration to America during Heinrich event 1, *Geology*, 34(3), 141, doi:10.1130/G22200.1, 2006.
- Savoskul, O. S.: Holocene glacier advances in the headwaters of Sredniaya Avacha, Kamchatka, Russia. *Qual. Res.* 52, 14–26, 1999.
- Schaefer, K., Zhang, T., Bruhwiler, L., and Barrett, A. P.: Amount and timing of permafrost carbon release in response to climate warming. *Tellus B*, **63**, 165–180, 2011.
- Schefuss, E., Schouten, S. and Schneider, R. R.: Climatic controls on central African hydrology during the past 20,000 years., *Nature*, 437(7061), 1003–6, doi:10.1038/nature03945, 2005.
- Schiller, A., Mikolajewicz, U., and Voss, R.: The stability of the North Atlantic thermohaline circulation in a coupled ocean- atmosphere general circulation model, *Clim. Dyn.*, 13(5), 325–347, doi:10.1007/s003820050169, 1997.
- Schlitzer, R.: Ocean Data View, <http://odv.awi.de>, 2011
- Schmitt, J., Schneider, R., Elsig, J., Leuenberger, D., Laurantou, A., Chappellaz, J., Köhler, P., Joos, F., Stocker, T. F., Leuenberger, M. and Fischer, H.: Carbon isotope constraints on the deglacial CO₂ rise from ice cores, *Science*, 336(6082), 711–4, doi:10.1126/science.1217161, 2012.
- Schmittner, A., Saenko, O. A. and Weaver, A. J.: Coupling of the hemispheres in observations and simulations of glacial climate change, *Quat. Sci. Rev.*, 22(5-7), 659–671, doi:10.1016/S0277-3791(02)00184-1, 2003.

- Schneider von Deimling, T. S., Meinshausen, M., Levermann, A., Huber, V., Frieler, K., Lawrence, D. M., and Brovkin, V.: Estimating the near-surface permafrost-carbon feedback on global warming. *Biogeosciences*, **9**, 649–665, 2012.
- Schouten, S., Hopmans, E. C., Schefuß, E. and Sinninghe Damsté, J. S.: Distributional variations in marine crenarchaeotal membrane lipids: a new tool for reconstructing ancient sea water temperatures?, *Earth Planet. Sci. Lett.*, 204(1-2), 265–274, doi:10.1016/S0012-821X(02)00979-2, 2002.
- Schouten, S., Hopmans, E. C. and Sinninghe Damsté, J. S.: The organic geochemistry of glycerol dialkyl glycerol tetraether lipids: A review, *Org. Geochem.*, **54**, 19–61, doi:10.1016/j.orggeochem.2012.09.006, 2013.
- Schouten, S., Huguet, C., Hopmans, E. C., and Sinninghe Damsté, J. S.: Improved analytical methodology of the TEX₈₆ palaeothermometry by high performance liquid chromatography/atmospheric pressure chemical ionization-mass spectrometry, *Anal. Chem.*, **79**, 2940–2944, 2007.
- Schuur, E. A. G., Abbott, B. W., Bowden, W. B., Brovkin, V., Camill, P., Canadell, J. G., Chanton, J. P., Chapin, F. S., Christensen, T. R., Ciais, P., Crosby, B. T., Czimeczik, C. I., Grosse, G., Harden, J., Hayes, D. J., Hugelius, G., Jastrow, J. D., Jones, J. B., Kleinen, T., Koven, C. D., Krinner, G., Kuhry, P., Lawrence, D. M., McGuire, A. D., Natali, S. M., O'Donnell, J. A., Ping, C. L., Riley, W. J., Rinke, A., Romanovsky, V. E., Sannel, A. B. K., Schädel, C., Schaefer, K., Sky, J., Subin, Z. M., Tarnocai, C., Turetsky, M. R., Waldrop, M. P., Walter Anthony, K. M., Wickland, K. P., Wilson, C. J. and Zimov, S. A.: Expert assessment of vulnerability of permafrost carbon to climate change, *Climatic Change*, **119** (2), 359–374, doi:10.1007/s10584-013-0730-7, 2013.
- Schuur, E. A. G., Bockheim, J., Canadell, J. G., Euskirchen, E., Field, C. B., Goryachkin, S. V., Hagemann, S., Kuhry, P., Lafleur, P. M., Lee, H., Mazhitova, G., Nelson, F. E., Rinke, A., Romanovsky, V. E., Shiklomanov, N., Tarnocai, C., Venevsky, S., Vogel, J. G. and Zimov, S. A.: Vulnerability of Permafrost Carbon to Climate Change: Implications for the Global Carbon Cycle, *Bioscience*, **58**(8), 701–714, doi:10.1641/B580807, 2008.
- Schuur, E. A. G., McGuire, A. D., Grosse, G., Harden, J. W., Hayes, D. J., Hugelius, G., Koven, C. D. and Kuhry, P.: Climate change and the permafrost carbon feedback, *Nature*, **520**, 171–179, doi:10.1038/nature14338, 2015.
- Schuur, E. A. G., Vogel, J. G., Crummer, K. G., Lee, H., Sickman, J. O. and Osterkamp, T. E.: The effect of permafrost thaw on old carbon release and net carbon exchange from tundra., *Nature*, **459**(7246), 556–559, doi:10.1038/nature08031, 2009.
- Seki, O., Bendle, J. a., Harada, N., Kobayashi, M., Sawada, K., Moossen, H., Inglis, G. N., Nagao, S. and Sakamoto, T.: Assessment and calibration of TEX₈₆ palaeothermometry in the Sea of Okhotsk and sub-polar North Pacific region: Implications for palaeoceanography, *Prog. Oceanogr.*, **126**, 254–266, doi:10.1016/j.pocean.2014.04.013, 2014.
- Seki, O., Ikehara, M., Kawamura, K., Nakatsuka, T., Ohnishi, K., Wakatsuchi, M., Narita, H. and Sakamoto, T.: Reconstruction of palaeoproductivity in the Sea of Okhotsk over the last 30 kyr, *Palaeoceanography*, **19**, PA1016, doi:10.1029/2002PA000808, 2004a.
- Seki, O., Ishiwatar, R., and Matsumoto, K.: Millennial climate oscillations in NE Pacific surface waters over the last 82 kyr: New evidence from alkenones, *Geophys. Res. Lett.*, **29**(23), 2144, doi:10.1029/2002GL015200, 2002.

- Seki, O., Kawamura, K., Ikehara, M., Nakatsuka, T. and Oba, T.: Variation of alkenone sea surface temperature in the Sea of Okhotsk over the last 85 kyrs, *Org. Geochem.*, 35(3), 347–354, doi:10.1016/j.orggeochem.2003.10.011, 2004 b.
- Seki, O., Nakatsuka, T., Kawamura, K., Saitoh, S.-I. and Wakatsuchi, M.: Time-series sediment trap record of alkenones from the western Sea of Okhotsk. *Mar. Chem.*, 104(3-4), 253–265, doi:10.1016/j.marchem.2006.12.002, 2007.
- Seki, O., Sakamoto, T., Sakai, S., Schouten, S., Hopmans, E. C., Sinninghe Damste, J. S. and Pancost, R. D.: Large changes in seasonal sea ice distribution and productivity in the Sea of Okhotsk during the deglaciations, *Geochemistry, Geophys. Geosystems*, 10(10), Q10007, doi:10.1029/2009GC002613, 2009.
- Self, A. E., Klimaschewski, A., Solovieva, N., Jones, V. J., Andrén, E., Andreev, A. A., Hammarlund, D. and Brooks, S. J.: The relative influences of climate and volcanic activity on Holocene lake development inferred from a mountain lake in central Kamchatka, *Glob. Planet. Change*, 134, 67–81, doi:10.1016/j.gloplacha.2015.06.012, 2015.
- Seppä, H., Bjune, A. E., Telford, R. J., Birks, H. J. B. and Veski, S.: Last nine-thousand years of temperature variability in Northern Europe, *Clim. Past* 5, 523–535, 2009.
- Sergin, S. Y., Scheglova, M. S.: Beringia climate during ice ages as result of influence of global and local factors, In: *Beringia in the Cenozoic*. Nauka Press, Vladivostok, pp. 171-175, 1976. (in Russian).
- Siegert, M.J., Dowdeswell, J.A., Hald, M., Svendsen, J.: Modelling the Eurasian Ice Sheet through a full (Weichselian) glacial cycle, *Global Planet. Change* 31, 367–385, 2001.
- Sinninghe Damsté, J. S., Rijpstra, W. I. C., Hopmans, E. C., Weijers, J. W. H., Foesel, B. U., Overmann, J., et al.: 13, 16-Dimethyl Octacosanedioic Acid (iso-Diabolic Acid), a common membrane- spanning lipid of Acidobacteria subdivisions 1 and 3, *Appl. Environ. Microbiol.* 77, 4147–4154. doi: 10.1128/AEM.00466-11, 2011.
- Shah, S. R., and Pearson, A.: Ultra-microscale (5–25 µg C) analysis of individual lipids by ¹⁴C AMS: Assessment and correction for sample processing blanks, *Radiocarbon*, 49 (1), 69, 2007.
- Shahgedanova M., Perov, V., Mudriv, Y.: In: *The Physical Geography of Northern Eurasia*, Shahgedanova M. (ed.). Oxford University Press: Oxford, 284-313, 2002.
- Shakun, J. D., Clark, P. U., He, F., Marcott, S. A., Mix, A. C., Liu, Z., Otto-Bliesner, B., Schmittner, A. and Bard, E.: Global warming preceded by increasing carbon dioxide concentrations during the last deglaciation, *Nature*, 484(7392), 49–54, doi:10.1038/nature10915, 2012.
- Shanahan, T. M., Huguen, K. A. and Van Mooy, B. A. S.: Temperature sensitivity of branched and isoprenoid GDGTs in Arctic lakes, *Org. Geochem.*, 64, 119–128, doi:10.1016/j.orggeochem.2013.09.010, 2013.
- Sher, A. V., Kuzmina, S. A., Kuznetsova, T. V. and Sulerzhitsky, L. D.: New insights into the Weichselian environment and climate of the East Siberian Arctic, derived from fossil insects, plants, and mammals, *Quat. Sci. Rev.*, 24(5-6), 533–569, doi:10.1016/j.quascirev.2004.09.007, 2005.
- Shin, S. I., Liu, Z., Otto-Bliesner, B., Brady, E. C., Kutzbach, J. E., and Harrison, S. P.: A simulation of the Last Glacial Maximum climate using the NCAR-CCSM. *Clim. Dyn.*, 20(2-3), 127–151, doi:10.1007/s00382-002-0260-x, 2003.
- Skinner, L. C., Fallon, S., Waelbroeck, C., Michel, E. and Barker, S.: Ventilation of the deep Southern Ocean and deglacial CO₂ rise., *Science*, 328(5982), 1147–1151, doi:10.1126/science.1183627, 2010.

- Slater, A. G. and Lawrence, D. M.: Diagnosing present and future permafrost from climate models, *J. Clim.*, 26(15), 5608–5623, doi:10.1175/JCLI-D-12-00341.1, 2013.
- Smirnova, M. A., Kazarina, G. K., Matul, A. G. and Max, L.: Diatom Evidence for Palaeoclimate Changes in the Northwestern Pacific during the Last 20000 Years, *Mar. Geol.*, 55(3), 425–431, doi:10.1134/S0001437015030157, 2015.
- Smith, S. L., et al.: Thermal state of permafrost in North America: A contribution to the International Polar Year. *Permafr. Periglac. Process.*, **21**, 117–135, 2010.
- Smith, L. C., MacDonald, G. M., Velichko, A. A., Beilman, D. W., Borisova, O., Frey, K. E., Kremenetski, K. V. and Sheng, Y.: Siberian Peatlands a Net Carbon Sink and Global Methane Source Since the Early Holocene, *Science*, 303 (5656), 353–356, doi:10.1126/science.1090553, 2004.
- Solomina, O., Calkin, P.: Lichenometry as applied to moraines in Alaska, USA, and Kamchatka, Russia, *Arct., Antarc., Apl. Res.*, 35, 129-143, 2003.
- Solovieva, N., Klimaschewski, A., Self, A. E., Jones, V. J., Andrén, E., Andreev, A. A., Hammarlund, D., Lepskaya, E. V. and Nazarova, L.: The Holocene environmental history of a small coastal lake on the north-eastern Kamchatka Peninsula, *Glob. Planet. Change*, 134, 55–66, doi:10.1016/j.gloplacha.2015.06.010, 2015.
- Soulet, G., Ménot, G., Bayon, G., Rostek, F., Ponzevera, E., Toucanne, S., Lericolais, G. and Bard, E.: Abrupt drainage cycles of the Fennoscandian Ice Sheet., *Proc. Natl. Acad. Sci. U. S. A.*, 110(17), 6682–7, doi:10.1073/pnas.1214676110, 2013.
- Stabeno, P. J., and Reed, R. K.: Circulation in the Bering Sea basin by satellite tracked drifters. *J. Phys. Oceanogr.*, 24(4), 848-854, 1994.
- Stanford, J.D., Hemmingway, R., Rohling, E.J., Challonor, P.G., Medina-Elizade, M., Lester, A.J.: Sealevel probability for the last deglaciation: A statistical analysis of far-field records, *Glob. Planet. Change* 79, 193-203, 2011.
- Stepanek, C., and Lohmann, G.: Modelling mid-Pliocene climate with COSMOS, *Geosci. Model Dev.*, 5, 1221-1243, 2012.
- St. John, K. E. K. and Krissek, L. A.: Regional patterns of Pleistocene ice-rafted debris flux in the North Pacific, *Palaeoceanography*, 14(5), 653–662, doi:10.1029/1999PA900030, 1999.
- Strauch, G. and Gualteri, L.: Late Quaternary Glaciations in northeastern Russia, *J. Quat. Sci.*, 23, 6-7, 2008.
- Stuiver, M., Polach, H.A.: Reporting of ¹⁴C Data, *Radiocarbon*. 19, 355-363, 1977.
- Sun, M.-Y., Wakeham, S.G.: Molecular evidence for degradation and preservation of organic matter in the anoxic Black Sea Basin, *Geochim. Cosmochim. Acta*. 58, 3395-3406, 1994.
- Synal, H.-A., Stocker, M., and Suter, M.: Micadas: a new compact radiocarbon AMS system, *Nuclear Instruments and Methods in Physics Research Section B: Beam Interactions with Materials and Atoms*, 259 (1), 7-13, 2007.
- Takahashi, K., Fujitani, N., and Yanada, M.: Long term monitoring of particle fluxes in the Bering Sea and the central subarctic Pacific Ocean, 1990-2000, *Prog. Oceanog.*, 55(1-2), 95–112, doi:10.1016/S0079-6611(02)00072-1, 2002.
- Tanaka, S., and Takahashi, K.: Late Quaternary palaeoceanographic changes in the Bering Sea and the western subarctic Pacific based on radiolarian assemblages, *Deep Sea Res., Part II*, 52(16-18), 2131-2149, doi: 10.1016/j.dsr2.2005.07.002, 2005.

- Tarnocai, C., Canadell, J. G., Schuur, E. a. G., Kuhry, P., Mazhitova, G. and Zimov, S.: Soil organic carbon pools in the northern circumpolar permafrost region, *Global Biogeochem. Cycles*, 23(2), GB2023, doi:10.1029/2008GB003327, 2009.
- Taylor, M. A., Hendy, I. L. and Pak, D. K.: Deglacial ocean warming and marine margin retreat of the Cordilleran Ice Sheet in the North Pacific Ocean, *Earth Planet. Sci. Lett.*, 403, 89–98, doi:10.1016/j.epsl.2014.06.026, 2014.
- Ternois, Y. T., Awamura, K. K., Hkouchi, N. O. and Eigwin, L. K.: Alkenone sea surface temperature in the Okhotsk Sea for the last 15 kyr, *Geochem. J.*, 34, 283–293, 2000.
- Tierney, J. E., Russell, J. M., Eggermont, H., Hopmans, E. C., Verschuren, D., and Sinninghe Damsté, J. S.: Environmental controls on branched tetraether lipid distributions in tropical East African lake sediments, *Geochim. Cosmochim. Acta* 74, 4902–4918. doi: 10.1016/j.gca.2010. 06.002, 2010.
- Timmermann, A., Menviel, L., Okumura, Y., Schilla, A., Merkel, U., O. Timm, O., Hu, A. S., Otto-Bliesner, B., and Schulz, M.: Towards a quantitative understanding of millennial scale Antarctic warming events. *Quat. Sci. Rev.*, 29(1-2), 74-85, 2010.
- Vaks, A., Gutareva, O. S., Breitenbach, S., Avirmed, E., Mason, A. J., Thomas, A. L., Osinzev, A. V., Kononov, A. M. and Henderson, G. M.: Speleothems Reveal 500,000-Year History of Siberian Permafrost, *Science*, 340, 183–186, doi:10.1126/science.1228729, 2013.
- Vandenberghe, J., French, H. M., Gorbunov, A., Marchenko, S., Velichko, A. a., Jin, H., Cui, Z., Zhang, T. and Wan, X.: The Last Permafrost Maximum (LPM) map of the Northern Hemisphere: permafrost extent and mean annual air temperatures, 25-17 ka BP, *Boreas*, doi:10.1111/bor.12070, 2014.
- VanLaningham, S., Piasias, N. G., Duncan, R. a. and Clift, P. D.: Glacial–interglacial sediment transport to the Meiji Drift, northwest Pacific Ocean: Evidence for timing of Beringian outwashing, *Earth Planet. Sci. Lett.*, 277(1-2), 64–72, doi:10.1016/j.epsl.2008.09.033, 2009.
- Velichko, A. A.: North Eurasian landscape and climate development. The Late Pleistocene/Holocene: Elements of Forecast. Iss. I. Regional Palaeogeography. Nauka Press, Moscow, 1993 (in Russian).
- Velichko, A.A., Wright, H.E., Barnosky, C.W.: Late Quaternary Environments of the Soviet Union, University of Minnesota Press, Minneapolis, 1984.
- Vellinga, M. and Wood, R. A.: Global climate impacts of a collapse of the Atlantic thermohaline circulation, *Clim. Chang.*, 54(3), 251-267, doi:10.1023/A:1016168827653, 2002.
- Veres, D., Bazin, L., Landais, A., Toyé Mahamadou Kele, H., Lemieux-Dudon, B., Parrenin, F., Martinerie, P., Blayo, E., Blunier, T., Capron, E., Chappellaz, J., Rasmussen, S. O., Severi, M., Svensson, A., Vinther, B. and Wolff, E. W.: The Antarctic ice core chronology (AICC2012): an optimized multi-parameter and multi-site dating approach for the last 120 thousand years, *Clim. Past* 9, 1733–1748, 2013.
- Vettoretti, G., Peltier, W. R., and McFarlane, N. A.: Global water balance and atmospheric water vapor transport at last glacial maximum: climate simulations with the Canadian Climate Center for Modelling and Analysis atmospheric general circulation model, *Can. J. Earth Sci.*, 37, 695–723, 2000.
- Volkman, J.K., Eglinton, G., Corner, E.D.S. and Forsberg, T.E.V.: Long-chain alkenes and alkenones in the marine coccolithophorid *Emiliania huxleyi*. *Phytochemistry*, 19, 2619-2622, 1980.
- Wacker, L. and Christl, M.: Data reduction for small radiocarbon samples, Annual Report of Ion Beam Physics laboratory ETH Zurich, 3, 36, 2011.

- Wacker, L., Fahrni, S. M., Hajdas, I., Molnár, M., Synal, H.-A., Szidat, S. and Zhang, Y. L.: A versatile gas interface for routine radiocarbon analysis with a gas ion source, *Nucl. Inst. Meth. B*, 294, 315–319, doi:10.1016/j.nimb.2012.02.009, 2013.
- Waelbroeck, C., Paul, A., Kucera, M., Rosell-Melé, A., Weinelt, M., Schneider, R., Mix, a. C., Abelmann, A., Armand, L., Bard, E., Barker, S., Barrows, T. T., Benway, H., Cacho, I., Chen, M.-T., Cortijo, E., Crosta, X., de Vernal, A., Dokken, T., Duprat, J., Elderfield, H., Eynaud, F., Gersonde, R., Hayes, A., Henry, M., Hillaire-Marcel, C., Huang, C.-C., Jansen, E., Juggins, S., Kallel, N., Kiefer, T., Kienast, M., Labeyrie, L., Leclaire, H., Londeix, L., Mangin, S., Matthiessen, J., Marret, F., Meland, M., Morey, A. E., Mulitza, S., Pflaumann, U., Pisias, N. G., Radi, T., Rochon, A., Rohling, E. J., Saffi, L., Schäfer-Neth, C., Solignac, S., Spero, H., Tachikawa, K. and Turon, J.-L.: Constraints on the magnitude and patterns of ocean cooling at the Last Glacial Maximum, *Nat. Geosci.*, 2, 127–132, doi:10.1038/ngeo411, 2009.
- Walker, C. B., de la Torre, J. R., Klotz, M. G., Urakawa, H., Pinel, N., Arp, D. J., Brochier- Armanet, C., Chain, P. S., Chan, P. P., Gollabgir, A., Hemp, J., Hügler, M., Karr, E. A., Könneke, M., Shin, M., Lawton, T. J., Lowe, T., Martens-Habben, W., Sayavedra-Soto, L. A., Lang, D., Sievert, A. M., Rosenzweig, A. C., Manning, G. and Stahl D. A.: *Nitrosopumilus maritimus* genome reveals unique mechanisms for nitrification and autotrophy in globally distributed marine Crenarchaea, *Proc. Natl. Acad. Sci. USA*, 107, 8818–8823, doi:10.1073/pnas.0913533107. Epub 2010 Apr 26, 2010.
- Walter, K. M., Erwards, M. E., Grosse, G., Zimov, S. A. and Chapin III, F. S.: Thermokarst Lakes as a Source of Atmospheric CH₄ during the Last Deglaciation, *Science* 318, 633–636, doi:10.1126/science.1142924, 2007.
- Wang, Y., Cheng, H., Lawrence Edwards, R., Kong, X., Shao, X., Chen, S., Wu, J., Jiang, X., Wang, X. and An, Z.: Millennial- and orbital-scale changes in the East Asian monsoon over the past 224,000 years, *Nature* 451, 1090–1093, 2008.
- Weber, M. E., Clark, P. U., Kuhn, G., Timmermann, A., Sprenk, D., Gladstone, R., Zhang, X., Lohmann, G., Meniel, L., Chikamoto, M. O., Friedrich, T. and Ohlwein, C.: Millennial-scale variability in Antarctic ice-sheet discharge during the last deglaciation, *Nature* 510, 134–138, doi:10.1038/nature13397, 2014
- Wei, W., Lohmann, G. and Dima, M.: Distinct modes of internal variability in the Global Meridional Overturning Circulation associated to the Southern Hemisphere westerly winds, *J. Phys. Oceanogr.*, 42, 785–801. doi:10.1175/JPO-D-11-038.1, 2012
- Wei, W., and Lohmann, G.: Simulated Atlantic Multidecadal Oscillation during the Holocene, *J. Climate*, 25, 6989–7002. doi:10.1175/JCLI-D-11-00667.1, 2012
- Weijers, J. W. H., Panoto, E., Van Bleijswijk, J., Schouten, S., Rijpstra, W. I. C., Balk, M., et al.: Constraints on the biological source(s) of the orphan branched tetraether membrane lipids, *Geomicrobiol. J.* 26, 402–414, doi: 10.1080/01490450902937293, 2009.
- Weijers, J. W. H., Schouten, S., Hopmans, E. C., Geenevasen, J. A. J., David, O. R. P., Coleman, J. M., Pancost, R. D. and Sinninghe Damsté, J. S.: Membrane lipids of mesophilic anaerobic bacteria thriving in peats have typical archaeal traits, *Environ. Microbiol.* 8, 648–657, 2006a
- Weijers, J. W. H., Schouten, S., Spaargaren, O. C. and Sinninghe Damsté, J. S.: Occurrence and distribution of tetraether membrane lipids in soils: Implications for the use of the TEX₈₆ proxy and the BIT index, *Org. Geochem.*, 37(12), 1680–1693, doi:10.1016/j.orggeochem.2006.07.018, 2006b.

- Weijers, J. W. H., Schouten, S., van den Donker, J. C., Hopmans, E. C. and Sinninghe Damsté, J. S.: Environmental controls on bacterial tetraether membrane lipid distribution in soils, *Geochim. Cosmochim. Acta*, 71(3), 703–713, doi:10.1016/j.gca.2006.10.003, 2007.
- Winterfeld, M.: Biomarker and carbon isotope constraints ($\delta^{13}\text{C}$, $\Delta^{14}\text{C}$) on sources and cycling of particulate organic matter discharged by large Siberian rivers draining permafrost areas. PhD-thesis, University of Bremen, 2014.
- Wuchter, C., Schouten, S., Coolen, M. J. and Sinninghe Damsté, J. S.: Temperature-dependent variation in the distribution of tetraether membrane lipids of marine Crenarchaeota: Implications for TEX₈₆ palaeothermometry. *Palaeoceanography*, 19, 2004.
- Yamamoto, M., Shimamoto, A., Fukuhara, T., Tanaka, Y. and Ishizaka, J.: Glycerol dialkyl glycerol tetraethers and TEX₈₆ index in sinking particles in the western North Pacific, *Org. Geochem.*, 53, 52–62, doi:10.1016/j.orggeochem.2012.04.010, 2012.
- Yanase, W. and Abe-Ouchi, A.: The LGM surface climate and atmospheric circulation over East Asia and the North Pacific in the PMIP2 coupled model simulations, *Clim. Past Discuss.*, 3(2), 655–678, doi:10.5194/cpd-3-655-2007, 2007.
- Yanase, W. and Abe-Ouchi, A.: A numerical study on the atmospheric circulation over the midlatitude North Pacific during the last glacial maximum, *J. Clim.*, 23(1), 135–151, doi:10.1175/2009JCLI3148.1, 2010.
- Yershov E.: *General Geocryology*, Cambridge (United Kingdom): Cambridge University Press, 1998.
- Zamoruyev, V.: Quaternary glaciation of north-east Asia, In: Ehlers, J., Gibbard, P.L. (Eds.), *Quaternary Glaciations - extent and chronology, Part III*. Elsevier, Netherlands, pp. 321–323, 2004.
- Zazula, G. D., Duk-Rodkin, A., Schweger, C. E. and Morlan, R. E.: Late Pleistocene chronology of glacial Lake Old Crow and the north-west margin of the Laurentide Ice Sheet, *Quat. Glaciat.*, 347–362, 2004.
- Zell, C., Kim, J.-H., Hollander, D., Lorenzoni, L., Baker, P., Silva, C. G., Nittrouer, C. and Sinninghe Damsté, J. S.: Sources and distributions of branched and isoprenoid tetraether lipids on the Amazon shelf and fan: Implications for the use of GDGT-based proxies in marine sediments, *Geochim. Cosmochim. Acta*, 139, 293–312, doi:10.1016/j.gca.2014.04.038, 2014.
- Zell, C., Kim, J.-H., Moreira-Turcq, P., Abril, G., Hopmans, E. C., Bonnet, M.-P., Lima Sobrinho, R. and Sinninghe Damsté, J. S.: Disentangling the origins of branched tetraether lipids and crenarchaeol in the lower Amazon River: Implications for GDGT-based proxies, *Limnol. Oceanogr.*, 58(1), 343–353, doi:10.4319/lo.2013.58.1.0343, 2013.
- Zhang, Y., Chen, W. J. and Riseborough, D. W.: Transient projections of permafrost distribution in Canada during the 21st century under scenarios of climate change. *Global Planet. Change*, 60, 443–456, 2008a.
- Zhang, Y., Chen, W. J. and Riseborough, D. W.: Disequilibrium response of permafrost thaw to climate warming in Canada over 1850–2100. *Geophys. Res. Lett.* 35, L02502, doi:10.1029/2007GL032117, 2008b.
- Zhang, X., Lohmann, G., Knorr, G. and Purcell, C.: Abrupt glacial climate shifts controlled by ice sheet changes. *Nature* 512, 290–294, DOI: 10.1038/nature13592, 2014.
- Zhang, X., Lohmann, G., Knorr, G. and Xu, X. Different ocean states and transient characteristics in Last Glacial Maximum simulations and implications for deglaciation. *Clim. Past* 9, 2319–2333, doi:10.5194/cp-9-2319-2013, 2013.

- Zhu, C., Weijers, J. W. H., Wagner, T., Pan, J.-M., Chen, J.-F. and Pancost, R. D.: Sources and distributions of tetraether lipids in surface sediments across a large river-dominated continental margin, *Org. Geochem.*, 42(4), 376–386, doi:10.1016/j.orggeochem.2011.02.002, 2011.
- Zimov, S. A., Schuur, E. A. G. and Chapin, F. S.: Climate change. Permafrost and the global carbon budget, *Science*, 312(5780), 1612–1613, doi:10.1126/science.1128908, 2006.
- Zimov, N. S., Zimov, S. A., Zimova, A. E., Zimova, G. M., Chuprynin, V. I. and Chapin, F. S.: Carbon storage in permafrost and soils of the mammoth tundra-steppe biome: Role in the global carbon budget, *Geophys. Res. Lett.*, 36(2), L02502, doi:10.1029/2008GL036332, 2009.

9. Description of Own Contributions

The sediment cores had already been retrieved when I started my PhD. Sampling of the cores was performed by myself. I processed the majority of samples from cores 12KL and 114KL through the subsequent geochemical sample treatment in the laboratories. I obtained help from two students during sample processing. One assisted to prepare samples for TOC measurements of cores 12KL and 114KL. The other student processed my samples of core 18-3/6 through the entire geochemical treatment. Supervising both students I instructed them during the lab-work. TOC-measurements were performed by two technicians at the University of Bremen. Measurements on the GC-FID, HPLC-APCI-MS and PC-GC were all conducted by myself. I performed the sample preparation for compound-specific radiocarbon analysis at ETH and also actively run the AMS measurements under the supervision and help of Cameron McIntyre.

TOC-measurements were performed by two technicians at the University of Bremen. Measurements on the GC-FID, HPLC-APCI-MS and PC-GC were all conducted by myself. Jens Hefter introduced me into the different instruments. I also actively conducted the AMS measurements at ETH-Zürich under the supervision and help of Cameron McIntyre and Negar Haghypour.

The research questions addressed in the manuscripts, the data-distribution among the manuscripts, the data processing (e.g. correction of radiocarbon-data) and the data interpretation were largely developed by myself. I developed the final details of the research questions. I wrote all manuscript-drafts and my co-authors made some suggestions where and how to improve the drafts. G. Lohmann produced the figures from the Earth System Model COSMOS (in Manuscript II) and wrote the model-setup description for the methods section of the manuscript. For manuscripts I, II and IV Jens Hefter helped with the accurate description of the instrumental setup.

Manuscript III resulted from a research stay at Queen's University Belfast where I was cooperating with Iestyn Barr. He introduced me to his degree-day-model and I applied it to my scientific questions.